AD 729330

AD

# USAAMRDL TECHNICAL REPORT 71-29

# SAFETY EVALUATION OF EMULSIFIED FUELS

By

L. Maurice Shaw

June 1971

DDC
RECEIVED
SEP 7 1971
D

EUSTIS DIRECTORATE
U. S. ARMY AIR MOBILITY RESEARCH AND DEVELOPMENT LABORATORY
FORT EUSTIS, VIRGINIA

CONTRACT DAAJ02-69-C-0030
DYNAMIC SCIENCE (THE AvSER FACILITY)
A DIVISION OF MARSHALL INDUSTRIES
PHOENIX, ARIZONA

Approved for public release;
distribution unlimited.

Reproduced by
NATIONAL TECHNICAL
INFORMATION SERVICE
Springfield, Va. 22151

193

Unclassified

Security Classification

**DOCUMENT CONTROL DATA - R & D**

*(Security classification of title, body of abstract and indexing annotation must be entered when the overall report is classified)*

| 1. ORIGINATING ACTIVITY (Corporate author) | 2a. REPORT SECURITY CLASSIFICATION |
|---|---|
| Dynamic Science (The AvSER Facility)<br>A Division of Marshall Industries<br>Phoenix, Arizona 85027 | Unclassified<br>2b. GROUP |

3. REPORT TITLE

SAFETY EVALUATION OF EMULSIFIED FUELS

4. DESCRIPTIVE NOTES (Type of report and inclusive dates)

Final Report

5. AUTHOR(S) (First name, middle initial, last name)

L. Maurice Shaw

| 6. REPORT DATE | 7a. TOTAL NO. OF PAGES | 7b. NO. OF REFS |
|---|---|---|
| June 1971 | 190 | 8 |

| 8a. CONTRACT OR GRANT NO. | 9a. ORIGINATOR'S REPORT NUMBER(S) |
|---|---|
| DAAJ02-69-C-0030<br>b. PROJECT NO.<br>1F162203A529<br>c.<br>d. | USAAMRDL Technical Report 71-29<br>9b. OTHER REPORT NO(S) (Any other numbers that may be assigned this report)<br>Dynamic Science Report 9130-71-3 |

10. DISTRIBUTION STATEMENT

Approved for public release; distribution unlimited.

| 11. SUPPLEMENTARY NOTES | 12. SPONSORING MILITARY ACTIVITY |
|---|---|
| None | Eustis Directorate, U. S. Army Air Mobility Research and Development Laboratory, Fort Eustis, Virginia |

13. ABSTRACT

A comprehensive test program was conducted to establish emulsified fuel screening test procedures, to obtain safety evaluation criteria, and to evaluate the safety performance of emulsified and gelled aviation fuels in a simulated full-scale crash environment. A series of screening tests was formulated and conducted to obtain fuel characteristics as a function of hot-surface ignition, wind shear, and impact dynamics associated with fuel breakup, atomization/dispersion, and ignition. The data obtained from these screening tests were used to establish emulsified fuel safety evaluation criteria. A simulated full-scale experiment was designed to simulate the full-scale helicopter crash environment adequately and, in addition, to be reproducibly controllable at minimal cost.

The screening tests revealed that, for the emulsified fuels tested, safety was directly dependent upon the fuel yield stress and its internal phase base fuel. The screening test data followed the expected trends within the data scatter associated with the type of tests conducted. A safety evaluation criterion was established in terms of an ignition susceptibility parameter which was shown to be related to an empirical equation containing fuel properties. The data obtained from the simulated full-scale tests provided definition of a nonhazardous limiting value for the ignition susceptibility parameter. This allowed the screening test results to become meaningful in predicting the performance of emulsified fuels under actual crash conditions. Further, tests were performed on gelled fuels to offer a comparison between the safety of emulsified and gelled fuels.

Three of the emulsified fuels tested were found to result in a nonhazardous postcrash fire: (1) EP8R-104H emulsion, (2) EP8R-104 emulsion, and (3) Jet-A EXP-4 emulsion. The gelled fuels did not perform as well as the emulsified fuels; however, one gel, Jet-A gel #1, indicated a sizeable advantage over liquid fuels.

In summary, the results of this program confirmed that aircraft fuel emulsions can be formulated which are nonhazardous within the helicopter survivable crash limit envelope as reproduced during the conduct of this evaluation.

DD FORM 1 NOV 68 1473 REPLACES DD FORM 1473, 1 JAN 64, WHICH IS OBSOLETE FOR ARMY USE.

Unclassified

Security Classification

## DISCLAIMERS

The findings in this report are not to be construed as an official Department of the Army position unless so designated by other authorized documents.

When Government drawings, specifications, or other data are used for any purpose other than in connection with a definitely related Government procurement operation, the US Government thereby incurs no responsibility nor any obligation whatsoever; and the fact that the Government may have formulated, furnished, or in any way supplied the said drawings, specifications, or other data is not to be regarded by implication or otherwise as in any manner licensing the holder or any other person or corporation, or conveying any rights or permission, to manufacture, use, or sell any patented invention that may in any way be related thereto.

Trade names cited in this report do not constitute an official endorsement or approval of the use of such commercial hardware or software.

## DISPOSITION INSTRUCTIONS

Destroy this report when no longer needed. Do not return it to the originator.

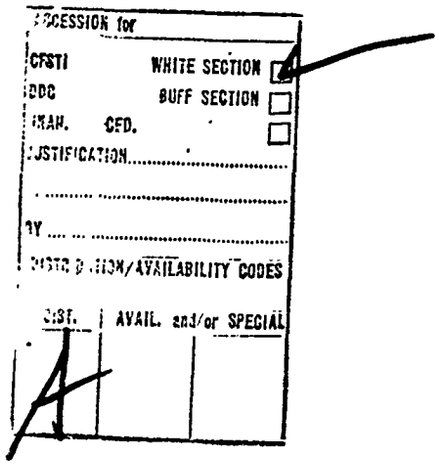

| 14. KEY WORDS | LINK A | | LINK B | | L |
|---|---|---|---|---|---|
| | ROLE | WT | ROLE | WT | ROL |
| Aircraft Postcrash Fire Protection | | | | | |
| Fuel Systems Safety | | | | | |
| Emulsified Fuels | | | | | |
| Gelled Fuels | | | | | |
| Laboratory Screening Tests | | | | | |
| Simulated Full-Scale Tests | | | | | |
| Ignition Susceptibility Parameter | | | | | |

DEPARTMENT OF THE ARMY
U. S. ARMY AIR MOBILITY RESEARCH & DEVELOPMENT LABORATORY
EUSTIS DIRECTORATE
FORT EUSTIS, VIRGINIA 23604

This report was prepared by Dynamic Science (The AvSER Facility), a Division of Marshall Industries, under the terms of Contract DAAJ02-69-C-0030. The technical monitor for this program was Mr. W. J. Nolan, of the Safety and Survivability Division, Eustis Directorate.

Since 1966, the U.S. Army has been conducting research in the areas of emulsified fuels composition, manufacture, rheology, combustion, and safety. This work was accomplished in the belief that fuel emulsions, because of their non-Newtonian characteristics, would provide an increased margin of safety in the aircraft flight and crash environments.

The purpose of this effort was to qualitatively evaluate the performance of emulsified fuels under realistically reproduced aircraft crash conditions. A series of laboratory tests was conducted in which the performance of fuels under dynamic conditions was observed. Based on these observations, a fuels susceptibility parameter was established as a means of predicting a fuel's behavior in the crash environment. Sixty full-scale fuel cell impact tests subsequently proved the validity of the susceptibility parameters. In addition, the impact tests conclusively demonstrated that emulsified kerosene fuels (JP-8, Jet A) significantly reduce the fire hazard associated with the aircraft post-crash environment.

The conclusions and recommendations contained in this report are concurred in by this Directorate. Also, this Directorate believes that the safety potential of emulsified kerosene fuels is of sufficient magnitude to warrant expedited program prosecution in an effort to develop usable systems for U.S. Army aircraft at the earliest possible date.

Project 1F162203A529
Contract DAAJ02-69-C-0030
USAAMRDL Technical Report 71-29
June 1971

# SAFETY EVALUATION OF EMULSIFIED FUELS

Final Report

Dynamic Science Report 9130-71-3

By

L. Maurice Shaw

Prepared by

Dynamic Science (The AvSER Facility)
A Division of Marshall Industries
Phoenix, Arizona

for

EUSTIS DIRECTORATE
U. S. ARMY AIR MOBILITY RESEARCH AND DEVELOPMENT LABORATORY
FORT EUSTIS, VIRGINIA

Approved for public release;
distribution unlimited.

## ABSTRACT

A comprehensive test program was conducted to establish emulsified fuel screening test procedures, to obtain safety evaluation criteria, and to evaluate the safety performance of emulsified and gelled aviation fuels in a simulated full-scale crash environment. A series of screening tests was formulated and conducted to obtain fuel characteristics as a function of hot-surface ignition, wind shear, and impact dynamics associated with fuel breakup, atomization/dispersion, and ignition. The data obtained from these screening tests were used to establish emulsified fuel safety evaluation criteria. A simulated full-scale experiment was designed to simulate the full-scale helicopter crash environment adequately and, in addition, to be reproducibly controllable at minimal cost.

The screening tests revealed that, for the emulsified fuels tested, safety was directly dependent upon the fuel yield stress and its internal phase base fuel. The screening test data followed the expected trends within the data scatter associated with the type of tests conducted. A safety evaluation criterion was established in terms of an ignition susceptibility parameter which was shown to be related to an empirical equation containing fuel properties. The data obtained from the simulated full-scale tests provided definition of a nonhazardous limiting value for the ignition susceptibility parameter. This allowed the screening test results to become meaningful in predicting the performance of emulsified fuels under actual crash conditions. Further, tests were performed on gelled fuels to offer a comparison between the safety of emulsified and gelled fuels.

Three of the emulsified fuels tested were found to result in a nonhazardous postcrash fire: (1) EF8R-104H emulsion, (2) EF8R-104 emulsion, and (3) Jet-A EXP-4 emulsion. The gelled fuels did not perform as well as the emulsified fuels; however, one gel, Jet-A gel #1, indicated a sizeable advantage over liquid fuels.

In summary, the results of this program confirmed that aircraft fuel emulsions can be formulated which are nonhazardous within the helicopter survivable crash limit envelope as reproduced during the conduct of this evaluation.

TABLE OF CONTENTS


| | Page |
|---|---|
| ABSTRACT | iii |
| LIST OF ILLUSTRATIONS | vii |
| LIST OF TABLES | xix |
| LIST OF SYMBOLS | xx |
| INTRODUCTION | 1 |
| APPROACH TO THE PROBLEM | 3 |
| ANALYTICAL CONSIDERATIONS | 6 |
| Rheological Considerations | 6 |
| Ignition and Vulnerability | 8 |
| Autoignition | 18 |
| Postcrash Fire Temperature Scaling | 18 |
| TEST METHODOLOGY | 21 |
| Nozzle Shear Tests | 22 |
| Hot-Source Ignition Tests | 23 |
| Wind Shear Tests | 27 |
| Impact Dispersion/Atomization Tests | 35 |
| Simulated Full-Scale Tests | 43 |
| TEST RESULTS | 61 |
| Results of Nozzle Shear Tests | 61 |
| Results of Hot-Surface Ignition Tests | 72 |
| Results of Wind Shear Tests | 79 |
| Results of Impact Dispersion/Atomization Tests | 99 |
| Results of Simulated Full-Scale Tests | 109 |
| TEST CORRELATION AND SAFETY EVALUATION CRITERIA | 130 |
| CONCLUSIONS | 149 |
| RECOMMENDATIONS | 150 |
| LITERATURE CITED | 151 |

TABLE OF CONTENTS (CONTD.)


Page

APPENDIXES

I. WIND SHEAR TEST DATA. . . . . 152

II. IMPACT DISPERSION/ATOMIZATION TEST DATA . . . 159

III. IMPACT IGNITION TEST DATA . . . . . 165

IV. SIMULATED FULL-SCALE TESTS DATA . . . . . 171

DISTRIBUTION . . . . . 174

## LIST OF ILLUSTRATIONS


| Figure | | Page |
|---|---|---|
| 1 | Shear Stress Versus Shear Rate . . . . . | 7 |
| 2 | Shear Stress Versus Shear Rate for Emulsified Fuel. . . . . | 9 |
| 3 | Critical Ignition Energy . . . . . | 10 |
| 4 | Critical Dependence of Ignition Energy on Fuel/Air Ratio for Typical Hydrocarbons. . . . | 11 |
| 5 | Interrelation of Processes Leading to Ignition . . . . . | 12 |
| 6 | Schematic of Emulsified Fuel Impingement Apparatus. . . . . | 23 |
| 7 | Front View of the Impingement Apparatus. . . . | 24 |
| 8 | Close View of the Nozzle Section . . . . . | 24 |
| 9 | Hot-Surface Ignition Apparatus . . . . . | 26 |
| 10 | Wind Shear Tunnel Test Apparatus . . . . . | 28 |
| 11 | Refrigeration Unit for Wind Shear Tunnel Test Apparatus . . . . . | 29 |
| 12 | Wind Tunnel Fuel Supply System . . . . . | 30 |
| 13 | Photographic Layout for Wind Shear Tunnel Test Apparatus . . . . . | 32 |
| 14 | Chromatograph Instrumentation Setup. . . . . | 34 |
| 15 | Fuel Impact/Dispersion Atomization Test Devices. . . . . | 36 |
| 16 | Fuel Piston for Impact/Dispersion Atomization Test Device. . . . . | 37 |
| 17 | Impact Dispersion/Atomization Facility . . . . | 39 |
| 18 | Impact Dispersion/Atomization Apparatus With Impact Area Inclosure . . . . . | 40 |
| 19 | Impact Ignition Configuration. . . . . | 42 |

## LIST OF ILLUSTRATIONS (CONTD.)


| Figure | | Page |
|---|---|---|
| 20 | Overall Test Setup | 44 |
| 21 | Impact Barrier | 45 |
| 22 | Test Fixture and Associated Equipment | 47 |
| 23 | View of Test Fixture From Side That is Next to Barrier on Impact | 48 |
| 24 | Fuel Tank Mount Pivot Arm and Energy-Absorption System | 49 |
| 25 | Fuel Tank and Fuel Tank Bladder | 50 |
| 26 | Tank Fabrication (Vacuum Formed Sandwich Construction) | 51 |
| 27 | Calorimeter Design | 53 |
| 28 | Fuel Temperature Regulation Assembly | 55 |
| 29 | Fuel Temperature Regulation Systems | 56 |
| 30 | On-Board (Engine Simulator) Igniter Configuration | 57 |
| 31 | On-Board (Engine Simulator) Igniter Assembly | 58 |
| 32 | On-Board Ignition Source Sequence | 59 |
| 33 | JP-4 Spray Atomization at Various Flow Velocities | 62 |
| 34 | JP-8 Spray Atomization at Various Flow Velocities | 63 |
| 35 | EF4R-104 Spray Atomization at Various Flow Velocities | 64 |
| 36 | EF4R-104H Spray Atomization at Various Flow Velocities | 65 |
| 37 | EF8-104H Spray Atomization at Various Flow Velocities | 66 |

## LIST OF ILLUSTRATIONS (CONTD.)


| Figure | | Page |
|---|---|---|
| 38 | Variation of Ligament and Droplet Characteristic Dimension for Different Fuel Impinging Velocities . . . . . | 68 |
| 39 | Ignition Susceptibility Parameter Versus Nozzle Shear Fuel Velocity for JP-4 Base Emulsion EF4R-104 ($\tau_y$ = 900 Dynes/cm$^2$) . . . . | 69 |
| 40 | Ignition Susceptibility Parameter Versus Nozzle Shear Fuel Velocity for JP-4 Base Emulsion EF4R-104H ($\tau_y$ = 1570 Dynes/cm$^2$) . . . | 70 |
| 41 | Ignition Susceptibility Parameter Based on JP-8 Versus Nozzle Shear Fuel Velocity for JP-8 Base Emulsion EF8-104H ($\tau_y$ = 800 Dynes/cm$^2$) . . . . . | 71 |
| 42 | Autoignition Characteristics for Liquid JP-4 Fuel. . . . . | 73 |
| 43 | Autoignition Characteristics for JP-4 Base Emulsion EF4R-104 ($\tau_y$ = 509 Dynes/cm$^2$) . . . . | 74 |
| 44 | Autoignition Characteristics for JP-4 Base Emulsion EF4R-104H ($\tau_y$ = 1153 Dynes/cm$^2$) . . . | 76 |
| 45 | Autoignition Characteristics for Liquid JP-8 Fuel. . . . . | 77 |
| 46 | Autoignition Characteristics for JP-8 Base Emulsion EF8-104H ($\tau_y$ = 750 Dynes/cm$^2$) . . . . | 78 |
| 47 | JP-4 Wind Shear Breakup, Wind Velocity = 40 fps . . . . . | 81 |
| 48 | JP-4 Wind Shear Breakup, Wind Velocity = 80 fps . . . . . | 81 |
| 49 | JP-4 Wind Shear/Fuel Flow Field, Wind Velocity = 40 fps. . . . . | 82 |
| 50 | JP-4 Wind Shear/Fuel Flow Field, Wind Velocity = 80 fps. . . . . | 82 |
| 51 | EF4R-104 Wind Shear Breakup, Wind Velocity = 40 fps ($\tau_y$ = 475 Dynes/cm$^2$). . . . . | 83 |

## LIST OF ILLUSTRATIONS (CONTD.)


| Figure | | Page |
|---|---|---|
| 52 | EF4R-104 Wind Shear Breakup, Wind Velocity = 50 fps ($\tau_y$ = 475 Dynes/cm$^2$) | 83 |
| 53 | EF4R-104 Wind Shear Breakup, Wind Velocity = 60 fps ($\tau_y$ = 475 Dynes/cm$^2$) | 84 |
| 54 | EF4R-104 Wind Shear Breakup, Wind Velocity = 70 fps ($\tau_y$ = 475 Dynes/cm$^2$) | 84 |
| 55 | EF4R-104 Wind Shear Breakup, Wind Velocity = 100 fps ($\tau_y$ = 400 Dynes/cm$^2$) | 85 |
| 56 | EF4R-104 Wind Shear/Fuel Flow Field, Wind Velocity = 60 fps ($\tau_y$ = 600 Dynes/cm$^2$) | 85 |
| 57 | EF4R-104 Wind Shear/Fuel Flow Field, Wind Velocity = 100 fps ($\tau_y$ = 600 Dynes/cm$^2$) | 86 |
| 58 | EF4R-104 Wind Shear/Fuel Flow Field, Wind Velocity = 60 fps ($\tau_y$ = 1200 Dynes/cm$^2$) | 86 |
| 59 | EF4R-104 Wind Shear/Fuel Flow Field, Wind Velocity = 80 fps ($\tau_y$ = 1300 Dynes/cm$^2$) | 87 |
| 60 | EF4R-104 Wind Shear/Fuel Flow Field, Wind Velocity = 100 fps ($\tau_y$ = 1050 Dynes/cm$^2$) | 87 |
| 61 | EF4R-104 Wind Shear/Fuel Flow Field, Wind Velocity = 50 fps ($\tau_y$ = 1733 Dynes/cm$^2$) | 88 |
| 62 | EF4R-104H Wind Shear/Fuel Flow Field, Wind Velocity = 60 fps ($\tau_y$ = 1733 Dynes/cm$^2$) | 88 |
| 63 | EF4R-104H Wind Shear/Fuel Flow Field, Wind Velocity = 70 fps ($\tau_y$ = 1733 Dynes/cm$^2$) | 89 |
| 64 | EF4R-104 Wind Shear/Fuel Flow Field, Wind Velocity = 80 fps ($\tau_y$ = 1733 Dynes/cm$^2$) | 89 |
| 65 | EF4R-104 Wind Shear/Fuel Flow Field, Wind Velocity = 90 fps ($\tau_y$ = 1733 Dynes/cm$^2$) | 90 |
| 66 | EF4R-104H Wind Shear/Fuel Flow Field, Wind Velocity = 100 fps ($\tau_y$ = 1733 Dynes/cm$^2$) | 90 |

LIST OF ILLUSTRATIONS (CONTD.)


| Figure | | Page |
|---|---|---|
| 67 | EF4R-104H Wind Shear/Fuel Flow Field, Wind Velocity = 120 fps ($\tau_y$ = 1733 Dynes/cm$^2$) . . . | 91 |
| 68 | EF4R-104H Wind Shear/Fuel Flow Field, Wind Velocity = 60 fps ($\tau_y$ = 2470 Dynes/cm$^2$). . . . | 91 |
| 69 | EF4R-104 Wind Shear/Fuel Flow Field, Wind Velocity = 80 fps ($\tau_y$ = 2470 Dynes/cm$^2$). . . . | 92 |
| 70 | EF4R-104H Wind Shear/Fuel Flow Field, Wind Velocity = 100 fps ($\tau_y$ = 2470 Dynes/cm$^2$) . . . | 92 |
| 71 | Ignition Susceptibility Parameter Versus Wind Shear Velocity for JP-4 Base Emulsion EF4R-104 ($\tau_y$ = 437 Dynes/cm$^2$) . . . . . | 94 |
| 72 | Ignition Susceptibility Paramater Versus Wind Shear Velocity for JP-4 Base Emulsion EF4R-104 ($\tau_y$ = 645 Dynes/cm$^2$) . . . . . | 95 |
| 73 | Ignition Susceptibility Parameter Versus Wind Shear Velocity for JP-4 Base Emulsion EF4R-104 ($\tau_y$ = 1400 Dynes/cm$^2$). . . . . | 97 |
| 74 | Ignition Susceptibility Parameter Versus Wind Shear Velocity for JP-4 Base Emulsion EF4R-104H ($\tau_y$ = 1192 Dynes/cm$^2$ and 1886 Dynes/cm$^2$). . . . . | 98 |
| 75 | Ignition Susceptibility Parameter Versus Wind Shear Velocity for JP-8 Liquid Fuel and JP-8 Base Emulsion EF8-104H ($\tau_y$ = 1000 Dynes/cm$^2$). . . . . | 100 |
| 76 | Ignition Susceptibility Parameter Based on JP-8 Versus Wind Shear Velocity for JP-8 Base Emulsion EF8-104H ($\tau_y$ = 1000 Dynes/cm$^2$) . | 101 |
| 77 | Ignition Susceptibility Parameter Versus Impact Kinetic Velocity for JP-4 Base Emulsion EF4R-104 ($\tau_y$ = 508 Dynes/cm$^2$) . . . . | 103 |
| 78 | Ignition Susceptibility Parameter Versus Impact Kinetic Velocity for JP-4 Base Emulsion EF4R-104H ($\tau_y$ = 1143 Dynes/cm$^2$) . . . | 105 |

## LIST OF ILLUSTRATIONS (CONTD.)


| Figure | | Page |
|---|---|---|
| 79 | Ignition Susceptibility Parameter Versus Impact Kinetic Velocity for Liquid JP-8 | 106 |
| 80 | Ignition Susceptibility Parameter Versus Impact Kinetic Velocity for JP-8 Base Emulsion EF8-104H ($\tau_y$ = 755 Dynes/cm$^2$) . . . . | 106 |
| 81 | Ignition Susceptibility Parameter Based on Liquid JP-8 Versus Impact Kinetic Velocity for JP-8 Base Emulsion EF8-104H ($\tau_y$ = 755 Dynes/cm$^2$) . . . . . | 107 |
| 82 | Ignition Rating Value Versus Ignition Susceptibility Parameter Obtained From Impact Ignition Tests . . . . . | 110 |
| 83 | Maximum Temperature Data Obtained From Open-Flame Igniter Tests . . . . . | 111 |
| 84 | Maximum Temperature Data Obtained From Open-Flame Igniter Tests | 112 |
| 85 | Average Maximum Temperature Data Obtained From Spark and Hot-Surface Igniter Tests (Shaded Area Denotes Temperature Envelope) . . | 116 |
| 86 | Average Maximum Temperature Data Obtained From Spark and Hot-Surface Igniter Tests (Shaded Area Denotes Temperature Envelope) . . | 117 |
| 87 | Average Maximum Temperature Data Obtained From Spark and Hot-Surface Igniter Tests (Shaded Area Denotes Temperature Envelope) . . | 118 |
| 88 | Average Maximum Temperature Data Obtained From Spark and Hot-Surface Igniter Tests (Shaded Area Denotes Temperature Envelope) . . | 123 |
| 89 | Average Maximum Temperature Data Obtained From Spark and Hot-Surface Igniter Tests (Shaded Area Denotes Temperature Envelope) . . | 124 |
| 90 | Average Maximum Temperature Data Obtained From Spark and Hot-Surface Igniter Tests (Shaded Area Denotes Temperature Envelope) . . | 125 |

LIST OF ILLUSTRATIONS (CONTD.)


| Figure | | Page |
|---|---|---|
| 91 | Maximum Temperature Data Obtained From On-Board Igniter Test on the Jet-A Gel #2 . . . . . | 126 |
| 92 | Yield Stress Versus K for Wind Shear Data. . . | 131 |
| 93 | Yield Stress Versus $V_j$ for Wind Shear Data . . | 132 |
| 94 | Yield Stress Versus K for Impact Dispersion/Atomization Data. . . . . | 133 |
| 95 | Yield Stress Versus $V_i$ for Impact Dispersion/Atomization Data. . . . . | 134 |
| 96 | Simulated Full-Scale Test Results for the Open-Flame and Spark/Hot-Surface Igniter Tests. . . . . | 137 |
| 97 | Simulated Full-Scale Test Results for the On-Board (Engine Simulator) Igniter Tests. . . | 138 |
| 98 | Simulated Full-Scale Test Results for the Gelled Fuel Tests. . . . . | 143 |
| 99 | Ignition Susceptibility Parameter Versus Time for Test Temperature to Reach 400°F for the Open-Flame and Spark/Hot-Surface Igniter Tests. . . . . | 144 |
| 100 | Ignition Susceptibility Parameter Versus Time for Test Temperature to Reach 400°F for On-Board (Engine Simulator) Igniter Tests. . . . . | 146 |
| 101 | Ignition Susceptibility Parameter Versus Extrapolated Time to Reach Aluminum Melting Temperature for Open-Flame and Spark/Hot-Surface Igniter Tests. . . . . | 147 |
| 102 | Ignition Susceptibility Parameter Versus Extrapolated Time to Reach Aluminum Melting Temperature for On-Board (Engine Simulator) Igniter Tests . . . . . | 148 |

## LIST OF TABLES


| Table | | Page |
|---|---|---|
| I | Wind Shear Safety Performance . . . . . | 136 |
| II | Impact Dispersion/Atomization Safety Performance . . . . . | 136 |
| III | Simulated Postcrash Fire Results. . . . . | 141 |
| IV | Wind Shear Test Conditions and Associated Data. . . . . | 152 |
| V | Impact Dispersion/Atomization Test Conditions and Associated Data. . . . . | 159 |
| VI | Impact Ignition Test Conditions and Associated Data . . . . . | 165 |
| VII | Simulated Full-Scale Test Conditions and Associated Data . . . . . | 171 |

## LIST OF SYMBOLS

| | |
|---|---|
| A | Airstream cross-sectional area (wind tunnel cross-sectional area), Equation 14; constant related to activation energy, Equation 25; constant, Equation 30. |
| $A_n$ | Fuel droplet surface area |
| $\dot{A}_n$ | Total fuel surface area formation rate |
| $A_s$ | Total exposed area of fuel |
| B | Constant, Equation 30 |
| $C_p$ | Specific heat |
| F/A | Fuel-to-air ratio |
| K | Fluid consistency |
| $K_1$ | Windshear-fuel relationship constant |
| $K_2$ | Fuel-impact relationship constant |
| $K_E$ | Kinetic energy |
| Q | Constant related to diffusion rate and vapor pressure |
| T | Spontaneous ignition temperature |
| $T_i$ | Calorimeter temperature at maximum heating rate |
| $T_o$ | Ambient or initial temperature |
| $T_{skin}$ | Aircraft skin temperature |
| V | Impact velocity |
| $V_{air}$ | Air velocity |
| $\dot{V}_F$ | Total volume rate of flow of fuel |
| $V_i$ | Fuel-impact velocity constant |
| $V_j$ | Fuel-wind shear velocity constant |
| $V_n$ | Droplet volume |
| $\dot{W}_F$ | Fuel flow rate |

## LIST OF SYMBOLS (CONTD.)

| | |
|---|---|
| $d$ | Droplet diameter |
| $h$ | Gas film coefficient |
| $k$ | Ignition delay constant |
| $n$ | Degree of non-Newtonian behavior, Equation 2; carbon subscript, Equation 5 |
| $\dot{n}$ | Fuel droplet formation rate |
| $\dot{q}$ | Heating rate |
| $t$ | Time |
| $t_i$ | Time between initial impact and time to reach maximum heating rate |
| $t_n$ | Ignition lag time at an infinite spontaneous ignition temperature |
| $x$ | Formation distance |
| $\dot{\gamma}$ | Shear rate |
| $\varepsilon$ | Surface emittance |
| $\theta$ | Impact angle, Equation 20; aircraft skin thickness, Equation 29 |
| $\theta_i$ | Impact angle |
| $\mu$ | Viscosity |
| $\mu_\alpha$ | Apparent viscosity |
| $\mu_\rho$ | Plastic viscosity |
| $\mu_\infty$ | Viscosity at infinite shear rate |
| $\rho$ | Aircraft skin density |
| $\rho_F$ | Fuel density of $\rho_{Fuel}$ |
| $\sigma$ | Stefan-Boltzmann constant |
| $\tau$ | Shear stress |

## LIST OF SYMBOLS (CONTD.)

| | |
|---|---|
| $\tau_y$ | Yield stress or $\tau_{yield}$ |
| $\psi$ | Ignition susceptibility parameter |

## INTRODUCTION

A significant number of injuries and fatalities that occur in light aircraft accidents are a result of postcrash fire, because the aviation fuels presently being used are readily dispersed, atomized, and ignited, resulting in extensive fire envelopes over damaged aircraft. Various approaches to this problem are being investigated. Included are:

- Component/system improvements to upgrade the functional performance of all flammable fluids systems in the crash environment.

- Inerting systems that sense the imminence of a crash, then actuate integral devices to prevent ignition of postcrash fires by curtailing the fuel supply, de-energizing the host of potential electrical ignition sources, cooling hot surfaces, and/or releasing agents which will make the ambient environment incapable of supporting combustion.

- Fuels technology research devoted to identification of fuels that possess properties less conducive to crash fire ignition and propagation.

This report details an extensive effort that was made in the fuels technology area.

A recognized method for decreasing postcrash fire casualty rates is to decrease the susceptibility of aircraft fuel to disperse and atomize. This can be achieved by the use of thickened fuels such as emulsified or gelled fuels. The thixotropic nature of emulsified fuels embodies a decreased tendency to flow after crash-induced fuel system failures. The viscous nature of gelled fuels also tends to decrease flow after crash-induced fuel system failures. For these types of fuel, less fuel is released for burning. Also, fire propagation is retarded through the resistance of the emulsified and gelled fuels to break up and atomize during exposure to shearing forces such as wind shear and surface impact.

Various fuel emulsions and gels have been formulated and manufactured that possess the basic viscous properties desired. Outwardly, these fuels all possess desirable traits from a fire retardation standpoint. Research over the past several years in modifying liquid fuels has proven the feasibility of manufacturing fuels without degrading their combustion efficiency in operating turbine engines.

Before any modified fuel can be designated as a safe fuel for aircraft, it is necessary to identify the individual combustibility characteristics. This will facilitate selection of optimum candidate fuels that are worthy of consideration and further refinement.

A good way to accomplish this goal is to establish a set of rules, i.e., criteria, which, when applied equally to any modified fuel, will assess its safety performance. Such criteria must evolve from both laboratory and full-scale testing under conditions that closely simulate the actual crash environment in a realistic and repeatable manner.

The purpose of the test program reported herein was to devise emulsified fuel screening test procedures, establish fuel safety evaluation criteria, and conduct a comprehensive, simulated full-scale, fuel tank impact test effort to define emulsified fuel performance in a helicopter crash environment. Simulated full-scale tests were also performed for two gelled fuels. The program entailed design and construction of laboratory facilities which were then utilized to test and study emulsified fuels under simulated crash environments. These tests involved fundamentals tests resulting in basic fuel characteristic data which were used primarily to guide the performance of simulated postcrash environmental testing. The fuel fundamentals tests consisted of (1) nozzle shear tests to help define the breakup of emulsified fuels as a function of input kinetic energy and (2) hot-surface ignition tests to define the ignition characteristics of the fuels. The postcrash environmental tests consisted of wind shear tests to simulate fuel spillage from a moving, crashed aircraft and impact dispersion/atomization tests to simulate fuel impact on surrounding surfaces in a crash environment.

Full-scale tests are desirable to define the crash environment effects on the dispersion and ignition of a fuel and to determine a postcrash fire hazard limit associated with the above screening test results. Unfortunately, it is probably financially prohibitive to test enough cases to adequately cover the range of test variables. Therefore, tests were designed to simulate the actual full-scale crash environments which a helicopter fuel tank experiences during a crash impact. These tests were conducted at a large enough scale to adequately represent the full-scale crash environment and still provide an economical test program.

This report describes the test methodology used for the program and presents the results obtained therefrom. Analytical considerations, the test results, and the resultant safety evaluation criteria are presented herein. Recommendations and areas requiring further research are also discussed.

## APPROACH TO THE PROBLEM

The actual safety that a particular fuel displays can best be determined by full-scale crash testing. However, with the advent of many different fuel compositions and flammability characteristics, the amount of full-scale testing to determine safety criteria covering all such fuels is economically prohibitive. If a scaled-down or screening test program can be formulated to obtain safety criteria involving the basic fuel characteristics, the ability to screen out undesirable fuels (from a fire-hazard standpoint) can be obtained inexpensively. Although the results of such testing may not offer the actual ability for a fuel to be designated "safe" in a postcrash environment, such results will determine the fuel formulas and characteristics which perform in the most optimum manner. With these safer (from a screening criterion standpoint) fuels, fewer scaled-up tests can be performed with a great decrease in the funding involved.

Some fuels will perform better than others in the postcrash environment. Therefore, the purpose of screening tests is to eliminate potentially hazardous fuels from further investigation.

To study screening test procedures and obtain safety criteria for investigating emulsified fuels, a systematic step-by-step program was formulated to study the emulsified fuel characteristics under simulated postcrash fire environments. The results of the screening tests were then used to determine safety criteria to measure the performance of emulsified fuels.

Although the screening test results offer an approach to determining a safety evaluation parameter for emulsified fuels, the actual value of such a safety parameter which represents a safe limit must be determined from full-scale or simulated full-scale environmental tests. With the determination of this safety limit, further screening tests can be related to the full-scale crash condition.

As with any criteria, a baseline must be determined. The obvious choice was to use the performance of a standard presently used fuel. JP-4 was selected because of its extensive use in Army aircraft. The existence of extensive postcrash fire data on aircraft which use JP-4 was also considered in this selection.

The overall program involved the conduct of three different test series: (1) fuel fundamentals testing, (2) fuel environmental testing, and (3) simulated full-scale testing. The fuel fundamentals tests were designed as an inexpensive method of

determining basic fuel characteristic data to guide the design and testing of the fuel environmental tests. The fuel environmental tests offered the development of safety performance criteria which could be finalized and verified by the simulated full-scale testing.

The fuel fundamentals tests were not designed to yield a direct method for determining fuel safety criteria, but were utilized to help correlate the results of fuel environmental tests. Two types of fuel fundamentals tests were conducted: (1) nozzle shear tests and (2) hot-surface ignition tests. The nozzle shear tests provided basic emulsified fuel breakup data as a function of the kinetic energy imparted to the fuel. The hot-source ignition tests were conducted to measure the ignition susceptibility of the fuels in contact with hot surfaces as they might be exposed during the postcrash environment. The test configurations, procedures, and results are discussed in detail later in this report.

The mechanics involved in producing combustible mixtures of fuel during a crash environment can be classified into two areas: (1) wind shear during fuel tank spillage and (2) fuel impact with surrounding environment. Accordingly, two types of fuel environmental tests were designed and performed: (1) wind shear tests and (2) impact dispersion/atomization tests. The wind shear tests were designed to simulate overboard spillage and, therefore, to show the effects of wind shear energies imparted to the fuel escaping from ruptured fuel lines and tanks during the deformation of a crashing aircraft. The impact dispersion/atomization tests were designed to simulate the fuel impact with surrounding crash surfaces and the associated fuel dispersion and atomization.

With JP-4 as a standard baseline fuel, the comparison of the test results obtained from modified fuels provides guidelines on which safety evaluation criteria can be based. Here we assume the JP-4 test results to be a maximum hazardous condition.

Previously established knowledge of screening test values of a safety performance parameter provides the means to determine a fire hazard limit based on the simulated full-scale test results. By using the full-scale data to correlate the results of the screening tests, evaluative criteria can be formulated that will qualitatively and accurately assess the safety performance of a given fuel. Thus, the desired objective of relating the screening test results to a full-scale crash situation can be accomplished.

Simulated full-scale crash tests can be effectively scaled-up to the full-scale situation, provided attention is given to detailed simulation of the crash environment physics. This not only reduces costs but allows a suitably controlled evaluation. To simulate the full-scale crash environment, several conditions must be met: (1) testing at a sufficiently large scale to simulate the full-scale impact, dispersion, ignition, and resulting fire environment; (2) conducting tests with impact energy conditions which approximate the maximum crash survival impact limit; (3) reproducing ignition sources that simulate all potential ignition sources in a full-scale environment such as electrical sparks, friction sparks, hot metal surfaces, engine flaming, and residual flame sources such as those propagating from oil spillage, etc.; and (4) testing fuel tank structures that correspond to the full-scale fuel tank configuration.

The basic test procedure for the simulated full-scale tests was to impact simulated helicopter fuel tanks, filled with various fuels, onto a barrier which simulates terrain corresponding to a full-scale impact environment. The fuel tanks, each containing 13 gallons of fuel, were mounted on a sled fixture and accelerated into the barrier. Each fuel tank was constructed to simulate the tank structure of a typical U. S. Army helicopter. A 65-ft/sec impact velocity with a 45-degree impact was used in each test. Three types of igniters were used to reproduce full-scale ignition sources: open-flame igniters, spark igniters, and hot-surface igniters.

## ANALYTICAL CONSIDERATIONS

Accurate analytical solutions for the characteristics and combustion processes involved for fuels in a postcrash environment are difficult to model for a liquid (or Newtonian fluid) fuel and become prohibitive for the fuel properties characteristic of emulsified fuels. However, basic analytical approaches exist which can be used to understand modified fuel characteristics and to enhance their data reduction and correlation when applied to the postcrash environment. Several such analytical considerations discussed in this section are characteristic of all postcrash environments.

### RHEOLOGICAL CONSIDERATIONS

Solidified fuels, such as emulsified or gelled fuels, fall under a non-Newtonian fluid classification. Several analytical models have been classified as the result of current and past investigations[1,2,3,4]. Three of these classifications are the Bingham plastics, pseudo-plastics, and real plastics (see Figure 1). Each of these is a departure from the Newtonian fluid in that the shear stress can no longer be related to shear rate as

$$\tau = \mu\dot{\gamma}$$

where $\tau$ is shear stress, $\mu$ the viscosity of the fluid, and $\dot{\gamma}$ the shear rate.

Bingham Plastics have the characteristic that a yield stress must be overcome before the fluid can flow. Once the yield stress is exceeded, the material structure disintegrates and behaves as a Newtonian fluid. The relationship between shear stress and shear rate then takes on the following form:

$$\tau - \tau_{yield} = \mu_p\dot{\gamma} \qquad (1)$$

where $\mu_p$ is the plastic viscosity or coefficient of rigidity. Materials composed of micro-visible particles and liquid droplets suspended in a liquid medium contain these characteristics.

Fluid structures such as gels, fluids with suspensions of asymmetric particles, or solutions of high polymers can be generally classed as pseudo-plastics. This viscoelastic fluid model assumes no yield stress value as in Bingham plastics, but the apparent viscosity, $\mu_a$, decreases progressively with an increase in shear rate. The value of $\mu_a$ approaches linearity and becomes $\mu_\infty$ as an infinite shear

1. BINGHAM FLUID (IDEAL PLASTIC)
2. TYPICAL EMULSIFIED FUEL (REAL PLASTIC)
3. PSEUDO-PLASTIC
4. NEWTONIAN FLUID

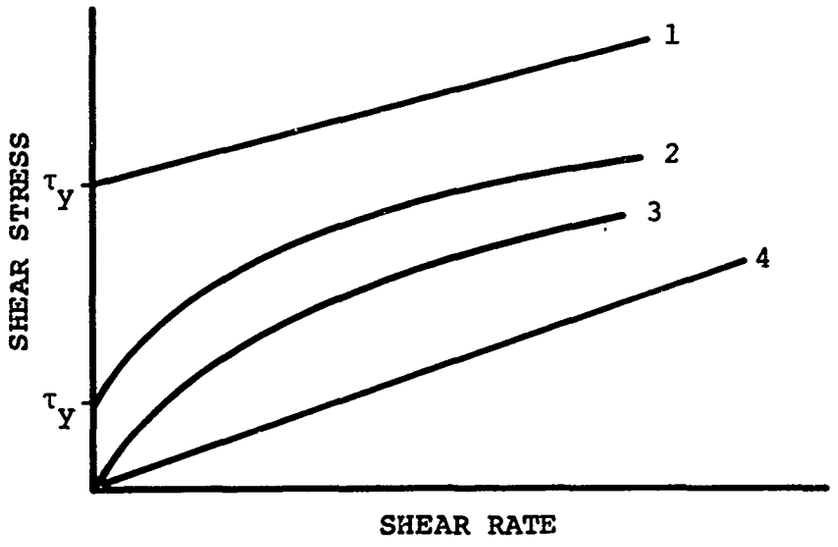


Figure 1. Shear Stress Versus Shear Rate.

rate is approached. The relationship between the shear stress and shear rate is generally taken as

$$\tau = K\dot{\gamma}^n, \quad (n < 1) \tag{2}$$

where K and n are constants and are the respective measures of the consistency of the fluid and the degree of non-Newtonian behavior of the fluid.

Emulsified fuels studied during this program are known to exhibit traits which compare to a Bingham fluid model for low shear rate values in that they possess a yield stress and are thixotropic. However, the shape of the shear stress versus shear rate curve (Figure 1), once the yield stress is overcome, compares with that of a pseudo-plastic fluid model. The resulting curve is like that associated with real plastic

fluid models. It follows, then, that the relacionship between shear stress and shear rate can be empirically formulated as

$$\tau - \tau_{yield} = K\dot{\gamma}^{n}, \quad (n < 1) \tag{3}$$

where, if $\tau_{yield}$ approaches zero, the shear characteristics approach a pseudo-plastic.

Although other empirical relations have been generated for non-Newtonian models, these illustrate the general form and expected tendencies for such materials.

From data obtained from "capillary" tube viscometer studies,[5] it is known that emulsified fuels follow a Bingham fluid model for shear stresses below some critical value. Above the critical shear stress, the shear rate increases substantially, finally becoming nearly linear with shear stress (see Figure 2). This behavior can be modeled initially by a Bingham fluid which, on reaching a critical shear stress, reverts to a Newtonian fluid or possibly a pseudo-plastic fluid. U. S. Army Fuels and Lubricants Research Laboratory researchers* have determined in preliminary analyses that this critical shear stress decreases with increasing yield stress, introducing the possibility that high yield-stress emulsified fuel would be less stable. The amount of energy necessary to break up an emulsified fuel should be a function of the difference between the critical yield stresses. Therefore, if the yield stress of the emulsion is increased and, in turn, the critical stress is decreased, then the energy required to break up the emulsion is decreased. U. S. Army Fuels and Lubricants Research Laboratory researchers felt that this type of phenomenon may be a function of the fact that the fuel globular diameter decreases with increased yield stress. As an emulsion is worked, the globular diameter decreases, increasing the fuel surface area. As this process continues, an inadequate amount of water to form a water matrix results. The breakdown in the matrix then accounts for the existence of the critical stress.

## IGNITION AND VULNERABILITY

The actual safety a fuel displays in a crash environment is dependent on the ability of that fuel to not form combustible fuel-to-air mixtures in the vapor phase. Ignition will not occur unless certain fuel/air ratios are present, either in the surrounding crash environment or in the tank ullage. However, for fuel-air mixtures within the combustible range, it is possible for safety to exist. This is demonstrated by

*Personal communication

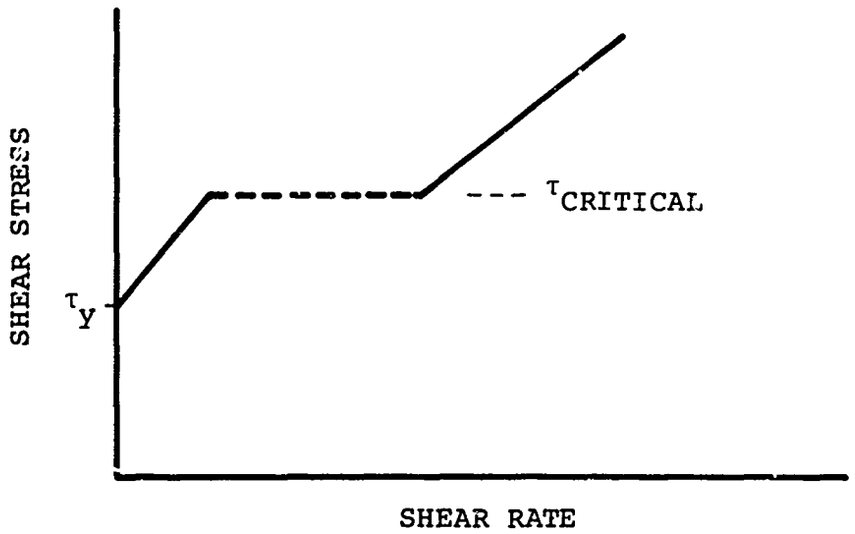


Figure 2. Shear Stress Versus Shear Rate for Emulsified Fuel.

the large increase in energy required for ignition for several hydrocarbon fuels as illustrated in Figure 3.

The fraction of stoichiometry in Figure 3 can be converted to fuel/air weight ratio by the relation

$$F/A = (\text{Fraction}) \frac{(14n + 2)}{(216n + 62)} \tag{4}$$

where n represents the carbon subscript associated with the equation

$$C_n H_{2n} + 2 + (\frac{3n + 1}{2})O_2 + (6n + 2)N_2 = nCO_2 + (n + 1)H_2O + (6n + 2)N_2 \tag{5}$$

As illustrated in Figure 4, the fuel/air ratio terms shown in Figure 3 are more meaningful. Therefore, to prevent post-crash fire, it is necessary that formation of combustible fuel/air ratios does not occur and then, failing this, that insufficient ignition potentials are present.

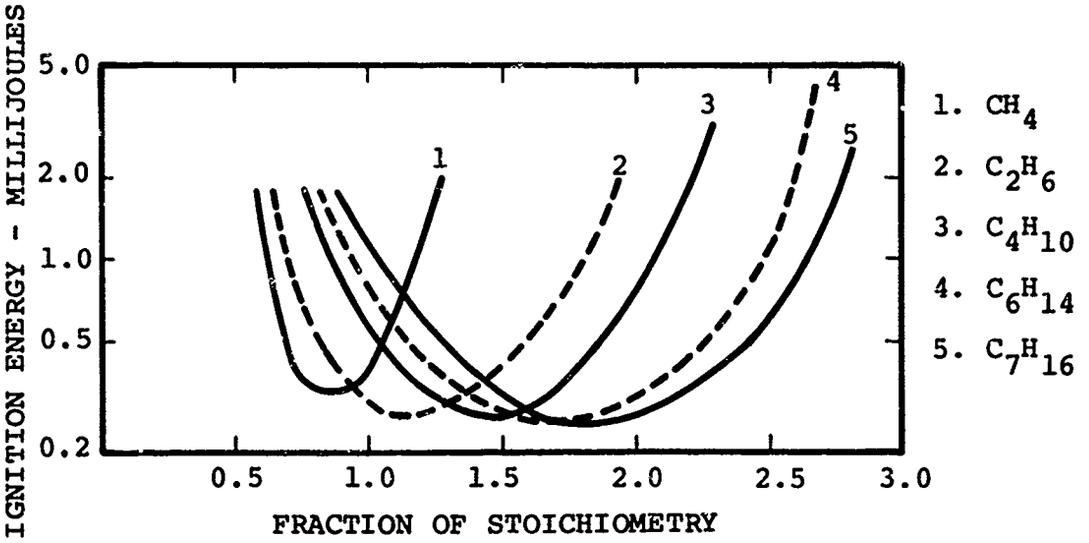


Figure 3. Critical Ignition Energy.

The interaction of properties and events leading up to an ignition hazard are outlined in Figure 5. The governing parameters are fuel properties, crash kinematics, ignition hazards, and ignition sources. Each element of Figure 5 can be characterized by certain physical properties. For example, the fuel properties are characterized by vapor pressure, viscosity ($\mu$), surface tension ($\sigma$), and yield stress ($\tau$). The crash kinematics can be characterized by crash configuration and input kinetic energy to the fuel. Although the statistical nature of a crash causes much difficulty, the fire hazard can be related to fuel properties even if the mechanism for formation of ignitable fuel/air ratios is not understood. If an ignitable fuel/air ratio is not generated, no ignition source can cause a fire hazard. Of special concern is how to determine the generation of fuel/air ignition limits for emulsified fuels. This demands testing to determine the fuel/air formation of emulsified fuels in postcrash environments.

If the formation of ignitable fuel/air ratios can be related to emulsified fuel properties, the fire hazard can be minimized by adopting emulsified fuels whose properties correspond to limited fuel/air ratio formation. Further, the understanding of both fuel/air and dispersion mechanisms will simplify the understanding of ignition sources. An electric or

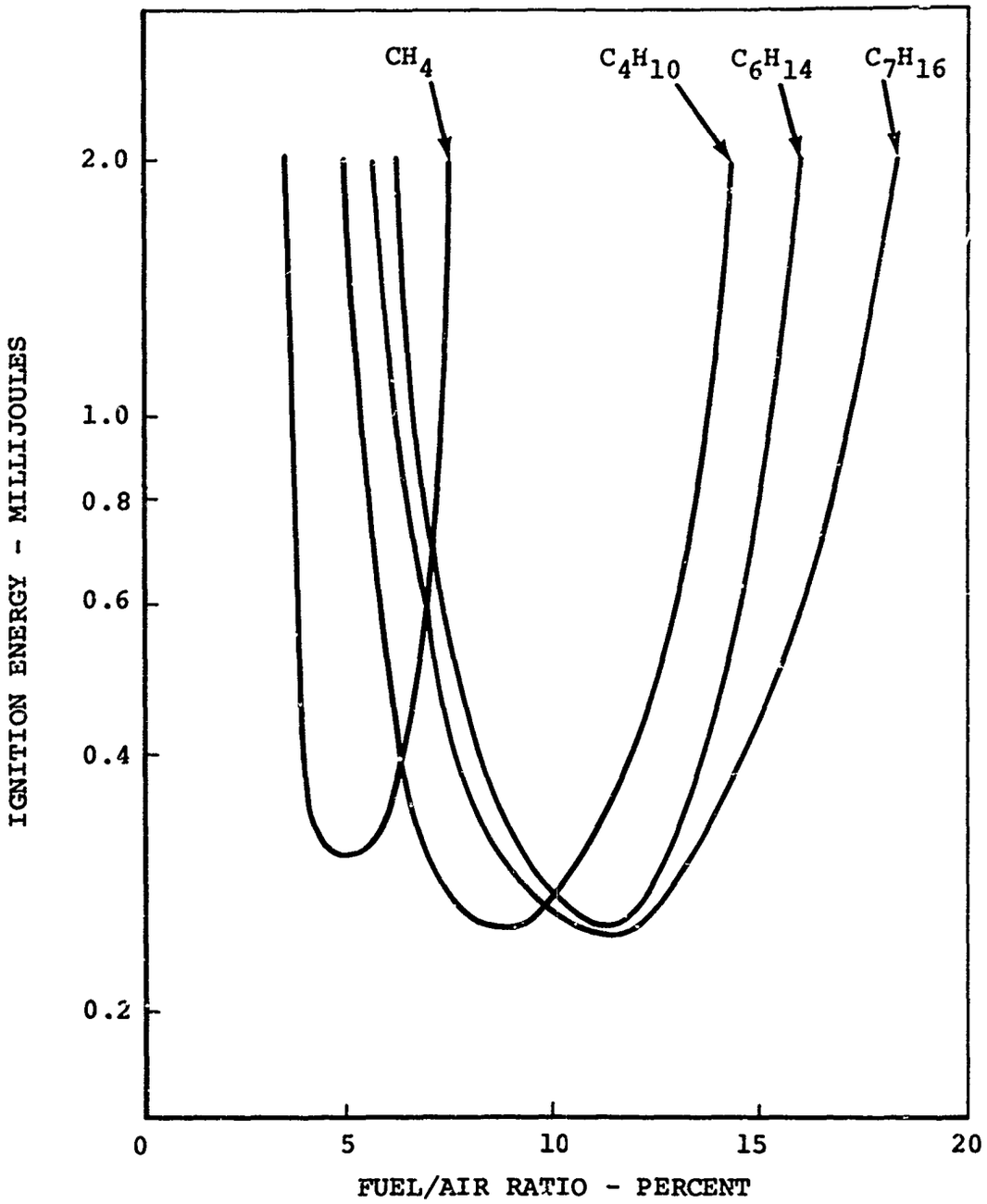


Figure 4. Critical Dependence of Ignition Energy on Fuel/Air Ratio for Typical Hydrocarbons.

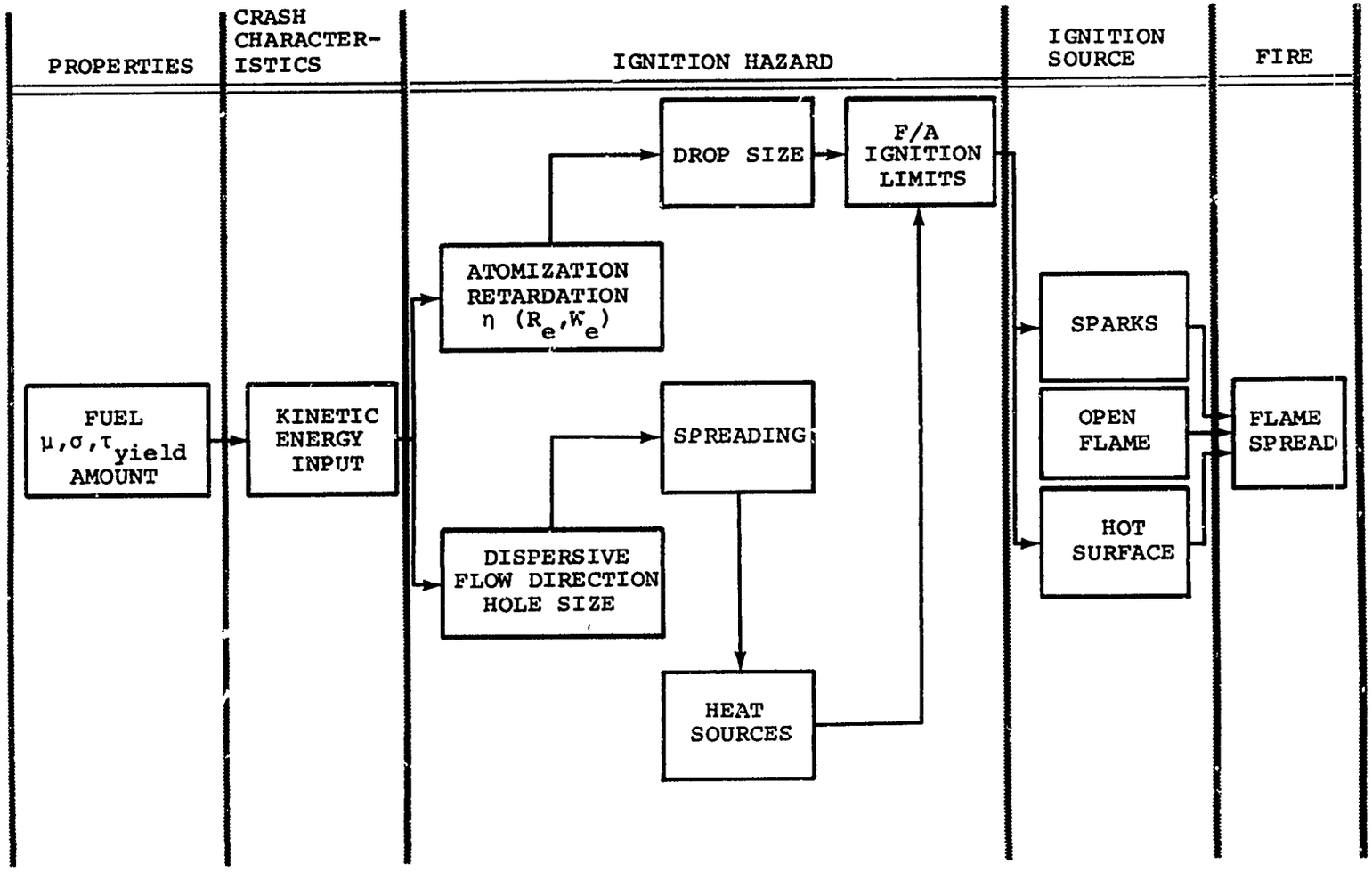


Figure 5. Interrelation of Processes Leading to Ignition.

friction spark may cause fuel/air ignition, while heat sources can create fuel/air ratios which, in turn, can be ignited by spark or hot-surface sources.

The extent of atomization during a crash environment determines the mean fuel droplet size, which determines, in turn, the fuel vaporization rate and thereby governs the formation of fuel/air ignition limits. Basically, the crash environment can be divided into two mechanisms for atomizing and dispersing fuel: (1) atomization due to wind shear (i.e., interaction between spilled fuel and a moving airstream) and (2) fuel impact with the surrounding crash environment.

The relationship between the mean fuel/air ratio and pertinent parameters in a wind shear environment is quite complicated to handle analytically. To simplify the analytical model, several simplifying assumptions must be made and, even with this, some empirical relations through data correlation are required. We first assume that the mean fuel droplets are spherical and that the formation of the droplets occurs at time zero. We further assume that the vapor pressures and diffusion rates do not vary between the fuels being studied. This, of course, is not the case. The results, however, will offer expected trends regarding the formation of fuel/air ratios in a wind shear environment which may be useful for data correlation. One further assumption, which is correct for the wind shear tests presented in this report, is that the fuel flow rate into the airstream is held constant.

The volume of each droplet can be expressed as

$$V_n = 4/3\pi \left(\frac{d}{2}\right)^3 \tag{6}$$

where d is the droplet diameter. The total volume rate of flow issuing into the airstream is then

$$\dot{V}_F = \frac{\dot{W}_F}{\rho_F} = \dot{n}\, V_n \tag{7}$$

where $\dot{W}_F$ and $\rho_F$ are the fuel flow rate and density and $\dot{n}$ is the droplet formation rate. The amount of vaporization and, in turn, the fuel/air ratio of a mixture of fuel droplets and air are a function of the exposed fuel surface area. For one droplet, the surface area is just

$$A_n = 4\pi \left(\frac{d}{2}\right)^2 \tag{8}$$

We can now show that the total surface area formed per second is

$$\dot{A}_F = \dot{n}\, A_n = \frac{3\dot{V}_F}{(\frac{d}{2})} \tag{9}$$

If we assume a time (t) which represents the exposure time in which the flowing air and fuel droplets mix before they reach the ignition source or, in test, the point of measurement, then the total area of fuel exposed can be expressed as

$$A_s = \dot{A}_F t = \frac{3\dot{V}_F t}{(\frac{d}{2})} \tag{10}$$

For large formation distances (x), the exposure time becomes

$$t \approx \frac{x}{V_{air}} \tag{11}$$

where $V_{air}$ is the airstream velocity. Therefore,

$$A_s = \frac{6\dot{V}_F x}{d\, V_{air}} \tag{12}$$

The fuel/air ratio can be expressed as

$$F/A = \frac{\text{Volume of Vaporized Fuel}}{\text{Volume of Air}} \tag{13}$$

The volume of vaporized fuel will be some function of the exposed surface area, while the volume of air will be a function of stream velocity. The fuel/air ratio then becomes

$$F/A = \frac{Q\ As}{A\ V_{air}} = \frac{6Q\ \dot{V}_F x}{Ad\ V_{air}^2} \tag{14}$$

where Q is a constant containing a diffusion rate relation and vapor pressure and A is the airstream cross-sectional area. Due to our initial assumptions and in our wind tunnel tests, Q, $\dot{V}_F$, x, and A are constants related to the test procedures. We can now express fuel/air ratio functionally as

$$F/A = f(\frac{1}{d\ V_{air}^2}) \tag{15}$$

The relationship between fuel/air ratio and $\left(\frac{1}{d\ V_{air}^2}\right)$ can be experimentally determined. However, since we have chosen a baseline fuel for the determination of evaluation criteria, the ratio between the fuel/air ratio of a specific emulsified fuel and the standard fuel (JP-4) for the same wind shear conditions is more appropriate. We can then define a new parameter ($\psi$) which is equated as

$$\psi_{JP-4} = \frac{(F/A)_{Fuel}}{(F/A)_{JP-4}} \tag{16}$$

For the same wind shear conditions ($V_{air}$ constant), we also observe that

$$\psi_{JP-4} = \frac{(F/A)_{Fuel}}{(F/A)_{JP-4}} = \frac{d_{JP-4}}{d_{Fuel}}, \tag{17}$$

which states that the ratio of the measured fuel/air ratios is directly proportional to the inverse ratio of the measured droplet diameters. It must be understood, however, that this relation is only valid if the emulsified fuel's base fuel is JP-4. Similar relationships can be used for other base emulsified fuels as long as the reference fuel is the base fuel for the emulsion.

It has been determined through examination of test data that a relation between $\psi$ and wind shear velocity exists for each emulsified fuel structure tested. This relation takes the form

$$\psi = \exp\left\{-\frac{(V_j - V_{Air})^2}{K_1}\right\},\ V_{Air} \leq V_j \tag{18}$$

where $V_j$ and $K_1$ are constants and are functions of the emulsified fuel yield stress. The term ($V_j$) also represents the lowest airstream velocity in which the emulsified fuel acts or demonstrates the same fuel/air ratio and droplet diameter as its base fuel. The test results illustrating these phenomena are presented in the Test Results section.

For the emulsion formulations studied in this program, the values of $V_j$ and $K_1$ could be expressed as functions of yield stress. This allows the above equation for the wind shear ignition susceptibility parameter to be written as

$$\psi = \exp\left\{ - \left(\sqrt{27.2\ \tau_y} - V_{Air}\right)^2 / (23 + 0.029\ \tau_y)^2 \right\}, \quad V_{Air} \leq \sqrt{27.2\ \tau_y} \tag{19}$$

The extent of the atomization and dispersion of a fuel when impacting surfaces in a crash environment is dependent upon the kinetic energy imparted to the fuel from its interaction with its environment. The generation of an accurate physical combustion/interaction model is difficult, but the mechanisms initiating the atomization and dispersion are relatively simple for uncomplicated surfaces. Here the amount of atomization and dispersion for a given fuel is a direct function of the imparted kinetic energy where

$$K.E. = \frac{1}{2}\rho_{Fuel} V^2_{Fuel} \sin^2\theta \tag{20}$$

and $\theta$ is the impingement angle with the impact surface (which is assumed to be flat). For curved impact surfaces, the $\sin^2\theta$ term must be integrated over the surface.

Considering the formation of ignitable fuel/air ratios, we can assume that fuel/air ratios after impact are generated from two sources. The first is the initial fuel/air ratio formation resulting from atomization of the fuel by the input kinetic energy. Here, similar to the wind shear, the resulting fuel/air ratio can be expressed functionally as

$$(F/A)_{Initial} = f\left(\frac{1}{d}\right) \tag{21}$$

where d, the mean droplet diameter, is a complicated function of the input kinetic energy.

The second source for the formation of fuel/air ratio results from the dispersion of the fuel after impact. Here the fuel/air ratio formation depends on the total surface area of the spilled fuel and the distribution of this exposed area on the impacted surface. Thus,

$$(F/A)_{Secondary} \approx f(A) \tag{22}$$

Of course, the above fuel/air ratios are functions of fuel properties such as yield stress, viscosity, surface tension, vapor pressure, and diffusion rates.

The fuel/air ratios accompanying the nozzle shear tests presented in this report can be expressed only by the first formation process. The impact dispersion/atomization tests must

include both processes. It should be understood that under certain conditions the initial fuel/air ratio could generate combustible mixtures whereas the secondary fuel/air ratio may not. In this situation, ignition might occur but would be self-extinguishing and not propagate a flame. Conversely, it is also possible that the initial fuel/air ratio formation may not generate combustible mixtures, whereas the secondary fuel/air ratio process may form combustible mixtures. In this situation, complete combustion is possible, producing a hazardous situation. Of course, the most hazardous situation results when both mechanisms produce combustible fuel/air ratios. The actual results of these processes are experimentally illustrated in the Test Results section of this report. Although the above discussion is analytically sound, one must not overlook the possibility that combustion of the initial (or mist phase) fuel/air ratio formation heats the distributed spill to aid the production of a combustible mixture. This more closely represents the actual crash environment where "fireballing" of the mist phase usually results in high-energy combustion.

In the impact dispersion/atomization tests conducted for this study, it was possible to measure only an average fuel/air ratio over a specific period of time after impact. As a result, the definition of the above process (as a function of fuel/air ratio) was not possible. It was determined through examination of test data, however, that a relation similar to that observed for wind shear between ($\psi$) and ($V_{Fuel}\ Sin\theta$) exists for each emulsified fuel structure where $\theta$ is the fuel impingement angle. This relation holds between the emulsion and its base fuel as

$$\psi = \exp\left\{ \frac{-(V_i - V_{Fuel}\ Sin\theta)^2}{K_2} \right\}, \quad V_{Fuel}\ Sin\theta \leq V_i \qquad (23)$$

where $V_i$ and $K_2$ are constants which are functions of the emulsified fuel yield stress. As in the wind shear results, $V_i$ also represents the lowest value of $V_{Fuel}\ Sin\theta$ in which the emulsified fuel demonstrates the same fuel/air ratio as its base fuel. Data illustrating these phenomena are also presented in the Test Results section.

For the emulsion formulations studied in this program, the values of $V_i$ and $K_2$ could be equated as functions of yield stress. This allowed the above equation for the impact dispersion/atomization ignition susceptibility parameter to be expressed as

$$\psi = \exp\left\{ - \left(\sqrt{10.63\ (\tau_y - 212)} - V\ \mathrm{Sin}\theta_i\right)^2 / (9.5 - 0.035\ \tau_y)^2 \right\},$$
$$V\ \mathrm{Sin}\theta_i \leq \sqrt{10.63\ (\tau_y - 212)} \quad (24)$$

AUTOIGNITION

In any powered aircraft crash, hot-surface sources that will ignite flammable fuels are always present. These sources can range from hot tailpipes to shorted electrical wires. It is therefore necessary to understand fuel ignition characteristics in order to determine not only the minimum autoignition temperature of the fuel but also the ignition characteristics of a fuel in contact with hot surfaces.

The minimum autoignition temperature as well as the ignition delay times associated with different surface temperatures for a fuel in air, is dependent upon the physical processes of diffusion, mixing with the oxidant, fuel heat conductivity, surface properties, and geometry as well as chemical processes. In aircraft crashes, the air pressure can, in general, be assumed constant at one atmosphere. Most hot surfaces in light Army aircraft are stainless steel.

The dependence of ignition delay time on the surface temperatures has been mathematically represented in Reference 6 as

$$\ln t = A/T + \ln k \quad (25)$$

where t is the ignition delay time, T is the spontaneous ignition temperature, k is a constant, and A is a constant related to the apparent "Activation Energy" of the controlling process.

Based on the test data contained in this report (Test Results section), a modified version of this mathematical relation was found to represent the data more accurately:

$$\ln(t - t_R) = \frac{A}{T} + \ln k \quad (26)$$

where $t_R$ is a constant for a given fuel which can be interpreted as the ignition lag time associated with an infinite spontaneous ignition temperature due to interface heat transfer resistance.

POSTCRASH FIRE TEMPERATURE SCALING

It is advantageous to relate the temperature and heating rate data obtained during the simulated tests to those expected in

an actual full-scale environment. Such an analysis not only allows the extrapolation of the scaled data, but offers an approach to validate the approach used in the design of the simulated tests.

Although the resulting ignition characteristics should be nearly identical between scaled and full-scale conditions, the resulting temperatures reached in the scaled test are limited by the burn time of the fuel and, therefore, by the amount of fuel. The heating rates associated with a scaled-down fire test should be nearly identical to those imposed in a full-scale postcrash fire. This has been shown to be the case for JP-4 fires in the test data presented herein. Thus, the full-scale fire environment should produce maximum heating rates (using JP-4) on the order of 10.5 Btu/ft$^2$ - sec. Approximately 89 percent of this total heating rate is due to radiation and the remainder is due to convection. The JP-4 scaled data gave heating rates on this order of magnitude. This can be expressed as

$$T_{skin} = \frac{\dot{q}\ (t)}{\rho C_p \theta} - T_o \tag{27}$$

where $T_{skin}$ is the aircraft skin temperature, $T_o$ is the initial or ambient temperature, $\rho$ is the skin material density, $C_p$ is the skin material specific heat, $\theta$ is the skin thickness, t is the time to reach a temperature $T_{skin}$, and $\dot{q}$ is the total heating rate. The total heating rate from a fuel fire can be expressed as

$$\dot{q} = \sigma\varepsilon(T_{flame}^4 - T_o^4) + h\Delta T \tag{28}$$

where $\sigma$ is the Stefan-Boltzmann constant, $\varepsilon$ is the surface emittance, h is the hot gas film coefficient, $T_o$ is the ambient or surface temperature, and $\Delta T$ is the temperature difference between gas and surface.

If it is assumed that the heating rates obtained for various fuels in the scaled tests are representative and that an infinite amount of fuel is available for combustion in the full-scale environment, then analytical extrapolation of aircraft skin burn-through time to the full-scale conditions is possible from the test data. It should be apparent that long burn-through times represent a less hazardous condition than short burn-through times. A skin temperature of 1100°F (melting point of aluminum) is chosen as the burn-through temperature. The burn-through time from initial impact can then be calculated as

$$t_{\substack{\text{burn} \\ \text{through}}} = \frac{\rho C_p \theta \ (1100 - T_i)}{\dot{q}_{max}} + t_i \qquad (29)$$

where $\rho$, $C_p$, and $\theta$ are the aluminum skin density, specific heat, and skin thickness, respectively, and $\dot{q}_{max}$ is the maximum heating rate obtained in the scaled test, $T_i$ is the calorimeter temperature corresponding to the point at which $\dot{q}_{max}$ is observed. The term $t_i$ is the time between initial impact and the point at which $\dot{q}_{max}$ was observed.

This analysis is somewhat conservative from a heating standpoint since the actual heating rate decreases as the skin temperature increases; however, it does indicate a maximum condition. The actual heating rate distribution with increasing skin temperature cannot be obtained without knowing the radiation characteristics of the environment. It was found in the test data that the extrapolated burn-through times for JP-4 were on the order of 20 seconds. This value corresponds to fuselage burn-through times of 20 to 35 seconds.[8]

It was found when plotting the extrapolated burn-through time versus the ignition susceptibility parameter for each fuel that a curve fit resulted which could be expressed as

$$t_{\substack{\text{burn} \\ \text{through}}} = A + \exp\ (B/\psi) \qquad (30)$$

where A and B are constants. Although there is no apparent analytical basis for this curve fit, it does portray a trend which would be expected from ignition observations of the tests.

## TEST METHODOLOGY

A comprehensive test effort was conducted to establish emulsified fuel screening test procedures for safety evaluation criteria. This entailed the design and construction of test facilities which were utilized to test emulsified fuels under simulated crash environments to obtain data for defining the safety characteristics of specific fuels.

The mechanics involved in producing combustible mixtures of fuel during a crash environment can be classified into two basic areas: (1) wind shear during fuel tank spillage and (2) fuel impact with the surrounding environment. With these mechanisms and the economics involved in mind, the following sequence of testing was developed:

| | |
|---|---|
| Nozzle Shear Tests<br>Hot Surface Ignition Tests | Fuel Fundamentals Tests |
| Wind Shear Tests<br>Impact Dispersion/ Atomization Tests | Fuel-Crash Environment Tests |

A second, equally comprehensive test effort was conducted to (1) establish a limiting value for the screening test safety parameter and (2) study the performance of emulsified fuels in a full-scale crash environment. This entailed the design and construction of a test facility which was used to test emulsified fuels under a simulated full-scale helicopter crash environment.

The mechanics involved in duplicating and simulating the full-scale crash environment can be classified into three basic areas: (1) duplication of impact kinetics and impact velocity, (2) duplication of tank structural design, and (3) simulation of full-scale ignition sources. With these mechanisms in mind, simulated crash tests were conducted at a velocity equal to the maximum crash-survivable velocity for helicopters using a fuel tank structure corresponding to full-scale helicopter fuel tank design, and ignition sources which represent those possible in a full-scale crash. The various ignition sources used to accomplish the latter item were:

Open flame igniter tests (one test per fuel)

Spark and hot-surface igniter tests (two tests per fuel)

On-board (engine simulator) igniter tests (three tests per fuel)

Descriptions follow of the theories and techniques devised to accomplish the required testing.

## NOZZLE SHEAR TESTS

Nozzle shear tests were designed to enable a quick preliminary study of the flow properties and atomization processes of emulsified aircraft fuels for comparison with liquid aircraft fuels. Further, the nozzle shear test data provided information to enhance the fuel environmental tests. The experimental technique involved photographic observation of the flow region resulting from impinging a fuel stream onto a lucite rod surface.

A schematic of the flow system is shown in Figure 6. It consists of a 1-gallon volume Freon tank and an emulsified fuel tank. Freon was chosen as the "pushing" liquid because of its immiscibility with emulsified fuel. The flow rate of the emulsified fuel was based on the measured volumetric flow rate of the Freon. Pressurization of the Freon tank was controlled by a hand regulator. Different fuel flow rates were easily attained by varying the pressure of the Freon tank. Freon flow rates, which in turn determined the emulsified fuel flow rates, were measured with turbine-type flowmeters. The signals of the flowmeters were fed via amplifiers into a recording oscillograph.

A 2-gallon aluminum cylinder, 8 inches in diameter, was used as the fuel tank. A well-fitted aluminum piston, 3 inches in length, was utilized in the fuel tank as a moving diaphragm to separate the Freon from the emulsified fuel. A 0.180-inch I.D. tube was used as the fuel nozzle. Nozzle alignment with the lucite rod surface was refined on the basis of flow patterns. The gap spacing between the nozzle exit and the lucite surface was maintained at 0.750 inch. Ball valves were used along the emulsified fuel flow lines to avoid small restrictions which could cause the breakdown of the emulsified fuel. Figure 7 presents a front view of the impingement apparatus. A detailed view of the nozzle and the impingement surface is shown in Figure 8.

The data were recorded with a 4-inch x 5-inch still camera and consisted of photographic observation of the fuel sheet that resulted from impinging the fuel stream onto the lucite surface. A micro-flash system was used to provide the proper lighting. Flash duration was approximately 1.0 microsecond

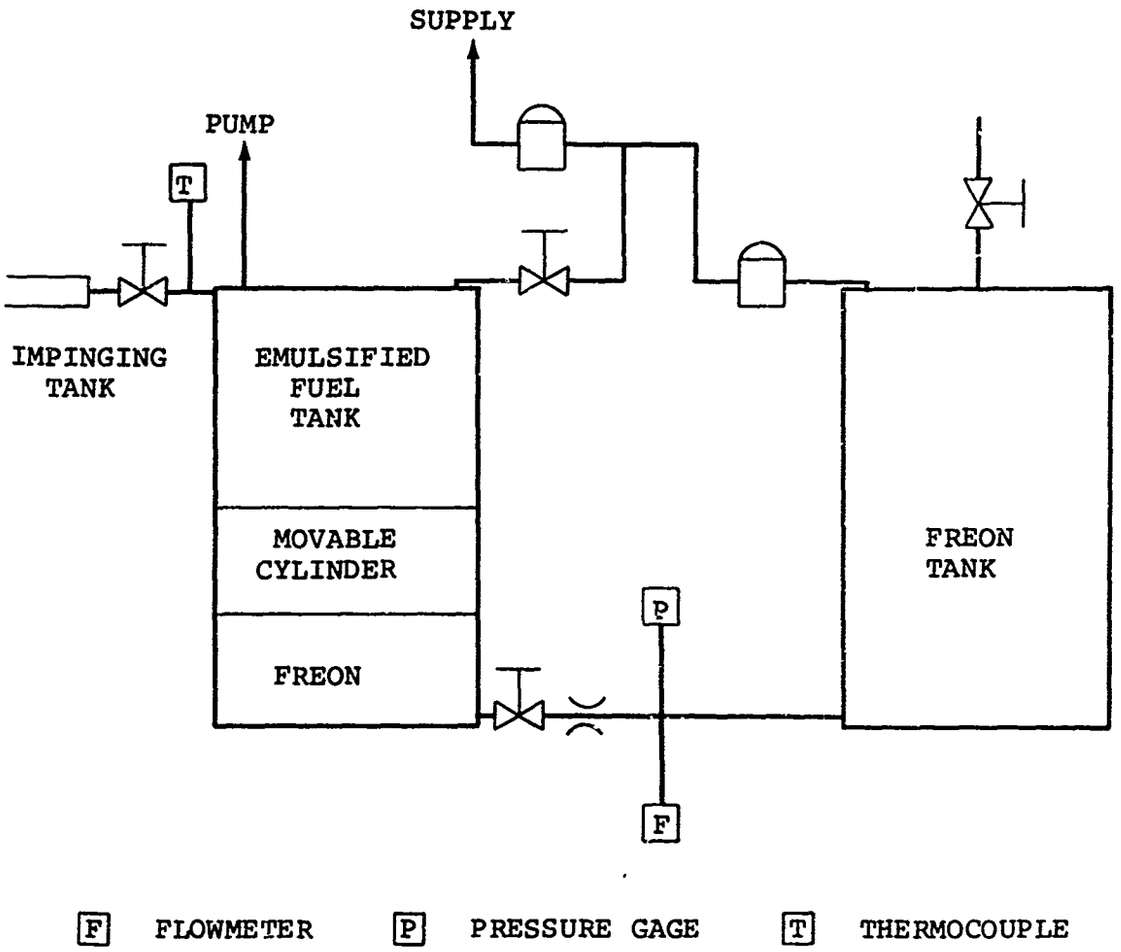


Figure 6. Schematic of Emulsified Fuel Impingement Apparatus.

with mean peak light intensity of 50,000,000-beam candlepower. The microsecond flash duration stopped the motion of fuel ligaments and droplet sizes. The camera was positioned perpendicular to the fuel sheet with the center of the film approximately 7 inches from the nozzle centerline.

## HOT-SOURCE IGNITION TESTS

The measurement of a minimum autoignition temperature is dependent upon the type and geometric configuration of the test apparatus. Therefore, a minimum autoignition temperature

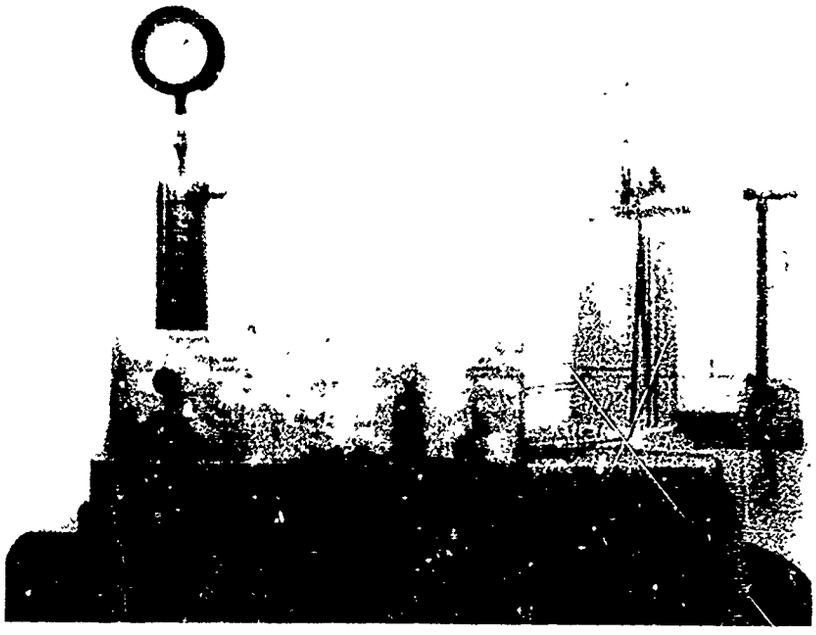

Figure 7. Front View of the Impingement Apparatus.

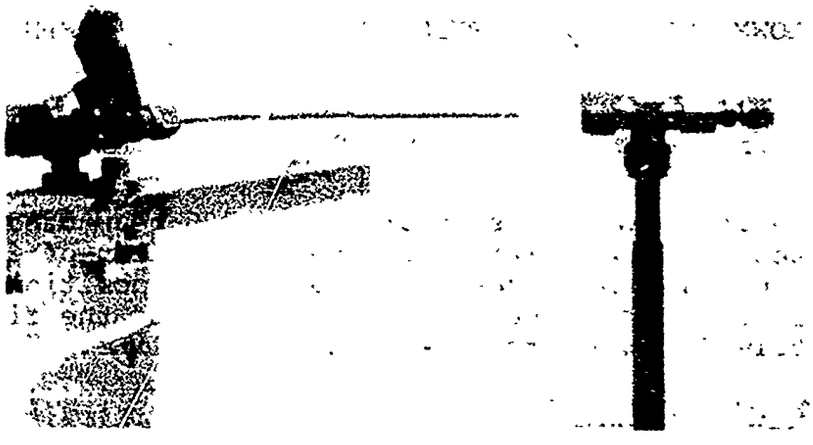

Figure 8. Close View of the Nozzle Section.

cannot be regarded as a physical constant but is dependent on such factors as vessel materials, vessel size, and oxidant mixing characteristics.

For the tests performed in this report, a heated vessel or "static" crucible method was used. A modification of the ASTM designation, D-2155-66 "Autoignition Temperature of Liquid Petroleum Products", was designed and incorporated. Because the majority of the hot surfaces existing in an aircraft crash are constructed of stainless steel, the heated vessel chosen was a 600-ml stainless steel beaker, replacing the 200-ml Erlenmeyer borosilicate glass flask. The static crucible method was chosen for its simplicity and ability to adequately simulate fuel spillage on hot crash surfaces. With this approach, no forced mixing of oxidant (air) is used. The static air in the test apparatus provides oxidant to the fuel.

The test apparatus is illustrated in Figure 9. A crucible furnace with a rheostat temperature control was used for heating the test crucible. The 600-ml beaker was instrumented with three iron-constantan thermocouples: (1) one located on the bottom and center of the beaker, (2) one located 2-1/2 inches from the top of the beaker, and (3) one located 1 inch from the top of the beaker. The test crucible was separated from contact with the bottom of the furnace by a 1/2-inch asbestos insulating ring. The top of the furnace was fitted with a 3/4-inch-thick asbestos cover with a 1-1/2-inch diameter hole provided to allow injection of the fuel sample and observation of ignition through the use of a mirror as shown. A 5cc hypodermic syringe calibrated in 0.1cc increments and equipped with a 3-inch No. 12 stainless needle was used to inject the fuel into the crucible. The ignition delay time was measured by a hand-operated stop watch.

The operational procedure for conducting the autoignition tests was similar to that set down by ASTM designation D-2155-65. The furnace temperature was adjusted so that the temperatures of the three thermocouple locations were within 5°F of the desired test temperature. A 0.10cc sample of the desired fuel was injected into the test crucible with the hypodermic syringe, and the syringe was quickly withdrawn. The time on the stop watch was started as the sample was injected into the crucible. Observation of the ensuing ignition, if any, was made with the aid of the observation mirror, at which time the ignition delay time was recorded on the stop watch. If a flame was not observed within 5 minutes, the sample was considered not flammable at the temperature measured. This procedure was repeated at various test temperatures.

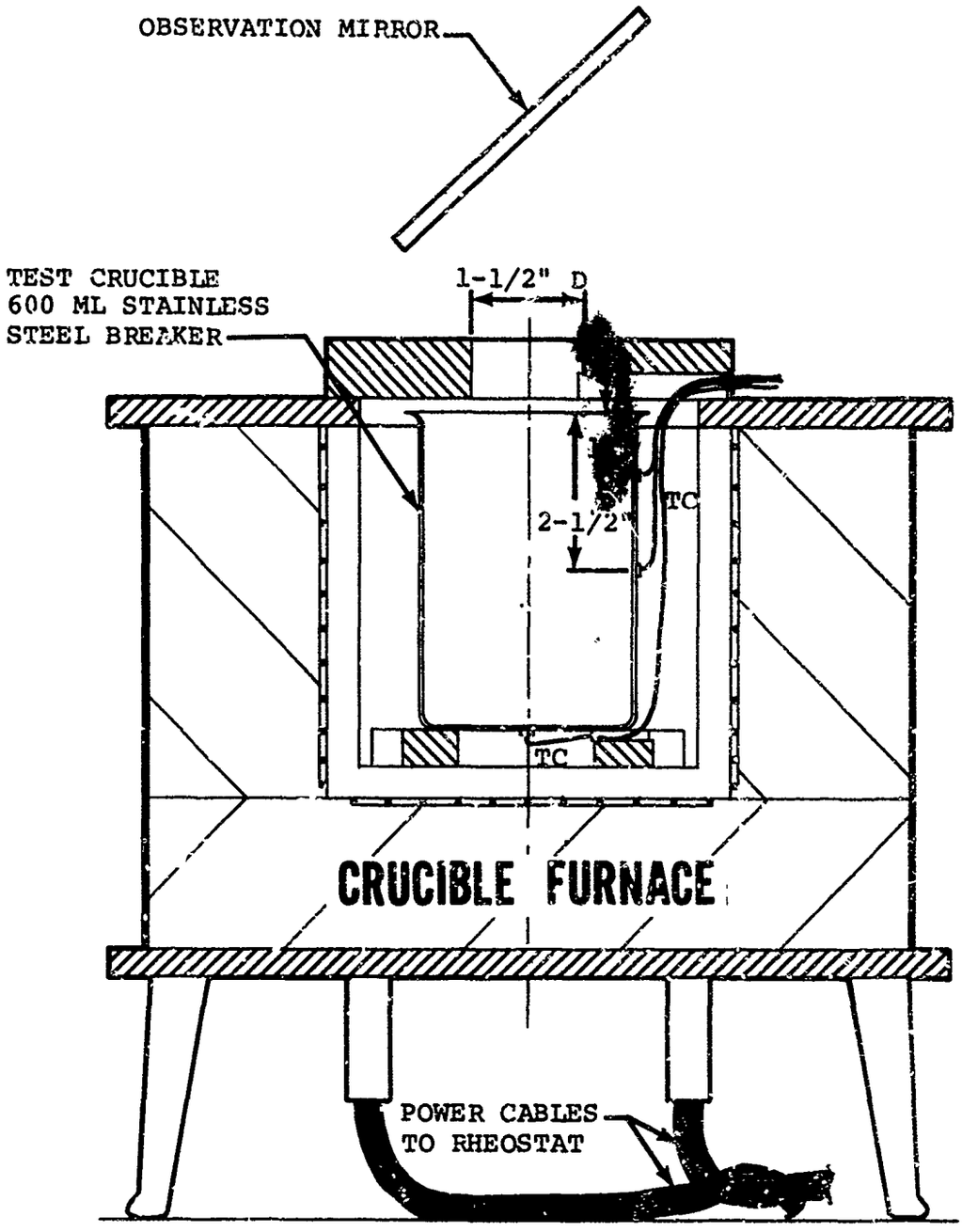


Figure 9. Hot-Surface Ignition Apparatus.

## WIND SHEAR TESTS

The wind shear tests were designed to determine the breakup and general flow field dispersion characteristics of fuels when subjected to air velocities typical of the crash environment. The basic wind shear tunnel test apparatus is shown in Figure 10. A blower, powered by an internal combustion engine, supplied air for the tunnel at velocities up to 146 fps. The blower flowed through a settling chamber provided with flow straightening devices. The 1-ft x 2-ft (cross section) test section had Plexiglas windows on one side along its 8-foot length for visual observation and photographic instrumentation. A smaller window was provided on the opposite side to allow the use of a strobe light for microphotography. Fuel was injected into the airstream through a port in the floor of the test section. Tunnel wind velocities were measured by a Pitot-static pressure probe, located at the forward end of the test section, that was connected to a water manometer. Air temperatures were measured by a thermocouple probe, also located at the forward end of the test section.

Test fuel temperature regulation was provided by the refrigeration unit shown in Figure 11. Tank No. 1 was a water reservoir fitted with refrigeration coils. The cooled water from Tank No. 1 was pumped through cooling coils in Tank No. 2 which contained the test fuel. The temperature-regulated fuel was transferred to the tunnel fuel pressurization tank (Tank No. 3) (shown in Figure 12) by a hand-operated vane pump. The temperature of Tank No. 3 was also controlled by pumping cooled water from Tank No. 1 through coils in the tank. The fuel pressurization tank was fitted with a pressure overload safety valve, a pressure relief valve, and a solenoid valve connected to the fuel flow rate pressure regulation system.

Fuel flow into the test section was provided by pressurizing the fuel pressurization tank. This flowed the fuel into a 1-inch flexible hose, through an on/off solenoid fuel valve, and into the test section through a 0.42-inch I.D. aluminum injection tube. The fuel line, solenoid valve, and injection tube were designed to provide adjustment of the injection tube with respect to the wind tunnel test section. A fuel drain with valve was provided at the bottom of the tank to allow measurement of emulsified fuel yield stresses prior to testing and to drain the tank.

The fuel flow rate was controlled by a pressure regulator valve fitted with a downstream orifice to insure a constant flow rate of air into the tank ullage. A second pressure regulator was connected to the tank to allow presetting of the

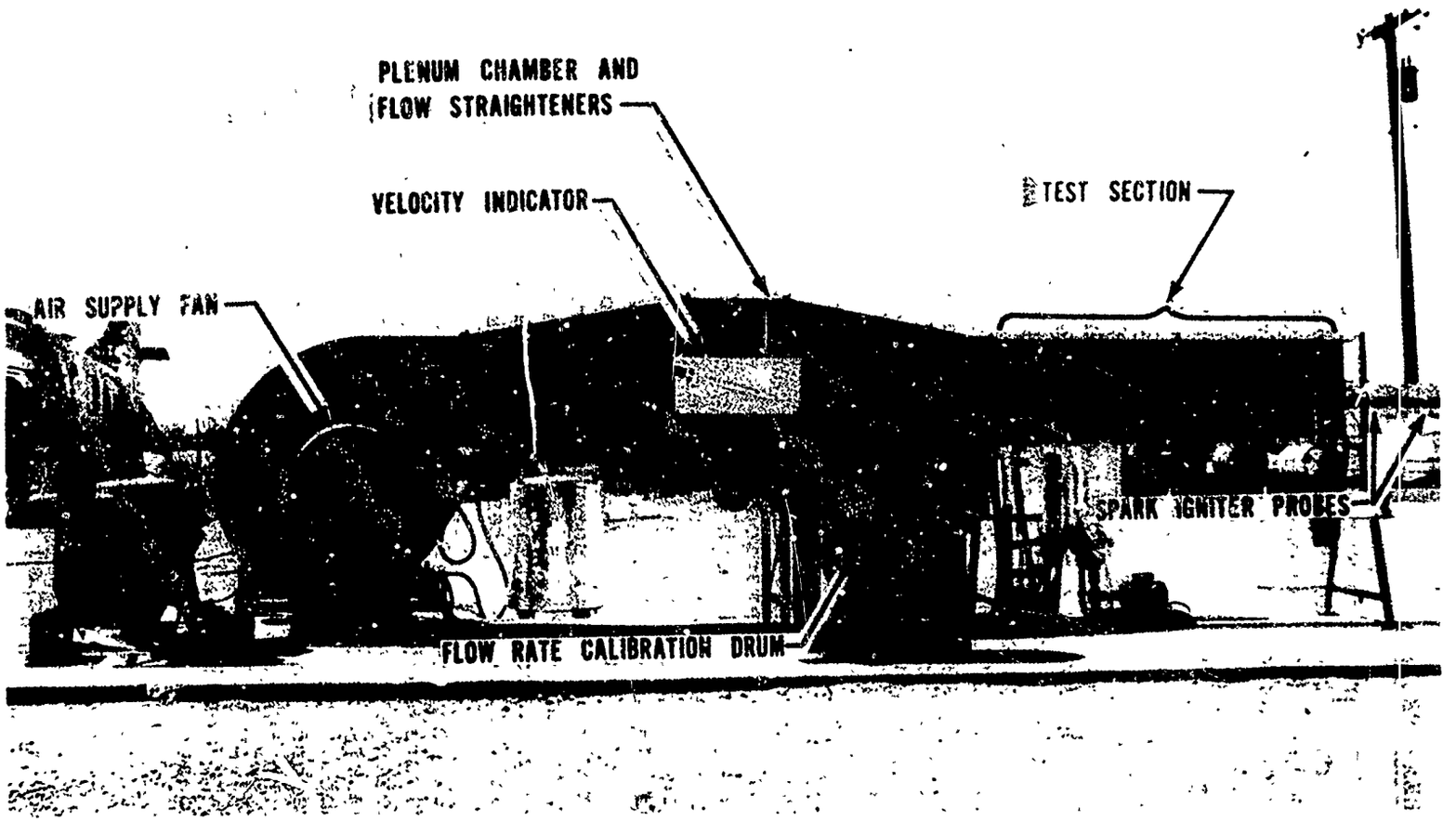


Figure 10. Wind Shear Tunnel Test Apparatus.

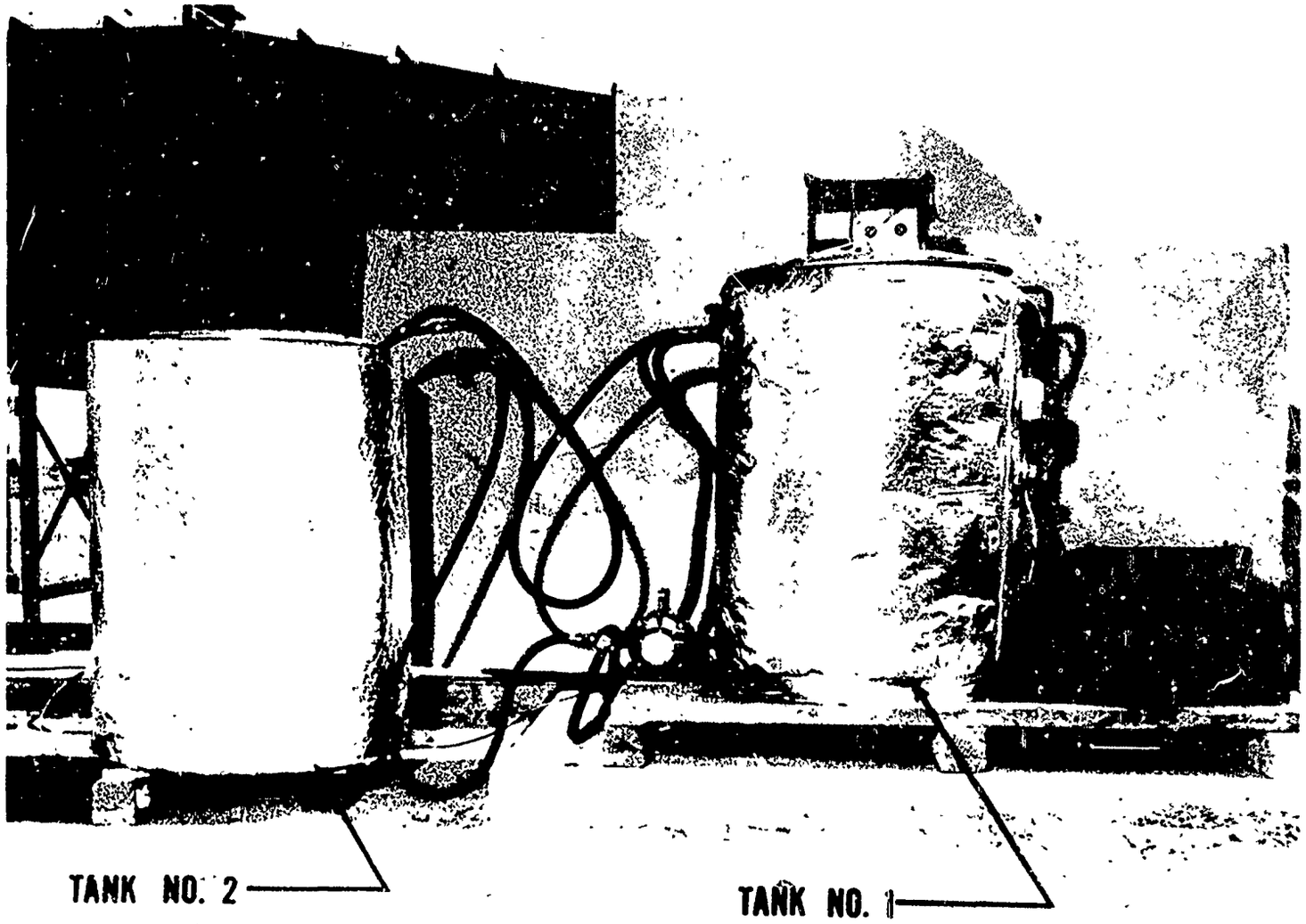


Figure 11. Refrigeration Unit for Wind Shear Tunnel Test Apparatus.

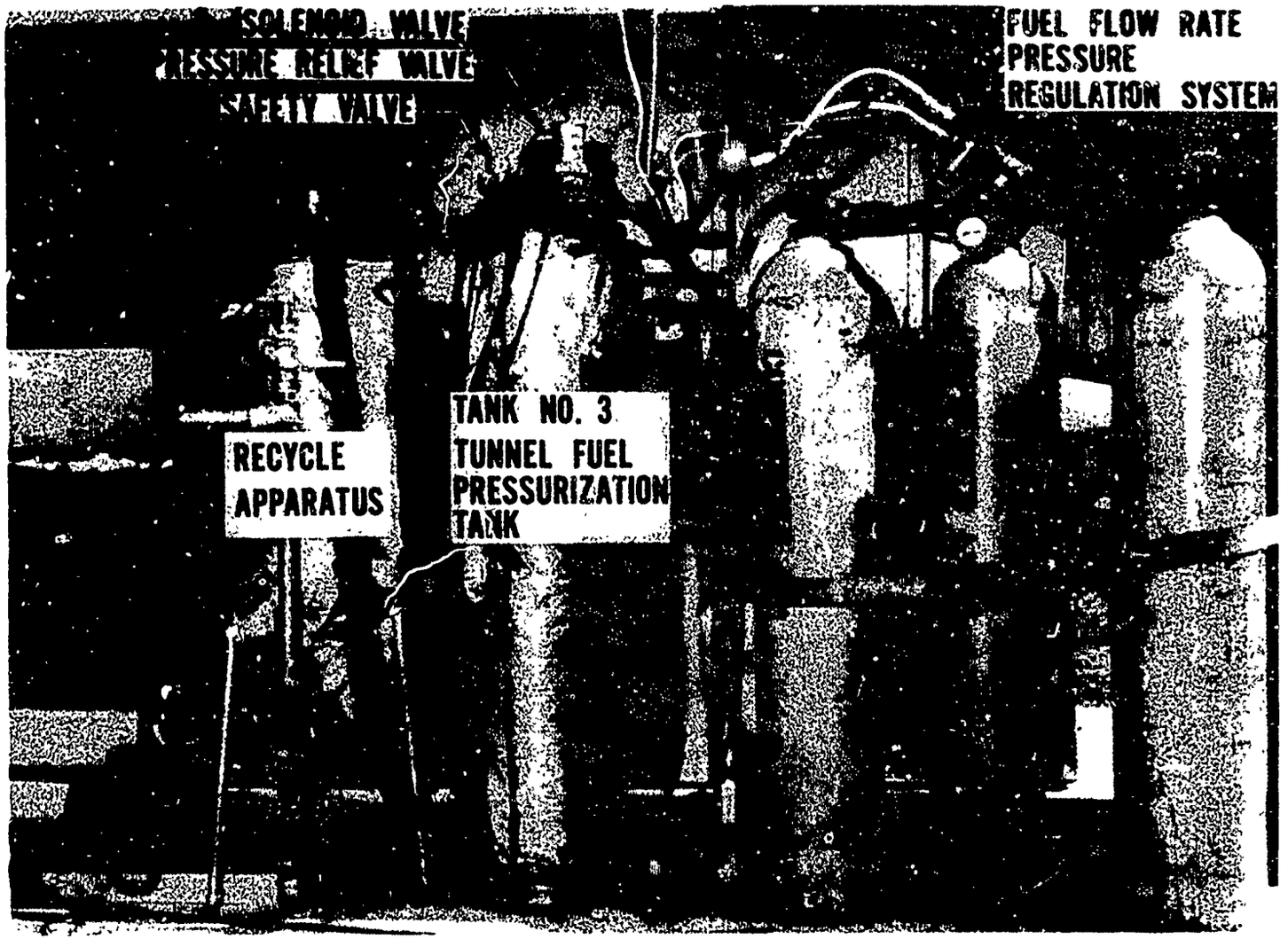


Figure 12. Wind Tunnel Fuel Supply System.

tank pressure to the steady-state pressure value downstream of the orifice.

Because the consistency and viscosity of the various fuels tested were different, it was necessary to calibrate the flow rate control system for each fuel. This was accomplished by flowing fuel into the flow rate calibration drum shown in Figure 10, which was weighed for a specific pressure setting and time. When required, the emulsified fuels were worked to higher yield stresses using the recycle apparatus shown in Figure 12.

Six basic types of data were obtained during wind shear testing: (1) wind tunnel condition data such as wind velocity and air temperature, (2) fuel property data, (3) spark ignition susceptibility data, (4) fuel droplet size data, (5) mean fuel/air ratio data, and (6) general fuel-wind flow field characteristic data.

The fuel property data consisted of type of fuel, yield stress value, and fuel temperature. The yield stress of the fuels was measured by a cone penetrometer technique developed by the U. S. Army Fuels and Lubricants Research Laboratory and described in USAAVLABS Technical Report 69-24, "Emulsified Fuels Characteristics and Requirements," March 1969.

The ignition susceptibility of wind-sheared fuel was obtained by placing spark igniter probes (70,000-volt capacitor discharge) aft of the test section as shown in Figure 10. Fuel ignition was observed and recorded visually.

Fuel droplet size measurements were obtained from microphotography of the dispersion flow field. The location of the microphotographic setup is illustrated in Figure 13. The setup consisted of a still camera with the field of view as shown in Figure 13, backed up by a 1 msec strobe light for capturing the flowing fuel droplets. The camera and strobe light were programmed to fire 4 seconds after injecting the fuel into the airstream.

The mean fuel/air ratio data were obtained from 11 sampling probes located at the aft end of the tunnel test section as illustrated in Figure 13. The probes were designed to sample an average fuel/air ratio over the full wind tunnel cross section. Each probe was constructed of 0.030-inch I.D. stainless steel tubing that incorporated a 60-degree scarfed end to minimize the digestion of solid fuel particles. The 11 probes were manifolded into a 3/8-inch-diameter stainless steel tube which was connected to a vacuum pump. A second vacuum pump

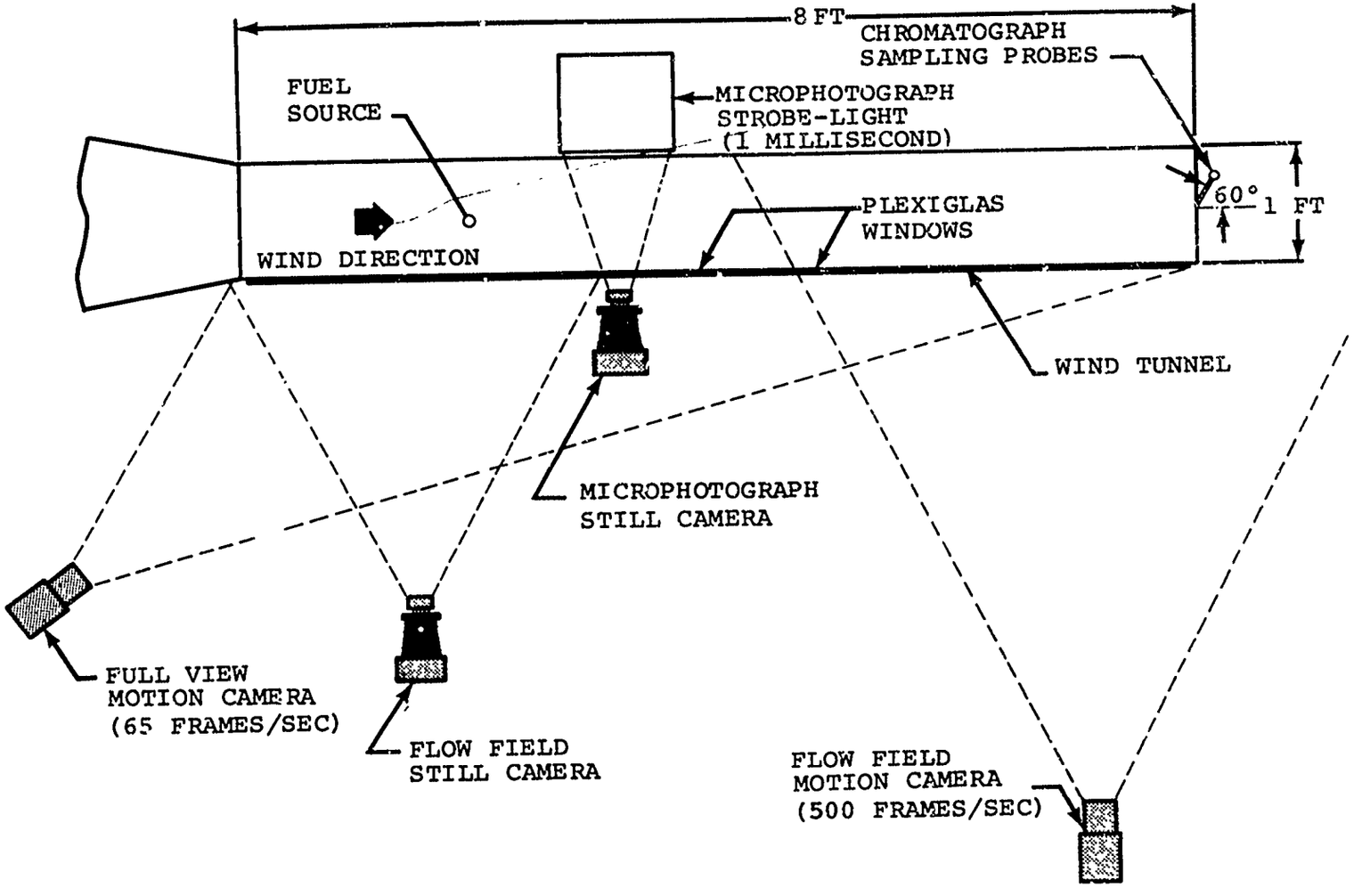


Figure 13. Photographic Layout for Wind Shear Tunnel Test Apparatus.

pulled a sample from the input manifold of the first vacuum pump through the chromatograph sampling coils. A chromatograph, connected to a recorder with integrator as shown in Figure 14, was used to record the sampled fuel/air ratio. The chromatograph was fitted with a silicone column which allowed the separate tracing of fuel compositions of varying molecular weight.

The general fuel dispersion patterns and fuel-air flow field interaction characteristics were obtained from three cameras. The flow field and fuel breakup kinetics were recorded by a hand-triggered still camera located as illustrated in Figure 13. A hand-triggered motion camera (65 frames per second) was also used to record fuel-wind interactions. A second motion camera (500 frames per second) was used as illustrated in Figure 13 to record the fuel breakup pattern and fuel droplet-air flow characteristics, and to determine the extent of fuel breakup downstream of the fuel injection point.

The data acquisition test procedure for the wind shear tests varied slightly depending upon the data being taken. The wind tunnel operating procedure, however, remained constant. Pretest preparations were as follows:

- Cameras were checked and loaded.
- Fuel/air sample vacuum pumps were turned on.
- The chromatograph was zeroed and set on the correct range.
- The yield stress of the fuel was taken.
- The fuel temperature was recorded.
- The fuel flow rate regulation system was set at the correct pressures which would produce a 10 fps fuel flow rate into the test section.
- The wind tunnel blower was started and set at a designated wind velocity.

The fuel flow rate regulator solenoid valve and fuel injection solenoid valve were programmed, through the use of an electronic counter, to open and close simultaneously to cause a 10-second fuel injection period into the wind tunnel test section.

Four seconds after fuel flow was started, the same counter system triggered the microphotograph camera and strobe light.

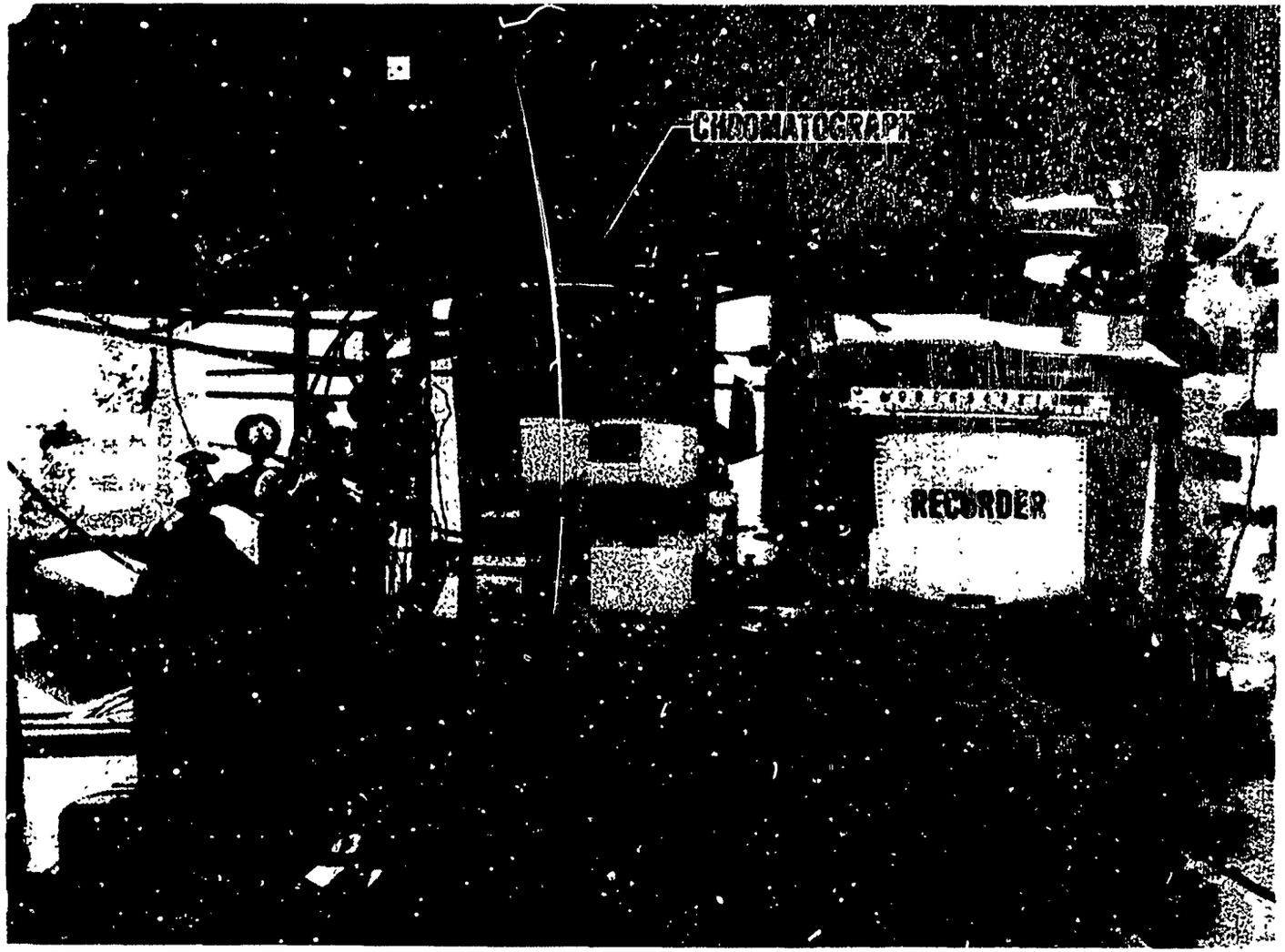


Figure 14. Chromatograph Instrumentation Setup.

The flow field still camera was hand triggered approximately 5 seconds after flow commenced. For motion camera data (which were taken without the two still cameras), the electronic counter triggered the flow field motion camera (500 frames per second) 4 seconds after flow was started and continued for 4 seconds. The full-view motion camera (65 frames per second) was hand operated and turned on for the complete 10-second run.

For spark ignition data, the spark was turned on prior to fuel flow injection and left on through the 10-second test period. Ignition was observed visually and recorded. Fifteen seconds after fuel flow commenced, the gas sample was switched into the chromatograph column to be analyzed. The wind tunnel test section was cleaned of residual fuel after each test before preparations for the next test commenced.

## IMPACT DISPERSION/ATOMIZATION TESTS

The impact dispersion/atomization test setup was designed to simulate fuel impact conditions of the crash environment on a laboratory scale. This was accomplished by impacting a slug of fuel onto a flat surface, representing the conditions existing when a fuel tank or fuel line ruptures during an actual crash.

The device for obtaining fuel impact velocities (Figure 15) was a 4-ft x 2-in. I.D. steel driver tube that inclosed a piston which contained the fuel sample. The sample was driven down the tube at a predesignated velocity by air pressure. The air supply entering the driver tube was fitted with a sonic orifice such that a known flow rate of air entered the tube for a given air supply pressure. Two 1/2-inch-diameter relief holes were located near the end of the piston travel to release the driver tube pressure when the fuel piston impacted a shock ring at the bottom of the driver tube. This prevented any flow of air through the piston into the fuel impact area.

The fuel piston was made of aluminum and held 3 cubic inches of fuel (Figure 15). The details of the fuel piston are illustrated in Figure 16. Fuel was held in the piston by placing an aluminum foil diaghragm over the face of the piston and clamping the diaphragm with a clamping ring. The clamping ring was constructed with an 85-degree knife edge to allow clean shearing of the diaphragm when the piston impacted the shock ring. O-rings were placed around the piston circumference to provide an air seal. A secondary piston was fitted inside the fuel piston to release the vacuuming effects of

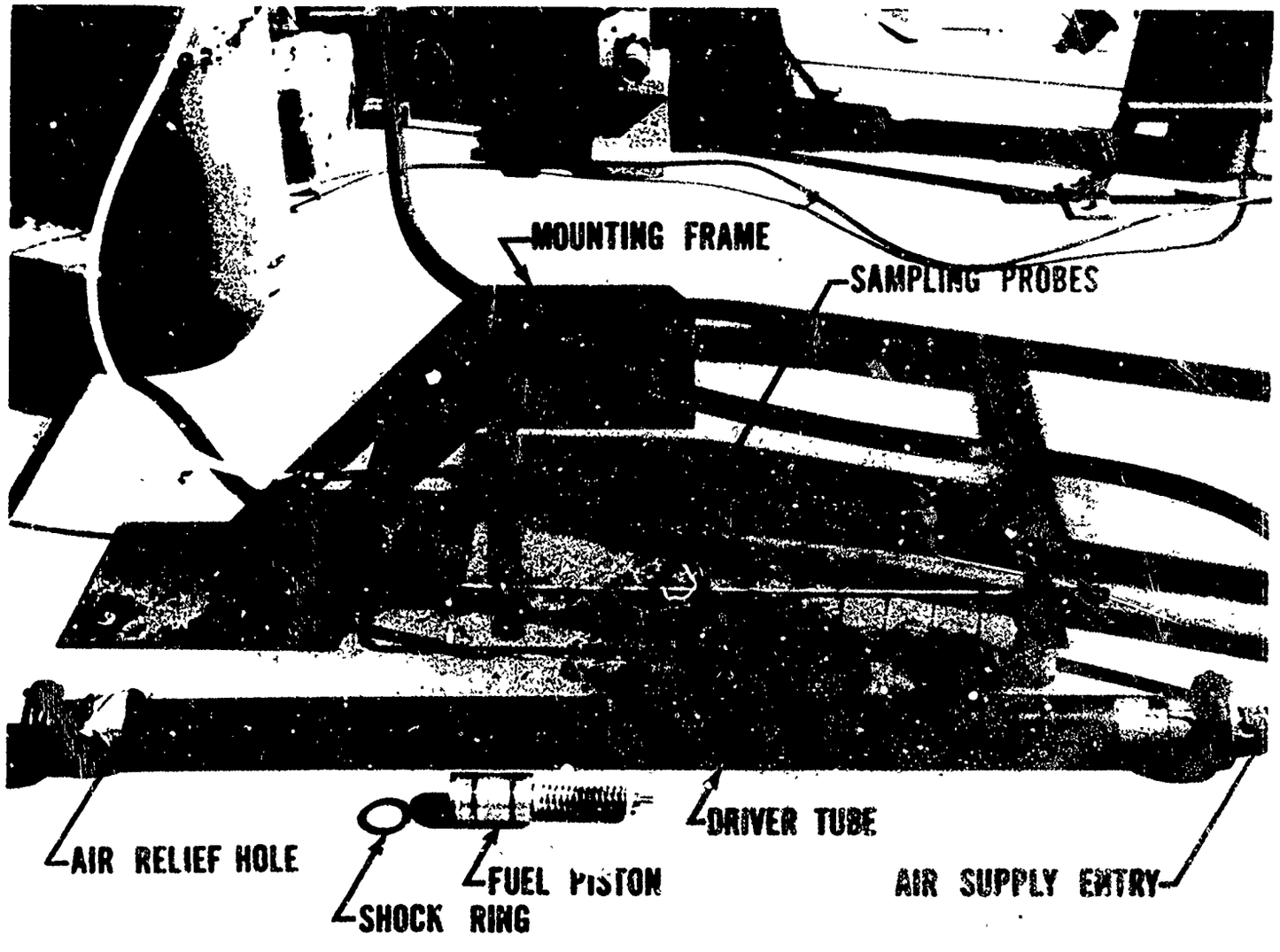


Figure 15. Fuel Impact/Dispersion Atomization Test Devices.

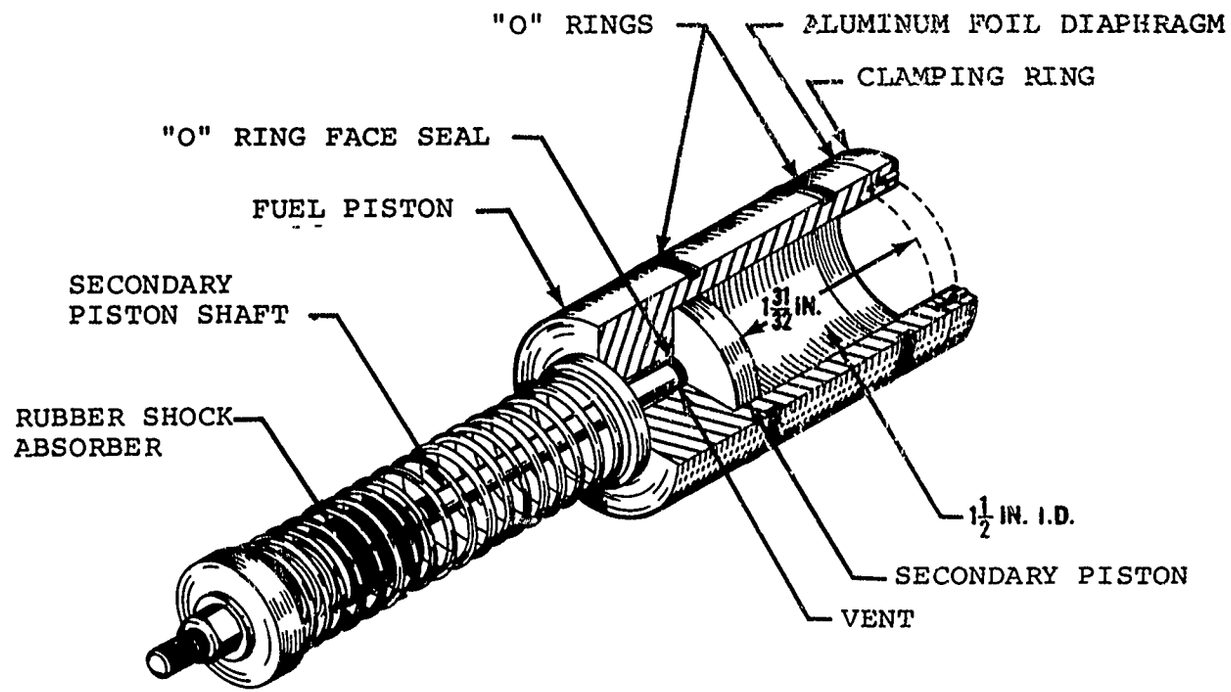


Figure 16. Fuel Piston for Impact/Dispersion Atomization Test Device.

the fuel exiting the piston. The O-ring face seal initially eliminated any liquid fuel leakage through the rear of the piston. The spring provided the initial seating force for the face seal as well as reduced the impact inertia forces on the secondary piston. The rubber shock absorber further attenuated these forces.

The driver tube-fuel piston assembly was mounted on the frame at the desired angle of impact (90, 45, or 15 degrees) as shown in Figure 17. The mounting frame was designed so that the fuel slug travel distance from the driver to its impact point was 1 foot for all three impingement angles.

Air to the driver tube was obtained from a supply bottle through an adjustable pressure regulator which fed an accumulator bottle. A solenoid valve programmed with the 500-frame-per-second camera released the air supply to the driver tube.

The sampling probes shown in Figures 15 and 17 contained 11 stainless steel tube probes (0.030-in. I.D.) which were connected to a vacuum pumping system for pulling a sample of vaporized gas. Care was taken to design the probes with a scarfed end so that ingestion of liquid fuel particles was held to a minimum. The 11 probes were located 2 inches from the impact surface and 6 inches from the impact centerline, starting adjacent to the point of impact.

To control wind and extraneous effects, a Plexiglas container was fitted over the impact area as shown in Figure 18. Inside, this container was 1 foot high, 2 feet wide, and 5 feet 7-1/2 inches long. These dimensions were based on a volume which, for JP-4, would give a fuel/air ratio of 0.1 by weight if all of the JP-4 fuel were vaporized for standard atmospheric conditions.

Data recorded for the impact dispersion/atomization tests consisted of: (1) fuel slug impact velocity, (2) air temperature, (3) impact surface temperature, (4) pressure regulator pressure, (5) fuel temperature, (6) fuel yield stress, and (7) mean fuel/air ratio.

A 500-frame-per-second camera, shown in Figure 18, recorded the actual fuel velocity and impact characteristics. Fuel yield stress was measured by a cone penetrometer.

The mean fuel/air ratios were measured by a chromatograph connected to a recorder with integrator as shown in Figure 14. A silicone column was used to trace various fuel molecular compositions. The chromatograph setup was the same as for the wind shear tests discussed earlier.


Figure 17. Impact Dispersion/Atomization Facility.

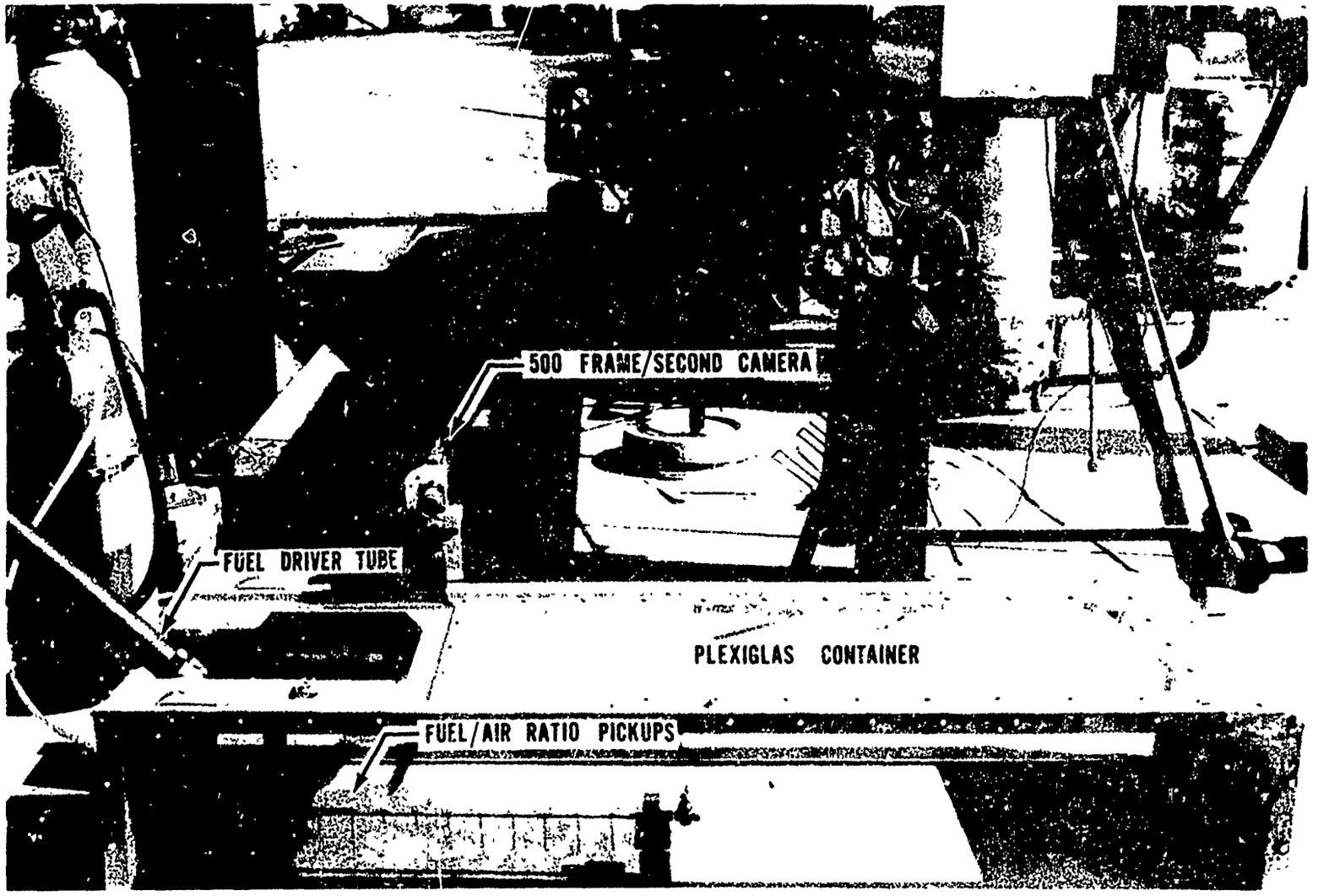


Figure 18. Impact Dispersion/Atomization Apparatus With Impact Area Inclosure.

The operational procedure for the impact dispersion/atomization tests was as follows:

- The camera was checked and loaded.
- Fuel/air sample vacuum pumps were turned on.
- The chromatograph was zeroed and set on the correct range.
- The yield stress of the fuel was taken.
- The fuel temperature was recorded.
- The impact surface and ambient air temperature were recorded.
- The air supply pressure regulator was set at the prescribed pressure to obtain specified impact velocity.
- The piston was filled with fuel and placed in the driver tube.
- The driver tube assembly was installed on the mounting frame.
- The camera was turned on for 3 seconds. After 1 second from camera start, the solenoid valve was automatically opened, accelerating the fuel to the impact point. When the camera was turned off, the solenoid valve closed.
- Fifteen seconds after the camera commenced, the gas sample was switched into the chromatograph column to be analyzed.
- Before the next test was run, the facility was cleaned of all residual fuel.

Only slight modification of the previously discussed facility and operational procedure was required to incorporate the ignition sources, a hot-surface source and a spark ignition source. The hot-surface ignition source was a stainless steel sheathed, nichrome heater strip (2 feet long and 3/8 inch in diameter) mounted on a frame as shown in Figure 19. The hot-surface ignition source was located at the same relative location as the gas sample pickups discussed previously. The heater strip was brought up to 1100°F by a rheostat while the temperature was measured by an iron-constantan thermocouple.

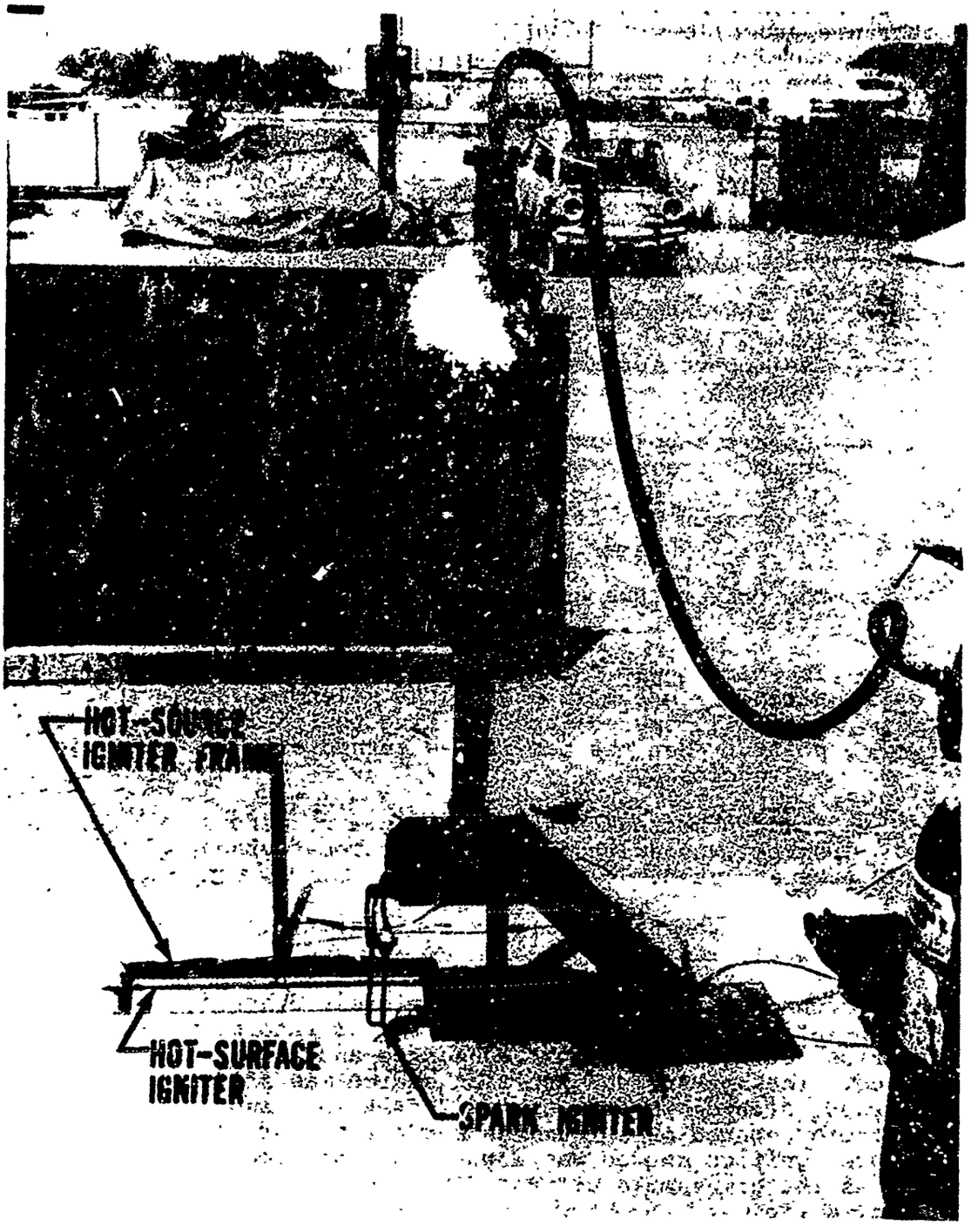


Figure 19. Impact Ignition Configuration.

The spark igniter was powered by a 12,000-volt transformer with an approximate spark gap of 0.1 inch. The spark igniter was located 5 inches from the fuel impact point and 1-3/4 inches from the surface.

The pretest operational procedure was similar to that already discussed except that chromatographic data were not obtained and the hot-surface and spark igniters were activated as required. The Plexiglas container was not used. The camera was set for a 4-second run period rather than a 3-second period so that complete combustion coverage could be obtained.

Recorded ignition characteristics were obtained from the 500-frame-per-second camera and visual observations and recordings.

Immediately after each run, the fire, if any, was extinguished, the spark igniter was turned off, and the hot surfaces were removed from the area. The facility was then cleaned and made ready for the next test.

SIMULATED FULL-SCALE TESTS

The basic overall test setup is illustrated in Figure 20. The test procedure consisted of accelerating a fuel tank mounted on a test fixture along a monorail, impacting the tank on a barrier, and recording ignition data photographically and in terms of electric analogs for the associated fire heating data.

A crash velocity of 65 ft/sec at an impact angle of 45 degrees was chosen to conduct the simulated full-scale tests. By conducting tests at the approximate crash-survivable energy limit, any fuel or test condition which indicated "safe" during these tests would be considered within the survival envelope during a full-scale crash.

The test impact barrier was an earthen fill constructed adjacent to a monorail as illustrated in Figure 21. The face of the barrier was constructed of concrete at a 45-degree incline with the horizontal and was 32 inches long and 5-1/2 feet wide. It was fitted with two steel tank cutters to insure that the fuel tank bladder would rupture as in full-scale crashes onto rough terrain. A concrete block wall was constructed adjacent to the monorail to provide a near vertical surface to contain the earthen fill, and to allow the impact area to be as close to the test fixture as possible within barrier-fixture clearance limits. The maximum height of the dirt fill was 3 feet 7 inches from ground level. The overall length of the impact barrier test area was 30 feet.

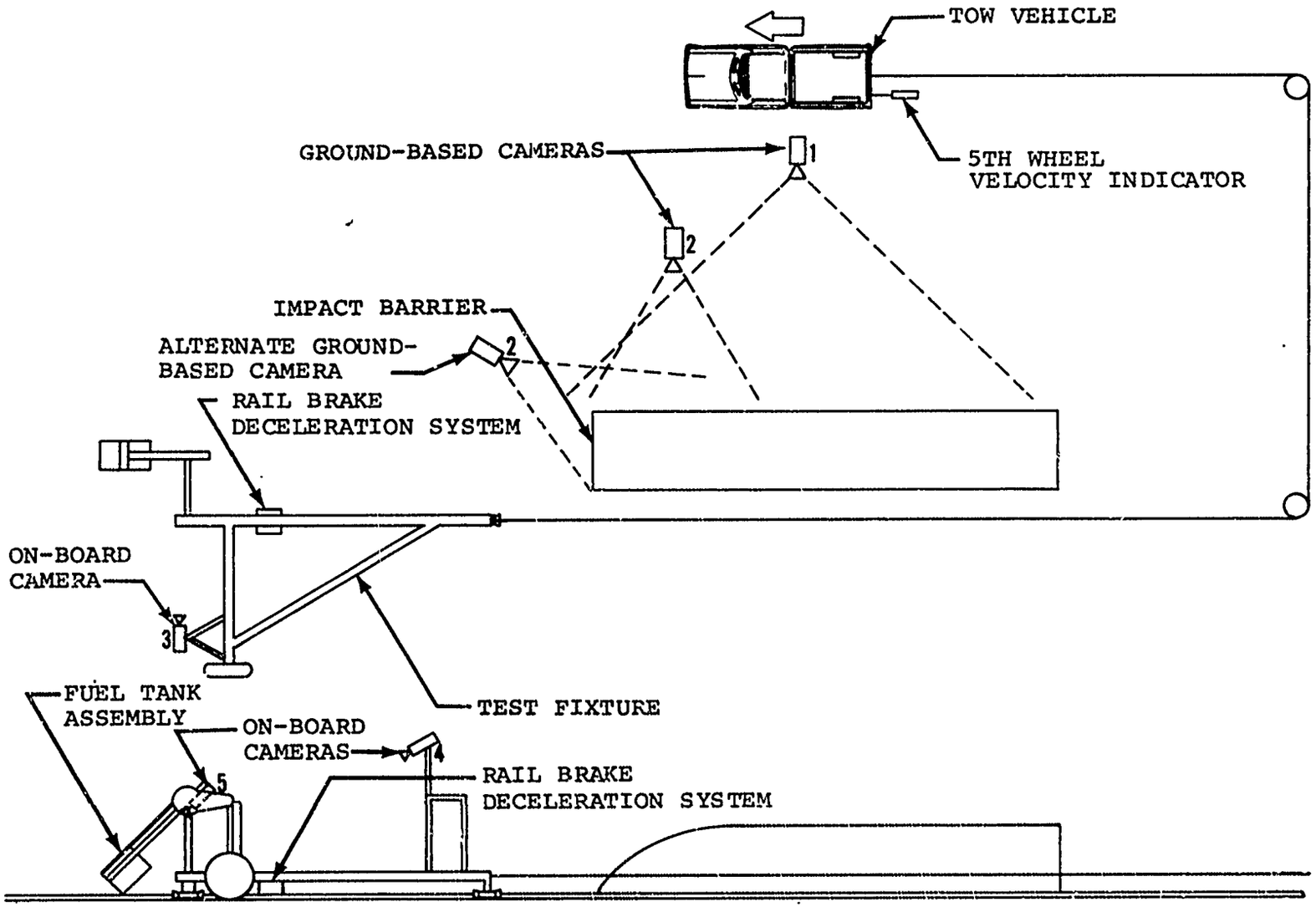


Figure 20. Overall Test Setup.

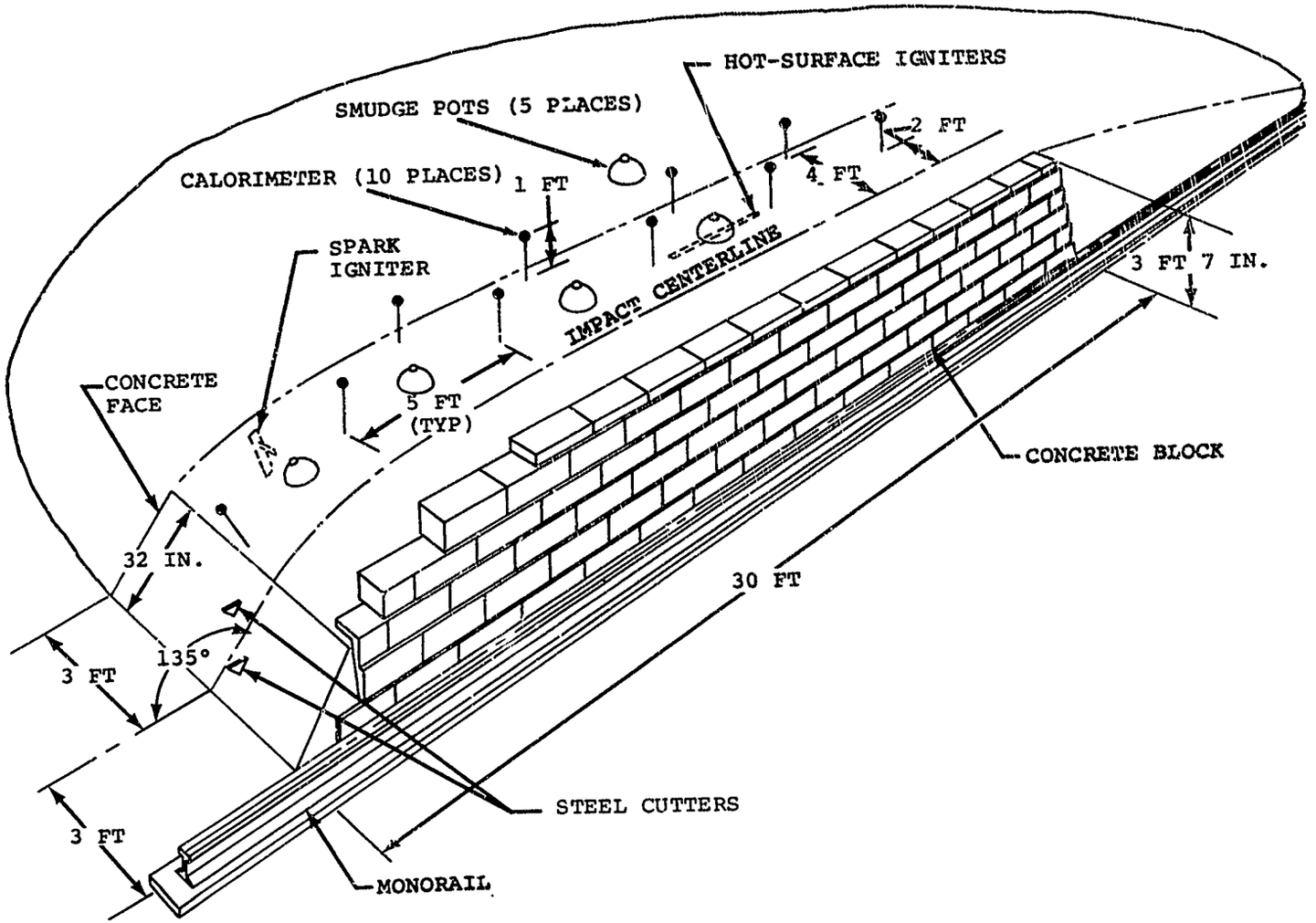


Figure 21. Impact Barrier.

Fifteen-hundred feet of monorail was used to accelerate the test fixture to a velocity of 65 ft/sec. Steel straps (48 feet long, 1/4 inch thick, and 2-1/2 inches wide) were attached to each side of the monorail in the vicinity of the impact barrier to provide a friction surface for the fixture stopping brake.

The test fixture was constructed to ride on the monorail, position the fuel tanks, and allow simulation of the impact kinetics and aircraft stopping distance after impact. The fixture is illustrated in Figures 22, 23, and 24. The tank mount and supporting structure consisted of a swinging pivot arm. An energy-absorbing brake system was incorporated to hold the pivot arm and fuel tank at the desired position prior to impact and to provide rotational energy absorption to duplicate impact kinetics during and after impact.

A rail caliper brake system was designed to stop the test fixture and fuel tank within 18 to 30 feet from initial impact. This system was designed to duplicate the stopping distance a crashing helicopter travels in the horizontal after initial impact at the energy condition tested. The brake system consisted of two brake shoes (2-1/2 in. x 12 in.) which clamped onto the steel strips attached to the monorail; see Figure 23. The brake was actuated by air pressure through use of a solenoid-actuated valve. A breaker wire switch triggered by a metal stake initiated brake actuation at a specific point in the fixture's travel into the barrier. The brake shoe material consisted of asbestos mil-board brake lining.

The simulated fuel tanks were constructed to duplicate the crash kinetics of actual full-scale configurations. Figure 25 shows the test fuel tank configuration and the tank bladder. The tanks were of honeycomb sandwich construction as illustrated in Figure 26, and were typical of those found on many U. S. Army helicopters. The dimensions of the tanks allowed an approximate fuel volume of 13 gallons (1 ft x 1 ft x 2 ft). The outer skin of the tank structure was made from 0.016-inch-thick 7075-T6 aluminum panels. The core was of aluminum honeycomb (1/2 in. x 1/8 in. x 0.07N). A 2-ply fiberglass cloth provided the inner skin material. These materials were bonded with epoxy resin to form the sandwich-constructed panels as illustrated in Figure 26. A 1-inch lip was provided at the panel edges to allow rivet attachment to the 0.06-inch angle framework. The top end frames were constructed of two 0.06-inch "T" sections to provide mounting brackets and attachment of the tank to the fixture mount. A thin-wall fuel cell bladder was constructed to fit inside the tank structure. A 2-inch filler cap was vulcanized to the top center of the fuel cell bladder and attached through a 3-inch-diameter hole cut into the tank top panel.

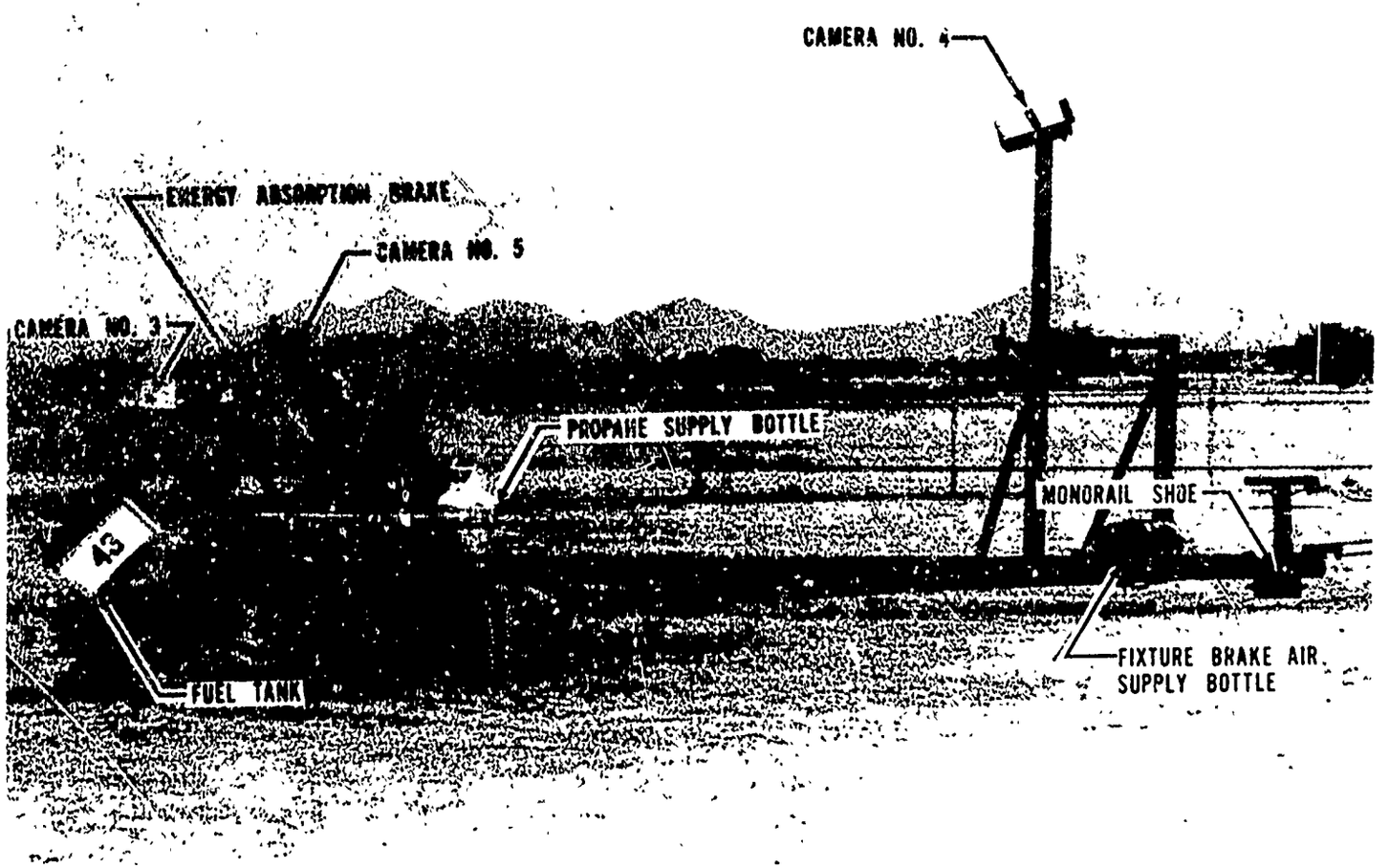


Figure 22. Test Fixture and Associated Equipment.

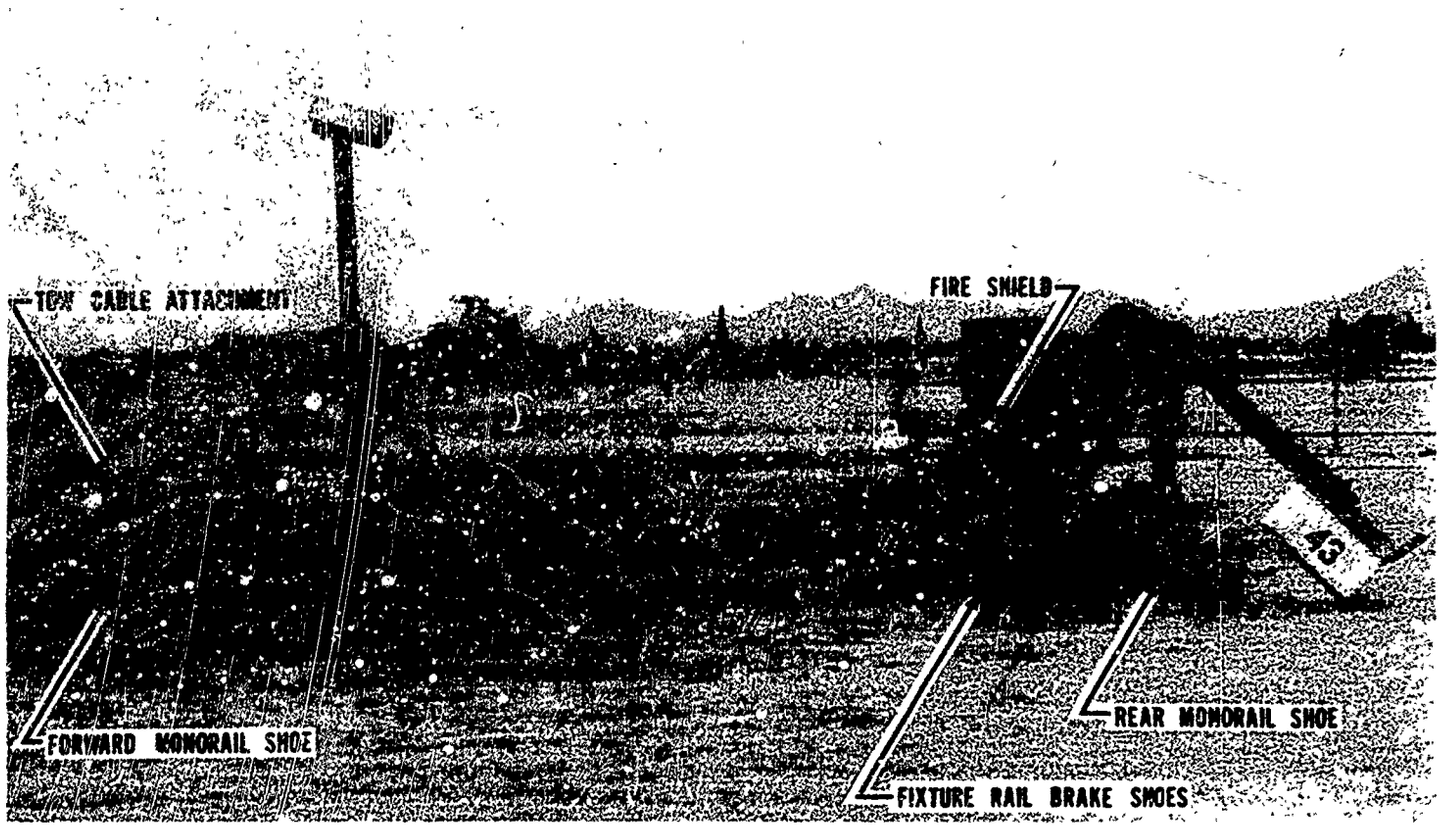


Figure 23. View of Test Fixture From Side That is Next to Barrier on Impact.

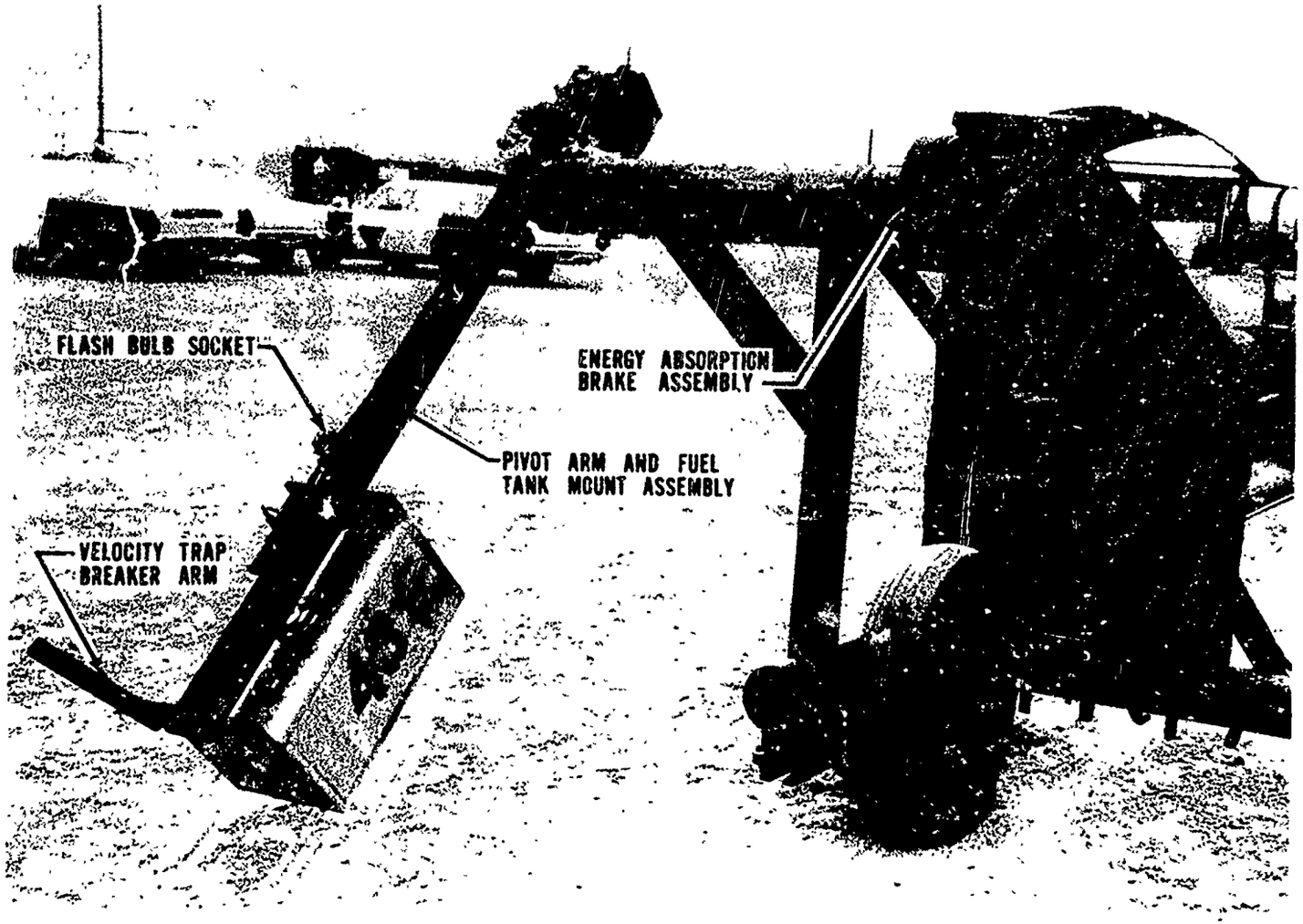


Figure 24. Fuel Tank Mount Pivot Arm and Energy-Absorption System.

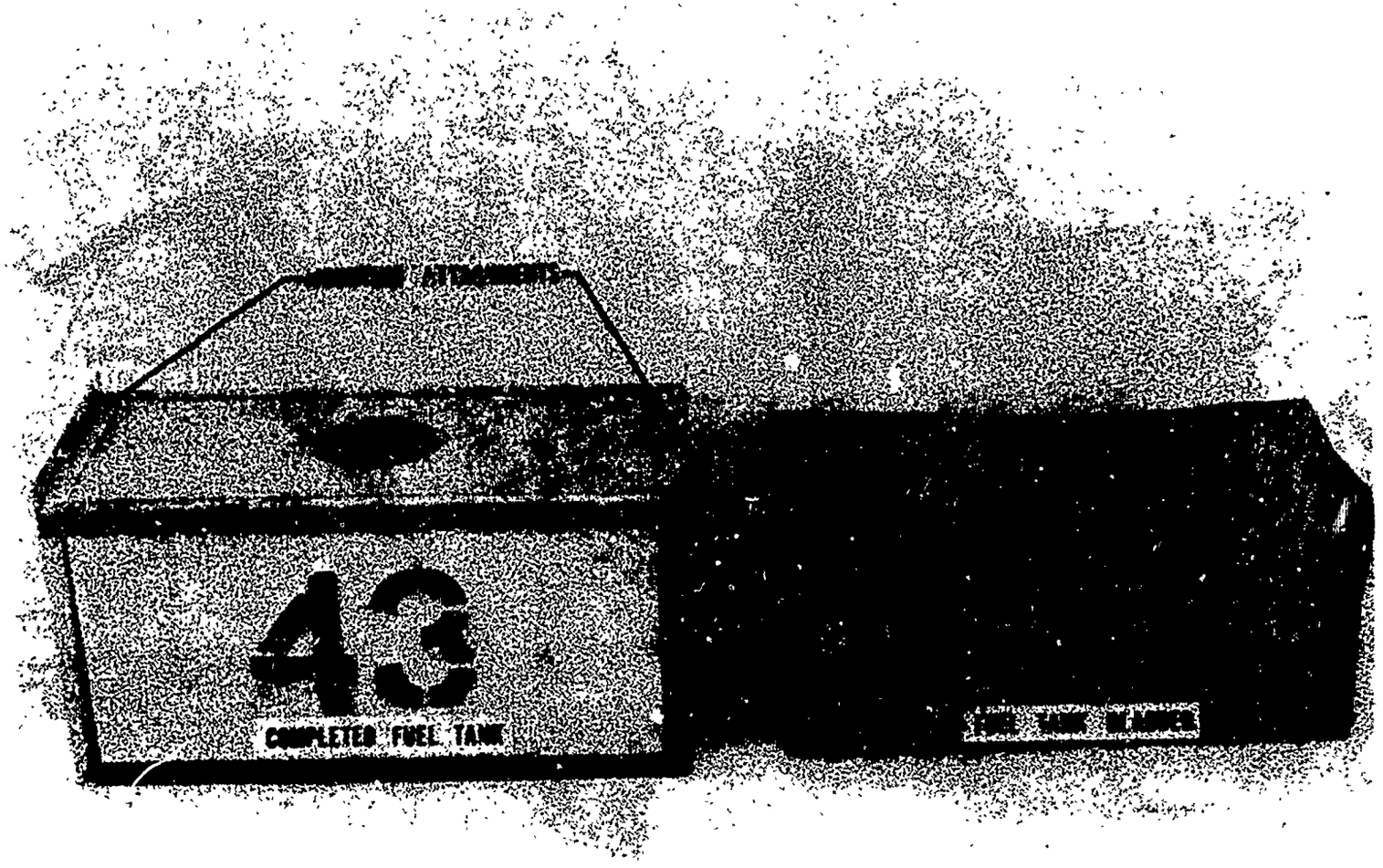


Figure 25. Fuel Tank and Fuel Tank Bladder.

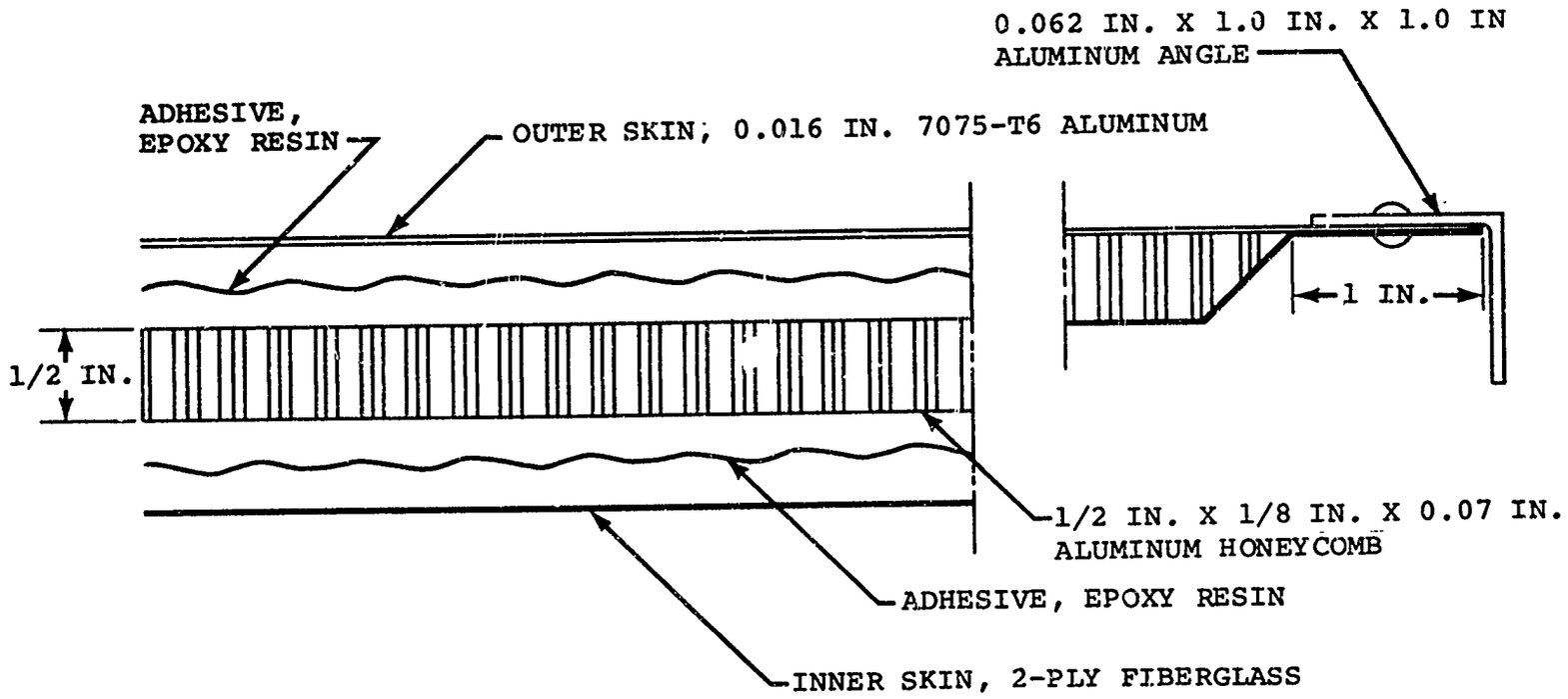


Figure 26. Tank Fabrication (Vacuum Formed Sandwich Construction).

Instrumentation was provided to measure and record the impact velocity, the fire intensity, and the test conditions. The impact velocity was obtained by towing the test fixture with a vehicle using a 1,500-foot cable; see Figure 20. The tow vehicle was instrumented with a fifth wheel velocity indicator and a speed control device. The speed control device provided accurate velocity regulation which eliminated the possibility of human error. This system provided an impact velocity of 65 ft/sec within ±2 ft/sec. An electrical breaker speed trap was placed just forward of the impact barrier to measure the actual impact velocity.

The fire intensity accompanying the impact and ignition of the fuel was measured versus time. Ten calorimeter probes, located as shown in Figure 21, were positioned vertically 1 foot from the barrier surface. The calorimeter devices were constructed as shown in Figure 27. They measured the environmental temperature versus time to allow computation of resulting heating rates. This system allowed the determination of relative fire intensity and provided a means to extrapolate the simulated test fire intensity to a full-scale condition.

Pretest environmental conditions were determined by measuring impact barrier surface temperature, fuel temperature, barometric pressure, air temperature, relative humidity, wind velocity, wind direction, and hot-surface igniter temperature when applicable. Impact barrier and fuel temperature were measured with a mercury thermometer prior to test initiation. Ambient wind velocity and direction were measured by a portable anemometer and direction indicator. Ambient air temperatures were recorded by an enclosed U. S. Weather Bureau ambient thermometer. The relative humidity and barometric pressure were obtained from the U. S. Weather Bureau at the Phoenix airport. The hot-surface igniter temperature was measured with a thermocouple.

Five high-speed cameras were used to provide photographic coverage of each test. Three cameras were installed on the test fixture for on-board photographic coverage as illustrated in Figures 20 and 22. Camera 5 was attached to the tank support pivot arm and Camera 3 was positioned to photograph a close-up side view of the impact sequence. Camera 4 was located to photograph a semioverhead view of the impact sequence. Two ground cameras were located as shown in Figure 20. Camera 1 provided an overall view of the impact test and Camera 2 was positioned to record a close-up view of the impact event. An alternate position for Camera 2 is illustrated in Figure 20. It was used in the on-board (engine simulator) igniter tests to provide coverage of both the igniter and impact sequence.

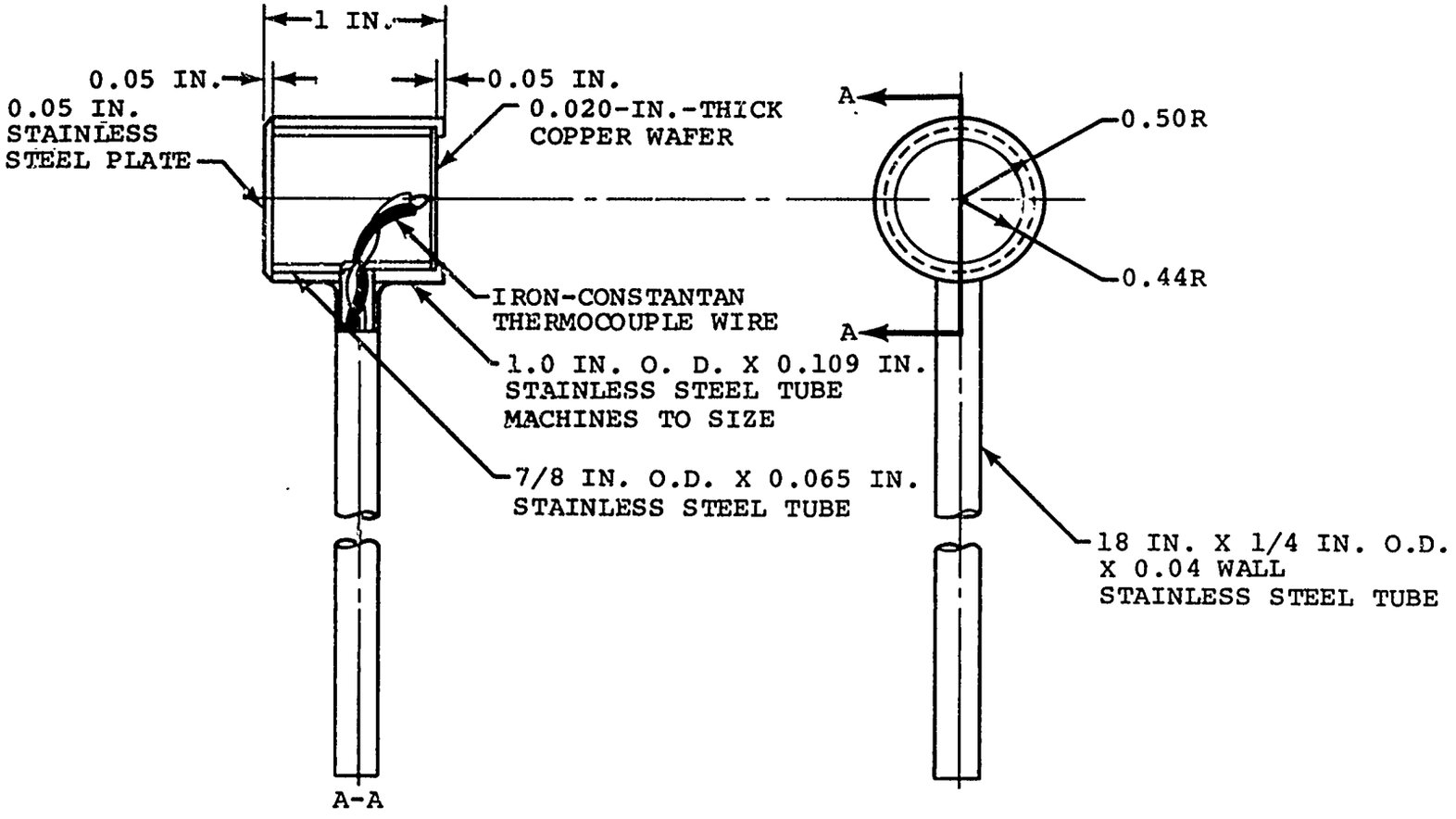


Figure 27. Calorimeter Design.

Fuel temperature was maintained throughout the tests between 97° and 103°F. This was accomplished by storing the test fuels in two identical fuel temperature regulation systems. The system is illustrated schematically in Figure 28, and photographically in Figure 29. Each fuel regulation system consisted of an insulated 55-gallon barrel which enclosed a 30-gallon fuel barrel. The space between the 55- and 30-gallon barrels was filled with water to allow a regulated heating control liquid. A barrel heater that was powered by a thermostat control device which regulated the water temperature by a thermometer submerged in the water was wrapped around the base of the 55-gallon barrel. The 30-gallon barrel was filled with the desired fuel and brought up to the desired fuel temperature.

Yield stress of the emulsified fuels was measured three times when the tank was filled for testing and then averaged. An ASTM D217 cone penetrometer (30-gram cone assembly) was used to measure the yield stress in dynes/cm$^2$.

Ignition sources were provided which simulated those sources observed in full-scale crashes. Basically, three types of ignition tests were studied: (1) a ground-based spark and hot-surface igniter configuration, (2) ground-based open flame igniters, and (3) an on-board (engine simulator) hot-surface and open-flame igniter system.

The spark igniter source was located 1 foot from the barrier surface as illustrated in Figure 21. Spark was obtained from a 12,000-volt transformer driving a 0.1-inch spark gap. The hot-surface igniter source, located as illustrated in Figure 21, was a stainless steel sheathed, nichrome heater strip (2 ft long and 3/8 inch I.D.), temperature controlled with a rheostat and monitored with a thermocouple. The heater strip was positioned level to the barrier surface and was maintained at 1100°F.

The open-flame igniter sources, five smudge pots burning JP-4, are illustrated in Figure 21.

The on-board ignition source (see Figure 30) was located over the fuel tank on the pivot arm as shown in Figure 31. This ignition source simulated the crash environment associated with turbine tailpipe conditions and was sequenced to simulate observed full-scale tailpipe conditions as illustrated in Figure 32. The ignition source sequence consisted of an initial hot-surface or tailpipe condition of approximately 900°F. At 0.7 second after impact, the propane burner was ignited to simulate the engine flaming which is observed as the engine spools are halted by friction. The open flame was

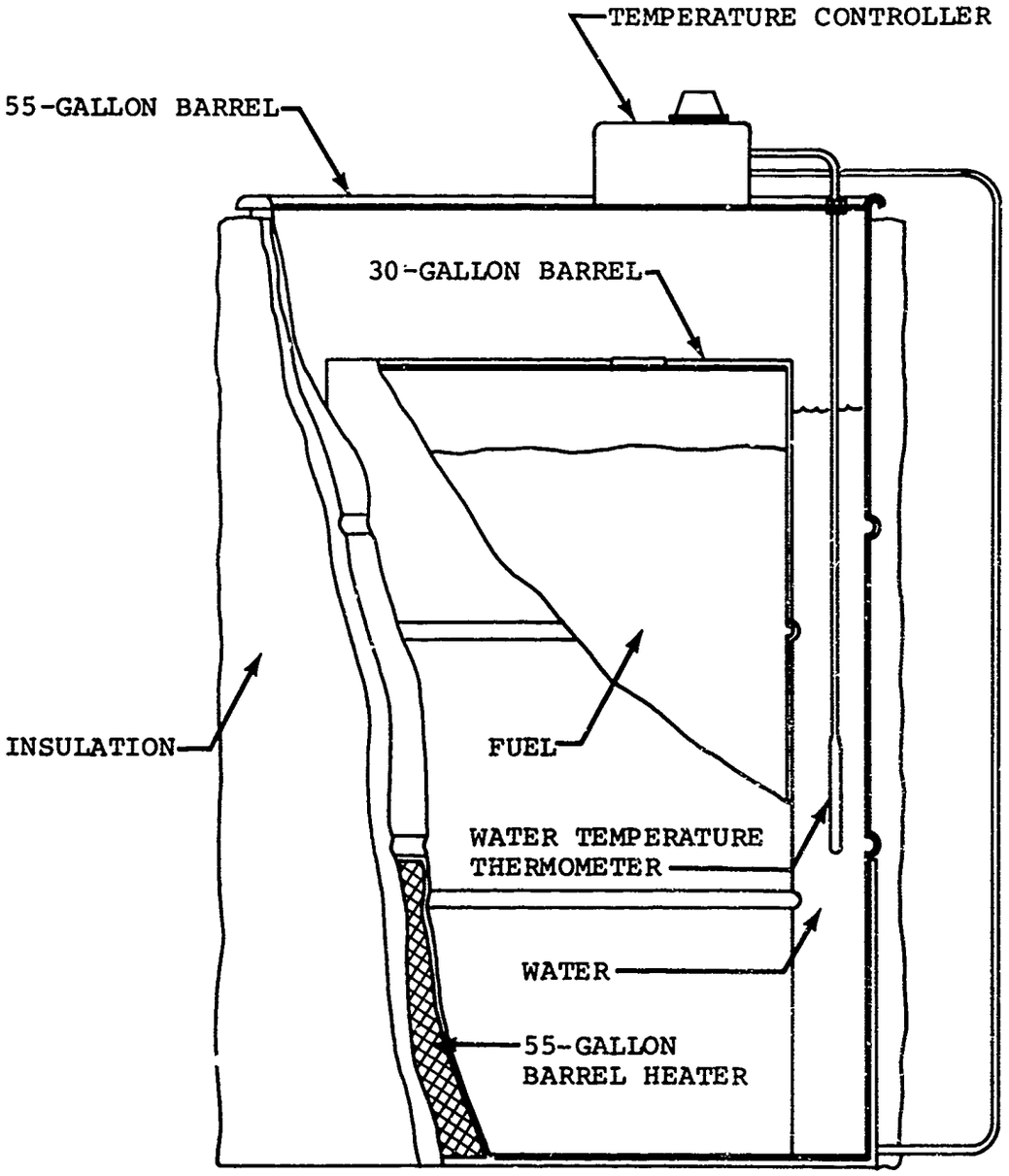


Figure 28. Fuel Temperature Regulation Assembly.


Figure 29. Fuel Temperature Regulation Systems.

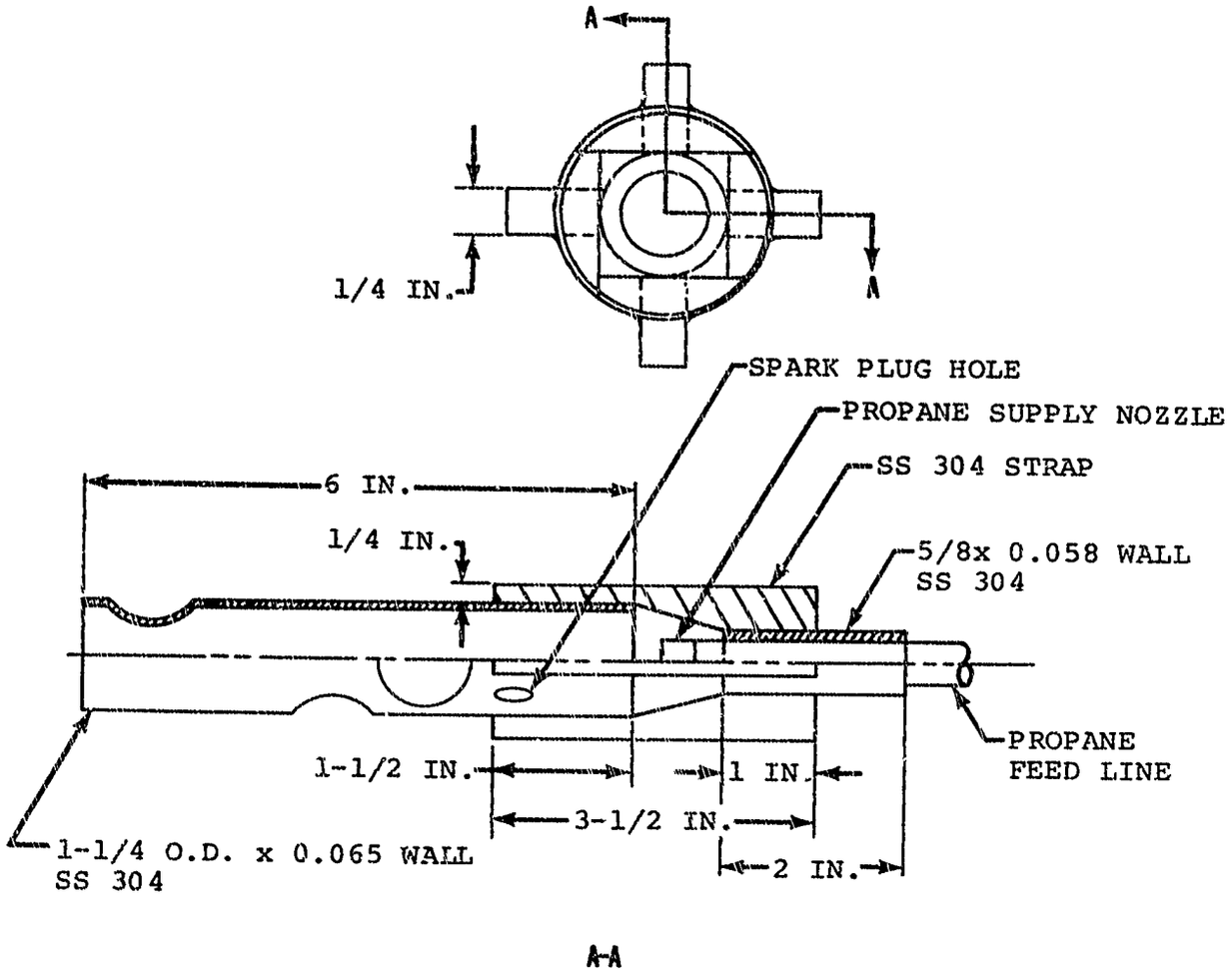


Figure 30. On-Board (Engine Simulator) Igniter Configuration.

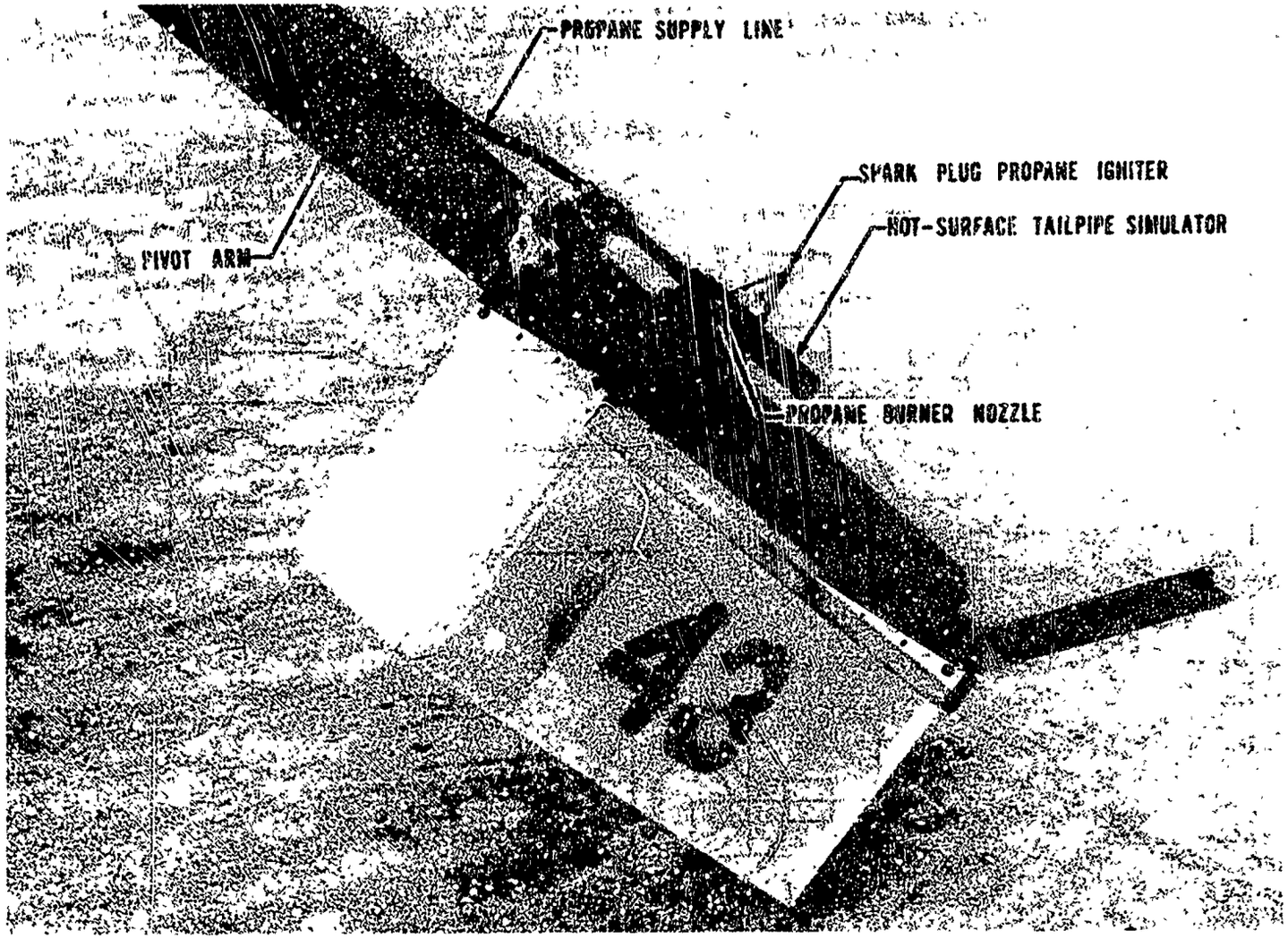


Figure 31. On-Board (Engine Simulator) Igniter Assembly.

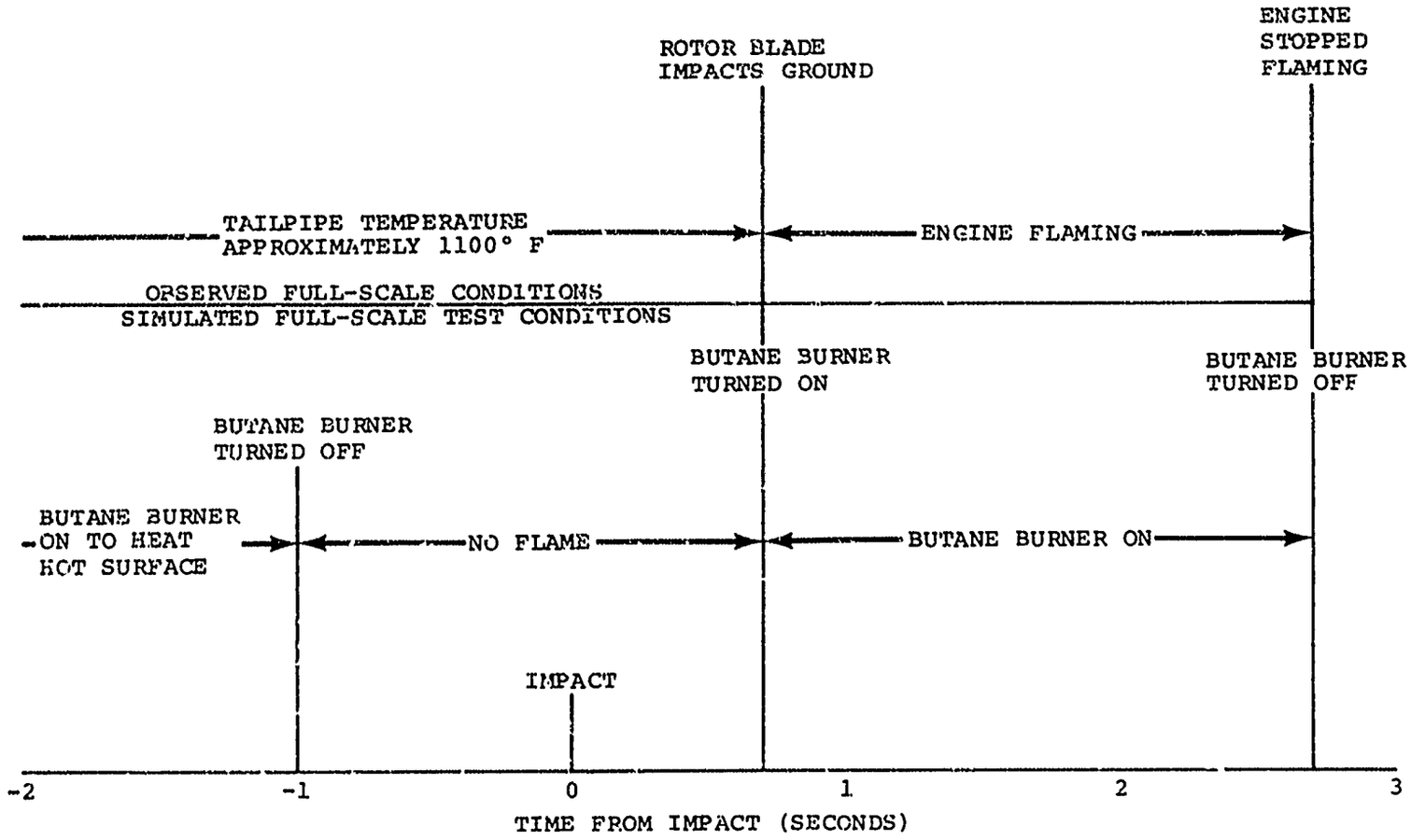


Figure 32. On-Board Ignition Source Sequence.

sustained for 2.0 seconds and then turned off. The time sequencing of this system was obtained with an electric timing device which was triggered at impact. The propane burner was left on prior to impact to keep the simulated tailpipe at the desired temperature. Just prior to impact, a triggering device shut off the propane burner and started the relight cycle. A spark plug was used to ignite the propane burner which was energized concurrently with the propane supply solenoid valve.

## TEST RESULTS

Using the laboratory screening test methodology detailed in the previous section, test data were obtained on five fuels:

1. Referee Grade JP-4
2. JP-4 Base Emulsion EF4R-104
3. JP-4 Base Emulsion EF4R-104H
4. JP-8
5. JP-8 Base Emulsion EF8R-104H

Using the simulated full-scale test methodology detailed in the previous section, test data were obtained on ten fuels:

1. Referee Grade JP-4
2. JP-4 Base Emulsion EF4R-104
3. JP-4 Base Emulsion EF4R-104H
4. JP-4 Base Emulsion JP-4 EXP-4
5. Referee Grade JP-8
6. JP-8 Base Emulsion EF8R-104
7. JP-8 Base Emulsion EF8R-104H
8. Jet-A Base Emulsion Jet-A EXP-4
9. Jet-A Gel #1
10. Jet-A Gel #2

### RESULTS OF NOZZLE SHEAR TESTS

Nozzle shear tests were performed on the five fuels at various flow velocities. Typical flow patterns that resulted from liquid JP-4 or JP-8 are shown in Figures 33 and 34, respectively. For both fuels, the dependence of droplet size on impinging fuel flow velocity is insignificant for the velocities tested.

The typical flow patterns resulting from impinging streams of EF4R-104, EF4R-104H, and EF8-104H fuel emulsions are shown in Figures 35, 36, and 37, respectively. The droplet diameter or

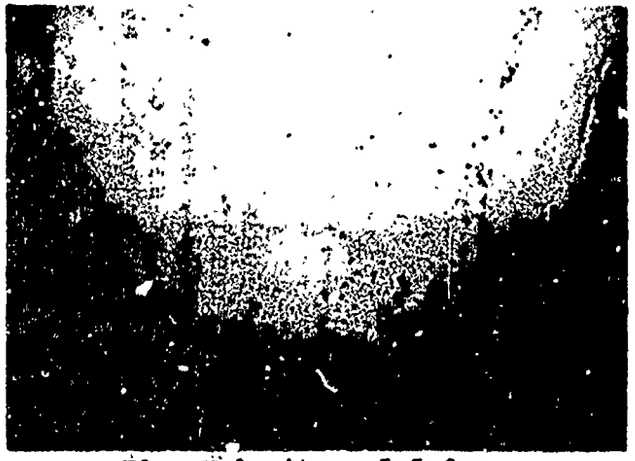

Flow Velocity = 5.5 fps

Flow Velocity = 21.8 fps

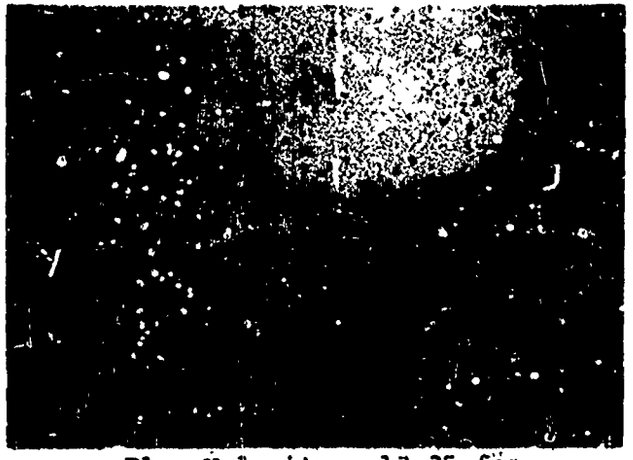

Flow Velocity = 13.35 fps

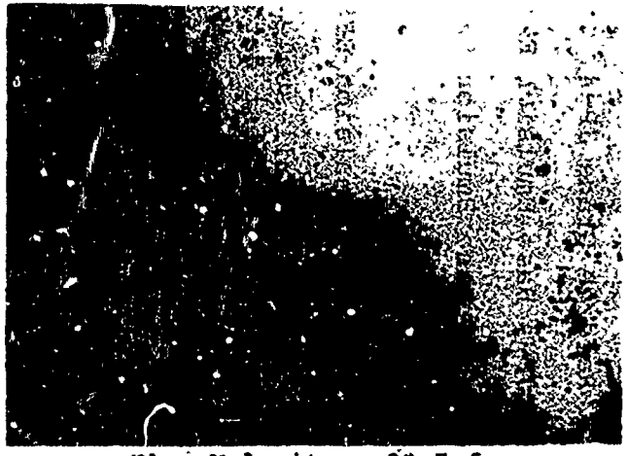

Flow Velocity = 23.7 fps

Figure 33. JP-4 Spray Atomization at Various Flow Velocities.

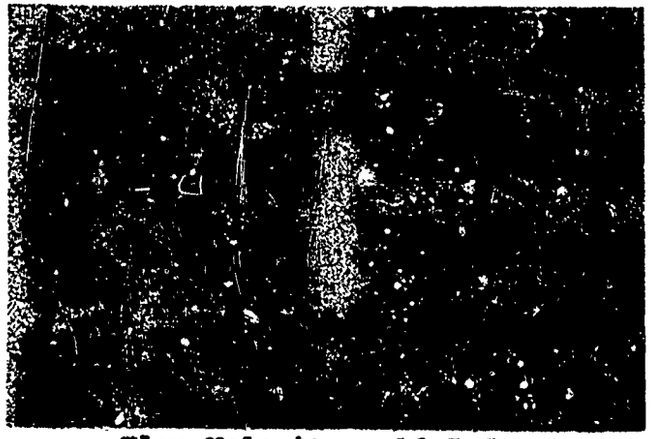

Flow Velocity = 16.7 fps

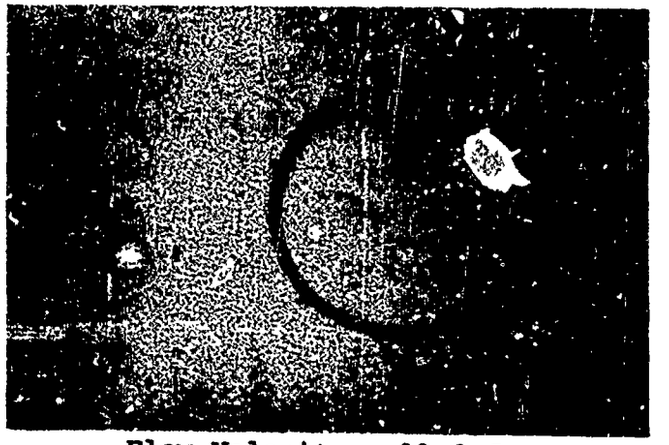

Flow Velocity = 19.8 fps

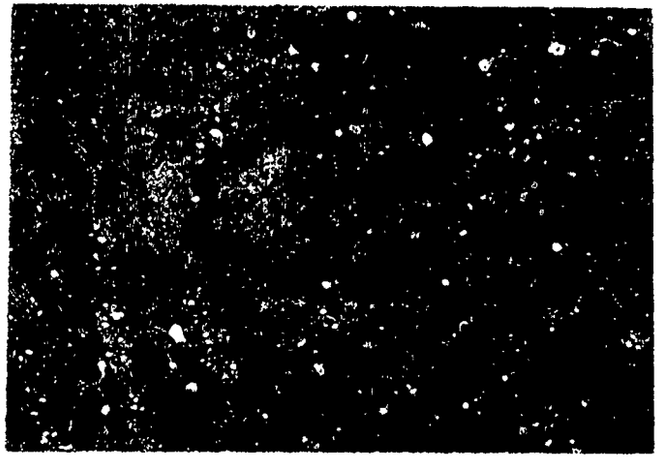

Flow Velocity = 42.7 fps

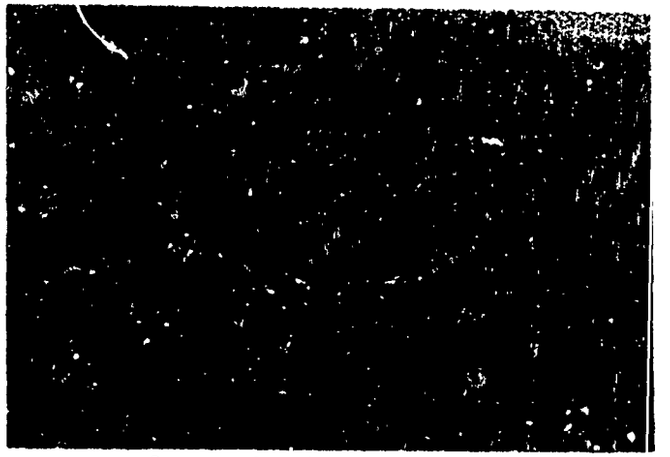

Flow Velocity = 55.3 fps

Figure 34. JP-8 Spray Atomization at Various Flow Velocities.

Flow Velocity = 13.35 fps

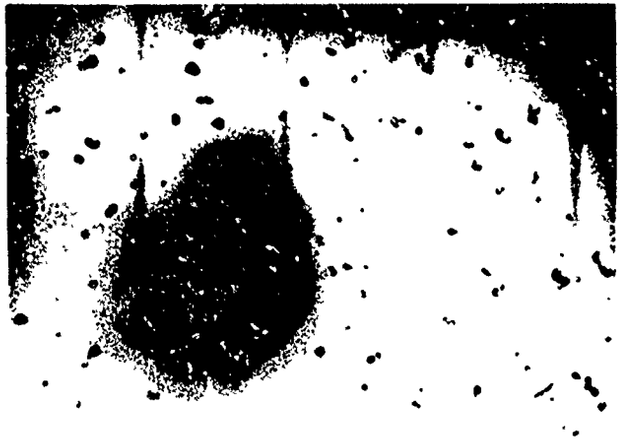

Flow Velocity = 20.5 fps

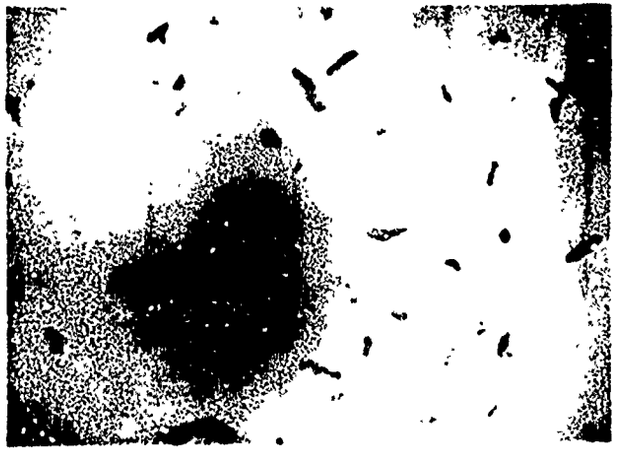

Flow Velocity = 16.05 fps

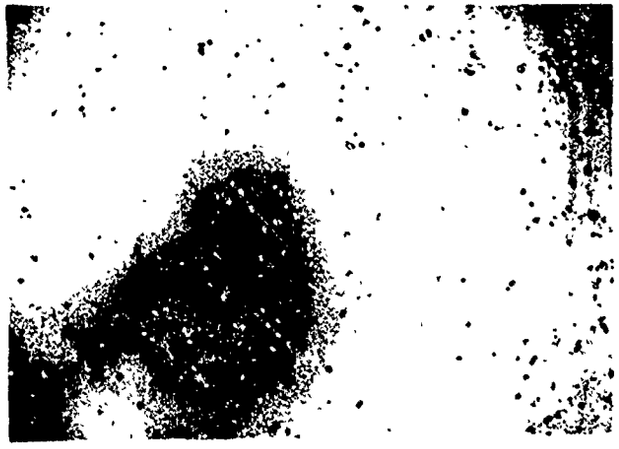

Flow Velocity = 26.0 fps

Figure 35. EF4R-104 Spray Atomization at Various Flow Velocities.

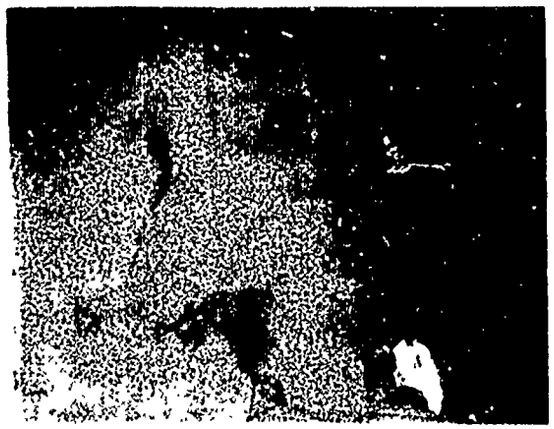

Flow Velocity = 21.8 fps

Flow Velocity = 32.0 fps

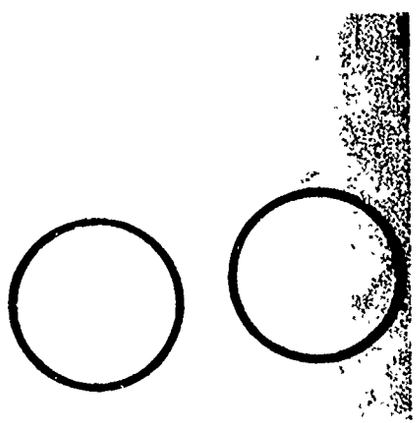

Flow Velocity = 25.0 fps

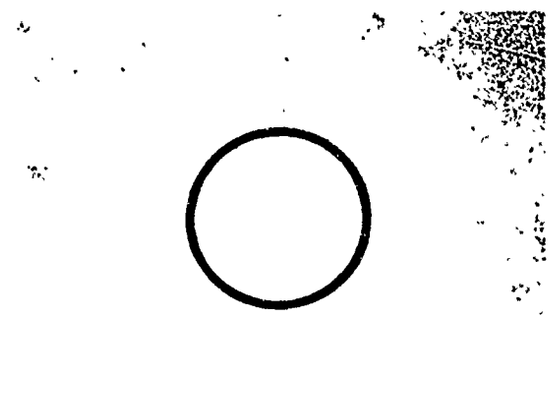

Flow Velocity = 67.0 fps

Figure 36. EF4R-104H Spray Atomization at Various Flow Velocities.

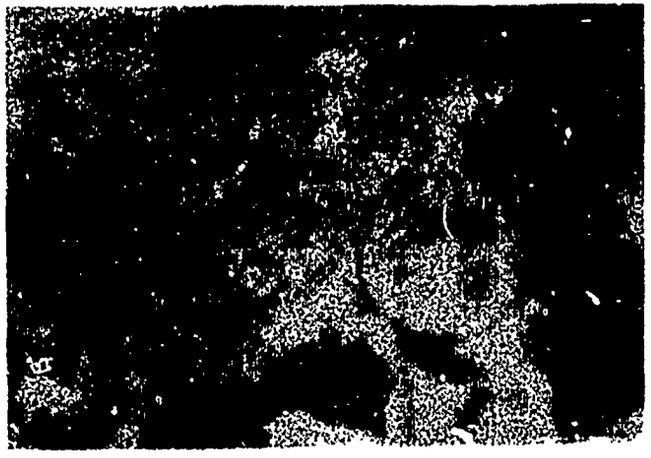

Flow Velocity = 22.1 fps

Flow Velocity = 26.0 fps

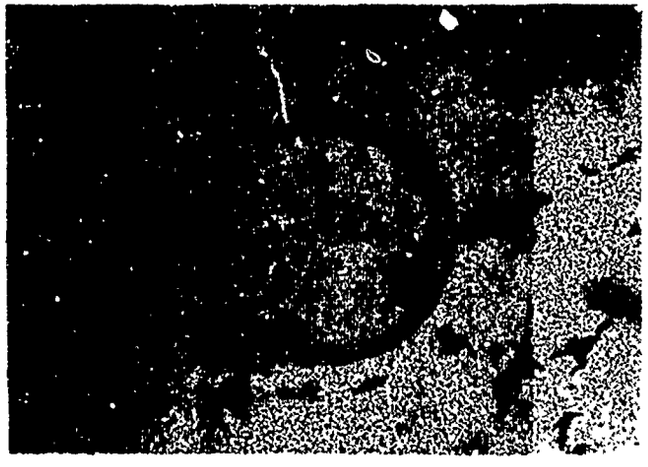

Flow Velocity = 29.4 fps

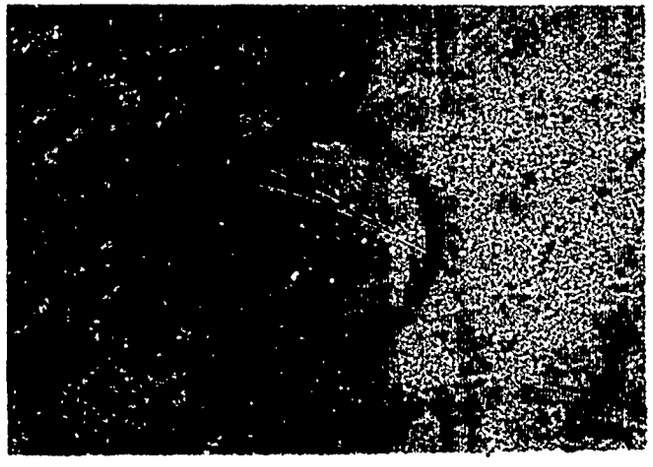

Flow Velocity = 61.7 fps

Figure 37. EF8-104H Spray Atomization at Various Flow Velocities.

characteristic ligament dimensions illustrate a direct dependence upon fuel velocity. It is apparent from comparison of EF4R-104 and EF4R-104H that the breakup is also a function of the emulsified fuel yield stress. It was observed during testing that, for fuel flow velocities less than 20 ft/sec, the emulsions appeared to "creep" out of the nozzle without impinging the lucite surface. For flow velocities greater than 20 ft/sec, the spray consisted mainly of large filaments with smaller ligaments. The particle size approached the liquid sizes as the fuel velocity increased. The measured yield stress was 900 dynes/cm$^2$ for the JP-4 base EF4R-104 emulsion and 1570 dynes/cm$^2$ for the EF4R-104H emulsion. The JP-8 base EF8-104H emulsion measured a yield stress of 800 dynes/cm$^2$.

Figure 38 shows the variation of mean droplet diameter or characteristic ligament size as a function of impinging fuel velocity for both emulsified and liquid fuels. It is observed that there is very little difference between the droplet diameters for the two liquid fuels. The emulsified fuels tend to generate an exponential relation between droplet diameter and fuel velocity. Using the empirical relation discussed in the Test Methodology section,

$$\psi_{\text{Base Fuel}} = \frac{d_{\text{Base Fuel}}}{d_{\text{Fuel}}} = \exp\left\{-\frac{(V_j - V)^2}{K}\right\}, \quad V \quad V_j, \qquad (31)$$

the data presented in Figure 38 can be replotted in terms of an ignition susceptibility parameter ($\psi_{\text{Base Fuel}}$). Figure 39 presents this data correlation ($\psi_{JP-4}$ versus fuel velocity) for JP-4 base EF4R-104 emulsified fuel at a yield stress of 900 dynes/cm$^2$. Using the above equation to fit a mean curve, it was found that ($V_j$) and (K) equalled 73.6 ft/sec and 1203, respectively. It may be observed that the data fit is very good for this type of testing.

Figure 40 presents the results plotted ($\psi_{JP-4}$ versus fuel velocity) for JP-4 base EF4R-104H emulsified fuel with a yield stress of 1570 dynes/cm$^2$. The resulting constants ($V_j$) and (K) were found to equal 82.25 ft/sec and 1345, respectively. In comparing these two fuels, it is apparent that an increase in yield stress decreases the corresponding fuel breakup. Again, the scatter is minimal for this type of testing. Figure 41 presents the corresponding curve for the JP-8 base EF8-104H emulsified fuel. The constants ($V_j$) and (K) were found to be equal to 56.25 ft/sec and 524 respectively at a yield stress of 800 dynes/cm$^2$.

Figures 39, 40, and 41 illustrate the dependence of the emulsified fuel breakup on the fuel impingement velocity. Each fuel

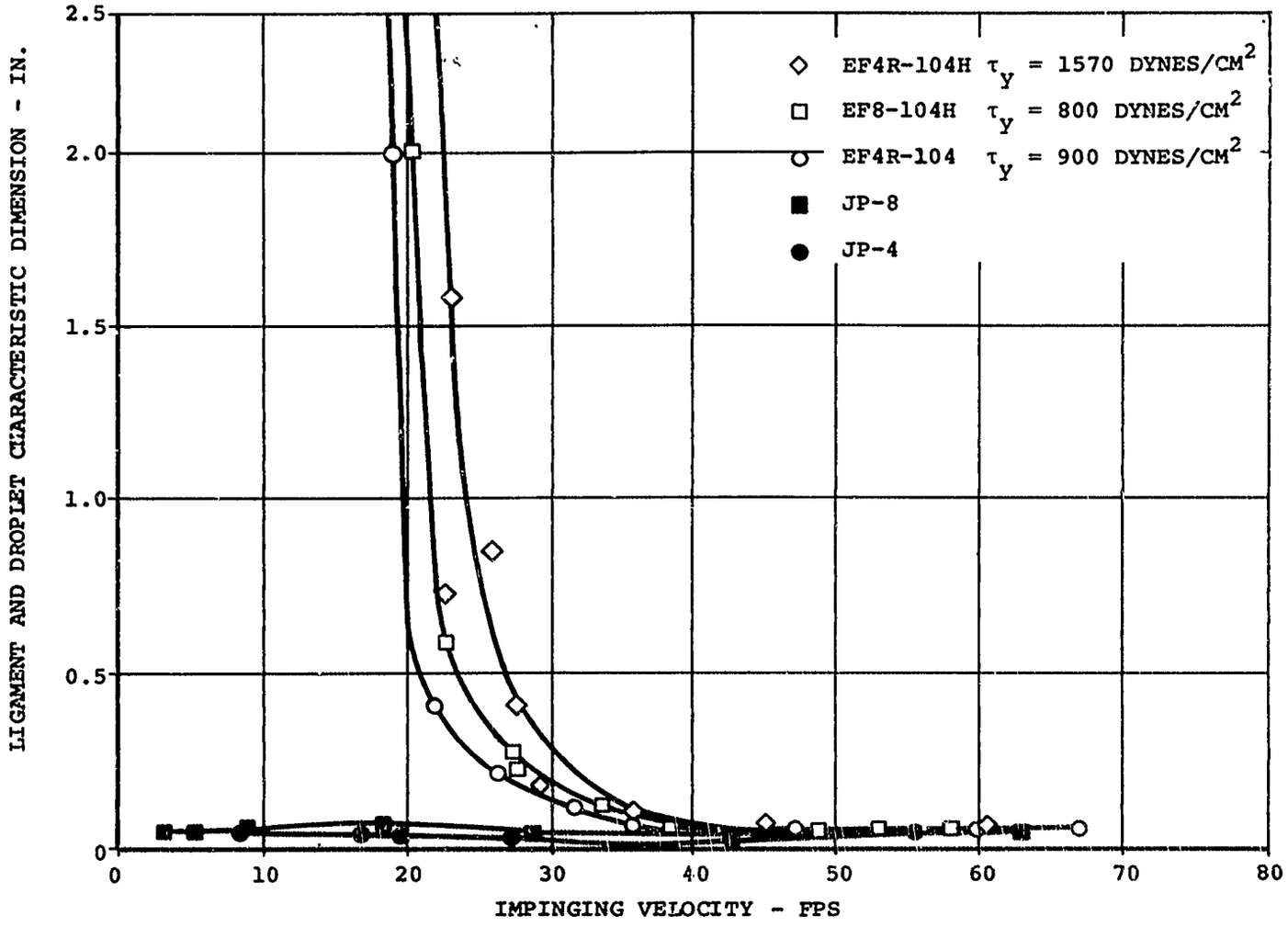


Figure 38. Variation of Ligament and Droplet Characteristic Dimension for Different Fuel Impinging Velocities.

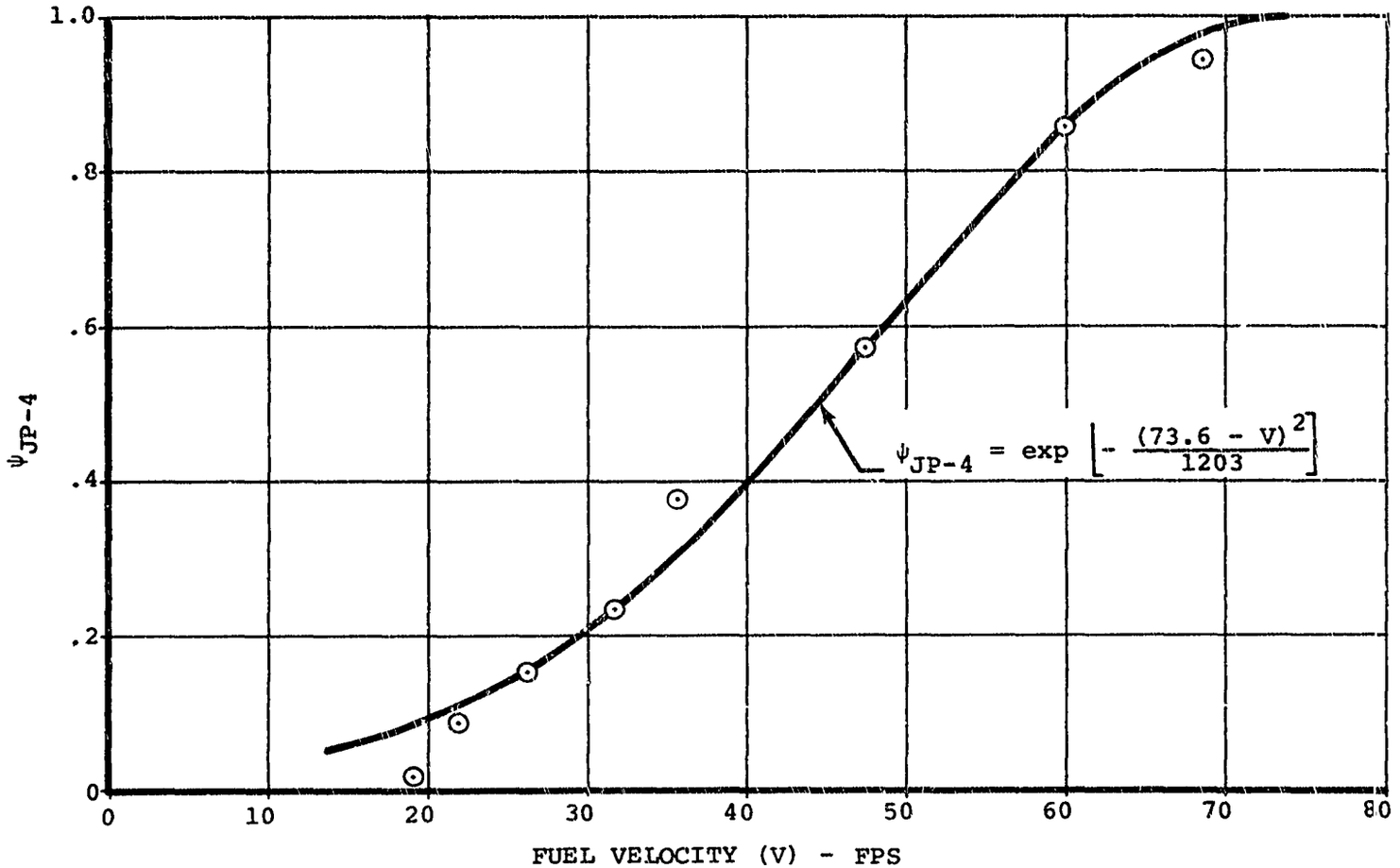


Figure 39. Ignition Susceptibility Parameter Versus Nozzle Shear Fuel Velocity for JP-4 Base Emulsion EF4R-104 ($\tau_y$ = 900 Dynes/cm$^2$).

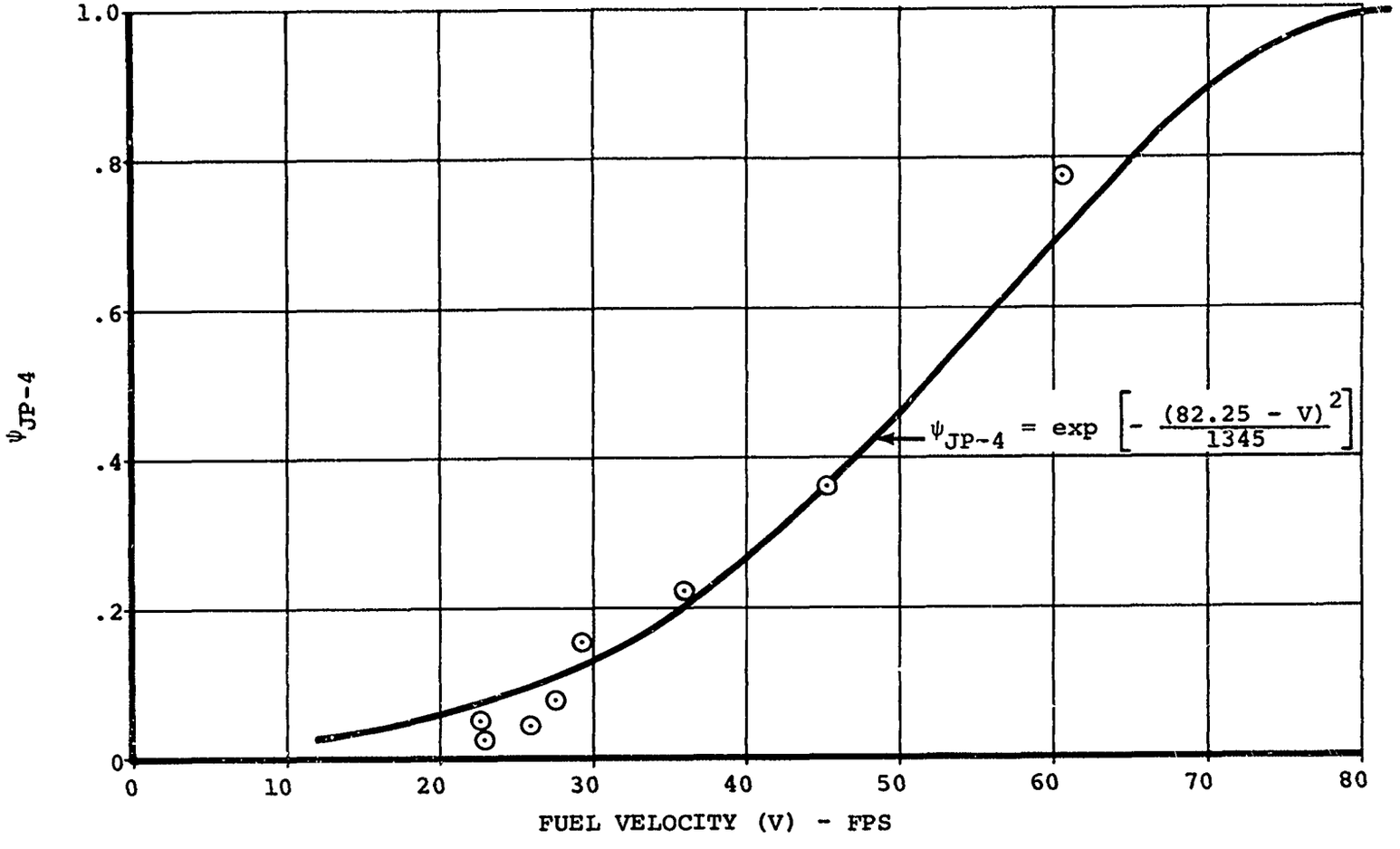


Figure 40. Ignition Susceptibility Parameter Versus Nozzle Shear Fuel Velocity for JP-4 Base Emulsion EF4R-104H ($\tau_y$ = 1570 Dynes/cm$^2$).

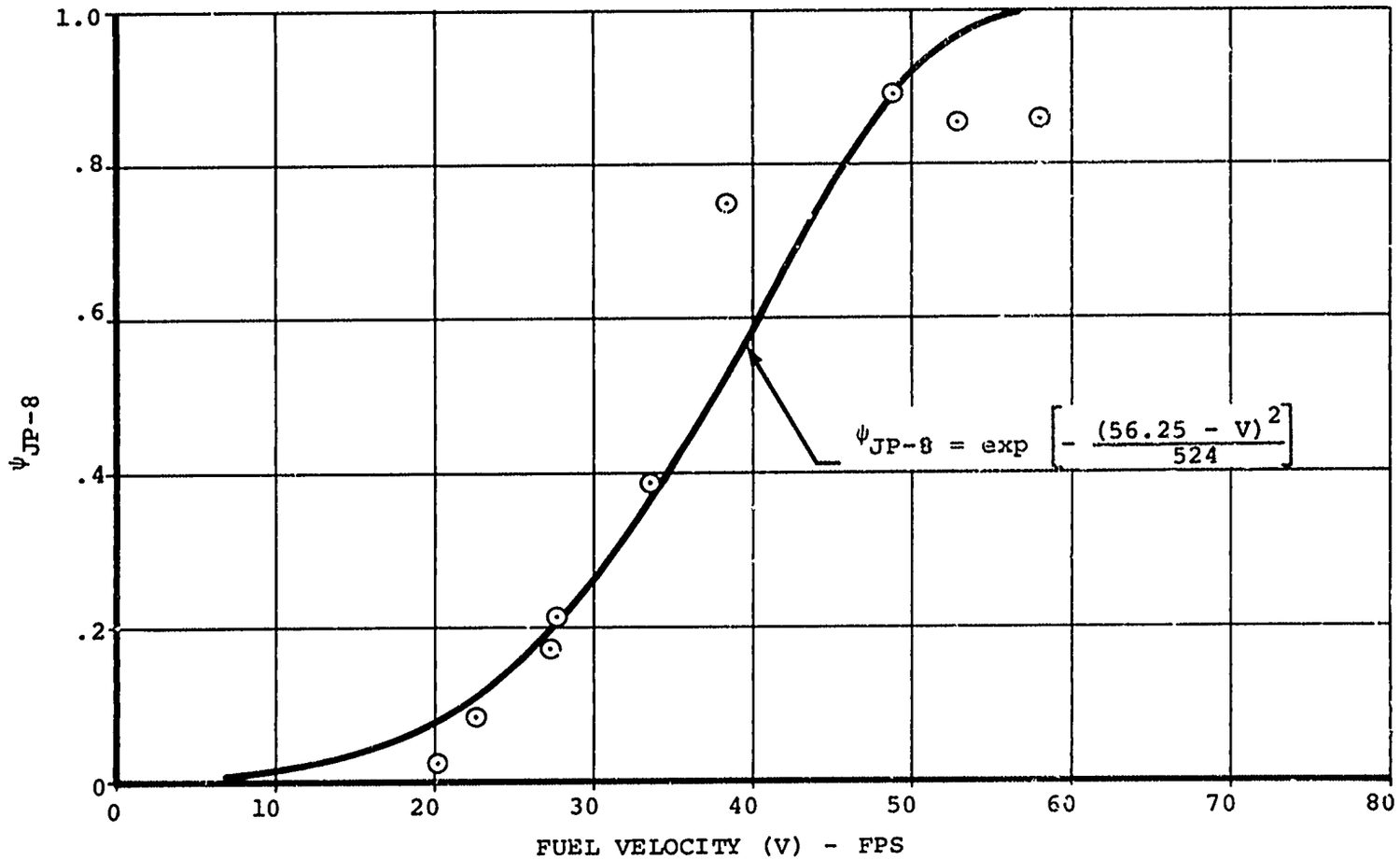


Figure 41. Ignition Susceptibility Parameter Based on JP-8 Versus Nozzle Shear Fuel Velocity for JP-8 Base Emulsion EF8-104H ($\tau_y$ = 800 Dynes/cm$^2$).

was characterized by a velocity at which a sharp decrease in droplet diameter began with a further increase in fuel velocity. The diameter approached the droplet diameters associated with the liquid base fuels. A rational comparison between the EF8-104H emulsion and JP-4 and its emulsions cannot be made unless the ignition susceptibility characteristic between JP-4 and JP-8 is known for the same conditions. As shown in the preceding section, when the base fuel is changed, the constant Q, which is a function of the vapor pressure and diffusion rate, changes. This variation must be known before the comparative ignition susceptibility characteristic between JP-4 and JP-8 can be computed. However, the results show the expected tendencies in that the fuel reaction to an input kinetic energy causes shear loads and, consequently, shear thinning of the emulsions.

## RESULTS OF HOT-SURFACE IGNITION TESTS

Using the methodology discussed previously, hot-surface ignition tests were performed on all five fuels. Figure 42 presents the hot-surface ignition data obtained for referee grade JP-4. The data is presented in terms of crucible temperature (degrees versus ignition delay time (seconds)). The modified mathematical relation discussed under Analytical Considerations was used to generate the curve representing the mean data results illustrated in Figure 42. Here (A) in the equation was found to be $2.342 \times 10^4$, ln k was found to be -20.52, and $t_r$ was equal to 0.9. Using this curve as a mean, the data were found to fall within the 5°F error tolerance incorporated in the test procedures.

Other methods of determining autoignition characteristics for liquid JP-4 have been studied.[7] The results of a dynamic autoignition test on JP-4 are illustrated by the dashed curve in Figure 42. This curve, taken from Reference 7, was obtained using a stainless cylinder with a flow-through fuel-air mixture. It may be observed that the two correlation curves compare favorably. References 6 and 7 indicate a minimum spontaneous ignition temperature of 468°F for JP-4. The test data obtained in this analysis indicate an autoignition temperature approximately 20°F higher than this.

The minimum autoignition temperature for emulsified fuels should not differ greatly from that of their base fuel. The data obtained for the JP-4 emulsions (EF4R-104 and EF4R-104H) indicate this trend. Figure 43 presents the autoignition data generated for the EF4R-104 fuel. Comparing the EF4R-104 data with the mean JP-4 data curves indicates that the emulsion autoignition data approached that obtained from JP-4. The

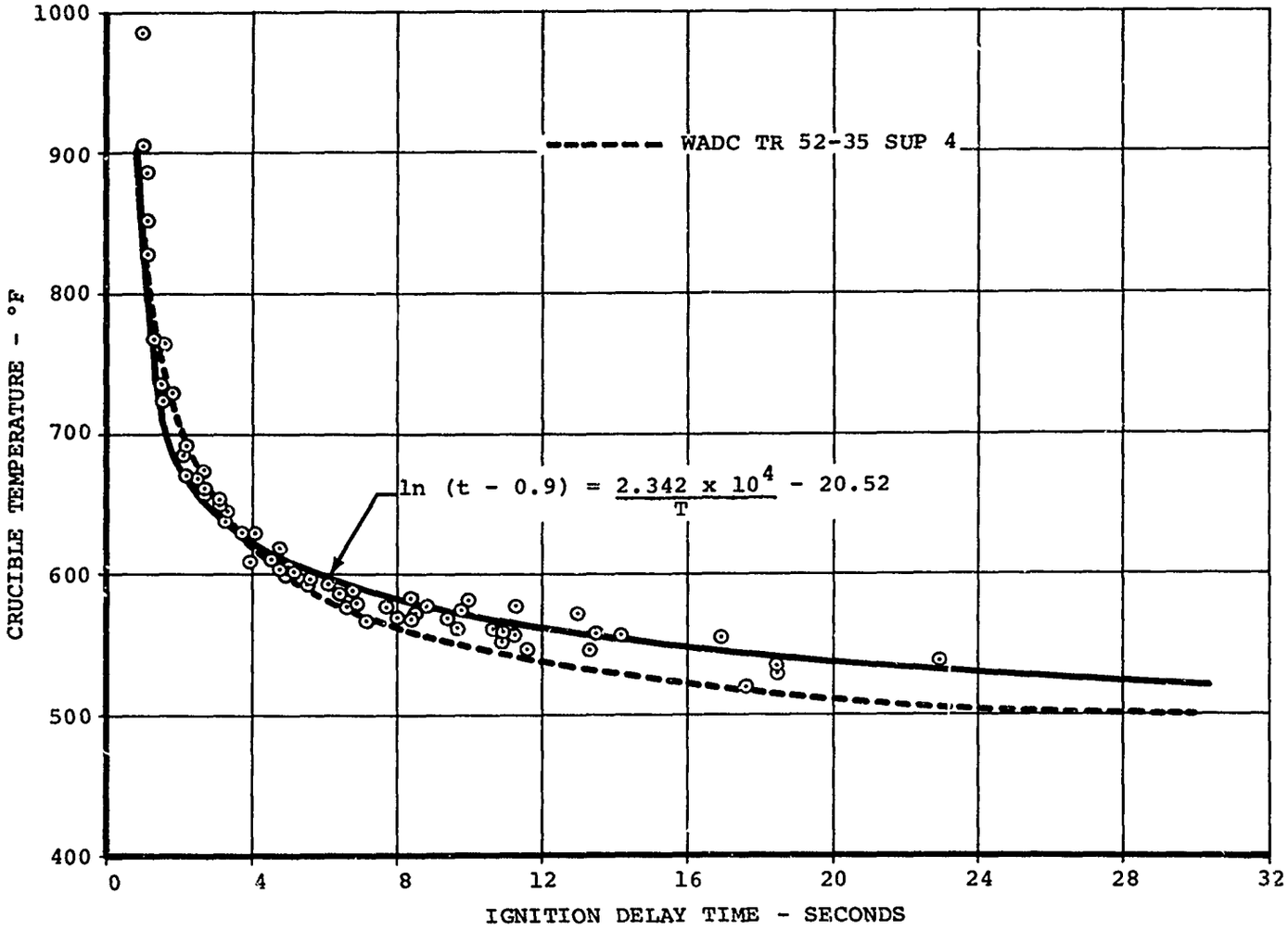


Figure 42. Autoignition Characteristics for Liquid JP-4 Fuel.

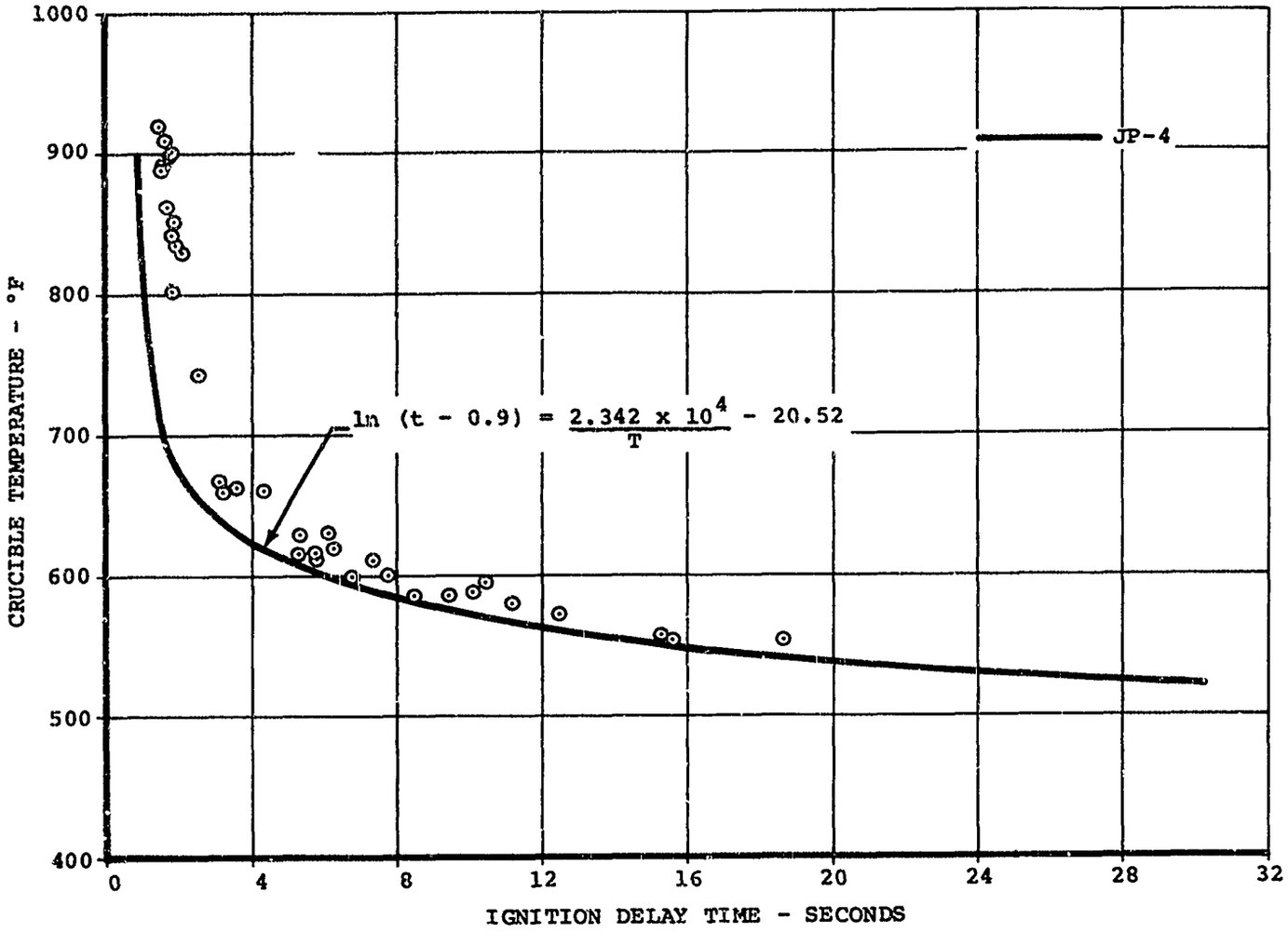


Figure 43. Autoignition Characteristics for JP-4 Base Emulsion EF4R-104 ($\tau_y$ = 509 Dynes/cm$^2$).

EF4R-104 emulsion does, however, indicate a longer ignition delay time of approximately 1.0 second for a given crucible temperature. This effect is to be expected since the water matrix present in the emulsion should change the heat transfer characteristics of the fuel in contact with the hot surface and result in slower fuel vaporization characteristics. The EF4R-104 tests were conducted with a mean yield stress of 509 dynes/$cm^2$, which is representative for this fuel in a near-relaxed state.

Figure 44 presents the autoignition data obtained from the EF4R-104H emulsion. Like that of EF4R-104, the autoignition temperature curve approaches that obtained for JP-4. Likewise, the ignition delay time is found to be longer for a given crucible temperature by about 1.0 second. It is noted, however, that the EF4R-104H emulsion curve approached the JP-4 curve at a higher temperature than the EF4R-104 emulsion. This might possibly be due to the higher yield stress (1153 dynes/$cm^2$) which is characteristic of the relaxed EF4R-104H fuel. The water matrix of the EF4R-104H surrounds smaller fuel globs; therefore, the thermal boundary layer is thinner and yields higher heat transfer rates. However, it is noted that this is only a hypothesis since this effect is not conclusively established by the data.

Vaporization and subsequent ignition are functions of various fuel properties such as hydrocarbon composition, diffusion rates, and heat transfer coefficient. The JP-8 fuel has a different hydrocarbon mixture than JP-4. The results of ignition tests on JP-8 are indicated in Figure 45 together with the mean autoignition curve for JP-4. Not only did the minimum autoignition temperature decrease, but the ignition delay time was much less for the JP-8 fuel. The indicated minimum autoignition temperature was approximately 40°F lower than for JP-4 or, from extrapolation, was 448°F. This lowering of the overall autoignition temperatures was contrary to expectations based on the ignition and fuel/air ratio data generated in the wind shear and impact dispersion/atomization tests as well as those based on the relative vapor pressure values (0.35 psi for JP-8 as compared to 3.0 psi for JP-4). All indications were that JP-8 was difficult to ignite at normal ambient temperatures. However, for the elevated temperatures used in the hot-surface tests, the data of Figure 45 show that JP-8 is a more easily ignitable fuel than JP-4.

Figure 46 presents the autoignition characteristics obtained from testing the EF8-104H emulsion. The data obtained for this fuel had considerable scatter. There appeared to be a temperature range between 600° and 800°F in which the autoignition

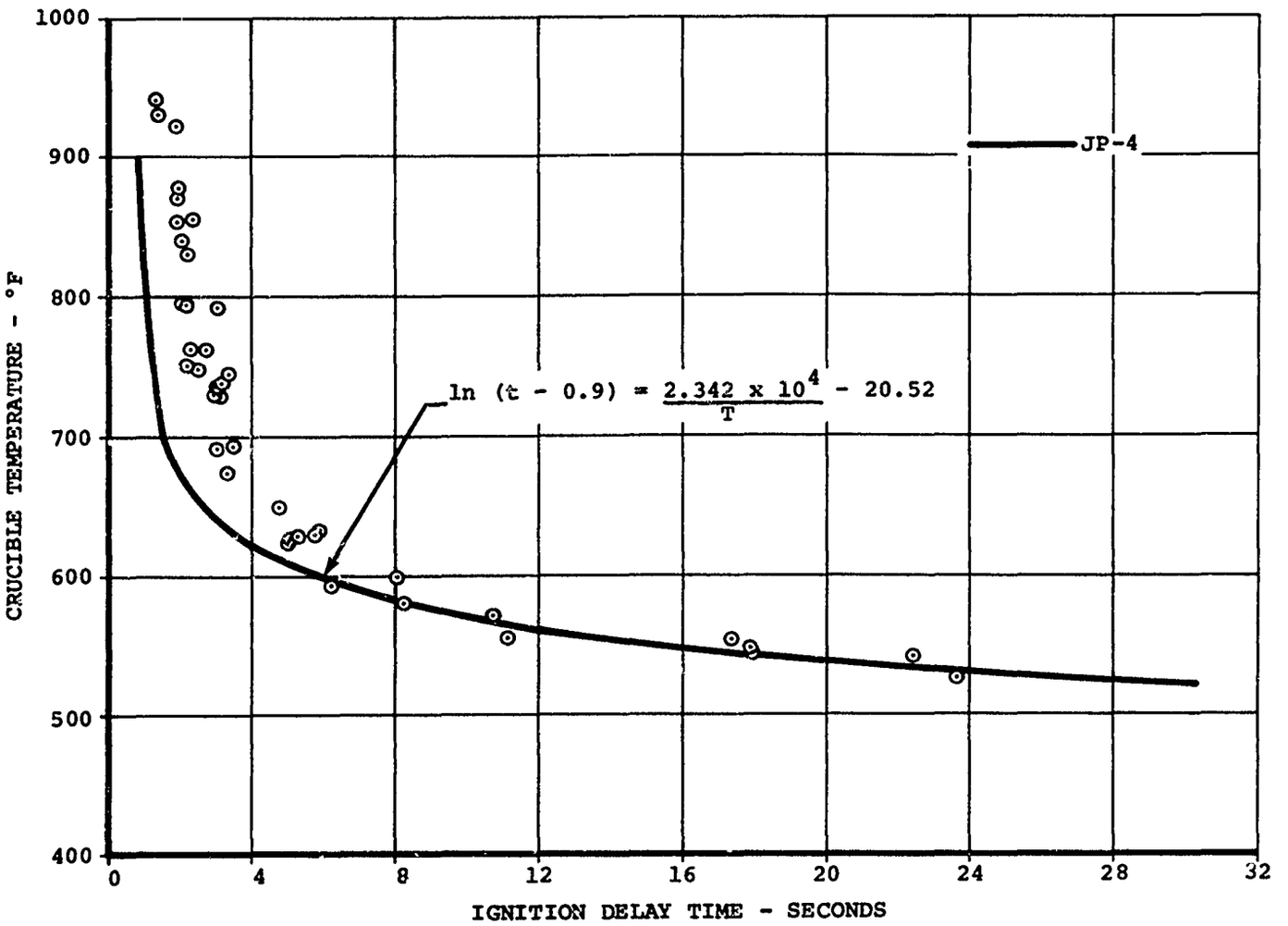


Figure 44. Autoignition Characteristics for JP-4 Base Emulsion EF4R-104H ($\tau_y$ = 1153 Dynes/cm$^2$).

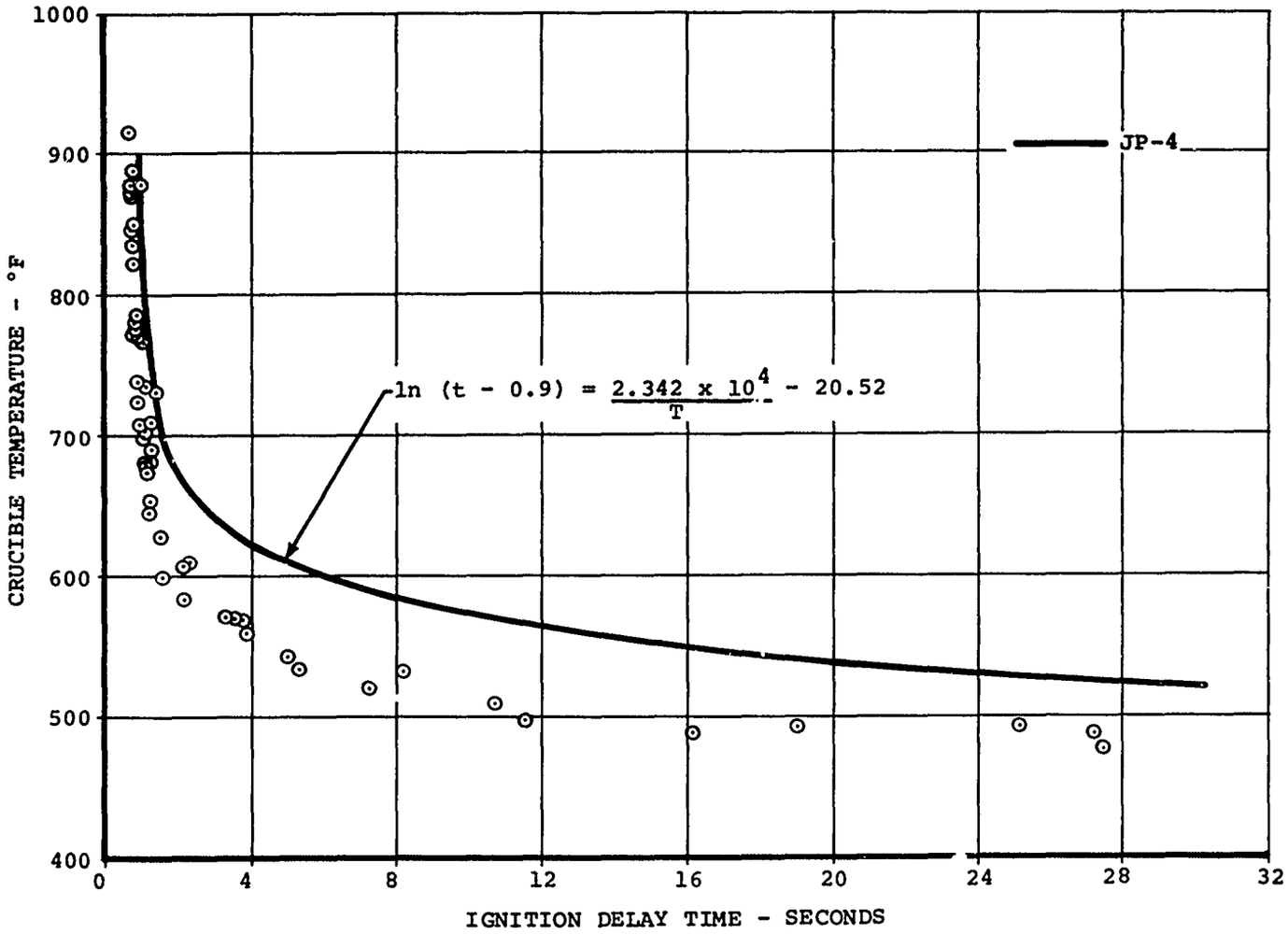


Figure 45. Autoignition Characteristics for Liquid JP-8 Fuel.

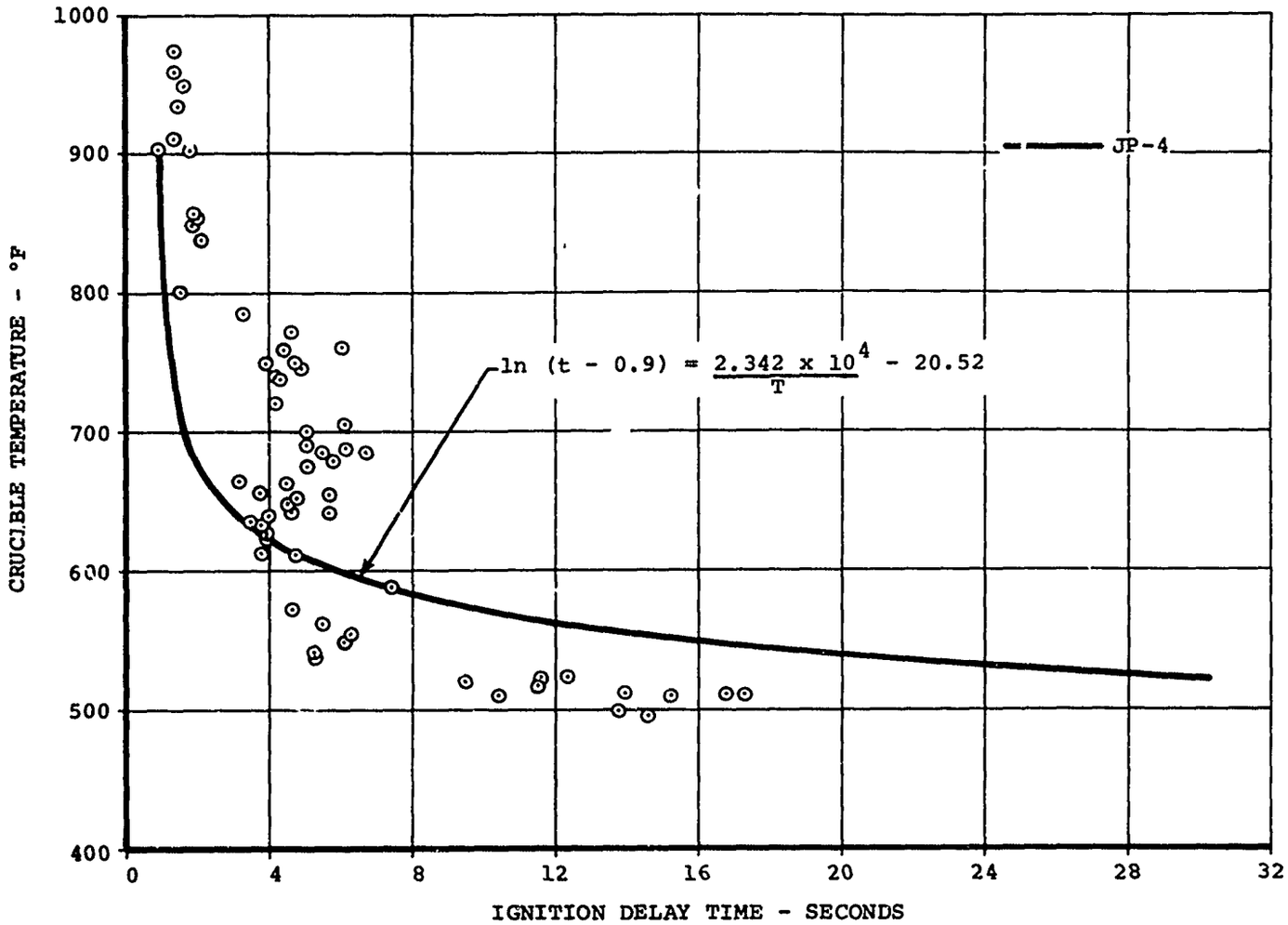


Figure 46. Autoignition Characteristics for JP-8 Base Emulsion EF8-104H ($\tau_y$ = 750 Dynes/cm$^2$).

behavior deviated from the characteristic trends of liquid or previously tested emulsified fuels. One explanation for the results obtained is that the EF8-104H emulsified fuel developed sporadic outgassing at the fuel/hot-surface interface, causing heat transfer delays in this temperature range. Once the temperature was dropped to below 600°F, the autoignition characteristics followed the expected trend and approached the JP-8 autoignition characteristics. As with the JP-4 emulsions, the ignition delay time for the JP-8 emulsion increased when compared to the base fuel.

It was observed that the emulsified fuels, in general, possessed more data scatter than their liquid base fuels. This is probably due to their more complicated structure.

RESULTS OF WIND SHEAR TESTS

Wind shear tests were performed on referee grade JP-4, JP-4 base emulsion EF4R-104, JP-4 base emulsion EF4R-104H, JP-8, and JP-8 base emulsion EF8-104H. The test wind velocities ranged from 30 to 120 ft/sec, enveloping the approximate maximum crash survivable velocity of 65 ft/sec. In all tests the fuel was injected into the airstream at 10 ft/sec. Wind shear test conditions and data results from each test are presented in Appendix I.

No fuel or velocity combination was found which would ignite with the spark ignition probes due to the absence of a combustible fuel/air ratio. It should be borne in mind, however, that this is a facility characteristic and does not necessarily lead to a noncombustible conclusion for a full-scale condition where much more fuel is involved. More important, however, are the relative trends developed in these tests in which the fuels performance is compared to the JP-4 standard.

Using the data correlation results obtained previously (Analytical Considerations), the droplet diameter and fuel/air ratio data are presented in terms of $\psi$, where

$$\psi_{\text{Base Fuel}} = \frac{(F/A)_{\text{Fuel}}}{(F/A)_{\text{Base Fuel}}} = \frac{d_{\text{Base Fuel}}}{d_{\text{Fuel}}} \qquad (32)$$

Basically, two types of test data were measured for fuel crashworthiness performance. These consisted of mean fuel/air ratio data and photographic data of the breakup, atomization, and dispersion of the fuels versus wind velocity. Photographic data were obtained from four cameras. The most important photographic data were obtained with the microphotographic

camera where actual fuel droplet diameters were determined. The full-view still camera gave secondary data results as to fuel flow characteristics. The data obtained from the two motion cameras were used to back up the droplet diameter data and indicate any trends not observed with the other types of data systems.

Figures 47 and 48 show the fuel droplet breakup for referee grade JP-4 fuel just downstream of the injection point. The fuel was injected at 10 ft/sec into the airstream at velocities of 40 and 80 ft/sec, respectively. Both figures show high amounts of breakup and dispersion for JP-4 with the mean droplet size being reduced slightly as the velocity increases. Figures 49 and 50 show the results from the full-view still camera for the same JP-4 tests and illustrate the overall flow pattern of the wind shear mechanism.

Figures 51 through 55 illustrate a sequence of tests performed on EF4R-104 emulsified fuel with yield stresses ranging from 400 to 500 dynes/cm$^2$. The five figures illustrate the breakup and dispersion characteristics of EF4R-104 emulsion when it was injected into a 40 to 100 ft/sec wind flow field. For the lower velocities, no breakup is visible and the fuel stays in a continuous strand. As the velocity is increased, small amounts of breakup and atomization are visible. At 100 ft/sec, the breakup and atomization are still small compared to liquid JP-4 at the same wind velocity. Even the smaller particles are still in an emulsified state. Figures 56 and 57 show the full view of the EF4R-104 fuel during wind shear for wind shear velocities of 60 and 100 ft/sec. These figures further illustrate the breakup susceptibility as the wind shear velocity increases.

To study the effects of yield stress on the breakup and atomization characteristics, the EF4R-104 emulsified fuel was worked to a yield stress of approximately 1200 dynes/cm$^2$ and tested at various wind shear velocities. Figures 58, 59, and 60 show the accompanying fuel-air flow field at wind velocities of 60, 80, and 100 ft/sec. It can be seen that the fuel breakup is less pronounced than the data shown in Figures 56 and 57. This indicates a potential increase in safety with increasing yield stress.

Figures 61 through 67 illustrate a sequence of tests performed on EF4R-104H emulsified fuel with an average yield stress of 1733 dynes/cm$^2$ for wind velocities from 50 to 120 ft/sec. It is evident that less breakup occurs with the higher yield stress of this fuel. Figures 68, 69, and 70 show photographs of EF4R-104H emulsified fuel which has been worked to a yield

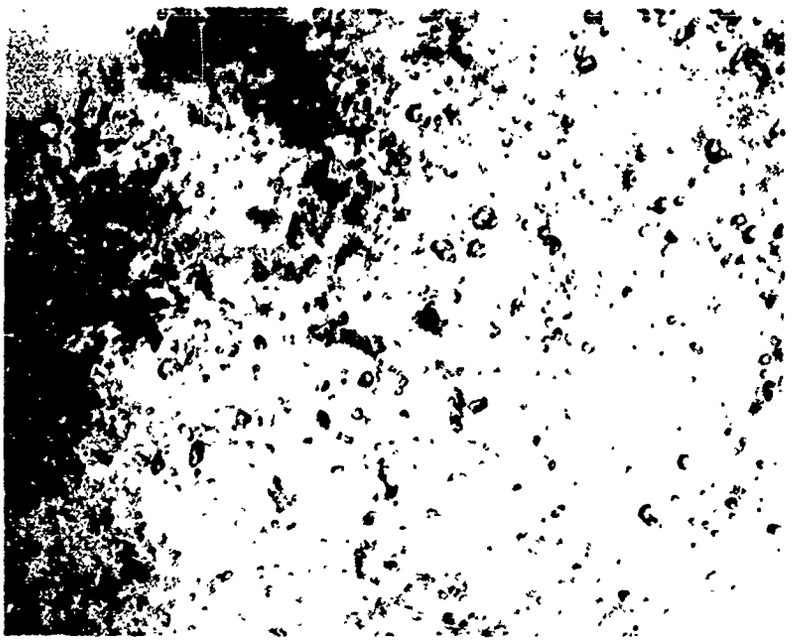

Figure 47. JP-4 Wind Shear Breakup, Wind Velocity = 40 fps.

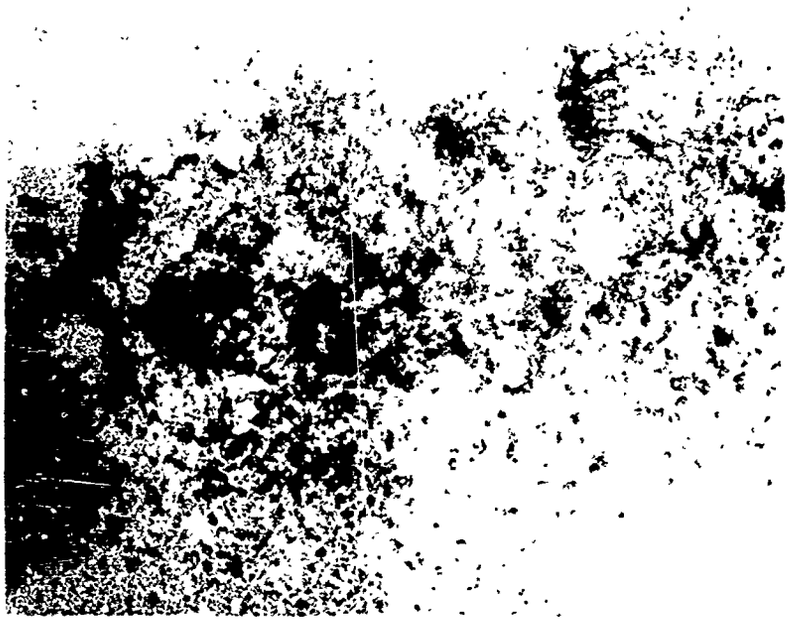

Figure 48. JP-4 Wind Shear Breakup, Wind Velocity = 80 fps.

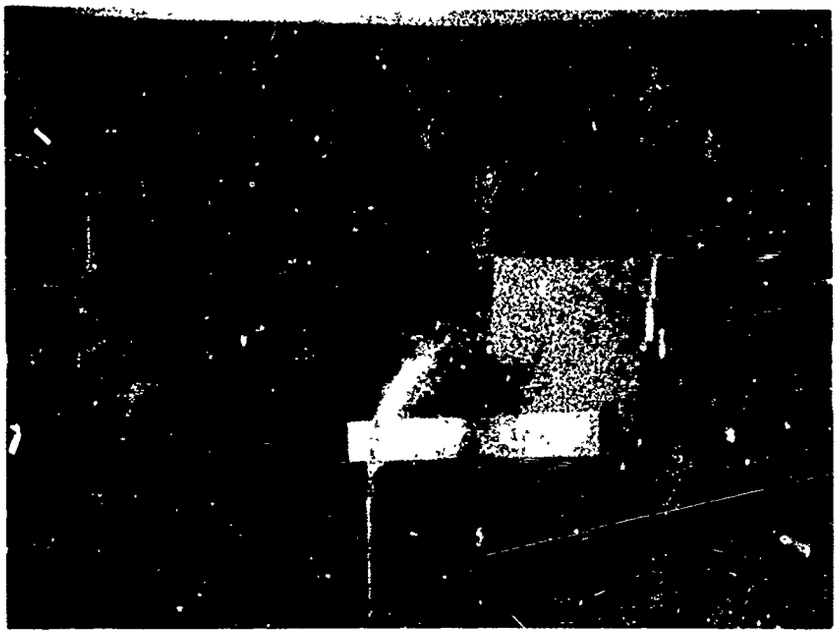

Figure 49. JP-4 Wind Shear/Fuel Flow Field, Wind Velocity = 40 fps.

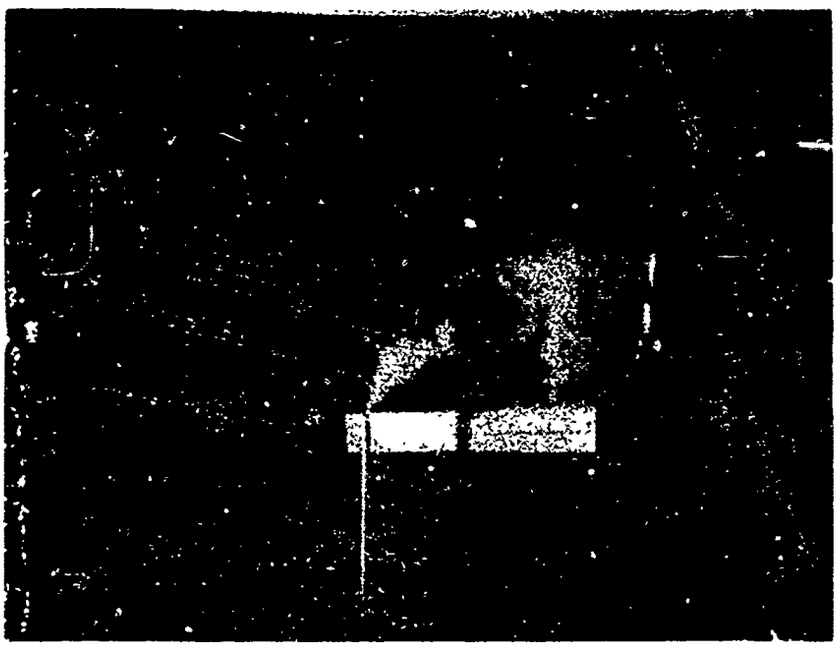

Figure 50. JP-4 Wind Shear/Fuel Flow Field, Wind Velocity = 80 fps.

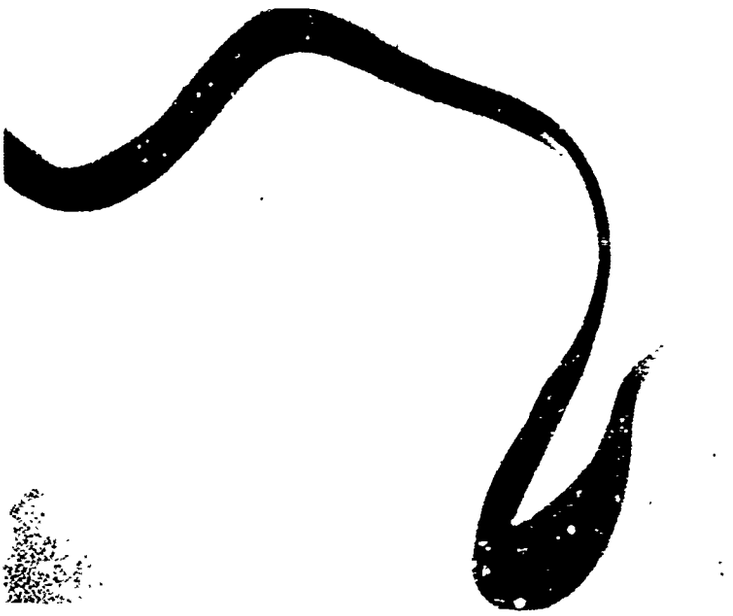

Figure 51. EF4R-104 Wind Shear Breakup, Wind Velocity = 40 fps ($\tau_y$ = 475 Dynes/cm$^2$).

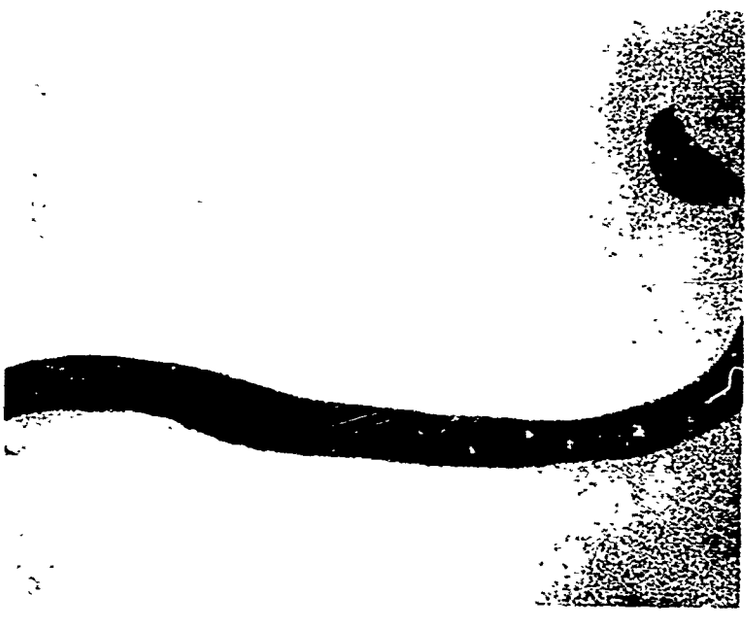

Figure 52. EF4R-104 Wind Shear Breakup, Wind Velocity = 50 fps ($\tau_y$ = 475 Dynes/cm$^2$).

Figure 53. EF4R-104 Wind Shear Breakup, Wind Velocity = 60 fps ($\tau_y$ = 475 Dynes/cm$^2$).

Figure 54. EF4R-104 Wind Shear Breakup, Wind Velocity = 70 fps ($\tau_y$ = 475 Dynes/cm$^2$).

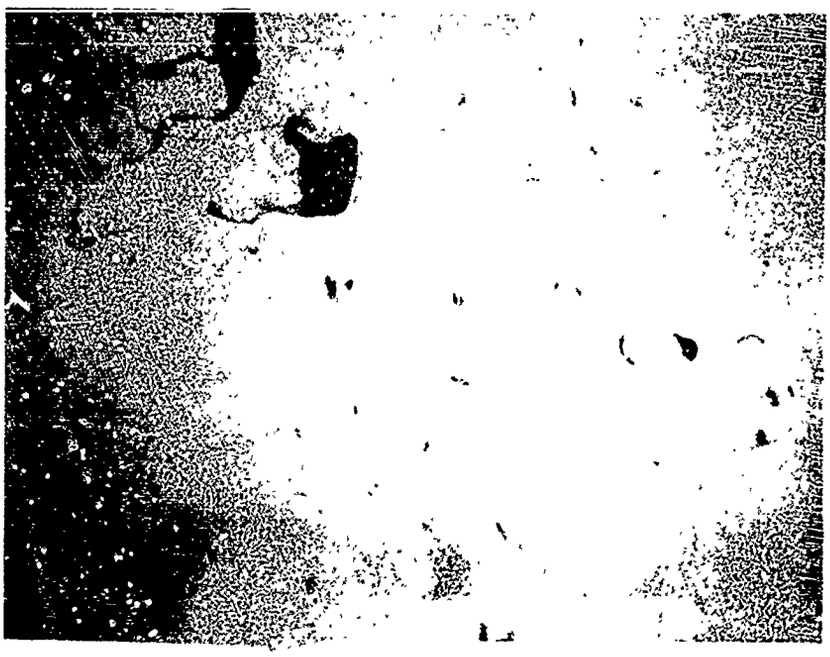

Figure 55. EF4R-104 Wind Shear Breakup, Wind Velocity = 100 fps ($\tau_y$ = 400 Dynes/cm$^2$).

Figure 56. EF4R-104 Wind Shear/Fuel Flow Field, Wind Velocity = 60 fps ($\tau_y$ = 600 Dynes/cm$^2$).

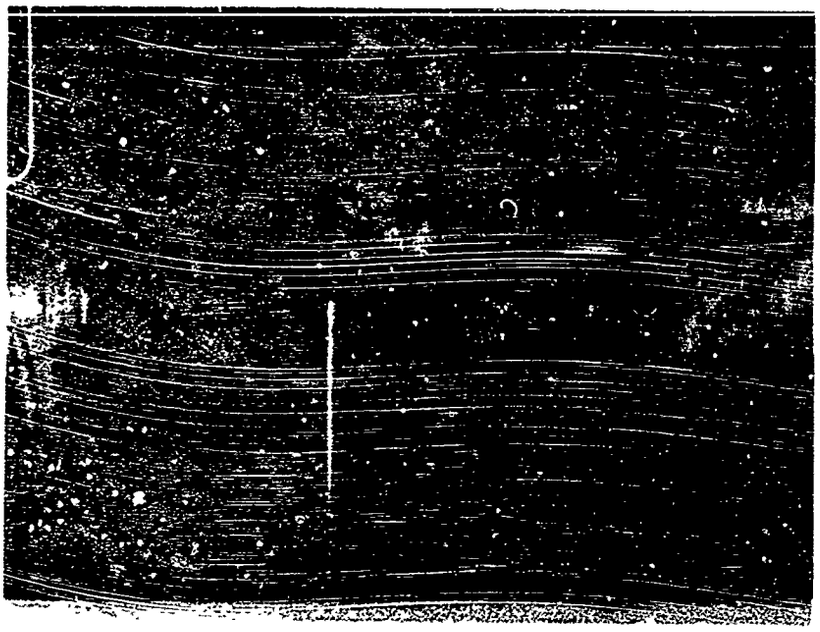

Figure 57. EF4R-104 Wind Shear/Fuel Flow Field, Wind Velocity = 100 fps ($\tau_y$ = 600 Dynes/cm$^2$).

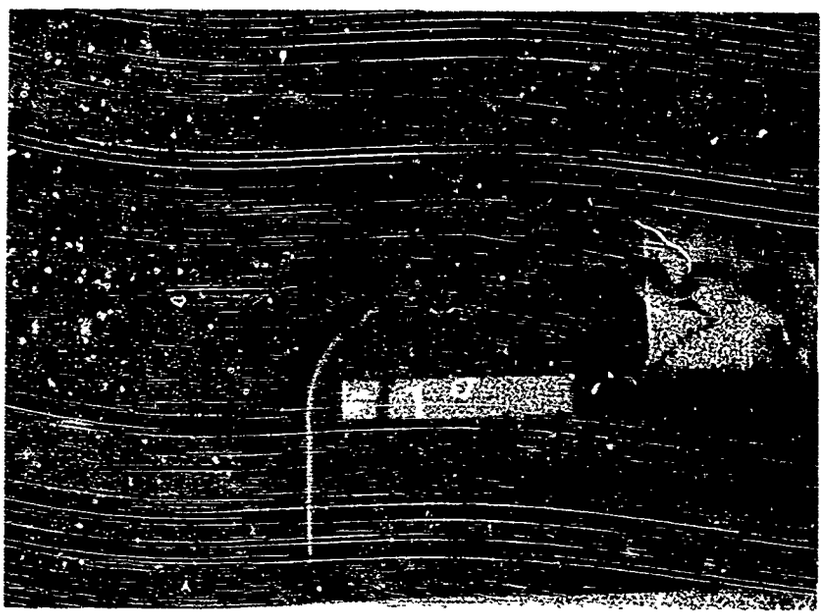

Figure 58. EF4R-104 Wind Shear/Fuel Flow Field, Wind Velocity = 60 fps ($\tau_y$ = 1200 Dynes/cm$^2$).

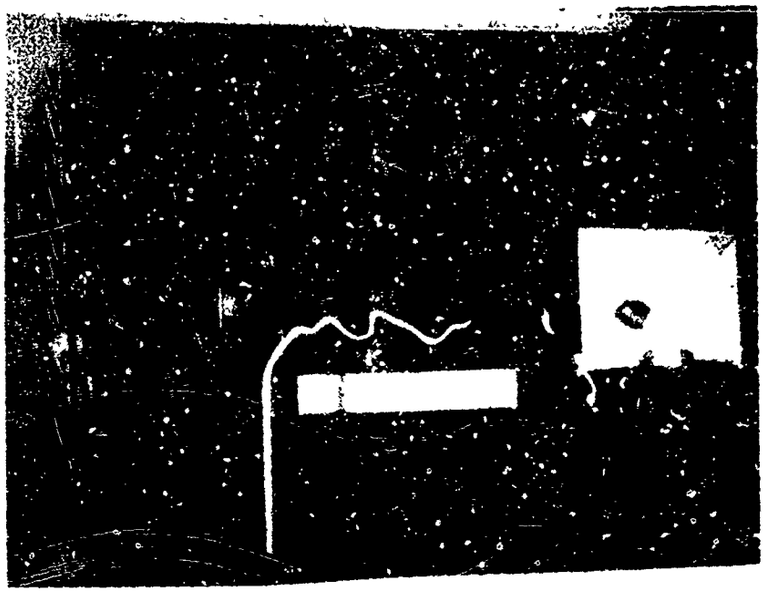

Figure 59. EF4R-104 Wind Shear/Fuel Flow Field, Wind Velocity = 80 fps ($\tau_y$ = 1300 Dynes/cm$^2$).

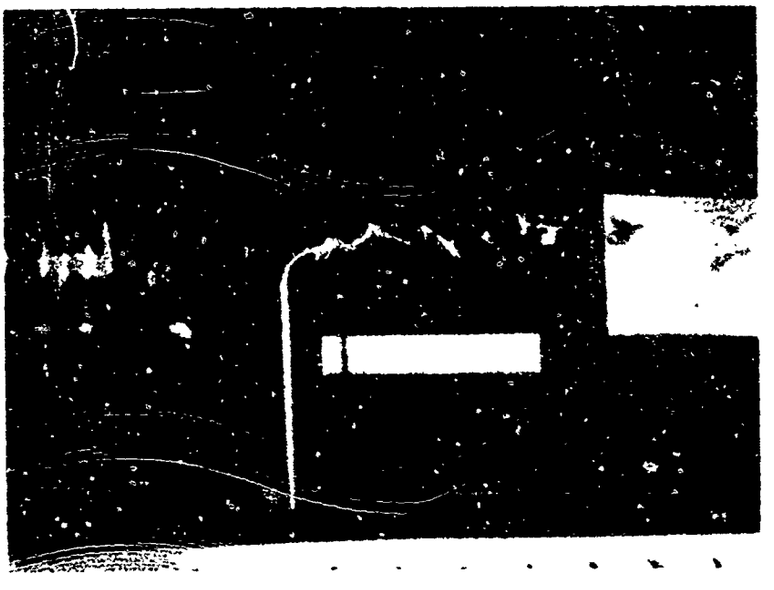

Figure 60. EF4R-104 Wind Shear/Fuel Flow Field, Wind Velocity = 100 fps ($\tau_y$ = 1050 Dynes/cm$^2$).

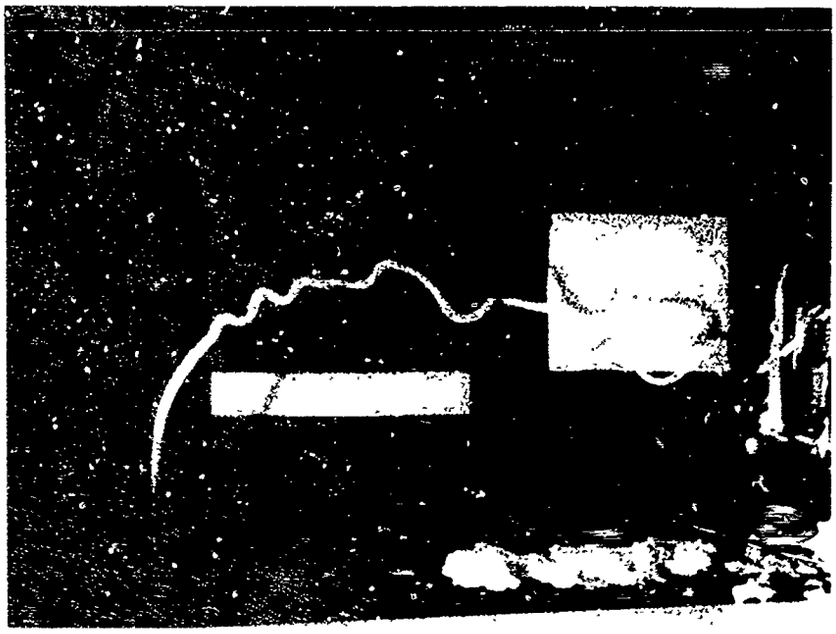

Figure 61. EF4R-104 Wind Shear/Fuel Flow Field, Wind Velocity = 50 fps ($\tau_y$ = 1733 Dynes/cm$^2$).

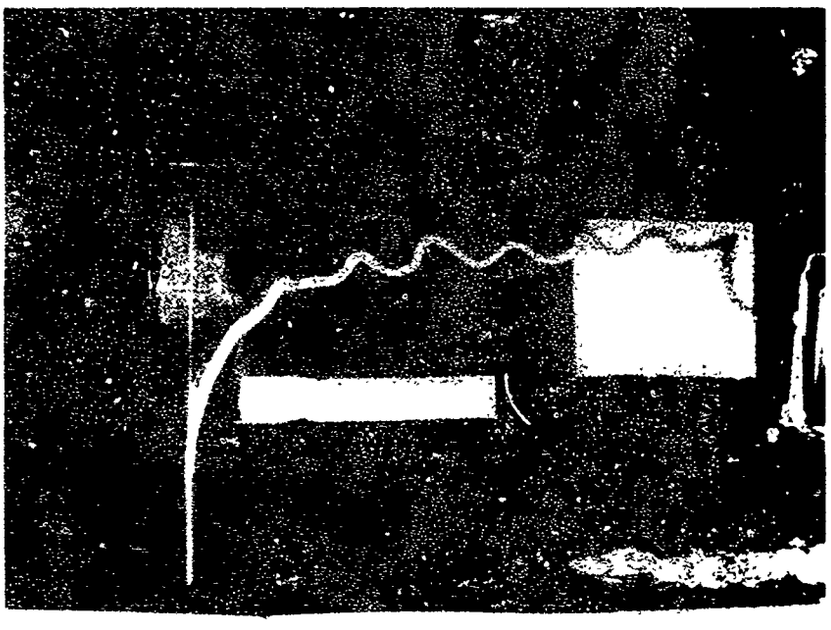

Figure 62. EF4R-104H Wind Shear/Fuel Flow Field, Wind Velocity = 60 fps ($\tau_y$ = 1733 Dynes/cm$^2$).

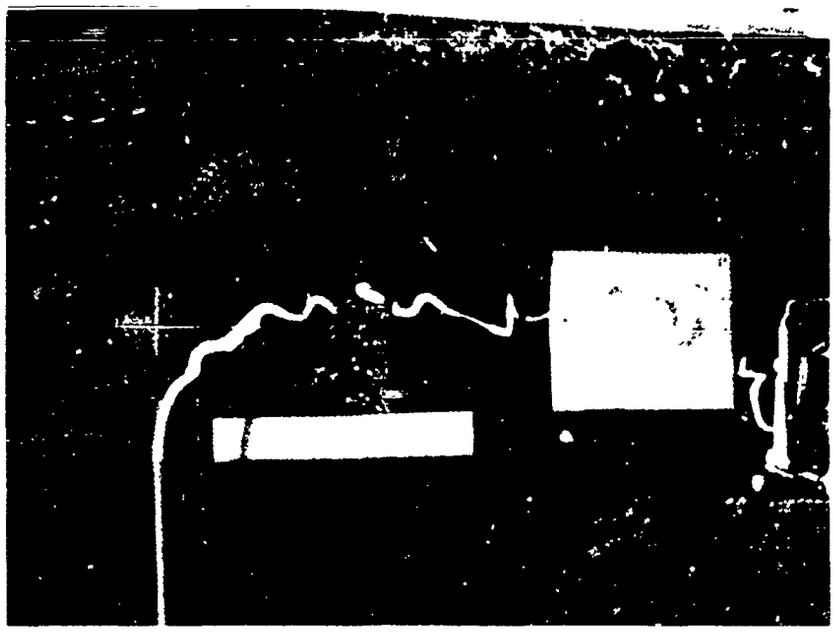

Figure 63. EF4R-104H Wind Shear/Fuel Flow Field, Wind Velocity = 70 fps ($\tau_y$ = 1733 Dynes/cm$^2$).

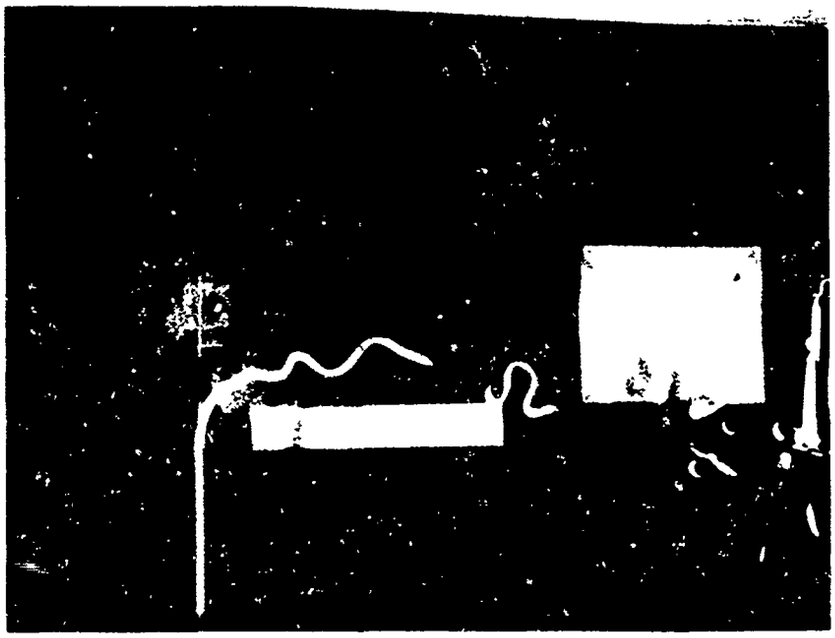

Figure 64. EF4R-104H Wind Shear/Fuel Flow Field, Wind Velocity = 80 fps ($\tau_y$ = 1733 Dynes/cm$^2$).

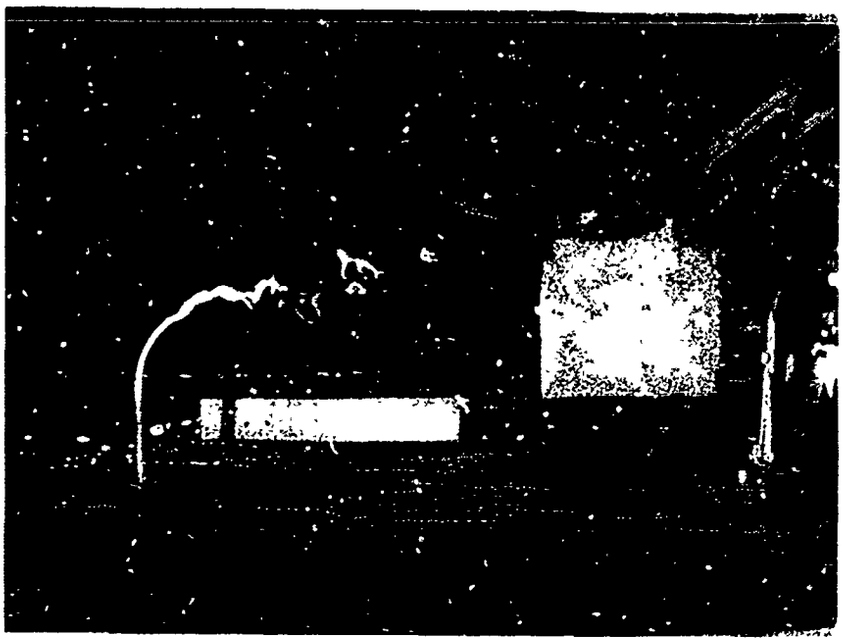

Figure 65. EF4R-104 Wind Shear/Fuel Flow Field, Wind Velocity = 90 fps ($\tau_y$ = 1733 Dynes/cm$^2$).

Figure 66. EF4R-104H Wind Shear/Fuel Flow Field, Wind Velocity = 100 fps ($\tau_y$ = 1733 Dynes/cm$^2$).

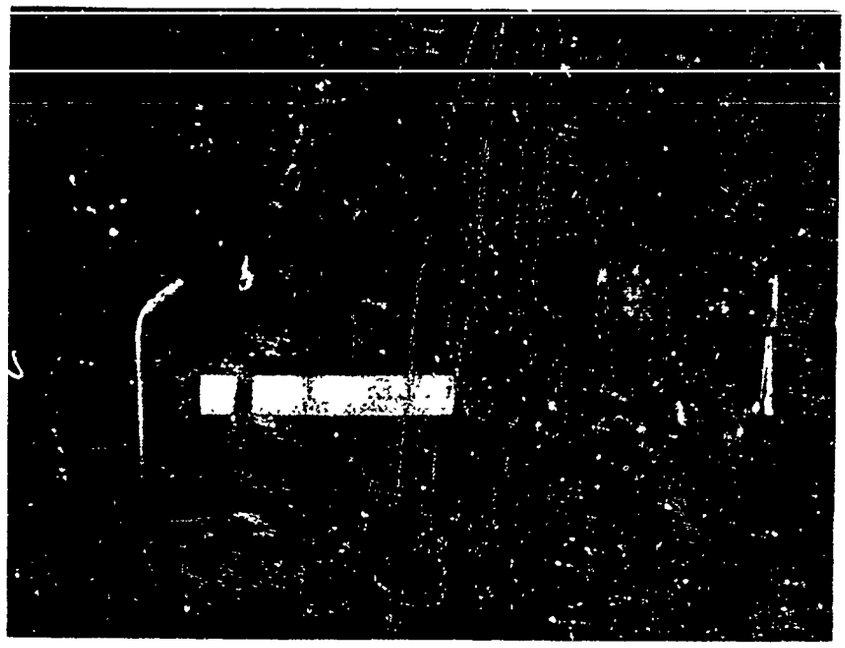

Figure 67. EF4R-104H Wind Shear/Fuel Flow Field, Wind Velocity = 120 fps ($\tau_y$ = 1733 Dynes/cm$^2$).

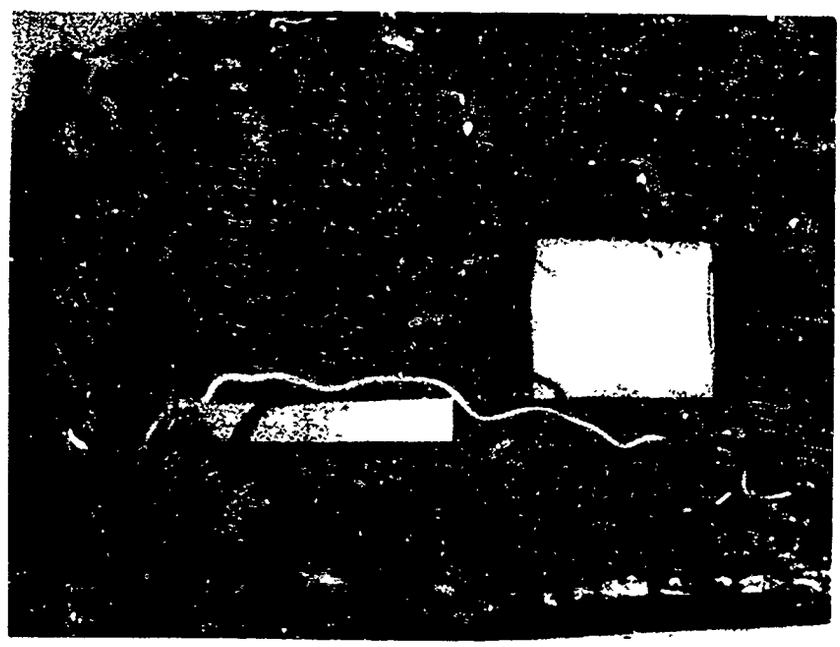

Figure 68. EF4R-104H Wind Shear/Fuel Flow Field, Wind Velocity = 60 fps ($\tau_y$ = 2470 Dynes/cm$^2$).

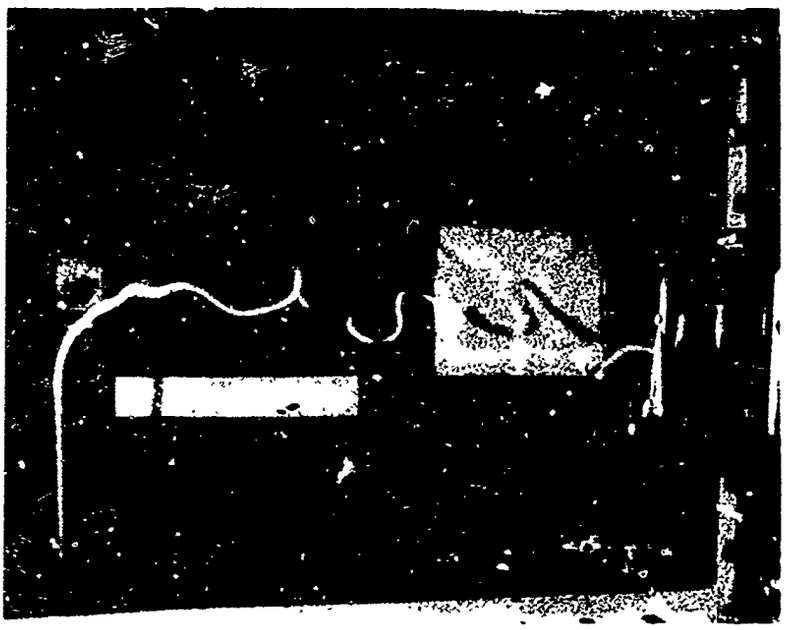

Figure 69. EF4R-104H Wind Shear/Fuel Flow Field, Wind Velocity = 80 fps ($\tau_y$ = 2470 Dynes/cm$^2$).

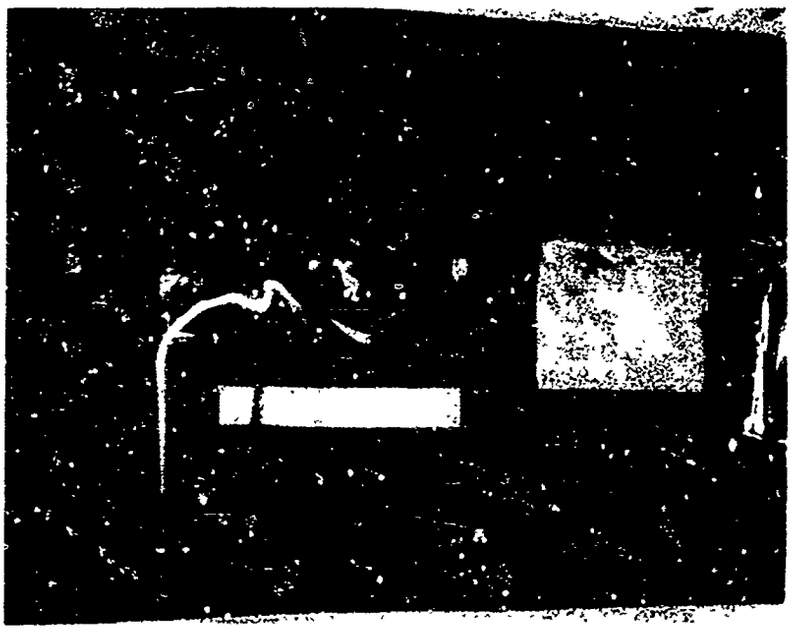

Figure 70. EF4R-104H Wind Shear/Fuel Flow Field, Wind Velocity = 100 fps ($\tau_y$ = 2470 Dynes/cm$^2$).

stress value averaging 2470 dynes/cm$^2$ and tested for velocities of 60, 80, and 100 ft/sec, respectively. At this yield stress, even less fuel breakup is apparent.

The actual safety a fuel displays is its ability to restrict formation of ignitable fuel/air mixtures in the crash environment. The best way to illustrate this point is to compare the performance of a tested fuel with that of a standard fuel, or with one for which much crash data is available. As was shown previously, a parameter ($\psi$) could be defined in which both fuel/air ratio data and droplet diameter data could be correlated to obtain a safety evaluation.

Figure 71 presents the fuel/air ratio data and droplet diameter data plotted in terms of $\psi_{JP-4}$ (as defined previously) versus wind shear velocity for the EF4R-104 emulsified fuel at an average yield stress of 437 dynes/cm$^2$ ($400 \leq \tau_y \leq 475$ dynes/cm$^2$). Very good correlation between the fuel/air ratio data and the droplet diameter data is evident which supports the analytical model generated previously. It was further found that the data presented in Figure 71, as well as the data presented in the forthcoming figures, can be represented by the relation

$$\psi_{\text{Base Fuel}} = \frac{(F/A)_{\text{Fuel}}}{(F/A)_{\text{Base Fuel}}} = \frac{d_{\text{Base Fuel}}}{d_{\text{Fuel}}} = \exp\left[-\frac{(V_j - V)^2}{K}\right], \quad V \leq V_j \qquad (33)$$

For the EF4R-104 emulsified fuel at an average yield stress of 437 dynes/cm$^2$, $V_j$ was found to equal 120.6 ft/sec and K was found to equal 1190. It can be seen in Figure 71 that the atomization and, therefore, fuel/air ratio increases rapidly and approaches that of liquid JP-4 when the wind shear velocity is increased beyond 60 ft/sec. $V_j$ can be interpreted as the wind shear velocity at which breakup and atomization would occur at the same rate for EF4R-104 as for liquid JP-4. Since it is known that liquid JP-4 is highly combustible in a crash environment, the value of $\psi_{JP-4}$ for a given wind shear velocity illustrates a fraction of the ignitability and combustibility expected for JP-4. There exists a value of the ignitability parameter ($\psi_{JP-4}$) under which ignition could not occur (at least to a hazardous extent) in a crash environment. Fuels with values equal to or less than this critical value of $\psi_{JP-4}$ for the approximate maximum crash survivable velocity (65 ft/sec) would be considered safe.

Figure 72 presents the fuel/air ratio data and droplet diameter data plotted in terms of $\psi_{JP-4}$ versus wind shear velocity for

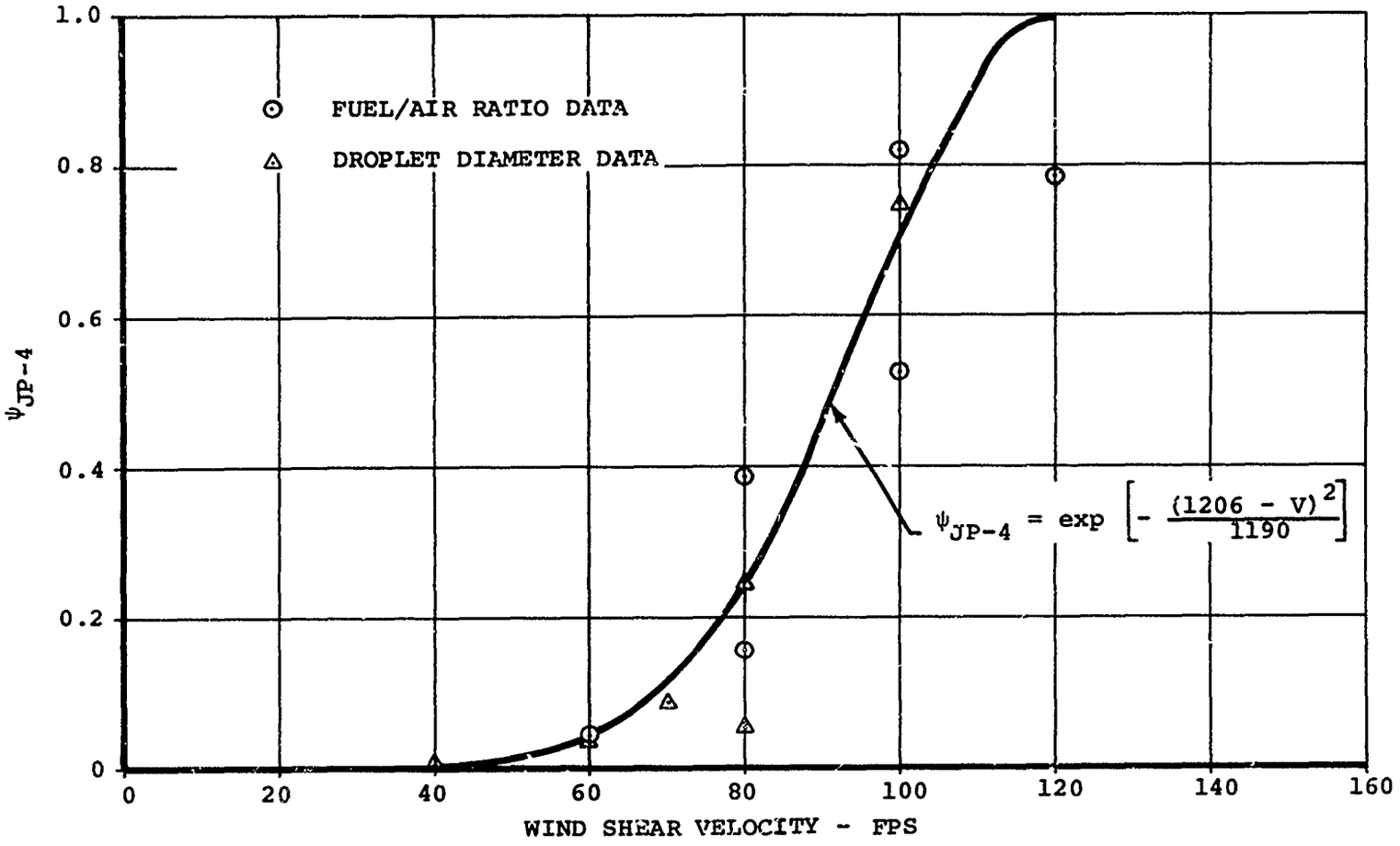


Figure 71. Ignition Susceptibility Parameter Versus Wind Shear Velocity for JP-4 Base Emulsion EF4R-104 ($\tau_y$ = 437 Dynes/cm$^2$).

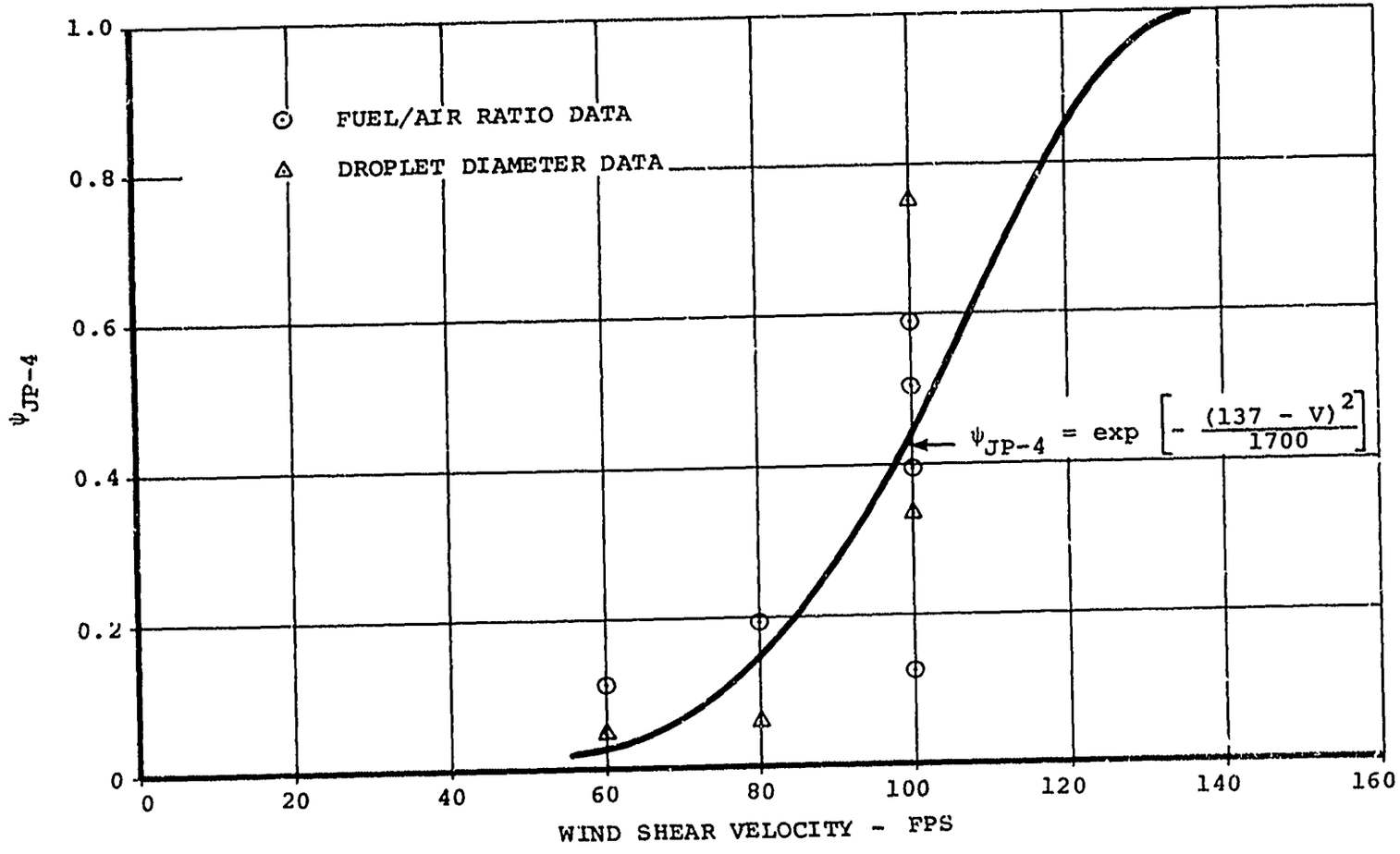


Figure 72. Ignition Susceptibility Parameter Versus Wind Shear Velocity for JP-4 Base Emulsion EF4R-104 ($\tau_y$ = 645 Dynes/cm$^2$).

EF4R-104 emulsified fuel with an average yield stress of 645 dynes/cm$^2$. (The yield stress for these data varied between 600 and 690 dynes/cm$^2$). Within the data scatter expected for this type of testing, the correlation between fuel/air ratio and droplet diameter was good. Using the equation for $\psi_{JP-4}$ to obtain a mean curve through the data resulted in a value for $V_j$ of 137 ft/sec and for K of 1700. Figure 72 indicates a sharp increase in $\psi_{JP-4}$ for wind shear velocities above 70 ft/sec. The increase in yield stress, as compared to Figure 71, offers an improvement in safety (i.e., lower values of $\psi$).

Figure 73 presents the fuel/air ratio data and droplet diameter data plotted in terms of $\psi_{JP-4}$ versus wind shear velocity for EF4R-104 emulsified fuel worked to an average yield stress of 1400 dynes/cm$^2$. The yield stress for these data varied between 1200 and 1700 dynes/cm$^2$. Within the data scatter expected for this type of testing, the fuel/air data and droplet diameter data correlation was good. Using the equation for $\psi_{JP-4}$ to obtain a mean curve through the data resulted in a value for $V_j$ of 190 ft/sec and for K of 4140. Figure 73 indicates a more gradual increase in $\psi_{JP-4}$ than observed in Figures 71 and 72 for wind shear velocities above 90 ft/sec. As the velocities increase, the value of $\psi_{JP-4}$ approaches 1.0, which represents liquid JP-4. Again, the increased yield stress appears to offer an improvement in safety.

Figure 74 presents the fuel/air ratio data and droplet diameter data plotted in terms of $\psi_{JP-4}$ versus wind shear velocity for EF4R-104H emulsified fuel. Two average yield stress curves are presented. The first average yield stress is 1192 dynes/cm$^2$ with a yield stress variation between 1125 and 1290 dynes/cm$^2$ and the second average yield stress is 1886 dynes/cm$^2$ with a yield stress variation between 1525 and 2520 dynes/cm$^2$. It is seen that quite a bit of data scatter is present. This is not unexpected for this type of testing; however, the wider range of yield stresses in these cases accounts for much of the scatter. For the average yield stress of 1192 dynes/cm$^2$, the mean curve obtained using the equation for $\psi_{JP-4}$ was found to give a value for $V_j$ of 180 ft/sec and for K of 3350. For the average yield stress of 1886 dynes/cm$^2$, the mean data curve resulted in a value for $V_j$ of 225.5 ft/sec and for K of 6100. As shown in Figure 74, the curve of $\psi_{JP-4}$ versus wind shear velocity indicates a gradual increase in $\psi_{JP-4}$ for velocities above 85 ft/sec for the 1192 dynes/cm$^2$ yield stress data and an even more gradual increase in $\psi_{JP-4}$ for velocities above 100 ft/sec for the 1886 dynes/cm$^2$ yield stress data. As was indicated in Figures 71, 72, and 73, the results shown in Figure 74 further confirm the potential safety improvement with increasing yield stress.

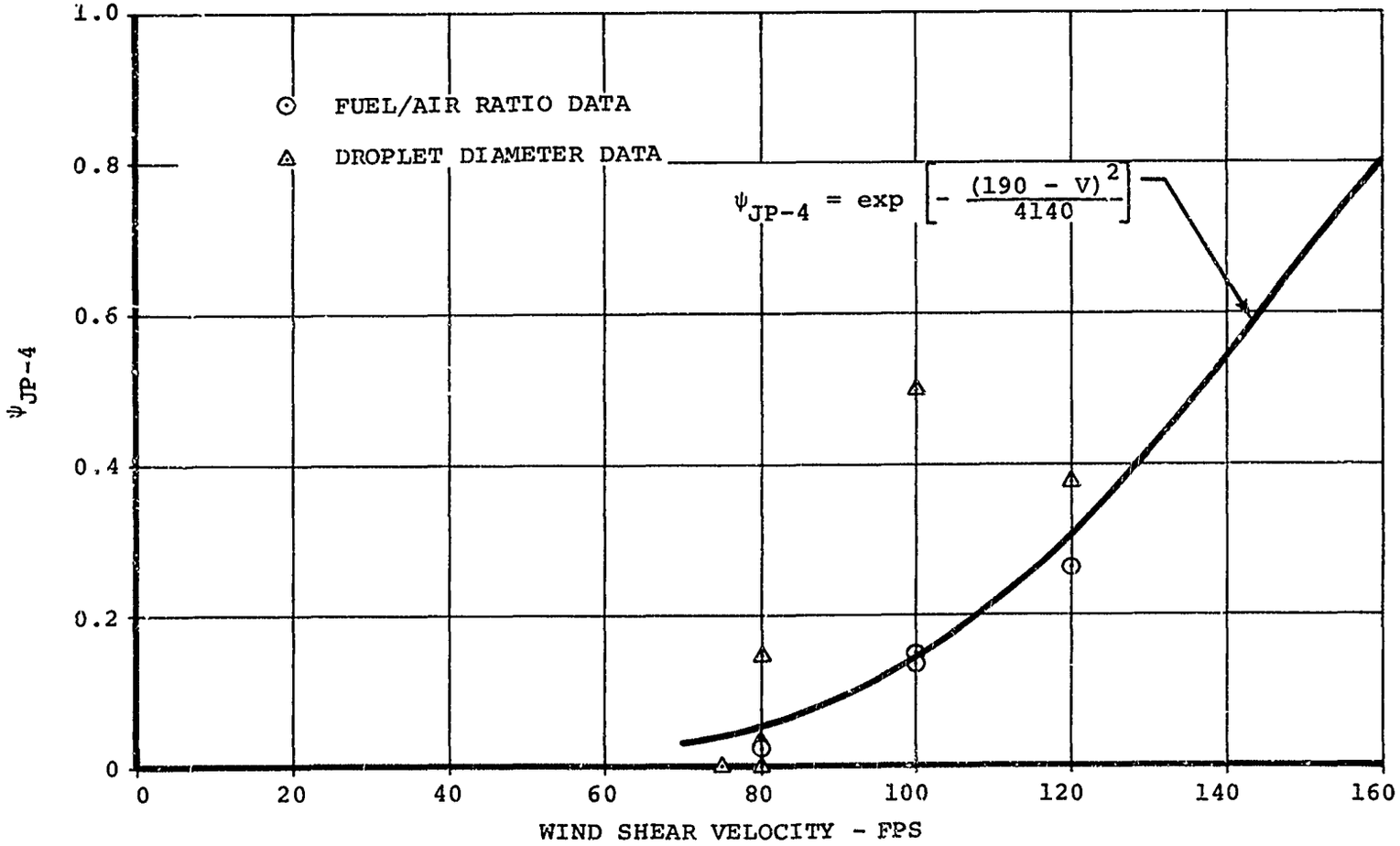


Figure 73. Ignition Susceptibility Parameter Versus Wind Shear Velocity for JP-4 Base Emulsion EF4R-104 ($\tau_y$ = 1400 Dynes/cm$^2$).

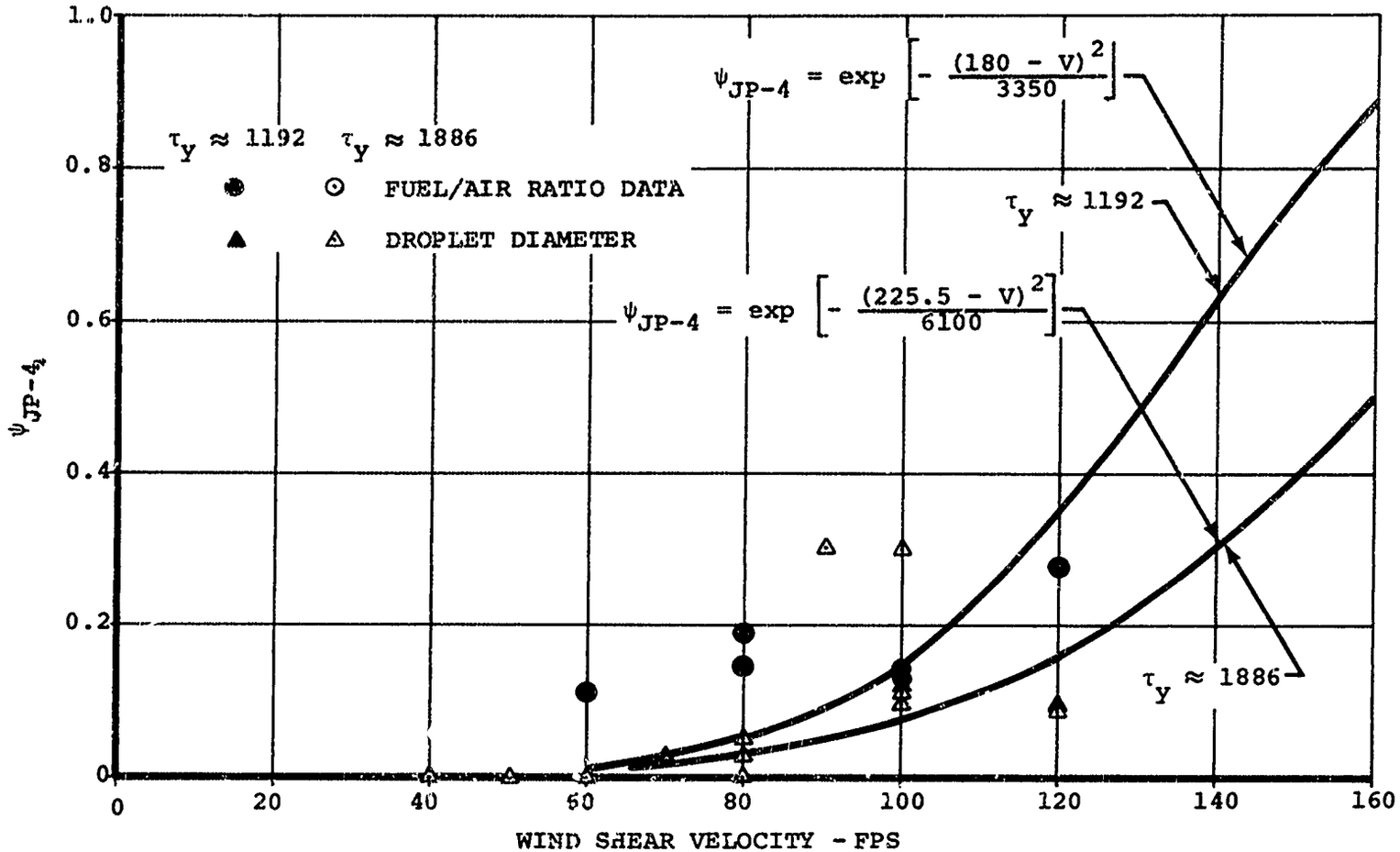


Figure 74. Ignition Susceptibility Parameter Versus Wind Shear Velocity for JP-4 Base Emulsion EF4R-104H ($\tau_y$ = 1192 Dynes/cm$^2$ and 1886 Dynes/cm$^2$).

Figure 75 presents fuel/air ratio data plotted in terms of $\psi_{JP-4}$ for liquid JP-8 and EF8-104H. The yield stress for liquid JP-8 is zero; however, the deviation of JP-8 from JP-4 is a function of the fuel properties such as vapor pressure, diffusion rates, and chemical composition. The average yield stress of the EF8-104H JP-8 base emulsified fuel is 1000 dynes/$cm^2$ with a yield stress variation between 750 and 1100 dynes/$cm^2$. The mean curve for the liquid JP-8 was taken as a straight line parallel to JP-4 data with a value of $\psi_{JP-4}$ corresponding to 0.8. These data do contain a fair amount of scatter, but it is within that expected for this type of testing. The mean curve representing EF8-104H was obtained from the equation for $\psi_{JP-8}$ using the JP-8 data to obtain the results shown in Figure 76 for $\psi_{JP-8}$ versus wind shear velocity. The mean EF8-104H data curve in Figure 75 was transferred from Figure 76 by a value of 9.8, representing the relationship between JP-8 and JP-4. Because JP-8 is the base fuel for EF8-104H, one would expect that $\psi_{JP-4}$ for EF8-104H would not become higher than 0.8. This mean data curve for EF8-104H resulted in a value for $V_j$ of 150 ft/sec and for K of 2700. The EF8-104H data scatter is a little greater than should be expected. No definite explanation is available; however, the hot-source ignition data presented previously also resulted in large amounts of scatter for this high yield stress fuel.

## RESULTS OF IMPACT DISPERSION/ATOMIZATION TESTS

Impact dispersion/atomization tests were performed on referee grade JP-4, JP-4 base emulsion EF4R-104, JP-4 base emulsion EF4R-104H, JP-8, and JP-8 base emulsion EF8-104H. The impact velocities tested ranged from 20 to 70 ft/sec. The tests were performed for each fuel at 45- and 90-degree impact angles. The results of each test are presented in Appendix II.

Using the data correlation results obtained from the analysis, the fuel/air ratio data is presented in terms of an ignition susceptibility parameter $\psi$, where

$$\psi_{\text{Base Fuel}} = \frac{(F/A)_{\text{Fuel}}}{(F/A)_{\text{Base Fuel}}} \qquad (34)$$

Two types of impact tests were performed and will be discussed separately. The first consisted of measuring mean fuel/air ratio results versus impact kinetic velocity and the second consisted of recording impact ignition susceptibility versus impact kinetic velocity.

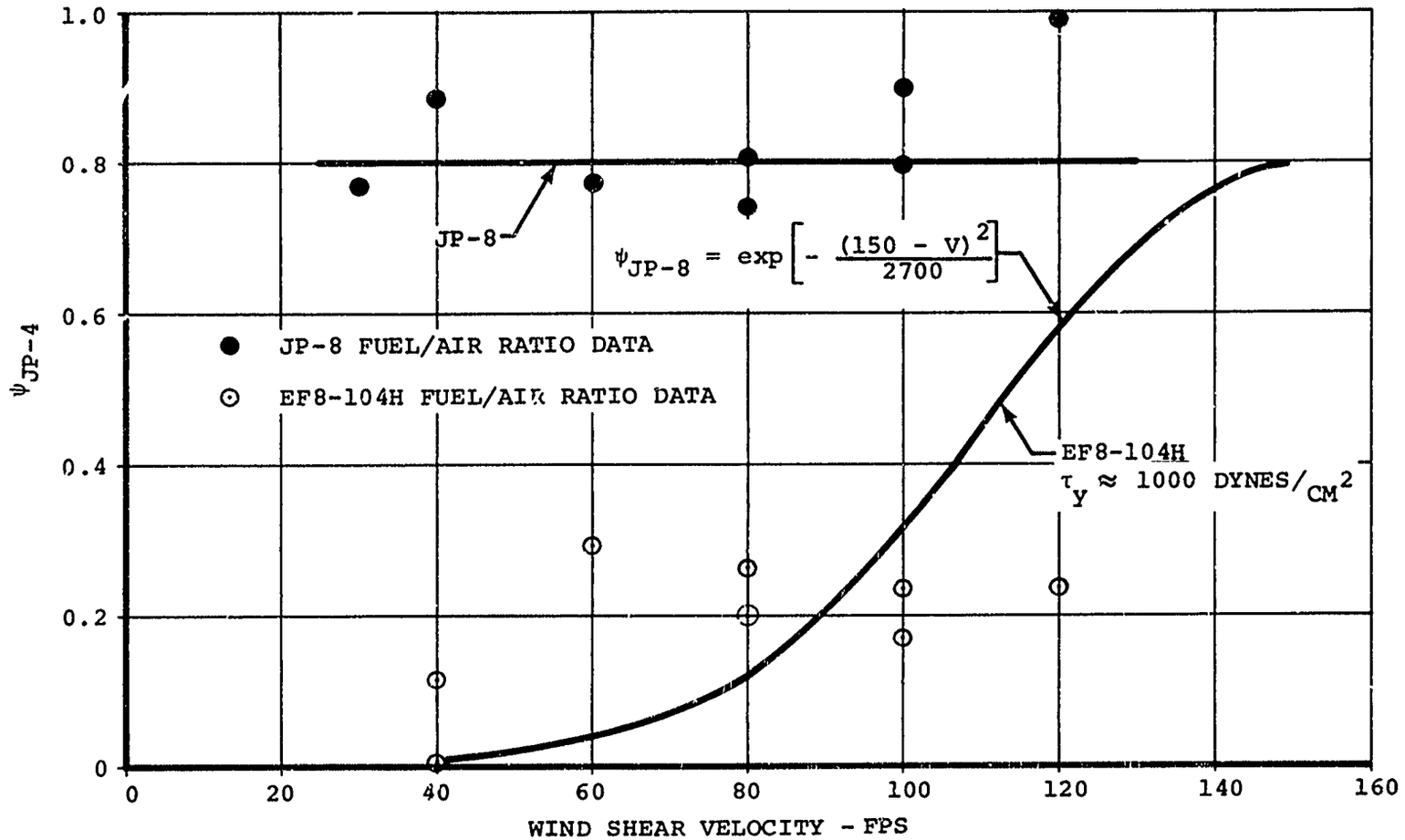


Figure 75. Ignition Susceptibility Parameter Versus Wind Shear Velocity for JP-8 Liquid Fuel and JP-8 Base Emulsion EF8-104H ($\tau_y$ = 1000 Dynes/cm$^2$).

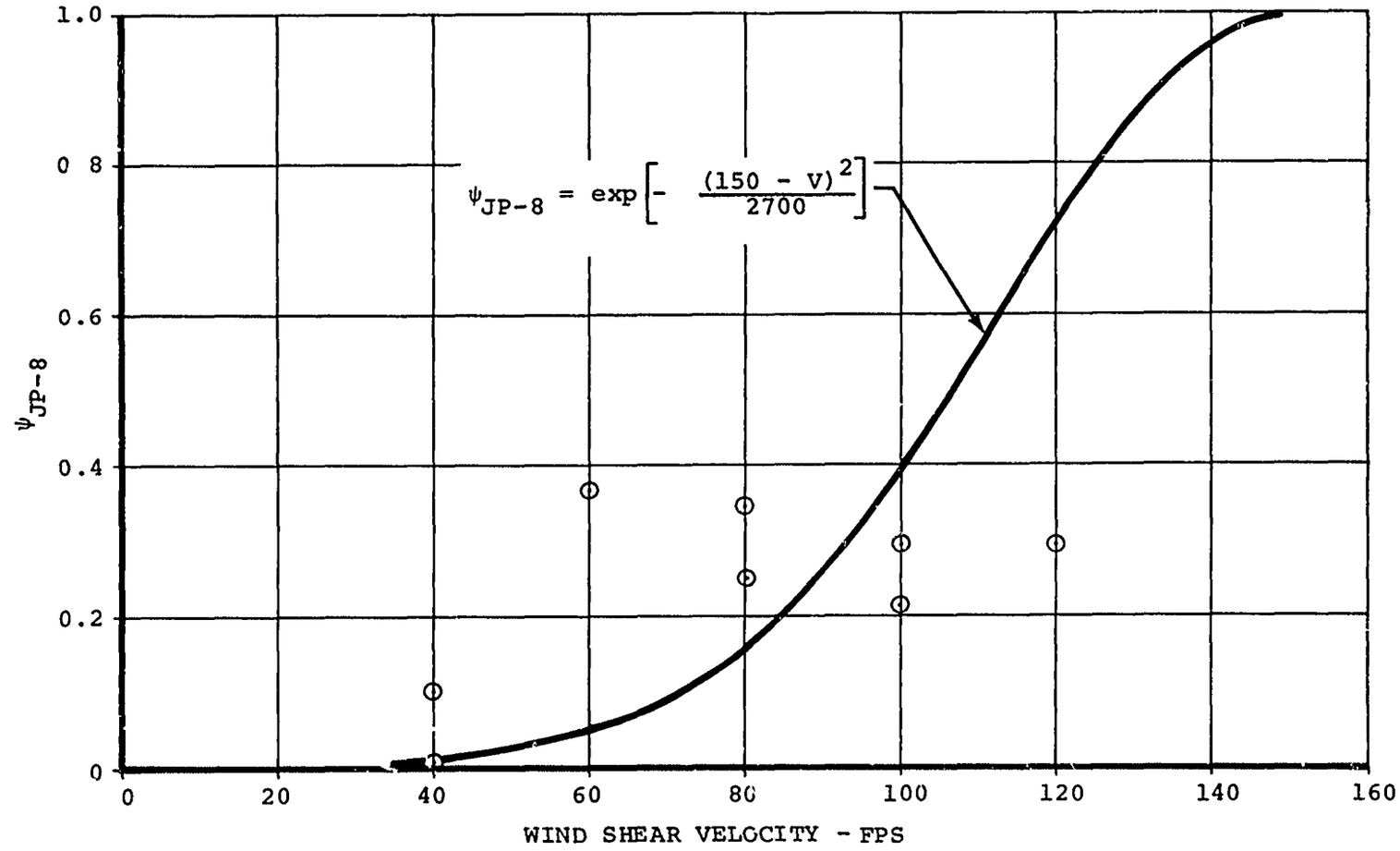


Figure 76. Ignition Susceptibility Parameter Based on JP-8 Versus Wind Shear Velocity for JP-8 Base Emulsion EF8-104H ($\tau_y$ = 1000 Dynes/cm$^2$).

## Fuel/Air Ratio Versus Impact Kinetic Velocity Tests

The mean fuel/air ratio data resulting from fuel impact with a surface, fuel impact velocity measurements, and test procedures were discussed in the Test Methodology section. The impact velocities were measured from the high-speed (500 frame-per-second) camera data.

The actual safety potential a fuel displays is its ability to restrict formation of ignitable fuel/air mixtures in the crash impact environment. The parameter ($\psi$) can be used to illustrate this ability by comparing the tested fuel with a standard fuel or with one for which crash data are available.

Figure 77 presents the fuel/air ratio data plotted in terms of $\psi_{JP-4}$ versus kinetic velocity (V Sin$\theta$) for the JP-4 base, EF4R-104 emulsified fuel at an average yield stress of 508 dynes/cm$^2$. The yield stress varied between 480 and 536 dynes/cm$^2$. Figure 77 consists of data taken for both 45 and 90 degrees; therefore, these results indicate that the impact dispersion and atomization dependence are a direct function of kinetic velocity for a given yield stress. Very little data scatter is present. It is found in Figure 77, as well as in the data presented in the forthcoming figures, that a similar relationship to that observed in the wind shear tests can represent the mean data, e.g.,

$$\psi_{\text{Base Fuel}} = \frac{(F/A)_{\text{Fuel}}}{(F/A)_{\text{Base Fuel}}} = \exp\left[-\frac{(V_j - V \text{ SIN}\theta)^2}{K}\right], \quad V \leq V_j \tag{35}$$

Based on the results of the EF4R-104 data presented in Figure 77, the mean curve resulted in a value of 60 ft/sec for $V_j$ and a value of 747.5 for K. It can be seen in Figure 77 that the atomization and dispersion and, therefore, the mean fuel/air ratio, increased rapidly when the kinetic velocity was increased beyond 15 ft/sec. Also, the data approached $\psi = 1.0$ (i.e., equal to that of liquid JP-4) near a kinetic velocity of 60 ft/sec. At this velocity, the impacted EF4R-104 would have atomization and dispersion characteristics similar to those expected for liquid JP-4. Since it is known that liquid JP-4 is highly combustible in a crash environment, the value of $\psi_{JP-4}$ for a given kinetic velocity illustrates a fraction of the ignitability and combustion expected for JP-4. It should be clear that there will exist a value of the ignitability parameter ($\psi_{JP-4}$) under which ignition could not occur (at least to a hazardous extent) in a crash environment. If we assume that the maximum survivable conditions for a crash

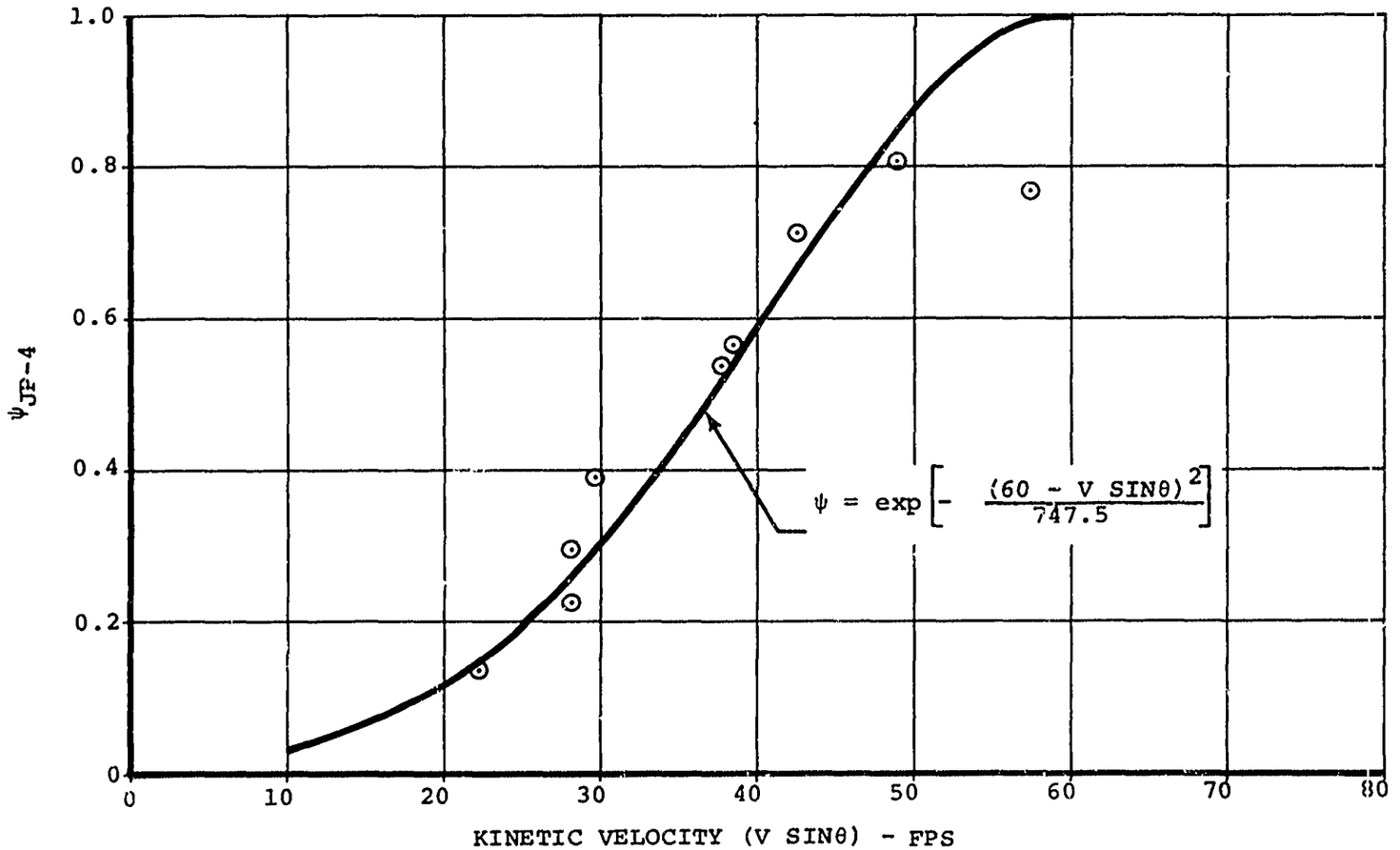


Figure 77. Ignition Susceptibility Parameter Versus Impact Kinetic Velocity for JP-4 Base Emulsion EF4R-104 ($\tau_y$ = 508 Dynes/cm$^2$).

environment are a velocity of 65 ft/sec at a 45-degree angle, then the maximum survivable kinetic velocity is 46 ft/sec. Fuels with values equal to or less than this critical value of $\psi_{JP-4}$ would be considered safe.

Figure 78 presents the fuel/air ratio data plotted in terms of $\psi_{JP-4}$ versus kinetic velocity for the JP-4 base EF4R-104H emulsified fuel at an average yield stress of 1143 dynes/cm$^2$. The yield stress varied between 1100 and 1185 dynes/cm$^2$ for the data. As in Figure 77, the data plotted in Figure 78 consists of tests run at both a 45- and 90-degree impact angle. Data scatter is not severe for this type of testing. Using the equation for $\psi_{JP-4}$ to obtain a mean data correlation curve resulted in a value for $V_j$ of 100 ft/sec and a value of 2450 for K. It can be seen in Figure 78 that the ignitability parameter $\psi_{JP-4}$ increases with increasing kinetic velocity less rapidly than the parameter in Figure 77. It is evident, as was the case in the wind shear test results, that increasing the yield stress of the emulsified fuel apparently enhances its safety characteristics.

Figure 79 presents the fuel/air ratio data plotted in terms of $\psi_{JP-4}$ versus kinetic velocity for liquid JP-8. The data presented in this figure were obtained for both a 45- and a 90-degree impact angle. Because the yield stress of JP-8 is zero, the lower fuel/air ratio data obtained, compared to JP-4, are the result of the inherent characteristics of JP-8, such as vapor pressure, diffusion rates, and chemical composition. Data scatter is no more than to be expected for this type of testing, especially at the lower fuel/air ratio ranges. The value of $\psi_{JP-4}$ for liquid JP-8 appears to taper off to a value between 0.2 and 0.3 for the larger kinetic velocities. This would correlate with the difference between vapor pressure of JP-8 and JP-4 (0.35 psi for JP-8 and 2.90 psi for JP-4).

Figure 80 presents the fuel/air ratio data plotted in terms of $\psi_{JP-4}$ versus kinetic velocity for the JP-8 base EF8-104H emulsified fuel with an average yield stress of 755 dynes/cm$^2$. The yield stress varied between 730 and 780 dynes/cm$^2$ for the data presented, which also included 45- and 90-degree impact angles. Using the equation for $\psi_{JP-8}$ and the mean JP-8 results, a mean data curve was generated for the EF8-104H data in terms of $\psi_{JP-4}$. This curve is shown in Figure 81. From this result, the values for $V_j$ and K were estimated at 73 ft/sec and 1310, respectively. As illustrated in Figure 81, there was considerable scatter. However, for the very low fuel/air ratios obtained with this fuel, such scatter is not unusual. As with the wind shear test and hot-surface ignition test results, it appears that this fuel will characteristically yield greater data scatter when compared to the others tested.

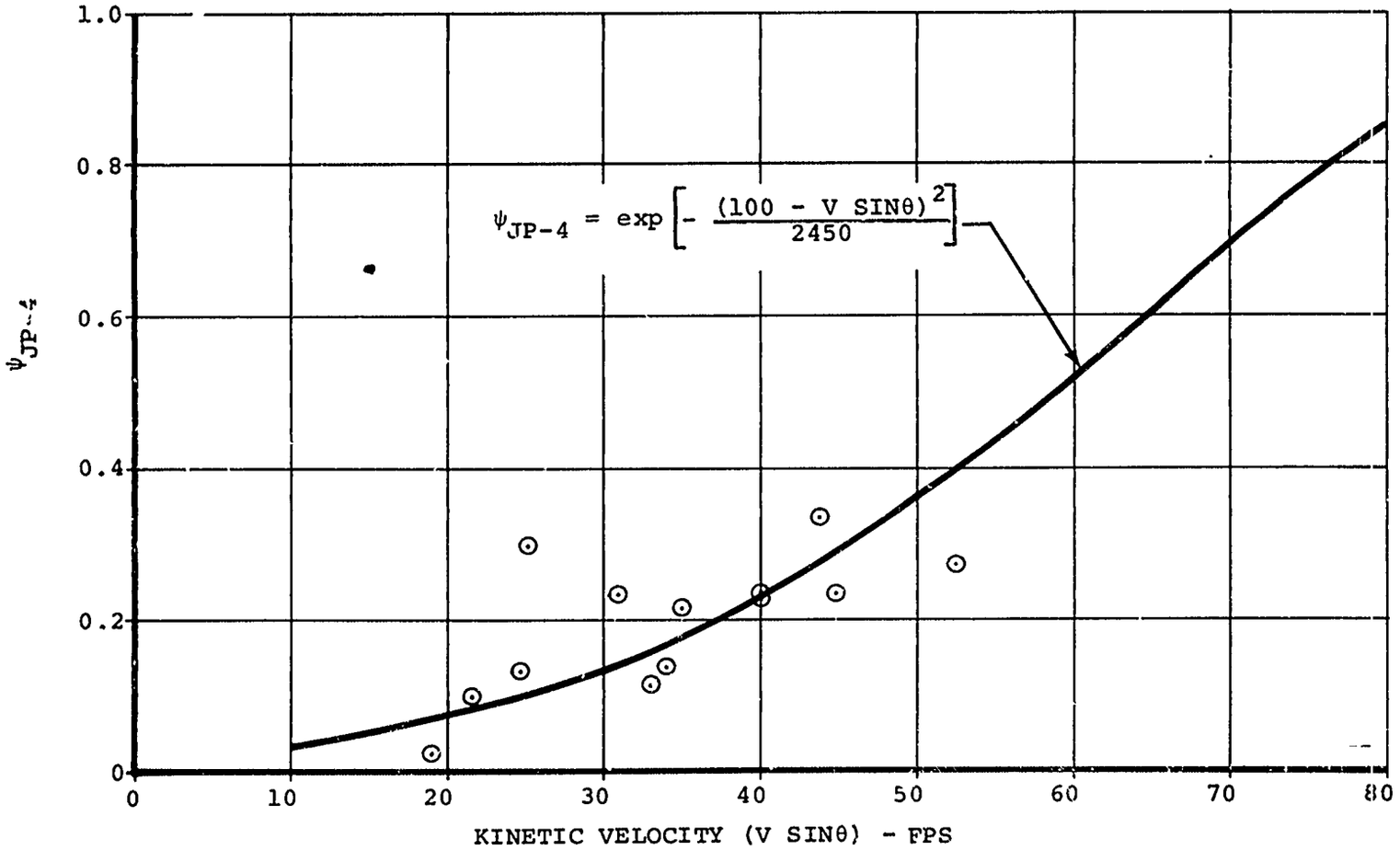


Figure 78. Ignition Susceptibility Parameter Versus Impact Kinetic Velocity for JP-4 Base Emulsion EF4R-104H ($\tau_y$ = 1143 Dynes/cm$^2$).

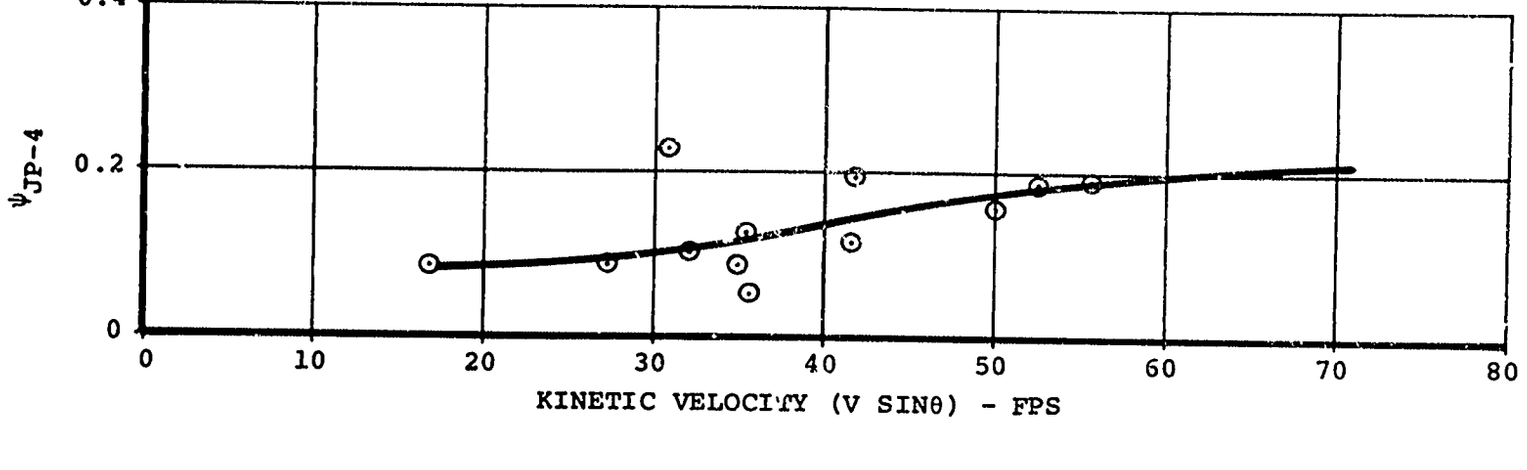


Figure 79. Ignition Susceptibility Parameter Versus Impact Kinetic Velocity for Liquid JP-8.

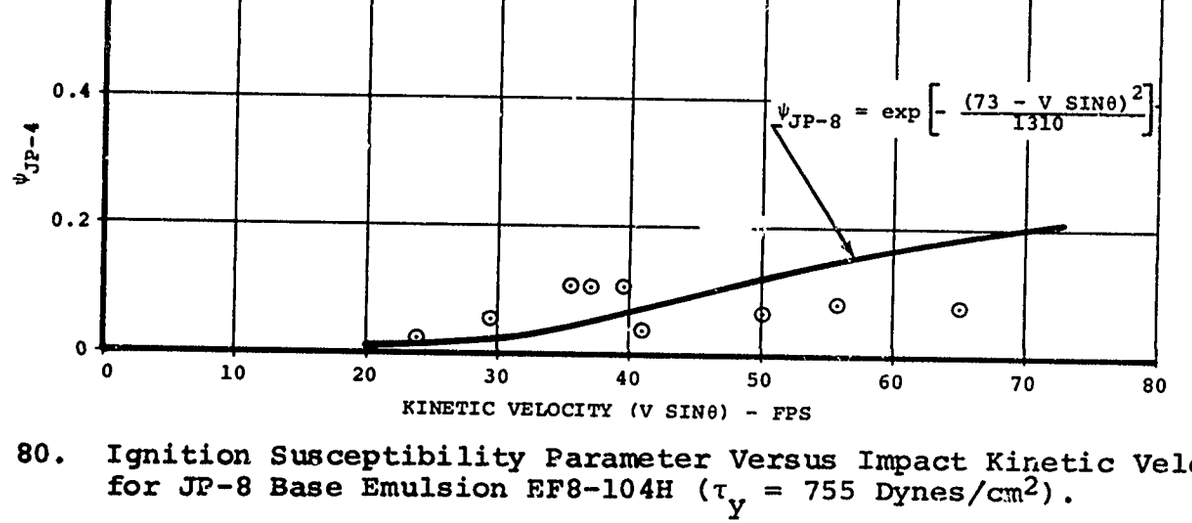


Figure 80. Ignition Susceptibility Parameter Versus Impact Kinetic Velocity for JP-8 Base Emulsion EF8-104H ($\tau_y$ = 755 Dynes/cm$^2$).

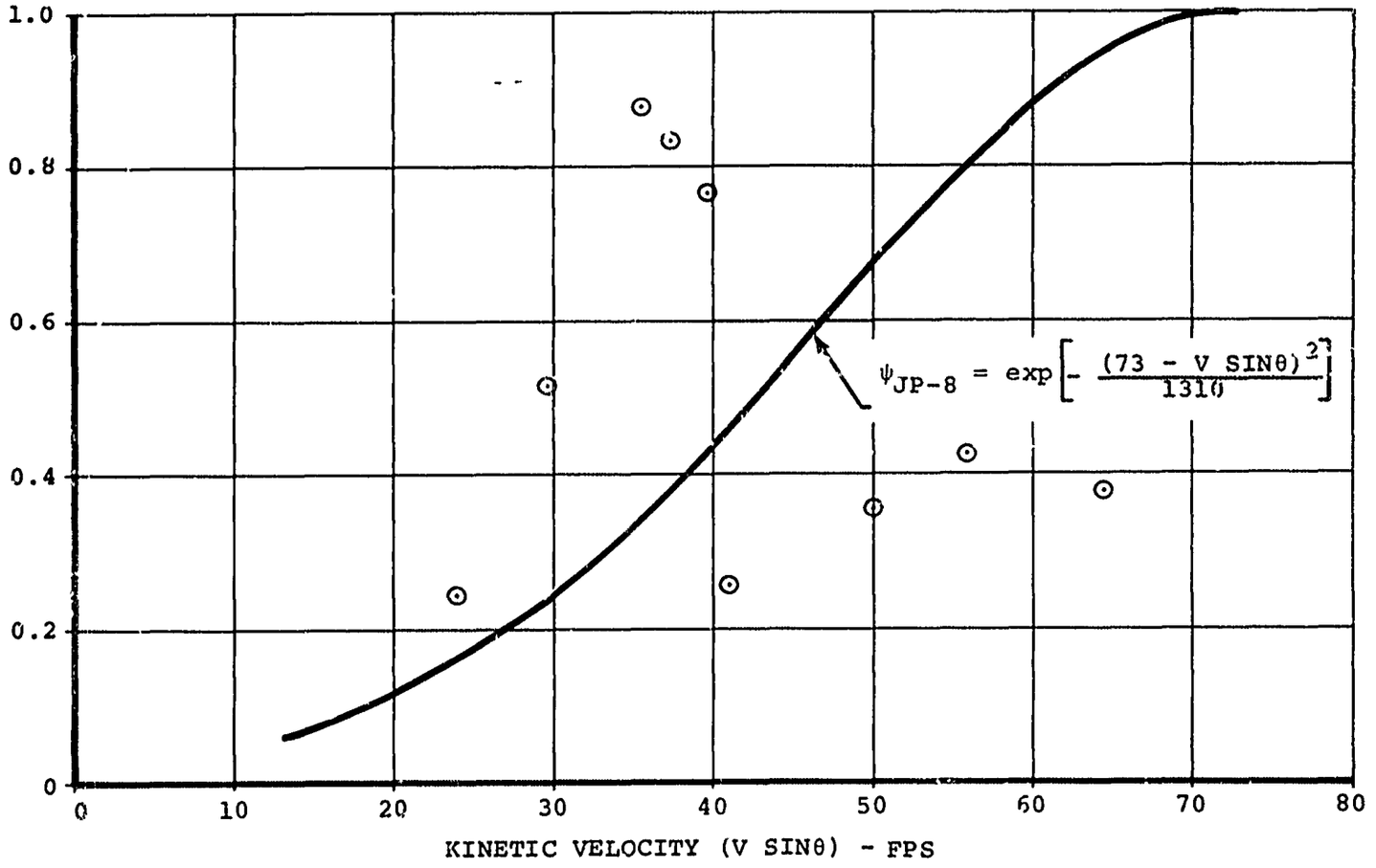


Figure 81. Ignition Susceptibility Parameter Based on Liquid JP-8 Versus Impact Kinetic Velocity for JP-8 Base Emulsion EF8-104H ($\tau_y$ = 755 Dynes/cm$^2$).

## Impact Ignition Susceptibility Versus Impact Kinetic Velocity Tests

An impact ignition test program was conducted to record ignition characteristics for referee grade JP-4, JP-4 base EF4R-104 emulsion, JP-4 base EF4R-104H emulsion, JP-8, and JP-8 base EF8-104H emulsion.

High-speed motion pictures (500 frames per second) were taken of each test to record the extent of fuel ignition from the spark and/or hot-surface ignition source and to determine the actual fuel impact velocity. Test conditions and data are presented in Appendix III.

It must be realized that the ignition results obtained in this test series do not necessarily represent the ignition expected in a full-scale crash environment. However, the ignition study does illustrate the ignition trends and how these trends relate to the impact dispersion/atomization results.

To illustrate graphically the ignition results, an ignition rating system numbering from 0 to 4 was devised. A rating of 0 indicated no ignition whereas a rating of 4 indicated a violent complete ignition, characteristic of the JP-4 results. A rating of 3 indicated a delayed complete ignition, lacking the initial fireball associated with light fuel spray. An ignition rating of 2 indicated a semi-fireball ignition which did not propagate a flame and was self-extinguishing. An ignition rating of 1 indicated only slight ignition without flame spreading.

Three tests were run for each fuel (except JP-4), velocity setting, and impact angle to obtain an adequate statistical analysis. Only two tests per condition were required for JP-4, as every velocity and impact angle tested resulted in an ignition rating of 4. It was found after analyzing the data that the actual impact velocities for nominally the same setting were not close enough to substantiate averaging for each test condition. Further, the yield stress of the fuels varied slightly during testing. Therefore, all the data were plotted rather than statistically averaged at a given condition.

To illustrate the effect of the ignition susceptibility parameter $\psi_{JP-4}$, the ignition rating of the test data was plotted versus the ignition susceptibility parameter $\psi_{JP-4}$. The value of $\psi_{JP-4}$ for each test was obtained from the governing equation using the measured kinetic velocity and the appropriate constants associated with yield stress (see section on Test Correlation and Safety Evaluation Criteria). The results are

presented in Figure 82. The data scatter is as expected in this type of data acquisition; however, there does appear to be a distinct border line which represents the limit of the occurrence of a specific ignition rating. If we assume that an ignition rating of 2 or under represents a nonhazardous condition, then it can be concluded that values of $\psi_{JP-4}$ equal to or less than 0.09 represent a safe condition. For values of $\psi_{JP-4}$ above this value, there is a finite probability of complete ignition. Figure 82 also allows prediction of ignition characteristics of other fuels if we know the appropriate value of $\psi_{JP-4}$ for the fuel.

To be able to define the limiting value of $\psi_{JP-4}$ from results with greater precision, either a much larger data sample or preferably much better reproducibility of the test condition would be required. It was observed in the tests that all ignitions were caused by the spark igniter rather than the hot-surface ignition source. Although the hot surface was kept at 1100°F, the contact time of the fuel apparently was not long enough to initiate combustion. The effect the hot source had on ignition by the spark igniter was not directly determined; however, it is possible that data with an ignition rating of 3 may have been affected by the hot source.

## RESULTS OF SIMULATED FULL-SCALE TESTS

The simulated full-scale test conditions and results are tabulated in Appendix IV.

### Results of Open-Flame Igniter Tests

One simulated full-scale impact test was performed using open-flame igniters for each of the ten fuels at an impact velocity of 65 ft/sec. The only environmental variable causing any change between the ten tests was the wind velocity and direction. Each test was conducted with a wind velocity of less than 10 mph. The maximum temperature observed at any position is illustrated for each test as a function of time from impact in Figures 83 and 84. Four tests resulted in no indicated temperature increase (zero heat rate). A malfunction occurred in the temperature data recorder in one test (liquid JP-8).

The ignition and postcrash fire resulting from the liquid JP-4 fuel test produced a violent reaction and a large fireball. A large amount of misted fuel ignited while airborne, and the fire spread over the test barrier, resulting in complete ignition of all the fuel. The maximum heating rate was found to be on the order of that expected for JP-4 postcrash fires (10 $Btu/ft^2$-sec).

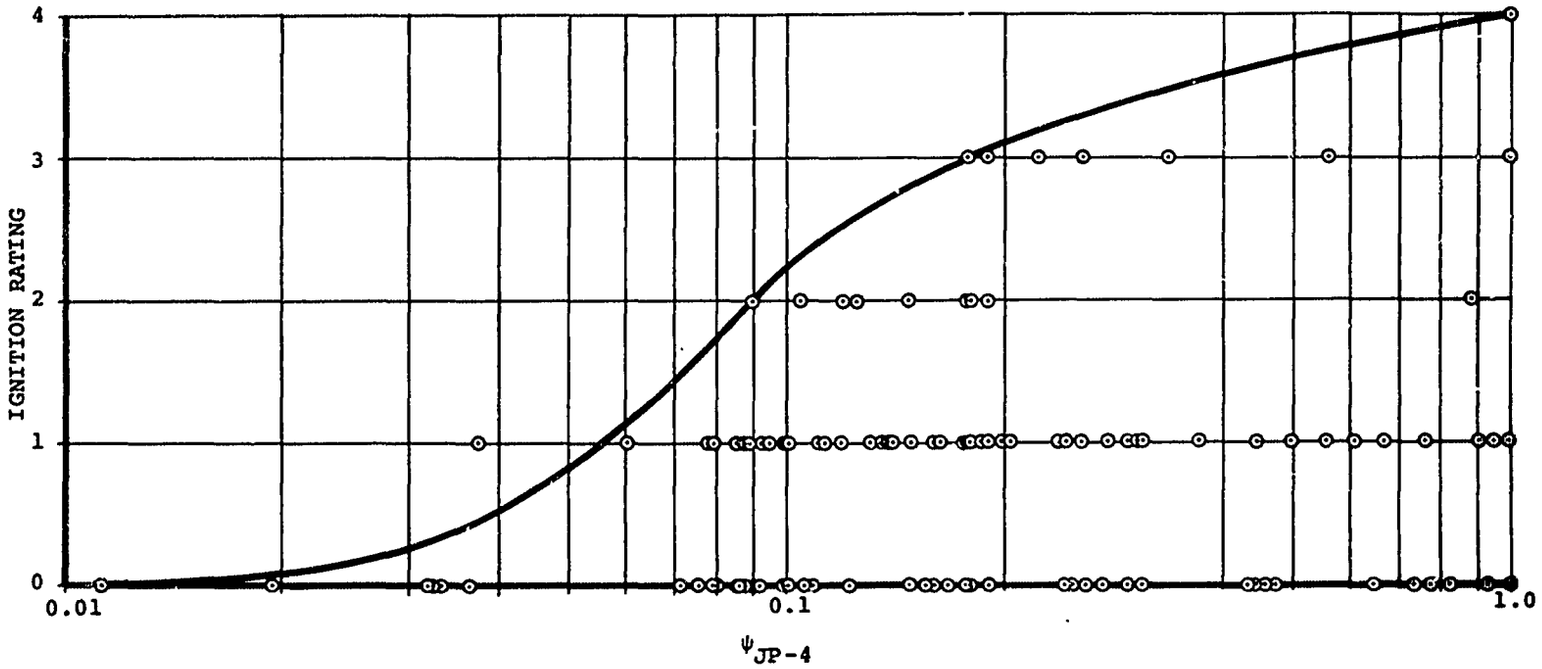


Figure 82. Ignition Rating Value Versus Ignition Susceptibility Parameter Obtained From Impact Ignition Tests.

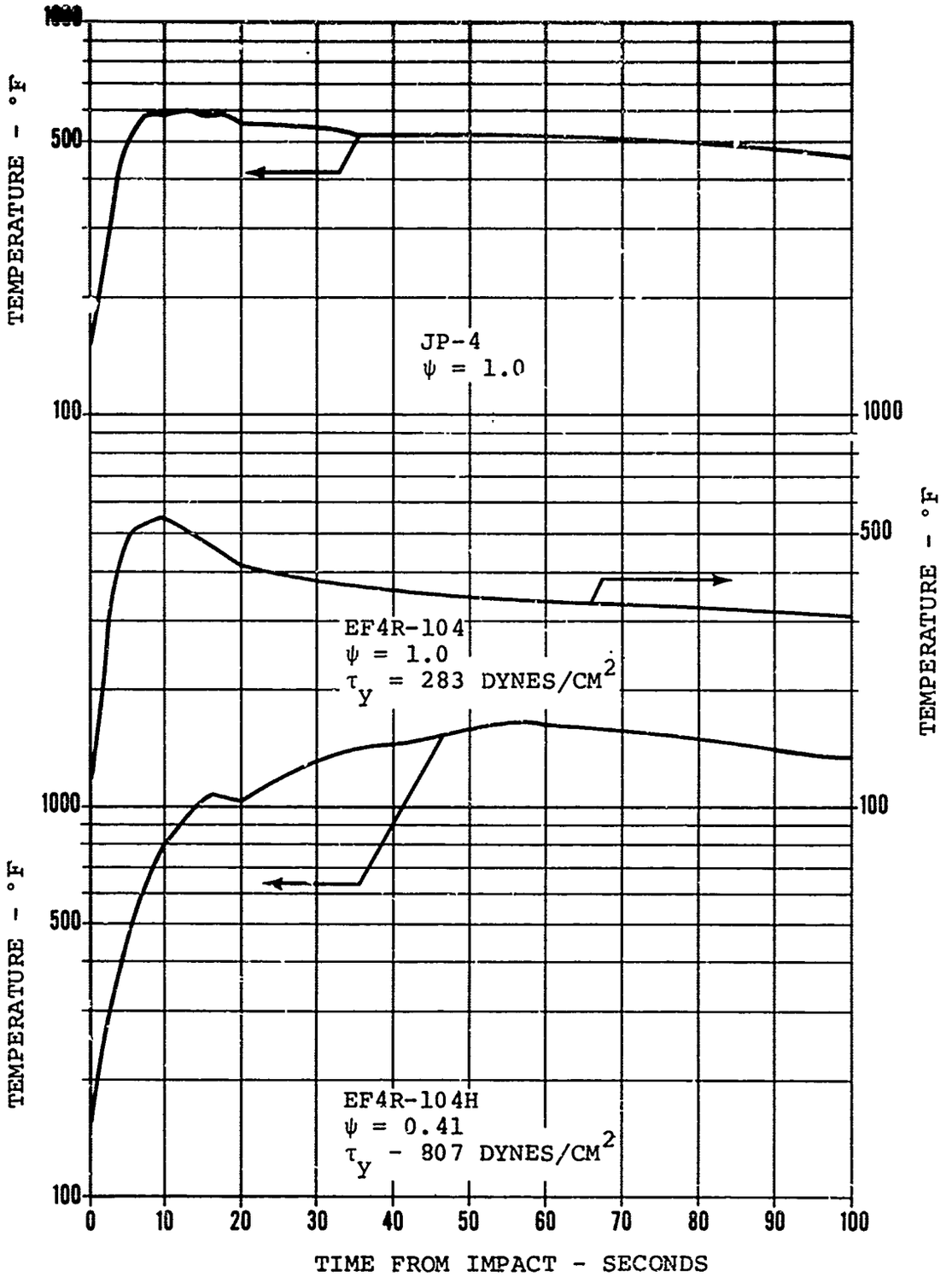


Figure 83. Maximum Temperature Data Obtained From Open-Flame Igniter Tests.

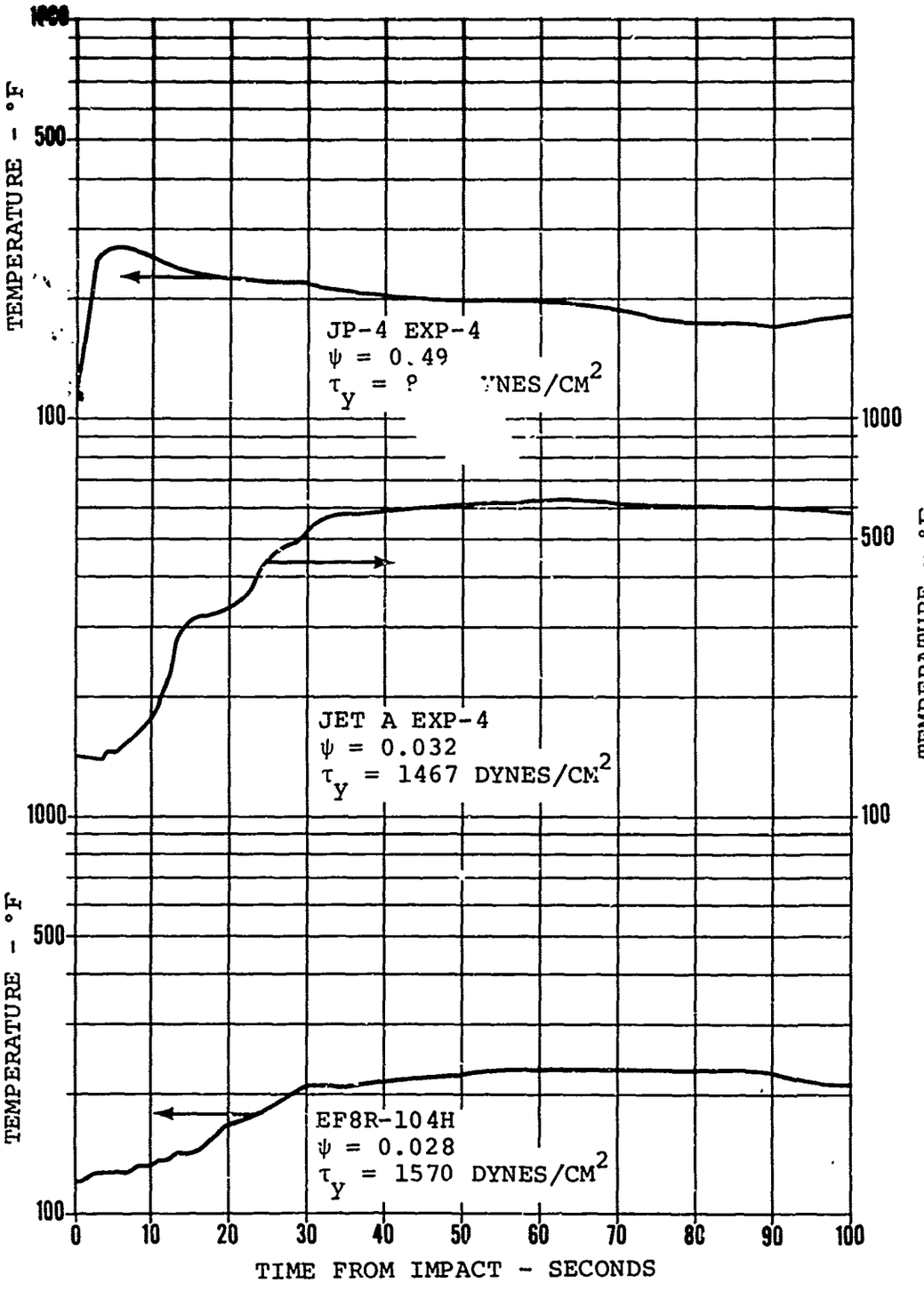


Figure 84. Maximum Temperature Data Obtained From Open-Flame Igniter Tests.

The JP-4 base emulsion EF4R-104, with a yield stress value of 283 dynes/cm$^2$, resulted in a violent ignition and postcrash fire of nearly the same magnitude as the JP-4 fuel. The resulting fireball was slightly smaller, which was as expected because fuel misting was reduced due to the emulsion's yield stress. The small globs of fuel, however, appeared to have been almost completely ignited while airborne. The resulting fire and fuel spread covered a somewhat larger area than JP-4 and also resulted in complete ignition of all the fuel. The postcrash fire burn time was increased over JP-4 as the emulsion tended to lay small globs over the ground which burned longer than the misted JP-4 fuel. The maximum heating rate was found to be nearly equal to that found for the JP-4 test. It was concluded that the postcrash fire hazard potential was as great or perhaps slightly greater than that of liquid JP-4.

The JP-4 base emulsion EF4R-104H, with a yield stress value of 807 dynes/cm$^2$, resulted in a violent ignition and postcrash fire. The resulting fireball was slightly reduced from the fireballs observed for JP-4 and EF4R-104 since the fuel globs were slightly increased in size. This resulted in a reduction in the available fuel in the vapor phase. However, nearly all the fuel globs were ignited while still airborne. The resulting fire and fuel spread covered a somewhat larger area than for JP-4 and resulted in nearly complete ignition of all the fuel with only small isolated unburned fuel globs. The postcrash fire burn time was increased as the larger globs of fuel lay on the barrier and burned until completely consumed. This longer burn time accounts for the higher temperatures acquired for this test over the JP-4 test since the JP-4 tended to be consumed in the initial fireball on impact. As with the EF4R-104 emulsion, the observed maximum heating rate was found to be nearly the same as JP-4. It was concluded that the postcrash fire hazard potential was as great as or greater than that of liquid JP-4.

The JP-4 base emulsion JP-4 EXP-4, with a yield stress of 800 dynes/cm$^2$, resulted in an ignition and postcrash fire nearly identical to that of the EF4R-104H fuel. The resulting temperatures, however, did not indicate as high an energy release as did the EF4R-104H fuel. However, the wind direction during this test may have been a factor since it was blowing the fire away from the temperature-calorimeter probes.

The liquid JP-8 fuel resulted in a violent ignition and postcrash fire that was nearly identical to the JP-4 test. The resulting fireball size was observed to be somewhat smaller than JP-4, which could be expected due to the reduced vaporization rate of JP-8. The fuel misting after impact appeared

much the same as JP-4, but the resulting flame speed through the mist was slower. Once the mist was heated by fire, the flame speed appeared to increase. As a result, fire spread was slower; however, nearly all the fuel was consumed by fire. No valid temperature or heating data were obtained in this test, as a malfunction occurred in the data recorder. It is expected that the heating data found in the spark hot-surface data would be representative of that expected here. The concluded postcrash fire hazard potential was considered slightly less than that for JP-4.

The Jet-A base emulsion Jet-A EXP-4, with a yield stress value of 1467 dynes/cm$^2$, resulted in a nonhazardous ignition and postcrash fire. An initial pilot ignition was observed as fuel globs impacted the open-flame igniters, but the fire did not propagate and tended to be self-extinguishing. Only the fuel that made direct contact with the igniters ignited and burned slowly around the igniters. Large fuel globs were formed after impact, and no visible misting occurred. The indicated temperature (Figure 84) resulted in a small localized burn in the vicinity of a temperature probe. The resulting heating rates were very low compared to JP-4 except for the one probe which indicated less than half the heating rate observed for JP-4. This occurred about 12 seconds after impact, as compared to 2 to 3 seconds after impact for JP-4. It was concluded that a nonhazardous postcrash fire condition resulted with this fuel.

The JP-8 base emulsion EF8R-104H, with a yield stress value of 1570 dynes/cm$^2$, resulted in a nonhazardous ignition and postcrash fire. An initial pilot ignition was observed as fuel globs impacted the open-flame igniter, but the fire did not propagate and tended to be self-extinguishing. Large fuel globs were formed after impact, and no visible misting occurred. The temperature data (Figure 84) indicated very little heating, with a maximum heating rate of one order of magnitude less than that observed for JP-4. This occurred 18 seconds after impact. It was concluded that a nonhazardous postcrash fire condition resulted with this fuel.

The JP-8 base emulsion EF8R-104, with a yield stress of 665 dynes/cm$^2$, resulted in a nonhazardous ignition and postcrash fire. An initial pilot ignition was observed off the first smudge pot as globs of fuel impacted the smudge pot igniter. The associated pilot fire did not propagate and tended to be self-extinguishing. Large to medium fuel globs, somewhat smaller than for the EF8R-104H fuel, were formed after impact, and no visible misting occurred. No temperature change was noted from the thermocouple calorimeters. An ignition susceptibility parameter of 0.1052 was calculated for this fuel and

test condition. It was concluded that a nonhazardous post-crash fire condition resulted with this fuel.

The Jet-A base gel #1, with a viscosity of 68 centipoise, resulted in a nonhazardous ignition and postcrash fire. An initial pilot ignition was observed off the first two smudge pots as the fuel impacted these igniters directly. The associated pilot fire did not propagate and tended to be self-extinguishing. Droplet formation after impact appeared to be relatively large with average fuel droplets the size of marbles. No visual misting was observed. No temperature change was noted from the thermocouple calorimeters. An ignition susceptibility parameter could not be calculated due to the lack of screening test data for gels. It was concluded that a nonhazardous postcrash fire condition resulted with this fuel.

The Jet-A base gel #2, with a viscosity of 40.7 centipoise, resulted in a potential hazardous ignition but with a nonhazardous postcrash fire. A small mist-phase fireball resulted from ignition off the first smudge pot igniter. A small ground fire resulted outside the thermocouple locations but did not propagate and therefore burned itself out. No temperature change was recorded. Fuel droplet sizes ranged from a mist phase to droplets somewhat smaller than for the gel #1. The presence of the mist-phase fireball provided an ignition potential for the rest of the fuel if more fuel had been available. Therefore, a hazardous postcrash fire rating must be recorded for this fuel.

For each of the above emulsified fuel tests, the ignition susceptibility parameter was computed using screening test criteria and the measured yield stress of each fuel. The value of the respective ignition susceptibility parameter is indicated for each fuel in Figures 83 and 84.

Results of Spark/Hot-Surface Tests

Two simulated full-scale impact tests were performed using the spark/hot-surface igniters for each of the ten fuels at an impact velocity of 65 ft/sec. The only environmental variable causing any change between the tests was the wind velocity and direction. Each test was conducted with a wind velocity of less than 10 mph. The maximum average temperature condition and associated maximum temperature envelope for each test are illustrated in Figures 85, 86, and 87. Two fuels resulted in no temperature increase (zero indicated heat rate).

The subsequent ignition and postcrash fire from the two liquid JP-4 tests resulted in a violent reaction and large fireball.

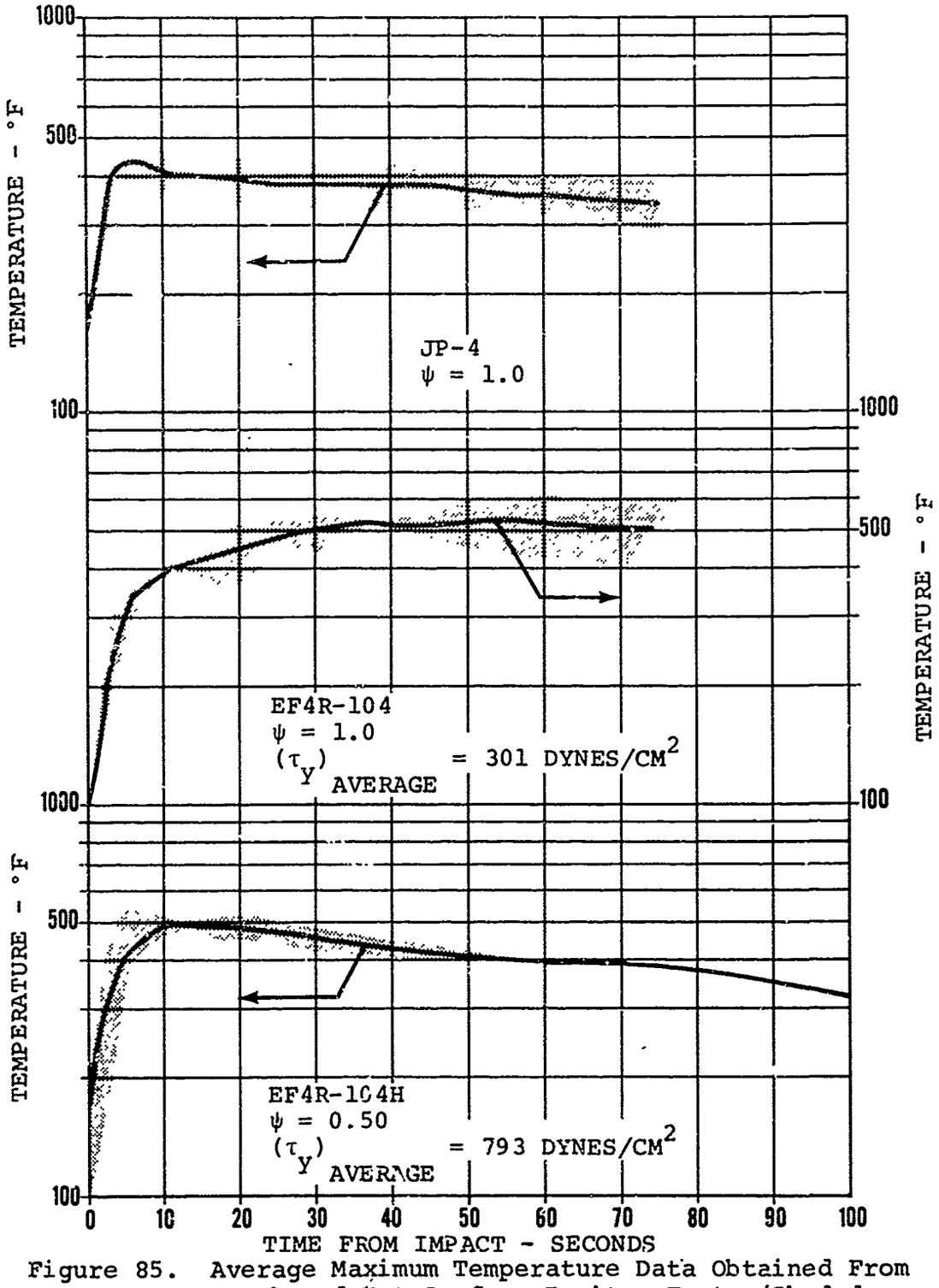


Figure 85. Average Maximum Temperature Data Obtained From Spark and Hot-Surface Igniter Tests (Shaded Area Denotes Temperature Envelope).

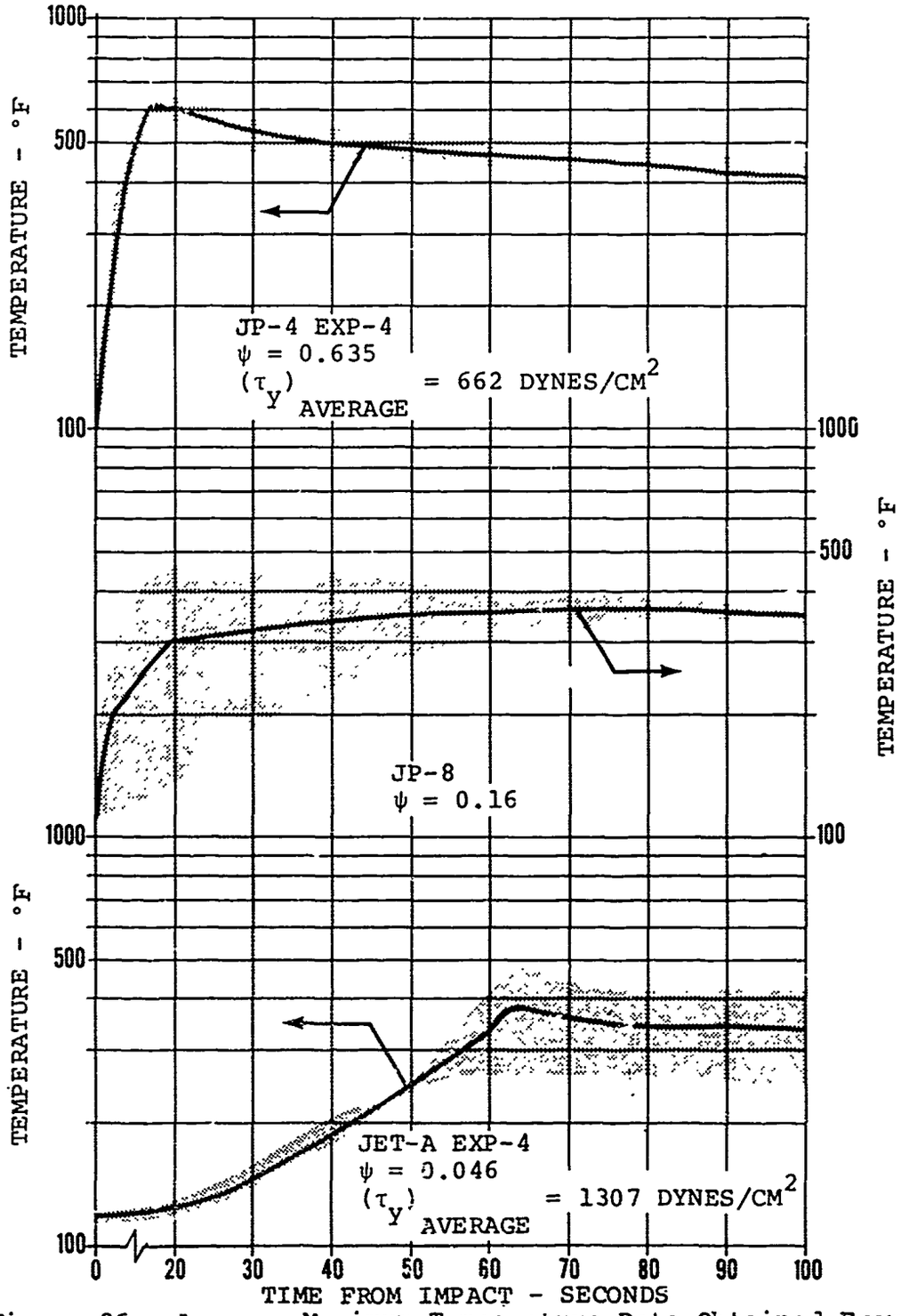


Figure 86. Average Maximum Temperature Data Obtained From Spark and Hot-Surface Igniter Tests (Shaded Area Denotes Temperature Envelope).

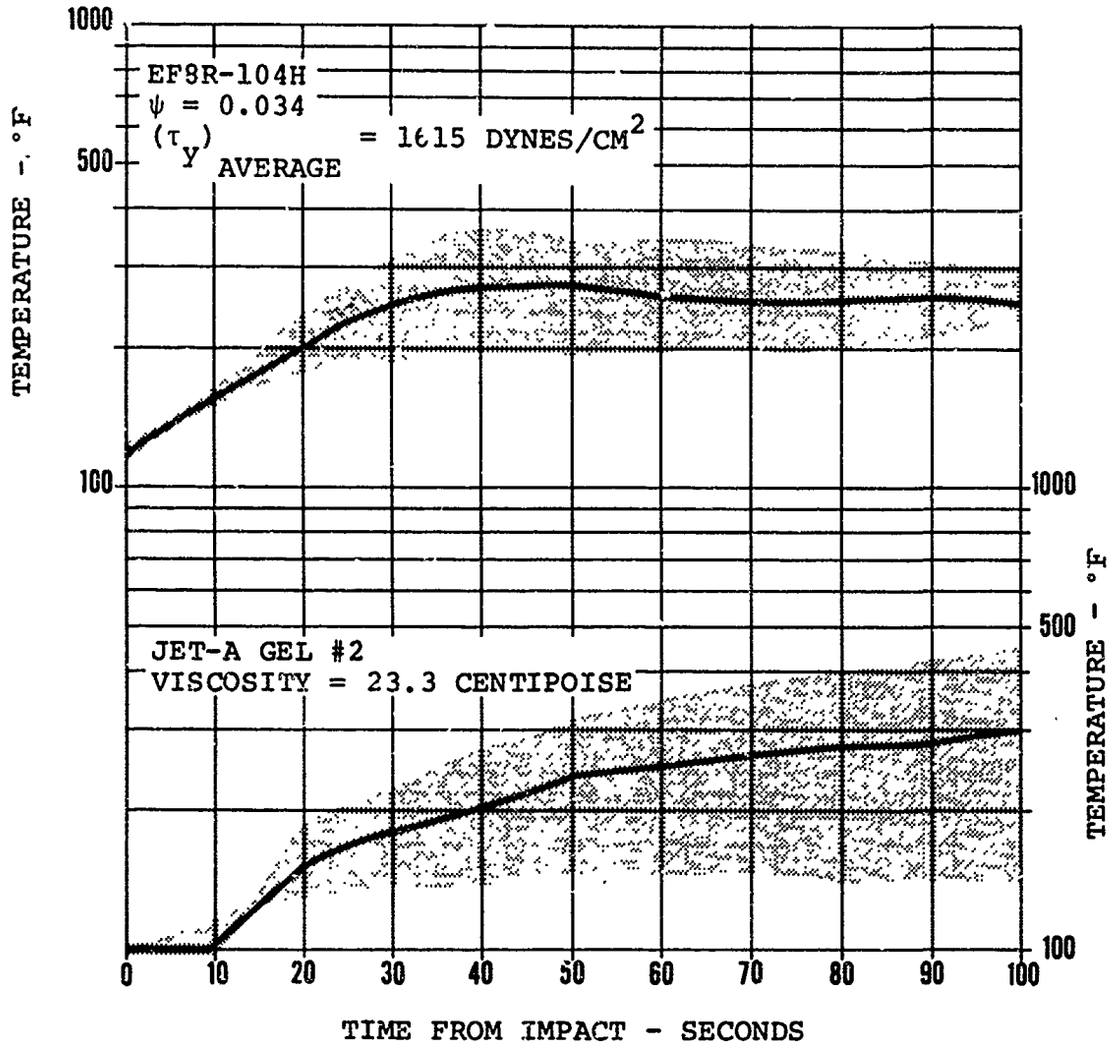


Figure 87. Average Maximum Temperature Data Obtained From Spark and Hot-Surface Igniter Tests (Shaded Area Denotes Temperature Envelope).

Nearly all the fuel was formed into a mist phase after impact. This fuel mist was ignited by the spark source, resulting in nearly complete combustion of the misted fuel while airborne. The fire spread over the test barrier, resulting in complete ignition of all the fuel. The maximum heating rates obtained in the tests were of the same order as those expected in JP-4 postcrash fires. The maximum average temperature condition, along with the maximum temperature envelope obtained in the two tests is presented in Figure 85.

Both of the JP-4 base emulsion EF4R-104 tests, with an average yield stress value of 301 dynes/cm$^2$, resulted in a violent ignition and postcrash fire of nearly the same magnitude as the JP-4 tests. The resulting fireball size was slightly smaller than for JP-4, but ignition off the spark resulted in nearly complete engulfment of the fuel in flame before reaching the ground. Small globs of fuel were observed with some fuel misting. The fire and fuel spread covered a larger area than that for JP-4 due to the fuel droplet size but resulted in complete burning of all the fuel. The postcrash fire burn time was longer than for JP-4 since the fuel globs slowed the burning rate of the fuel. The associated maximum heating rates were the same to slightly larger than those for the JP-4. It was concluded that the postcrash fire hazard potential was as great as or greater than that for the JP-4.

The JP-4 base emulsion EF4R-104H tests, with an average yield stress value of 793 dynes/cm$^2$, both resulted in a violent ignition and postcrash fire. The resulting fireball size was less than observed for JP-4. Ignition by the spark source was observed, and flame propagation through the airborne fuel globs was rapid. Much of the fuel was ignited before contacting the ground. Larger fuel globs were noted than were observed for the EF4R-104 with less fuel misting. The postcrash fire burn time was longer than for JP-4 due to the fuel droplet size; however, nearly complete burning of all fuel resulted. The associated maximum heating rates were the same to slightly larger than for the JP-4 fires. It was concluded that the postcrash fire hazard potential was as great as or greater than that for the liquid JP-4.

The JP-4 base emulsion JP-4 EXP-4 tests, with an average yield stress value of 662 dynes/cm$^2$, resulted in one test producing a violent ignition off the spark source and the other producing a slower ignition off the spark igniter with a hazardous postcrash fire as the fuel became heated. The fireball size for the former was nearly identical to the EF4R-104H fireball, whereas the latter resulted in a reduced fireball due to the slower ignition. The fuel glob sizes were nearly the same as for EF4R-104H. The fire and fuel spread covered a larger area

than the JP-4 tests but resulted in nearly complete burning of all the fuel. The associated maximum heating rates were the same to slightly larger than the JP-4 rates. The postcrash fire burn time was about the same as for EF4R-104H fuel. It was concluded that the postcrash fire hazard potential was as great as or greater than that for the liquid JP-4.

The liquid JP-8 fuel resulted in one test producing a violent ignition off the spark igniter and one test producing no ignition off the spark igniter but an ignition on the hot-source igniter followed by a slow flame propagation. Fuel misting from impact for both tests was similar to that observed with liquid JP-4. Flame spread in the violent reaction was slightly slower than for JP-4 with much the same characteristics observed in the open-flame igniter test. The observed heating rate for the violent reaction was found to be the same as for JP-4, whereas the nonviolent test resulted in heating rates of one order of magnitude less than those for JP-4. The average maximum temperature is illustrated in Figure 86. It was concluded that postcrash fire hazard potentials for the separate tests were (1) nearly as hazardous as JP-4 and (2) nonhazardous. Since one test resulted in a fire hazard, it was concluded that a hazardous rating must be placed on liquid JP-8 for this ignition source configuration.

Both of the Jet-A base fuel emulsion Jet-A EXP-4 tests, with an average yield stress value of 1307 dynes/cm$^2$, resulted in nonhazardous postcrash fires. Both tests produced slight ignition on the hot-surface igniter with little to no flame propagation. The ignition delay times compared with results reported in the screening tests for an 1100°F hot source. Maximum heating rates were one order of magnitude less than those obtained with JP-4. This is illustrated by the temperature data presented in Figure 86. Fuel globs were large, with no ignition from the spark igniter. It was concluded that a nonhazardous postcrash fire resulted for this fuel and igniter source configuration.

The JP-8 base fuel emulsion EF8R-104H tests, with an average yield stress of 1615 dynes/cm$^2$, as with the Jet-A EXP-4 fuel tests, resulted in nonhazardous ignition and postcrash fires. Both tests produced light ignition on the hot-surface igniter with little to no flame propagation. Flame propagation was slightly less than that of Jet-A EXP-4. No spark ignition was observed. The ignition delay times compared with those found in the screening tests for 1100°F hot surface. The maximum heating rates were one order of magnitude to less than those found for JP-4. Maximum temperature data are illustrated in Figure 87. Large fuel globs were observed after impact. It

was concluded that a nonhazardous postcrash fire resulted for this fuel and igniter source configuration.

The JP-8 base fuel emulsion EF8R-104 tests, with an average yield stress of 605 dynes/cm$^2$, both resulted in nonhazardous ignition and postcrash fires. Both tests resulted in no ignition from either the spark or hot-surface igniters. Misting was observed from fuel which contacted the hot surface. Fuel glob size following impact was observed to be slightly less than for the EF8R-104H fuel. No temperature increase was recorded due to the absence of fire. The calculated ignition susceptibility parameter was found to average 0.1092. A nonhazardous postcrash fire resulted from these tests.

The tests of the Jet-A based gel #1 with an average viscosity of 98 centipoise resulted in nonhazardous ignition and postcrash fires. Both tests resulted in a very slight fire on the spark igniter which did not propagate further. No ignition was observed off the hot surface; however, misting of fuel on hot surfaces was noted. Droplet formation resulted in an average size comparable to marbles, and little to no misting occurred. No temperature data were recorded due to a lack of fire. No ignition susceptibility parameter could be obtained due to lack of screening test results for gels. A nonhazardous postcrash fire resulted from these tests.

The tests of the Jet-A based gel #2 with an average viscosity of 26.6 centipoise resulted in hazardous ignition and postcrash fires. Both tests resulted in a small mist-phase fireball propagating from the spark igniter. One test resulted in a second fire from the hot-surface igniter. Fire spread was relatively slow but hazardous. Fuel droplet formation ranged from mist phase to droplets slightly smaller than gel #1. The maximum temperature data are shown in Figure 87. A maximum heating rate on the order of 5 times less than for a JP-4 fire was noted. No ignition susceptibility parameter could be obtained due to lack of screening test results for gels. A hazardous postcrash fire resulted from these tests.

For each of the spark and hot-surface tests just discussed, the ignition susceptibility parameter was computed for the emulsified fuels by using the screening test criteria and the average measured yield stress of each fuel. The value of the respective ignition susceptibility parameters is indicated for each fuel in Figures 85, 86, and 87, where applicable.

Results of On-Board (Engine Simulator) Igniter Tests

To provide a valid statistical analysis for the on-board igniter tests, three simulated full-scale impact tests were

performed for each of the ten fuels. Each test was conducted at an impact velocity of 65 ft/sec. The only environmental variable between the ten tests was the wind velocity and direction. Each test was conducted with a wind velocity of less than 10 mph. The average maximum temperature condition, along with the associated maximum temperature envelope for each fuel, is illustrated in Figures 88, 89, 90, and 91.

The ignition and postcrash fires from two of the three liquid JP-4 tests resulted in instant ignition when the igniter flame was produced. A violent postcrash fire resulted with rapid flame propagation on the ground. The timer for the on-board ignition device was incorrectly set and a 2- to 3-second delay time between impact and engine flaming (Figure 32) occurred rather than the desired 0.7-second delay time. The third JP-4 test resulted in a void run, as the burner device malfunctioned and did not ignite. The maximum heating rates for the two successful tests resulted in heating rate values that were slightly less than expected for JP-4 postcrash fires.

All the JP-4 base fuel emulsion EF4R-104 tests, with an average yield stress value of 351 dynes/$cm^2$, resulted in instant ignition when the burner flame was produced, followed by violent postcrash fires. Rapid flame propagation over the ground resulted. One test did not ignite on the initial igniter cycle. It appeared that the onslaught of fuel over the igniter either shorted the spark plug or produced too rich a fuel mixture to ignite. A relight cycle was made with a successful ignition by the flame, followed by a violent postcrash fire. Small fuel globs were produced upon impact. Maximum heating rate values were nearly the same as those experienced with JP-4 fires. Burn time was longer than for JP-4. It was concluded that the postcrash fire hazard potential was as great as or greater than that for liquid JP-4.

The JP-4 base fuel emulsion EF4R-104H tests, with an average yield stress value of 789 dynes/$cm^2$, all resulted in an instant ignition when the burner flame was produced, followed by a violent postcrash fire. A rapid flame propagation over the ground resulted. One test did not ignite on the initial igniter cycle. It appeared that the onslaught of fuel over the igniter either shorted the spark plug or produced too rich a fuel mixture to ignite. A relight cycle was made with a successful ignition by the flame, followed by a violent postcrash fire. Medium-sized fuel globs were produced upon impact. The burn time was longer than for JP-4 fuel. Maximum heating rate values were equal to those expected for JP-4 fires. It was concluded that the postcrash fire hazard potential was as great as or greater than that for liquid JP-4.

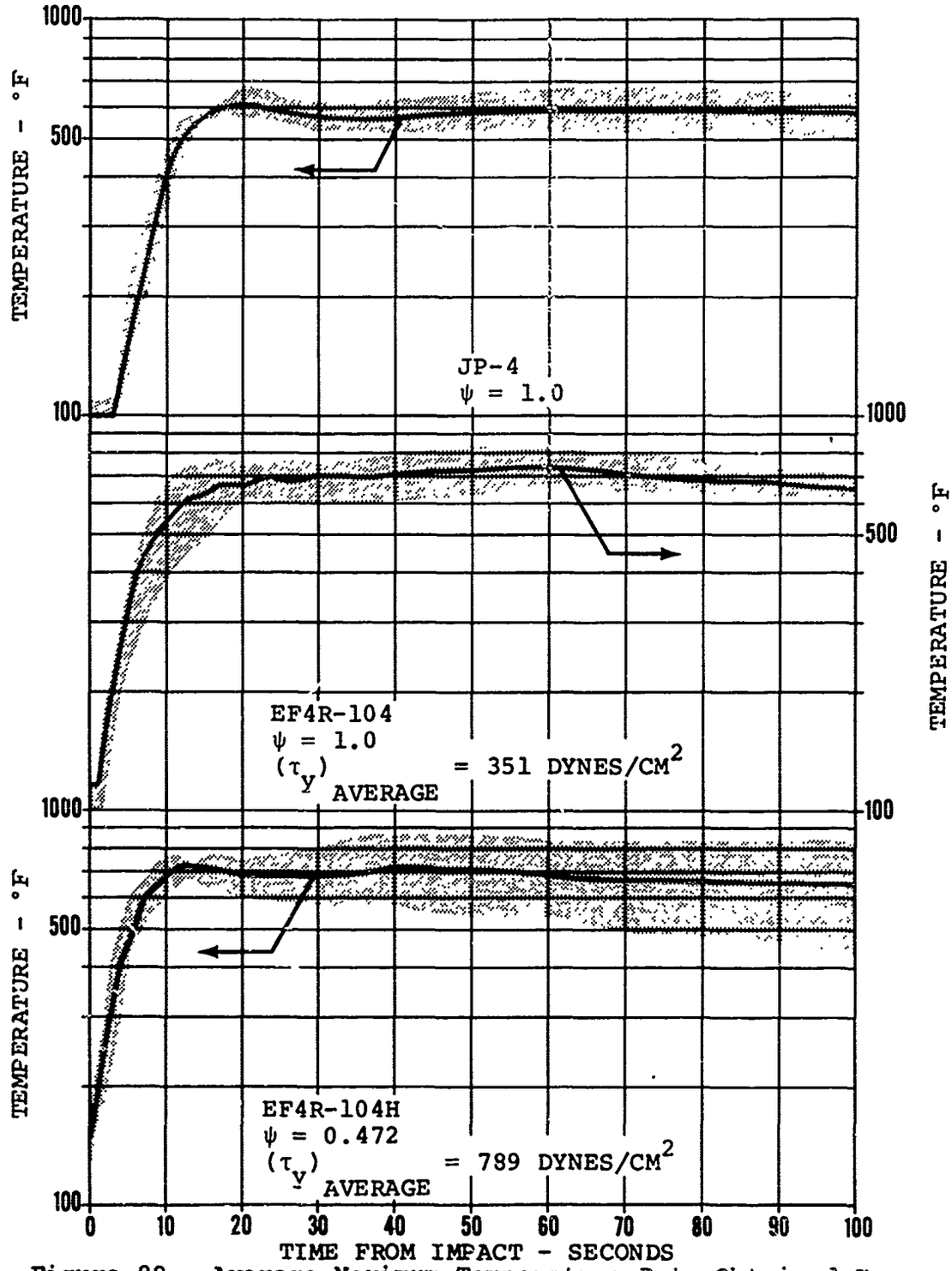


Figure 88. Average Maximum Temperature Data Obtained From On-Board Igniter Tests (Shaded Area Denotes Temperature Envelope).

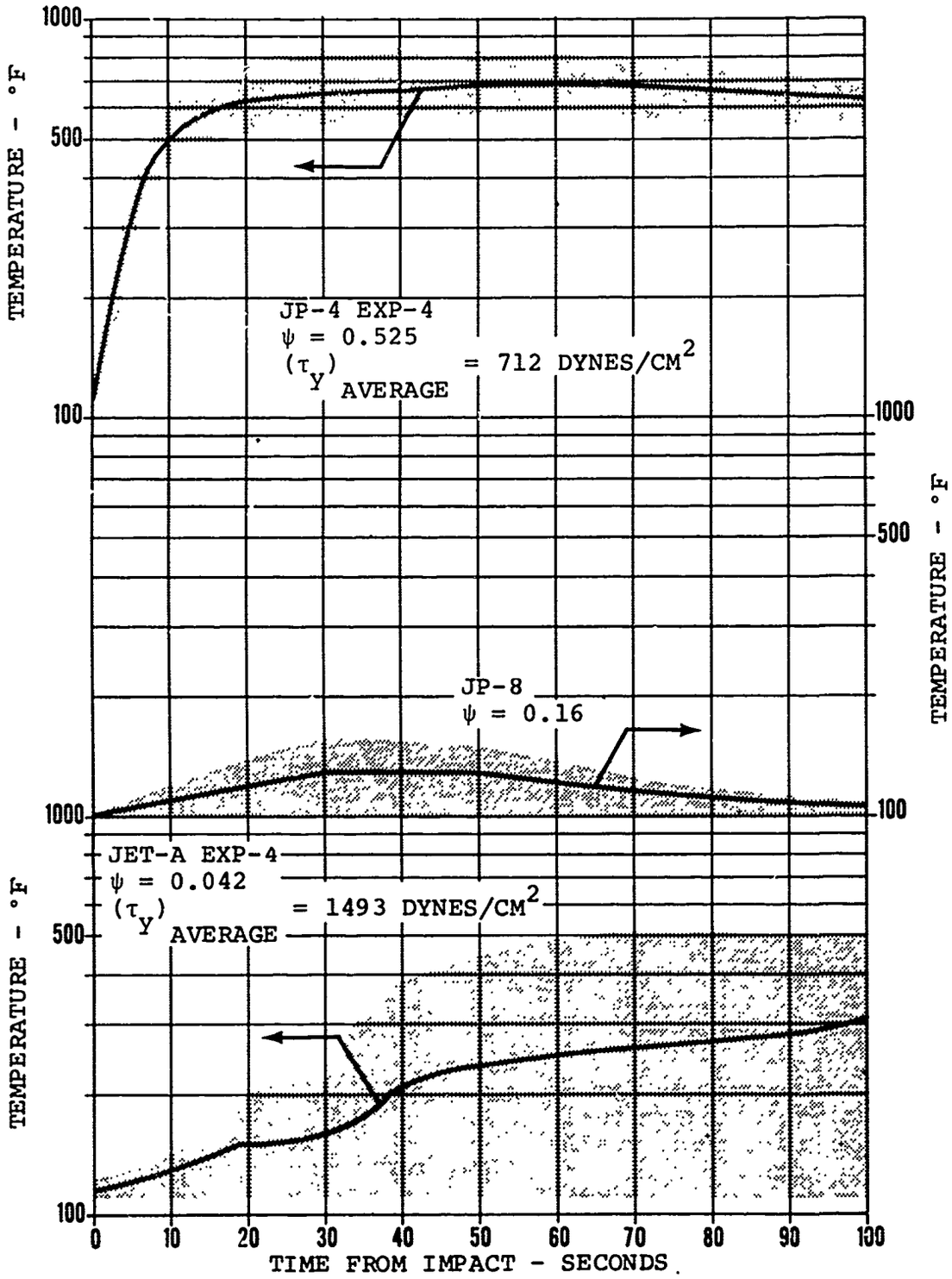


Figure 89. Average Maximum Temperature Data Obtained From On-Board Igniter Tests (Shaded Area Denotes Temperature Envelope).

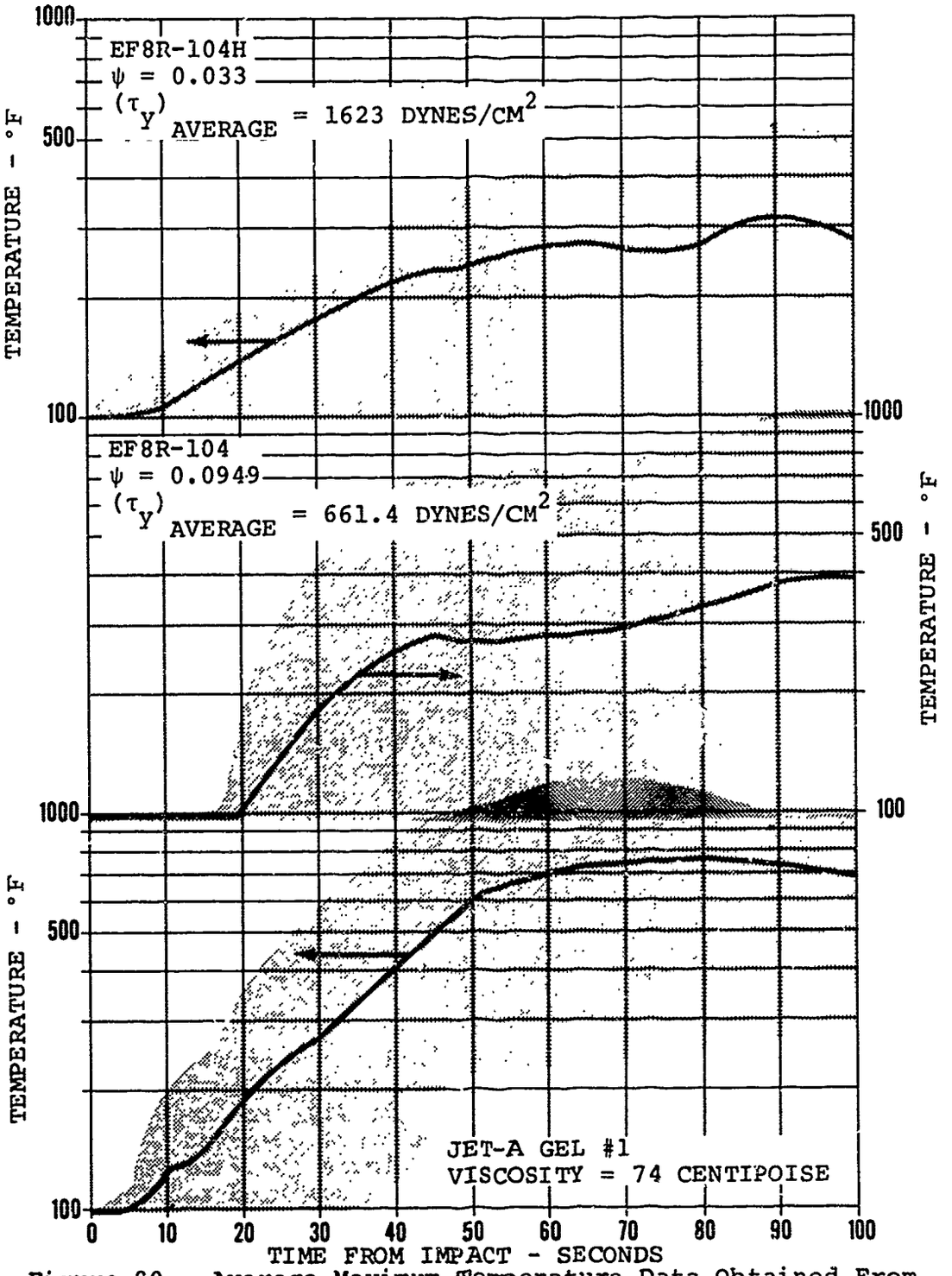


Figure 90. Average Maximum Temperature Data Obtained From On-Board Igniter Tests (Shaded Area Denotes Temperature Envelope).

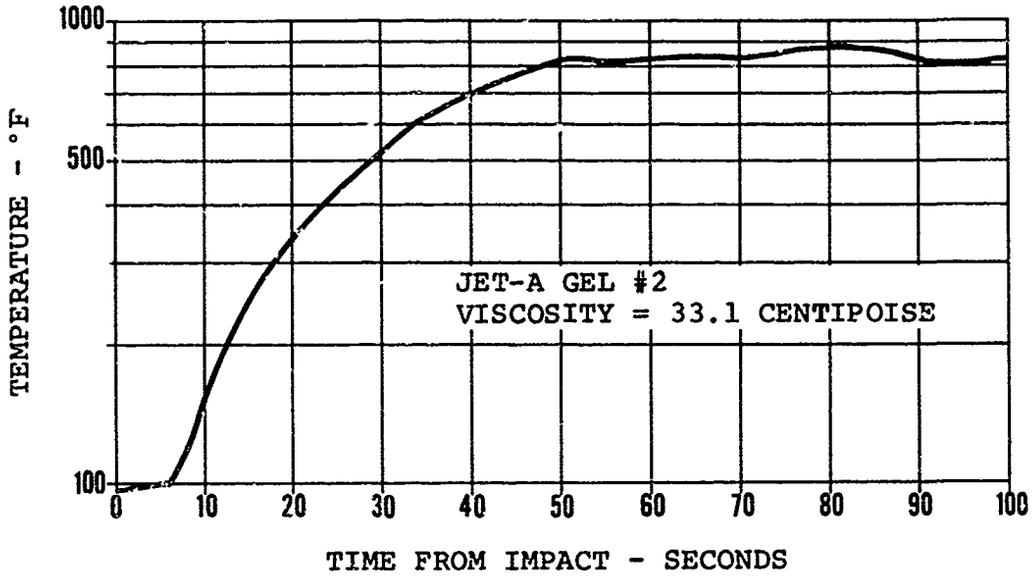


Figure 91. Maximum Temperature Data Obtained From On-Board Igniter Test on the Jet-A Gel #2.

The JP-4 base fuel emulsion JP-4 EXP-4 tests, with an average yield stress value of 712 dynes/cm$^2$, all resulted in an instant ignition when the burner flame was produced, followed by a violent postcrash fire. A rapid flame propagation over the ground resulted. One test did not ignite on the initial igniter cycle. It appeared that the onslaught of fuel over the igniter shorted the spark plug or produced too rich a fuel mixture to ignite. A relight cycle was made with a successful ignition by the flame, followed by a violent postcrash fire. Medium-sized fuel globs were produced upon impact. The maximum heating rates were the same as those experienced during JP-4 fires. Burn time was longer than for JP-4. It was concluded that the postcrash fire hazard potential was as great as or greater than that for liquid JP-4.

The liquid JP-8 fuel resulted in ignition and postcrash fire characteristics which ranged from no ignition to instant ignition from the burner flame, with light fire and very slow flame propagation over the ground. The maximum observed heating rates for this fuel and igniter configuration were found to be one order of magnitude less than those observed for JP-4 fires. The maximum average temperature with the maximum temperature envelope is illustrated in Figure 89. It was concluded that a nonhazardous postcrash fire resulted from JP-8 for this igniter configuration.

All the Jet-A base fuel emulsion (Jet-A EXP-4) tests, with an average yield stress value of 1493 dynes/cm$^2$, resulted in light ignition from the burner flame with zero to very slow flame propagation over the ground. Very little fuel was consumed by fire. Fuel globs produced from impact were large. The maximum heating rates observed were approximately one order of magnitude smaller than for JP-4 fires. The maximum average temperature and associated maximum temperature envelope are presented in Figure 89. It was concluded that a nonhazardous postcrash fire resulted with this fuel and igniter configuration.

The JP-8 base fuel emulsion EF8R-104H tests, with an average yield stress value of 1623 dynes/cm$^2$, all resulted in very light ignition on the fuel tank support arm (from either the flame or hot surface) with zero to very little postcrash fire and flame propagation. Large fuel globs were produced upon impact. The maximum heating rates observed were one order of magnitude less than for JP-4 fires. The maximum average temperature and associated maximum temperature envelope are presented in Figure 90. It was concluded that a nonhazardous postcrash fire resulted with this fuel and igniter configuration.

The JP-8 base fuel emulsion (EF8-104) tests, with an average yield stress value of 661.4 dynes/cm$^2$, resulted in two tests having a nonhazardous ignition and postcrash fire and a third test having a hazardous postcrash fire. The two nonhazardous tests resulted in a small flame on the support arm but the fire did not propagate. No temperature data were recorded for these tests due to the absence of sufficient fire. The hazardous test resulted in an initial small fire over the support arm with slow flame propagation. The fixture stopping distance for this test (10 feet) was considerably below the design values (18-30 feet) which resulted in a greater quantity of fuel in the vicinity of the support arm. Once enough heat was generated, the fuel vaporized sufficiently to support combustion and the fire spread more rapidly. The maximum temperature data for this test, along with the average for the three tests, are illustrated in Figure 90. Fuel globs slightly smaller than for the EF8R-104H fuel were noted after impact. The maximum heating data were in the order of five times less than for a JP-4 fire. Due to the atypical circumstances of the third test, it was concluded that a moderately hazardous postcrash fire rating should be given to this fuel.

The Jet-A base fuel gel #1 tests, with an average viscosity of 74 centipoise, all resulted in hazardous postcrash fires. Each test resulted in flame on the support arm with moderately

slow flame propagation until sufficient heat was generated to form a more combustible condition, at which time flame propagated readily. Droplet formation was much the same as the previous gel #1 tests with little to no mist phase observed. The maximum average temperature data are illustrated in Figure 90. The maximum heating data were just less than half that expected for JP-4 fires. It was concluded that a hazardous postcrash fire resulted for this fuel.

The Jet-A base fuel gel #2 tests, with an average viscosity of 33.1 centipoise, all resulted in hazardous ignition and postcrash fires. Each test resulted in flame on the support arm with moderately slow flame propagation until sufficient heat was generated to sustain continued combustion. Some fireballing was observed as fuel fell onto the igniter flame with a resultant increase in the fire spread rate. Fuel droplet formation was not unlike that observed in previous tests with this fuel, and some misting was observed. The maximum temperature data obtained from one of the tests are illustrated in Figure 91. No temperature rise data were obtained from two of the tests because the test fixture traveled out of the thermocouple range past the barrier. The maximum heating rate was found to be in the order of five times less than for JP-4 fires. It was concluded that a hazardous postcrash rating should be applied to this fuel.

For each of the above sets of tests, the ignition susceptibility parameter was computed for the emulsified fuels using screening test criteria and the average measured yield stress of each fuel. The value of the respective ignition susceptibility parameter is indicated for each fuel in Figures 88, 89, 90, and 91, except for the gelled fuel which could not be obtained due to insufficient knowledge of gelled fuel characteristics.

Several physical characteristics regarding emulsions and gels were observed in all the simulated full-scale tests but appeared to be particularly important for the on-board (engine simulator) igniter. From the previously discussed results, it was found that the on-board igniter produced a higher relative hazard rating with gelled fuel than with emulsified fuel or even liquid JP-8. A discussion of the various types of igniters with regard to combustible fuel characteristics therefore appears to be in order.

It was felt, throughout the screening and simulated full-scale tests, that the emulsified fuels tended to slip off hot surfaces readily. This is probably due to the weight associated with fuel globs as compared to fuel droplets or fuel film.

Another factor is the ability of the heat to break down the interface between the fuel glob and hot surface to form a very low viscosity medium. Although the emulsions ignite readily in a contained environment, such as the autcignition tester, the time which the fuel stays on an uncontained not surface is generally shorter than the ignition delay time, especially in a dynamic environment. Contrary to this, however, the gelled fuels tested tended to stick to hot surfaces and also did not have the heavier globular form, thus allowing time for ignition. For the on-board ignition device in particular, fuel impacting and sticking to the igniter and support arm (which is also hot in the vicinity of the igniter) is easily ignited by the hot surface or flame.

The various types of ignition sources used in the simulated full-scale test covered nearly every type of physical combustion between fuel and igniter. For fuels which form a mist phase upon impact, the spark source provides a catastrophic ignition source in which the fuel mist is ignited while following its trajectory after impact. This condition allows the ensuing high-energy fireball to propagate through the fuel in flight and descend upon any unburned fuel on the ground. The open-flame igniters, although igniting the fuel in either a fuel mist phase or fuel droplet phase, do so mainly as the fuel descends onto the barrier. The hot-surface igniter ignites fuels after the main portion of the fuel is on the ground (for instance in pools) according to their autoignition characteristics. For a hazardous fire to result from this igniter, flame speeds on the ground or in pools must be rapid.

The on-board igniter contains three different sources for ignition of fuel after the fuel has reached the ground: (1) the fuel on the hot surface can autoignite, (2) the belching flame can ignite any fuel in its vicinity, and (3) the hot surface can cause the fuel on it to form a mist which then can be readily ignited by the flame. In most cases, the third sequence of ignition resulted, and this generally resulted in a more hazardous situation, especially for those fuels which stayed in the vicinity of the igniter.

With the above types of igniters, some fuels were more hazardous with one ignition system, while others were more hazardous with another ignition system. For example, a fuel which forms a fuel mist is generally more hazardous with a spark igniter, while a fuel which does not form a mist and slips off hot surfaces is more hazardous when accompanied by open-flame igniters. Further, a fuel which does not form a mist and sticks to hot surfaces is generally more hazardous when accompanied by a hot-surface or the on-board type of igniter.

## TEST CORRELATION AND SAFETY EVALUATION CRITERIA

The laboratory screening test data presented in the Test Results section illustrate the performance and characteristics of several emulsified fuels under simulated crash conditions. The measure of safety has been shown to be a function of an ignitability parameter ($\psi$) which has also been related to an empirical equation. This equation includes a function of the characteristic kinetic energy and two constants which appear to be related to the yield stress and type of test conducted. If it can be shown that the constants ($V_j$, $V_i$ and $K_1$, $K_2$) in the equations for the ignitability parameter ($\psi_{\text{Base Fuel}}$) can be related anlytically or graphically to fuel yield stress from the test results, then an estimated value of ($\psi_{\text{Base Fuel}}$) versus input wind shear velocity and/or impact kinetic velocity can be calculated for any emulsified fuel where the yield stress is known.

Figure 92 presents the constant $K_1$ obtained from the mean data resulting from the wind shear tests versus emulsified fuel yield stress. A definite correlation between $K_1$ and yield stress exists. The bars accompanying the data points represent the range of measured yield stresses for which the mean $\psi_{\text{Base Fuel}}$ versus wind shear velocity curves for a particular emulsified fuel were obtained. Figure 93 presents a similar relationship for $V_j$ obtained from the wind shear data. As with Figure 72, a definite dependence of $V_j$ on yield stress is apparent.

Figure 94 presents the constant $K_2$ obtained from the relation for the mean data resulting from the impact dispersion/atomization tests versus emulsified fuel yield stress. As with the wind shear results, a definite correlation between $K_2$ and yield stress is apparent. Figure 95 presents the constant $V_i$ versus emulsified fuel yield stress; again, $V_i$ illustrates a definite dependence on emulsified fuel yield stress.

If the $\psi$ relationship is known between liquid JP-4 and the liquid base fuel of a given emulsified fuel, then the values of $\psi_{\text{JP-4}}$ for the emulsified fuel can be estimated from the following equation:

$$\psi_{\text{JP-4}} = (\psi_{\text{JP-4}})_{\text{Base Fuel}} \times (\psi_{\text{Base Fuel}})_{\text{Emulsified Fuel}} \quad (36)$$

As shown previously, for wind shear,

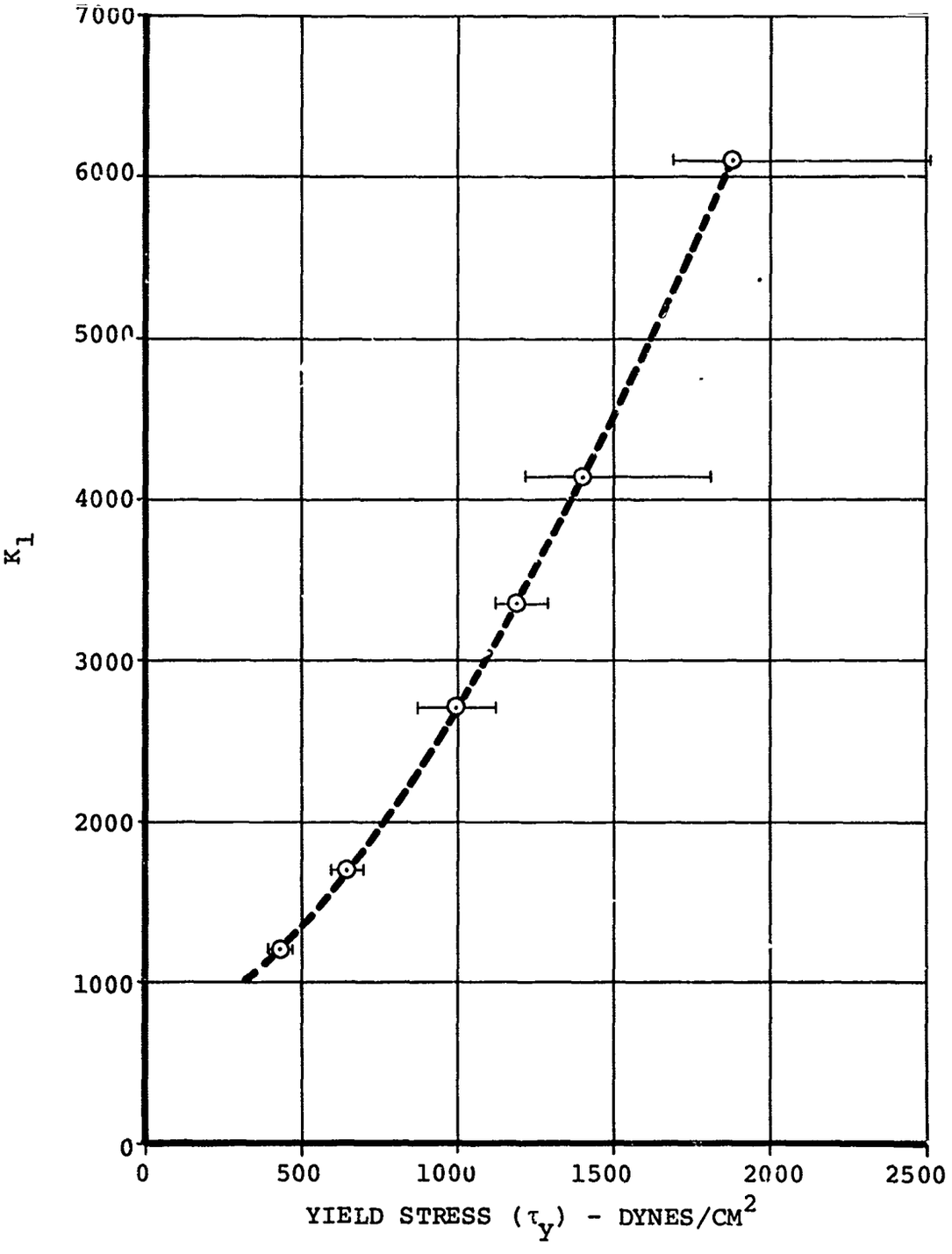


Figure 92. Yield Stress Versus K for Wind Shear Data.

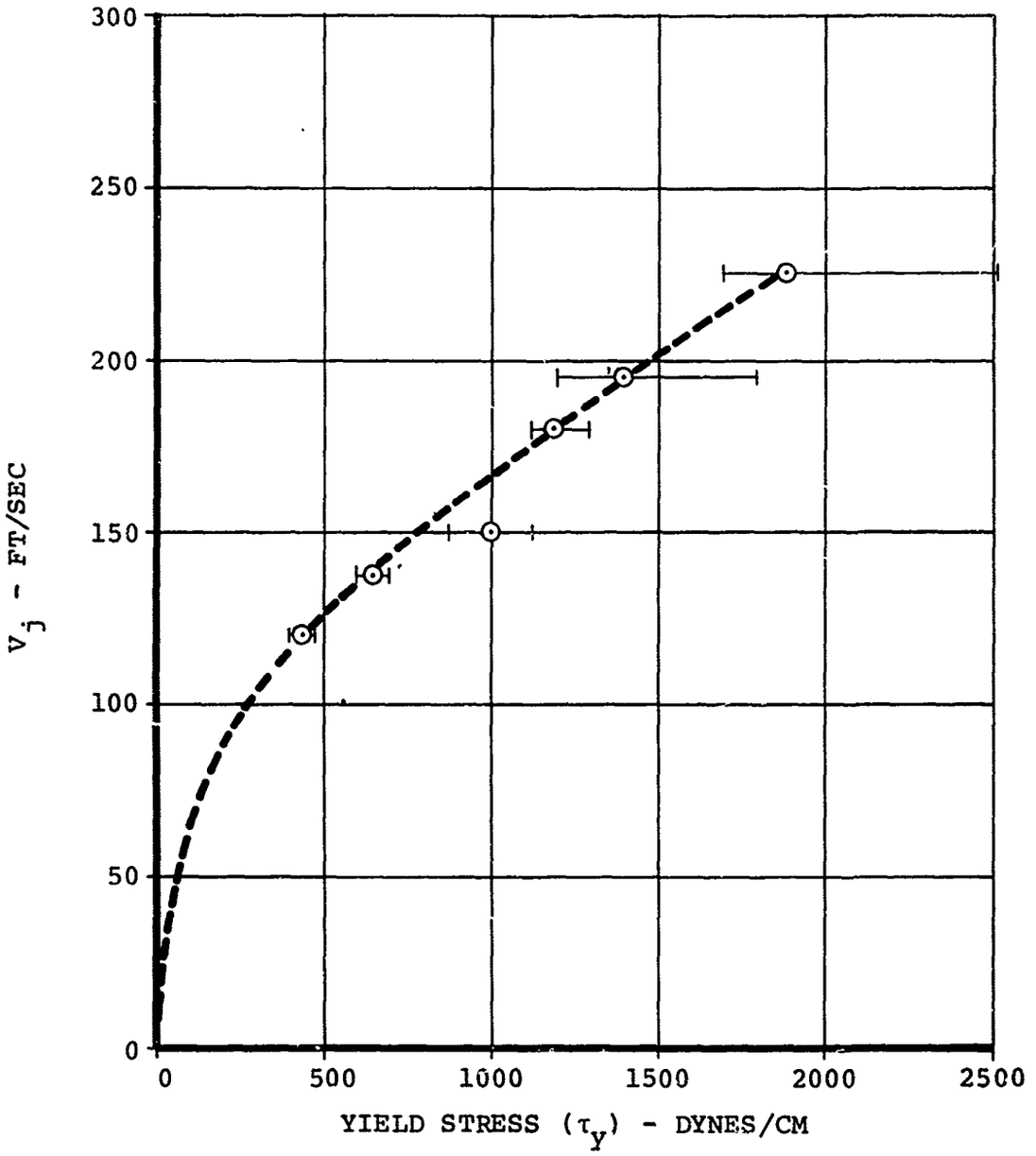


Figure 93. Yield Stress Versus $V_j$ for Wind Shear Data.

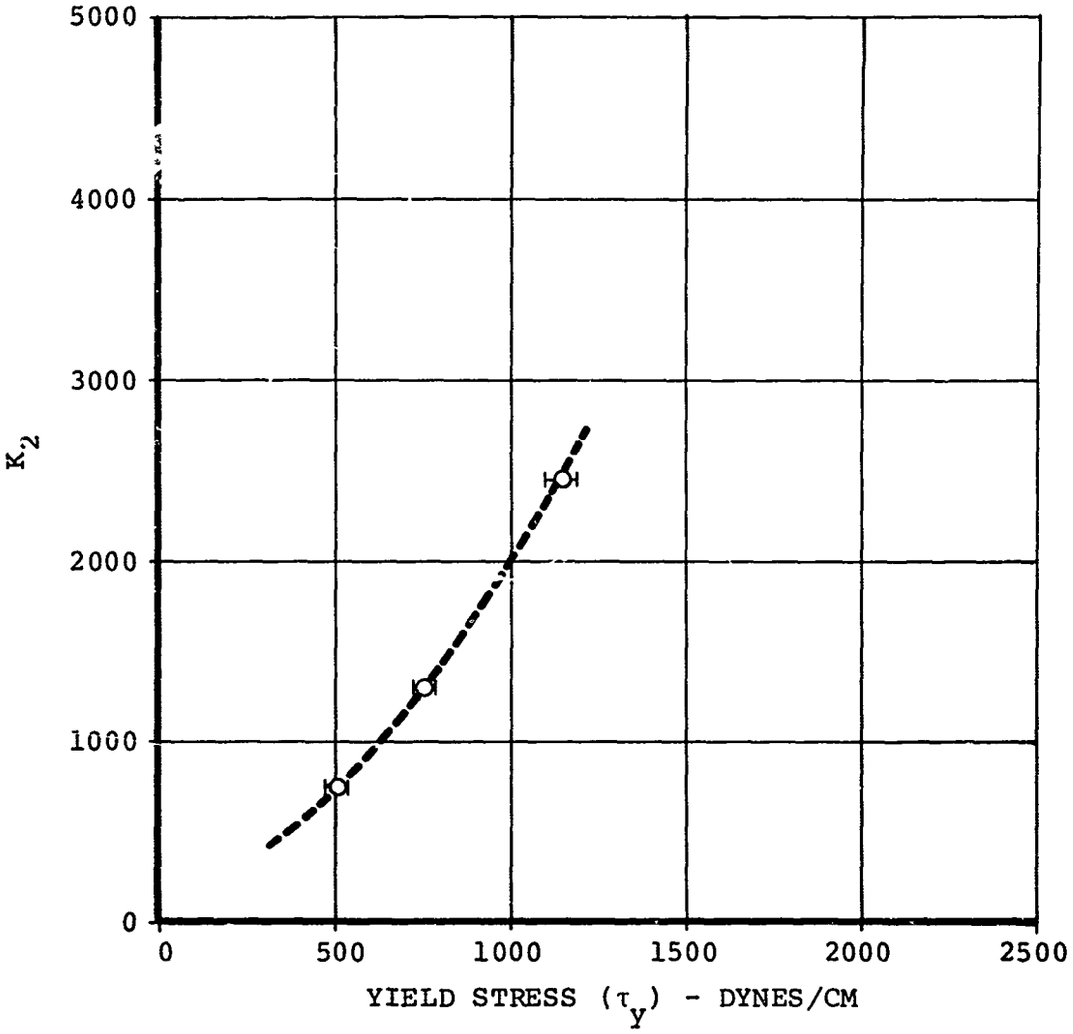


Figure 94. Yield Stress Versus K for Impact Dispersion/Atomization Data.

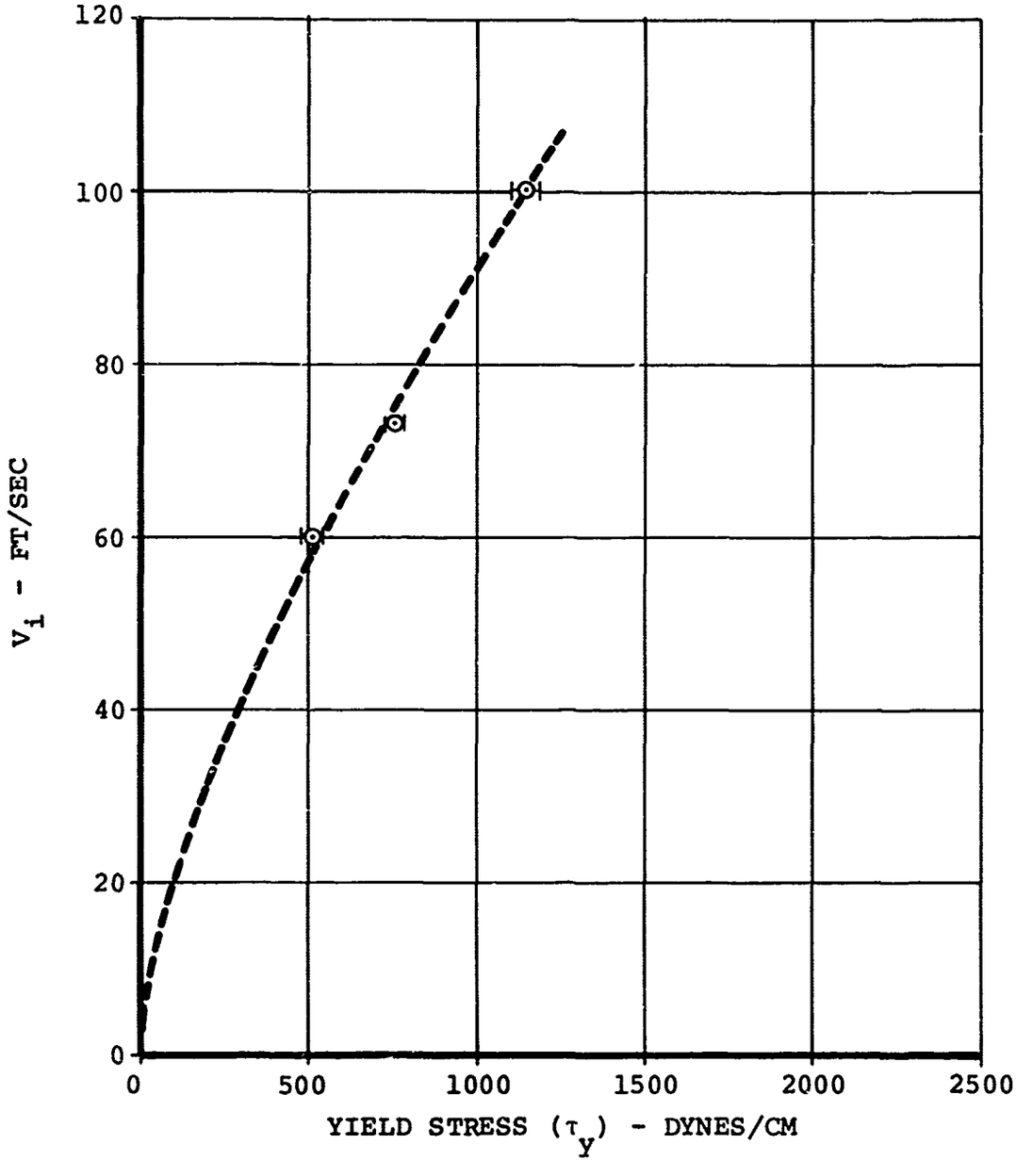


Figure 95. Yield Stress Versus $V_i$ for Impact Dispersion/Atomization Data.

$$\psi_{JP-4} = (\psi_{JP-4})_{\text{Base Fuel}} \exp\left[-\frac{(V_j - V)^2}{K_1}\right], \quad V \leq V_j \qquad (37)$$

or, if one equates the relationship between the constants and yield stress, this becomes

$$\psi_{JP-4} = (\psi_{JP-4})_{\text{Base Fuel}} \exp -\left[(\sqrt{27.2\tau_y} - V_{Air})^2/(23 + 0.029\ \tau_y)^2\right], \quad V_{Air} \leq \sqrt{27.2\ \tau_y} \qquad (38)$$

and for impact dispersion/atomization,

$$\psi_{JP-4} = (\psi_{JP-4})_{\text{Base Fuel}} \exp\left[-(V_i - V\ \text{SIN}\theta)^2/K_2\right], \quad V\ \text{SIN}\theta\ V_i \qquad (39)$$

or

$$\psi_{JP-4} = (\psi_{JP-4})_{\text{Base Fuel}} \exp -\left\{\left[\sqrt{10.63(\tau_y - 212)} - V\ \text{SIN}\theta_i\right]^2/(9.5 + 0.035\ \tau_y)^2\right\}, \quad V\ \text{SIN}\theta_i \leq \sqrt{10.63\ (\tau_y - 212)} \qquad (40)$$

Assuming a maximum crash survivability velocity of 65 ft/sec, the maximum expected wind shear velocity would also equal 65 ft/sec. Using a 45-degree average impact angle, the maximum impact survivable kinetic velocity is 46 ft/sec. Thus, the safety performance criterion for wind shear can be based on the value of $\psi_{JP-4}$ at a wind shear velocity of 65 ft/sec. Likewise, the safety performance criterion for fuel impact can be based on the value of $\psi_{JP-4}$ at a kinetic velocity of 46 ft/sec.

For the fuels tested in the laboratory screening tests study, Table I lists the safety performance of these fuels from a wind shear standpoint.

Table II lists the safety performance of the fuels tested obtained from an impact dispersion/atomization standpoint.

The smaller the value of $\psi_{JP-4}$, the safer the fuel is expected to be. In both types of crash environments, a characteristic value of $\psi_{JP-4}$ exists below which the performance is considered safe from a postcrash fire standpoint. This limiting value

| TABLE I. WIND SHEAR SAFETY PERFORMANCE | |
|---|---|
| Fuel | Safety Performance Parameter, $\psi_{JP-4}$ |
| JP-4 | 1.000 |
| EF4R-104 ($\tau_y$ = 437 Dynes/cm$^2$) | 0.074 |
| EF4R-104 ($\tau_y$ = 645 Dynes/cm$^2$) | 0.044 |
| EF4R-104 ($\tau_y$ = 1400 Dynes/cm$^2$) | 0.028 |
| EF4R-104H ($\tau_y$ = 1192 Dynes/cm$^2$) | 0.020 |
| EF4R-104H ($\tau_y$ = 1886 Dynes/cm$^2$) | 0.014 |
| JP-8 | 0.80 |
| EF8-104H ($\tau_y$ = 1000 Dynes/cm$^2$) | 0.053 |

| TABLE II. IMPACT DISPERSION/ATOMIZATION SAFETY PERFORMANCE | |
|---|---|
| Fuel | Safety Performance Parameter, $\psi_{JP-4}$ |
| JP-4 | 1.0 |
| EF4R-104 ($\tau_y$ = 508 Dynes/cm$^2$) | 0.763 |
| EF4R-104H ($\tau_y$ = 1143 Dynes/cm$^2$) | 0.303 |
| JP-8 | 0.166 |
| EF8-104H ($\tau_y$ = 755 Dynes/cm$^2$) | 0.099 |

was quite precisely determined as the primary result of the simulated full-scale tests (see Figures 96 and 97). The actual limiting value $\psi_{JP-4}$ in a full-scale environment could not be obtained without the simulated full-scale verification. With

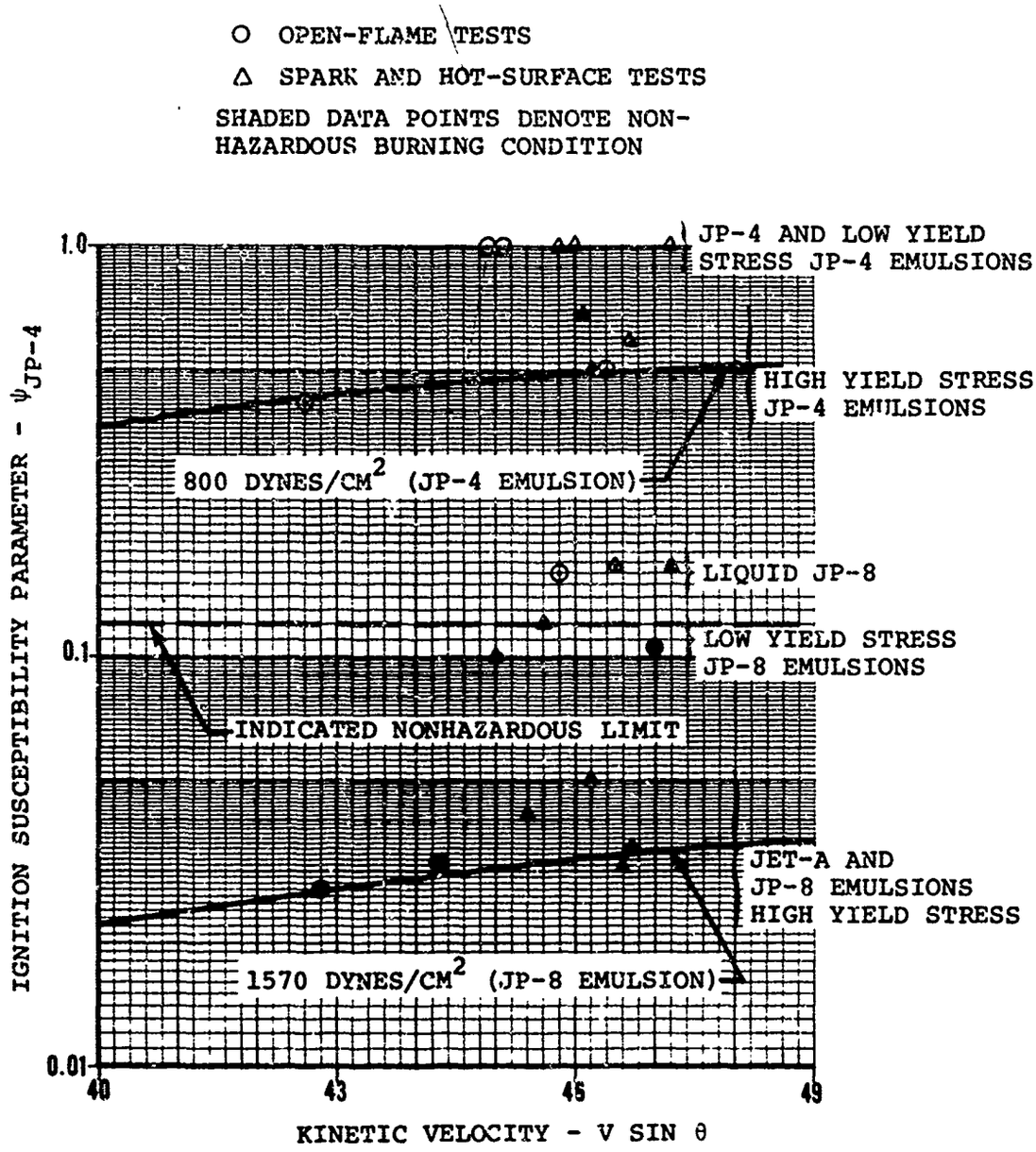


Figure 96. Simulated Full-Scale Test Results for the Open-Flame and Spark/Hot-Surface Igniter Tests.

SHADED POINTS DENOTE NONHAZARDOUS BURNING CONDITION

SUBSCRIPT "R" DENOTES RELIGHT CONDITION

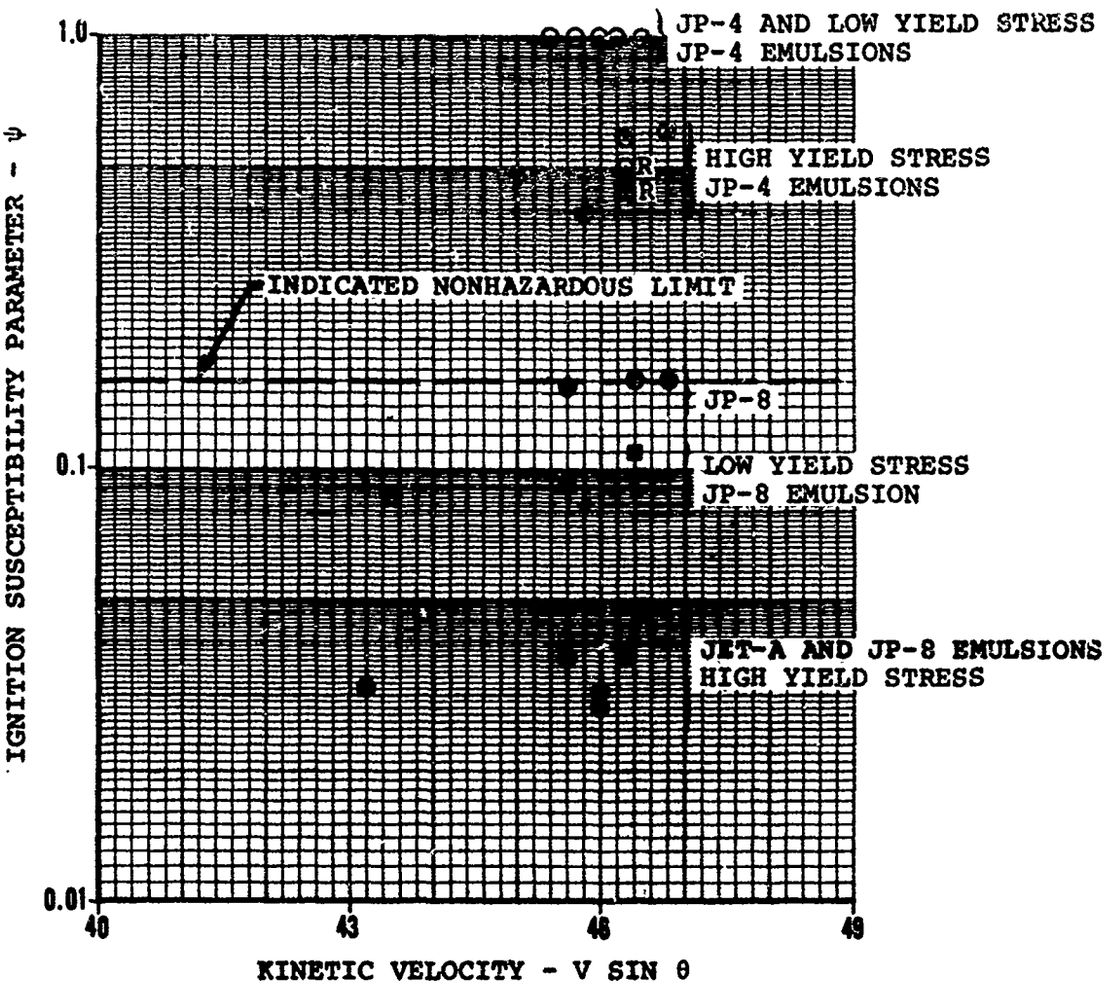


Figure 97. Simulated Full-Scale Test Results for the On-Board (Engine Simulator) Igniter Tests.

this additional information, the screening tests can be used to assess the full-scale safety performance of a specific fuel. An alternate approach to the determination of this limit was also illustrated in the impact ignition tests where specific ignition limits were found as a function of the parameter $\psi_{JP-4}$. This latter method was much less reliable, as pointed out previously.

In comparing the results of the nozzle shear tests, it was found that the data from these tests indicated the same trends as those found in the wind shear and impact tests. A direct correlation was not apparent, as was the case between wind shear and impact data, since the mechanisms were characteristic to each test system. It is significant, however, that the data from each type of test resulted in the same general trends and could be represented by the same form of empirical equation. The constants $V_i$, $V_i$ and $K_1$, $K_2$, therefore, are not only a function of input shear loads and yield stress but depend upon test facility conditions also.

In comparing the safety performance parameter results between wind shear and impact dispersion/atomization as illustrated in Tables I and II for JP-8 and emulsified JP-8, there appears to be a discrepancy. The values of the safety parameters for these fuels should correlate more closely with respect to the other fuel data. For example, the value of 0.8 for JP-8 in the wind shear results should more closely represent the ratio of vapor pressure between JP-4 and JP-8, as was the case for the impact dispersion/atomization results. It is felt that this discrepancy may be due to an instrumentation error in the calibration of fuel/air ratio for the JP-8 and EF8-104H wind shear data. Investigation of the calibration data results in a possible change in these values by a factor of 0.57 which would result in a wind shear safety parameter value of 0.43 for JP-8 and of 0.028 for EF8-104H.

It has been shown that safety apparently increases with an increase in yield stress for the same base fuel. However, other sources, as discussed under Analytical Considerations, have indicated mechanisms which might reduce the safety of an emulsified fuel by increasing its yield stress. Here it was hypothesized that increasing the yield stress decreases the critical stress and, in turn, decreases the shear energy necessary to break up the fuel. The physics for these effects appears to be sound. However, such a situation was not observed directly in the data obtained in this program, except possibly in the impact ignition tests where ignition of the higher yield stress EF4R-104H occurred more readily than the lower yield stress EF4R-104. Although, generally, no trend to more extensive breakup and atomization with the higher yield

stress fuels was observed, the yield stress values tested may not have been high enough to display this effect under the test conditions studied. Therefore, it is felt that if higher yield stress emulsions (in the relaxed state) than those tested here are to be considered, they should be screened through testing to verify the absence of these effects.

The discussion of the simulated full-scale tests in the Test Results section presented the observed (visual and photographic) and recorded results associated with the three igniter configurations and the 10 fuels tested. The performance of the fuels was presented as either a hazardous or nonhazardous postcrash fire condition. The ground rules on which a nonhazardous condition exists were based on the probability of whether there would be sufficient time available to allow a surviving human to egress the aircraft. In most cases for the test resulting in a nonhazardous condition, fire intensity was so small that neither an aircraft burn-through hazard or a ground fire hazard for occupant egress would have been encountered. For border-line observations, the temperature data were extrapolated to a full-scale condition to insure at least an order of magnitude increase in aircraft burn-through time.

Table III presents a synopsis of the postcrash fire hazard results for all three igniter configurations used in the simulated full-scale impact tests. These results for emulsified fuels may be generalized through the application of screening test criteria as discussed below.

By computing and comparing the ignition susceptibility parameters $\psi$ for each of the fuels tested, a value can be obtained for $\psi$ which represents the limiting, nonhazardous condition. This limiting value of $\psi$ (above which a hazardous condition may exist and below which a nonhazardous condition exists) allows full-scale safety performance predictions on the basis of the screening test results. Figure 96 presents the simulated full-scale data obtained from the open-flame and spark/hot-surface igniter tests. For each test, a value of $\psi$ was computed using the measured yield stress and the screening test performance equation applicable to the impact dispersion/atomization condition. This computed value was plotted versus impact kinetic velocity ($V\sin\theta_i$). In Figure 96, the shaded data points denote nonhazardous postcrash fire conditions while the open data points denote hazardous postcrash fire conditions. The indicated limiting value of $\psi$ from Figure 96 is 0.12.

It is observed that the test results for the open-flame igniter tests did not differ appreciably from those of the spark and hot-surface ignition tests. Although the open-flame test was

TABLE III. SIMULATED POSTCRASH FIRE RESULTS

| Fuel | Open-Flame Tests | Spark/Hot-Surface Tests | | On-Board (Engine Simulator) Tests | | |
|---|---|---|---|---|---|---|
| | | Test 1 | Test 2 | Test 1 | Test 2 | Test 3 |
| JP-4 | Hazardous | Hazardous | Hazardous | Hazardous | Hazardous | * |
| EF4R-104 | Hazardous | Hazardous | Hazardous | Hazardous | Hazardous | Hazardous** |
| EF4R-104H | Hazardous | Hazardous | Hazardous | Hazardous | Hazardous | Hazardous** |
| JP-4 EXP-4 | Hazardous | Hazardous | Hazardous | Hazardous | Hazardous | Hazardous** |
| JP-8 | Hazardous | Hazardous | Non-hazardous | Non-hazardous | Non-hazardous | Non-hazardous |
| Jet-A EXP-4 | Non-hazardous | Non-hazardous | Non-hazardous | Non-hazardous | Non-hazardous | Non-hazardous |
| EF8R-104H | Non-hazardous | Non-hazardous | Non-hazardous | Non-hazardous | Non-hazardous | Non-hazardous |
| EF8R-104 | Non-hazardous | Non-hazardous | Non-hazardous | Non-hazardous | Hazar-dous*** | Non-hazardous |
| Jet-A Gel #1 | Non-hazardous | Non-hazardous | Non-hazardous | Hazardous | Hazardous | Hazardous |
| Jet-A Gel #2 | Hazardous | Hazardous | Hazardous | Hazardous | Hazardous | Hazardous |

*On-board igniter malfunction.
**On-board igniter malfunction or swamped with fuel, igniter relight was successful.
***Stopping distance too short.

initially considered more severe from an ignition standpoint, this observation allowed the data from both series of tests to be plotted together in Figure 96.

Figure 97 presents the simulated full-scale data obtained from the on-board (engine simulator igniter) tests. As in Figure 96, the value of $\psi$ for each test is plotted versus kinetic velocity. The shaded data points denote nonhazardous post-crash fire conditions while the open data points denote hazardous postcrash fire conditions. With the on-board igniter, a limiting value of $\psi$ was obtained as 0.16. However, since it must be assumed that any ignition source could happen during a crash, the resultant limiting value of $\psi$ must be chosen as 0.12.

Figure 98 presents the simulated, full-scale data obtained from the Jet-A gels. The data are plotted in terms of the impact kinetic viscosity in centipoise. Specification of an ignition susceptibility parameter similar to that obtained for emulsified fuels was not possible due to the lack of information on the safety characteristics of the gels. There appears to be no definite limiting value of viscosity for which the gelled fuel performs in a nonhazardous manner. A hazardous condition existed for every on-board igniter test performed on gels. The chemical structure of the two gels was unknown; however, it was known that each manufacturer had a different formulation. This would further complicate the correlation between the two gels. The intent of testing the two gelled fuels was to offer a safety comparison between emulsions and gels under identical test conditions. The Jet-A gel #1 performed much better than the Jet-A gel #2. In the open-flame and spark/hot-surface igniter tests, the Jet-A gel #1 performed equally as well as the JP-8 emulsions; however, the on-board igniter tests all yielded a hazardous rating.

In addition to the fuel formulation, it was found that wind velocity and direction had a great deal to do with the heating rates and temperatures measured in the tests. Therefore, accurate temperature-heating rate evaluation becomes difficult. However, with the temperature data obtained, definite trends were apparent as to the effects the parameter $\psi$ had on probable energy release and aircraft burn-through characteristics. Although many tests did not indicate a temperature greater than 400°F at the temperature probes, Figure 99 presents an approximation of the effect of $\psi$ on the time to reach 400°F for open-flame and spark/hot-surface igniter data. The data shown follows an empirical equation involving $\psi$ which may be expressed as

$$t = 2.8 + \exp\ (0.19/\psi) \qquad (41)$$

○ OPEN-FLAME IGNITER TESTS

△ SPARK AND HOT-SURFACE IGNITER TESTS

□ ON-BOARD (ENGINE SIMULATOR) IGNITER TESTS

SHADED DATA POINTS DENOTE A NONHAZARDOUS BURNING CONDITION

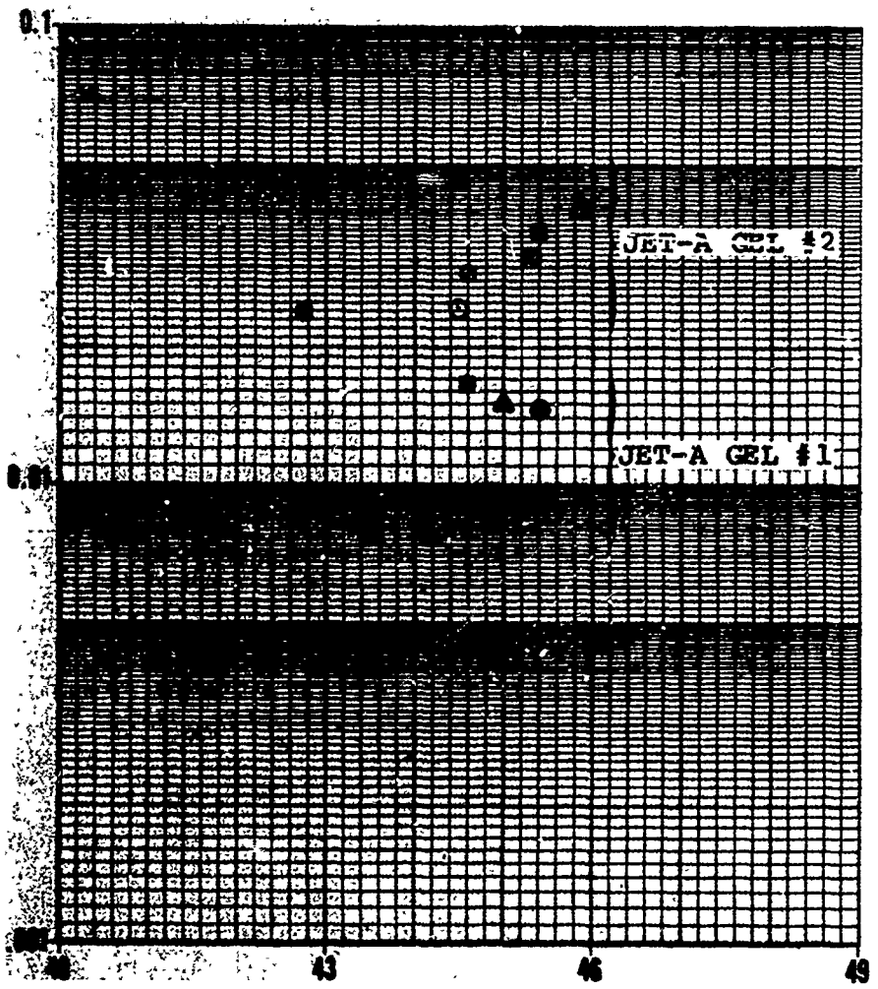


Figure 98. Simulated Full-Scale Test Results for the Gelled Fuel Tests.

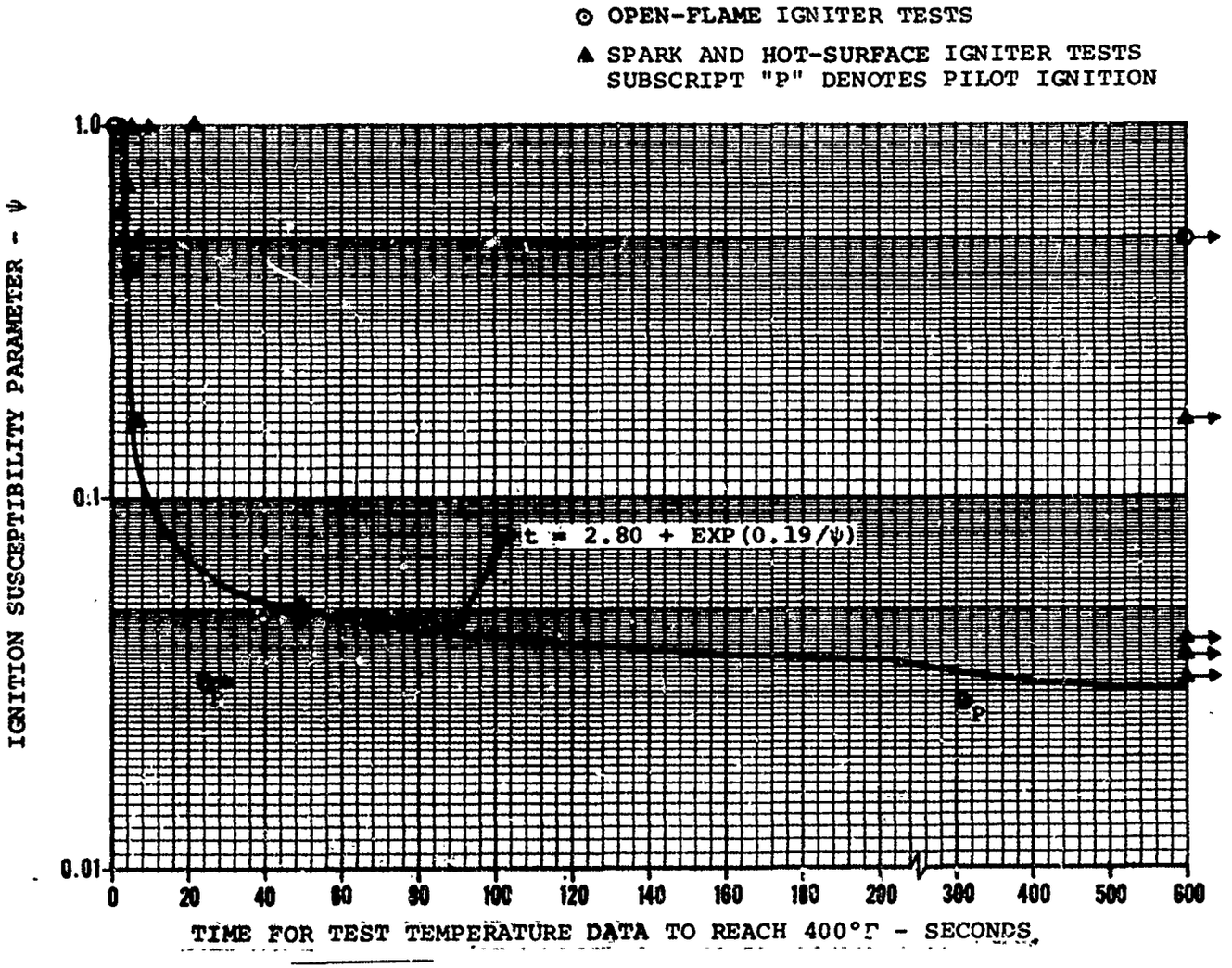


Figure 99. Ignition Susceptibility Parameter Versus Time for Test Temperature to Reach 400°F for the Open-Flame and Spark/Hot-Surface Igniter Tests.

Although no apparent scientific basis exists for this equation, it does portray the trend which was observed in the tests.

Figure 100 presents a similar curve for the on-board igniter tests with $\psi$ plotted versus the time to reach 400°F at the temperature probes. The empirical equation fitting this data takes the form

$$t = 6.0 + \exp\ (0.162/\psi) \qquad (42)$$

An analysis was conducted to extrapolate the simulated full-scale situation to an actual full-scale environment. This involved utilizing the maximum indicated heating rate for each test, assuming an unlimited supply of fuel, and calculating the time at which aircraft burn-through occurred (skin temperature = 1100°F). The analysis presented in the Analytical Considerations section of this report was employed for this extrapolation. The extrapolated resultant times were plotted versus $\psi$ in Figure 101 for the open-flame and spark/hot-surface igniter data and in Figure 102 for the on-board igniter data. In both cases, the effect of $\psi$ on burn-through time is an exponential function with the exponential constants being equal to those found in Figures 99 and 100, respectively. The curve-fit equations for each set of data are shown in each figure.

The data obtained in this test program back up those obtained in the prior screening test analysis. The safety performance of a given emulsified fuel in both test programs has been shown to follow a yield stress dependence. Furthermore, the results obtained in the simulated full-scale tests provided empirical definition of the limiting value for the ignition susceptibility parameter. Knowledge of this limit allows the screening tests conducted previously to be utilized in determining the safety of any fuel. A value of 0.12 for the ignition susceptibility parameter was found to be the upper limit of a nonhazardous environment. The only fuels tested which exhibited a value of 0.12 or less at the maximum crash survivable conditions were the JP-8 base fuel emulsion EF8R-104H, the JP-8 base fuel emulsion EF8R-104, and the Jet-A base fuel emulsion Jet-A EXP-4.

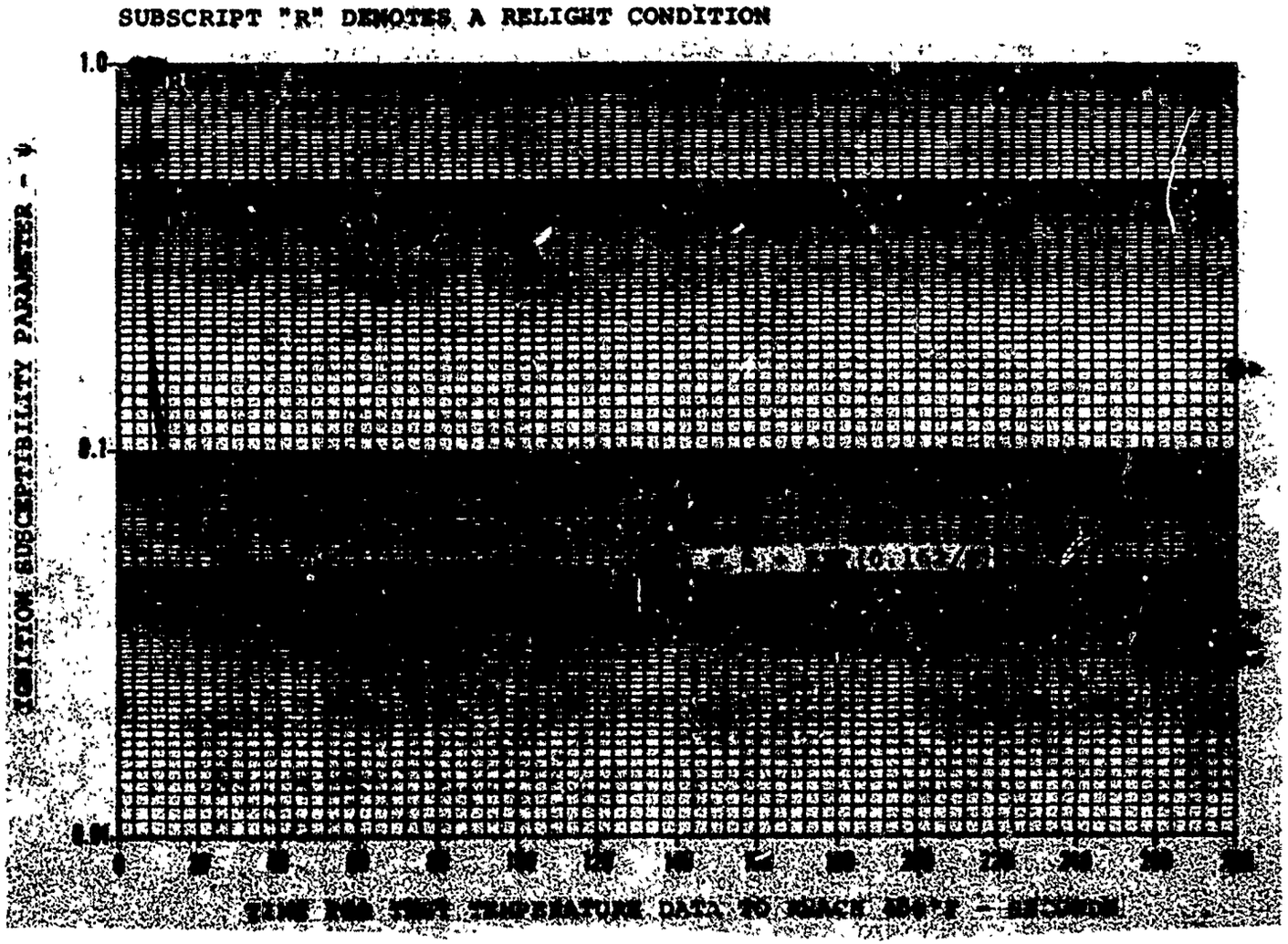


Figure 100. Ignition Susceptibility Parameter Versus Time for Test Temperature to Reach 400°F for On-Board (Engine Simulator) Igniter Tests.

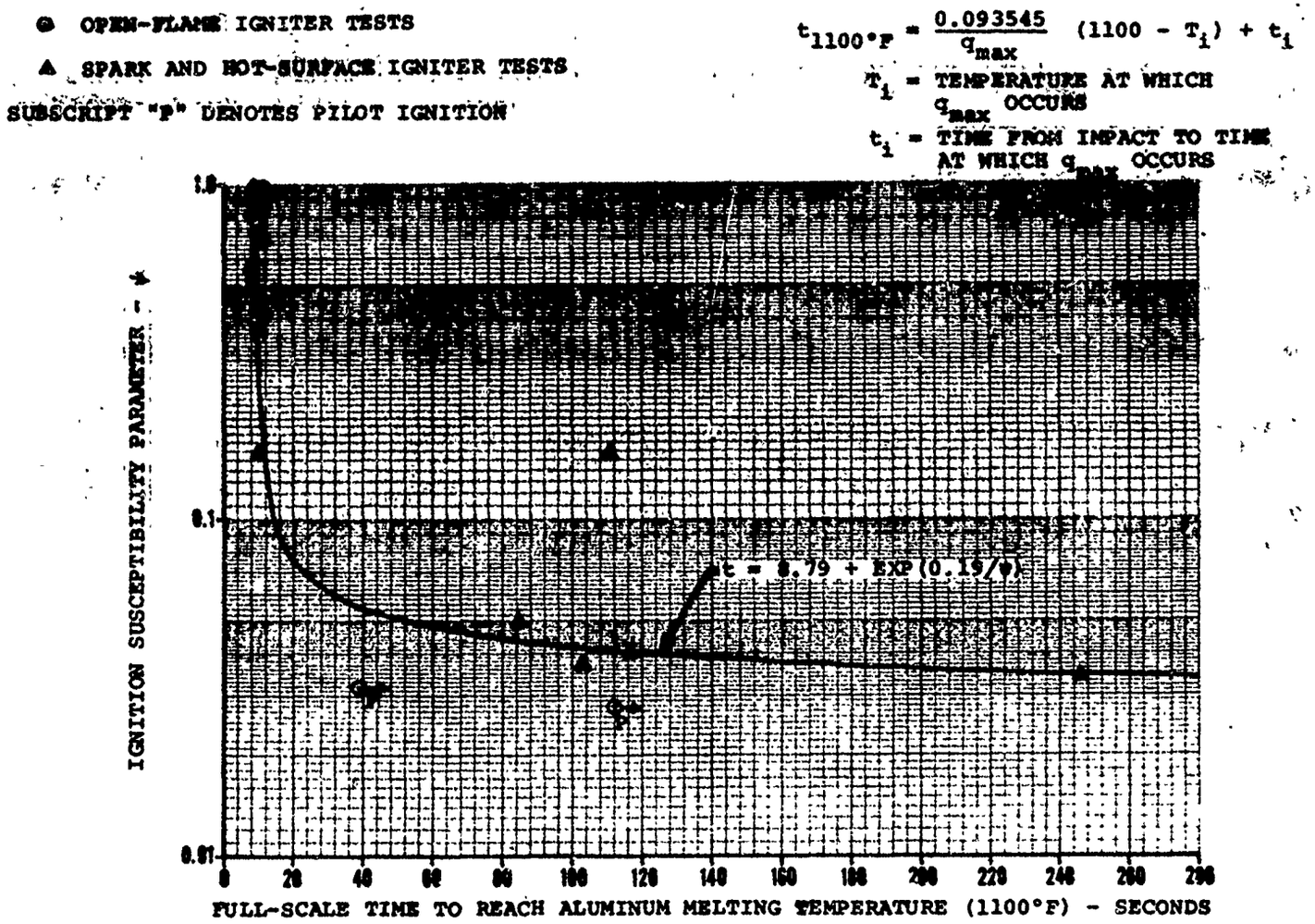


Figure 101. Ignition Susceptibility Parameter Versus Extrapolated Time to Reach Aluminum Melting Temperature for Open-Flame and Spark/ Hot-Surface Igniter Tests.

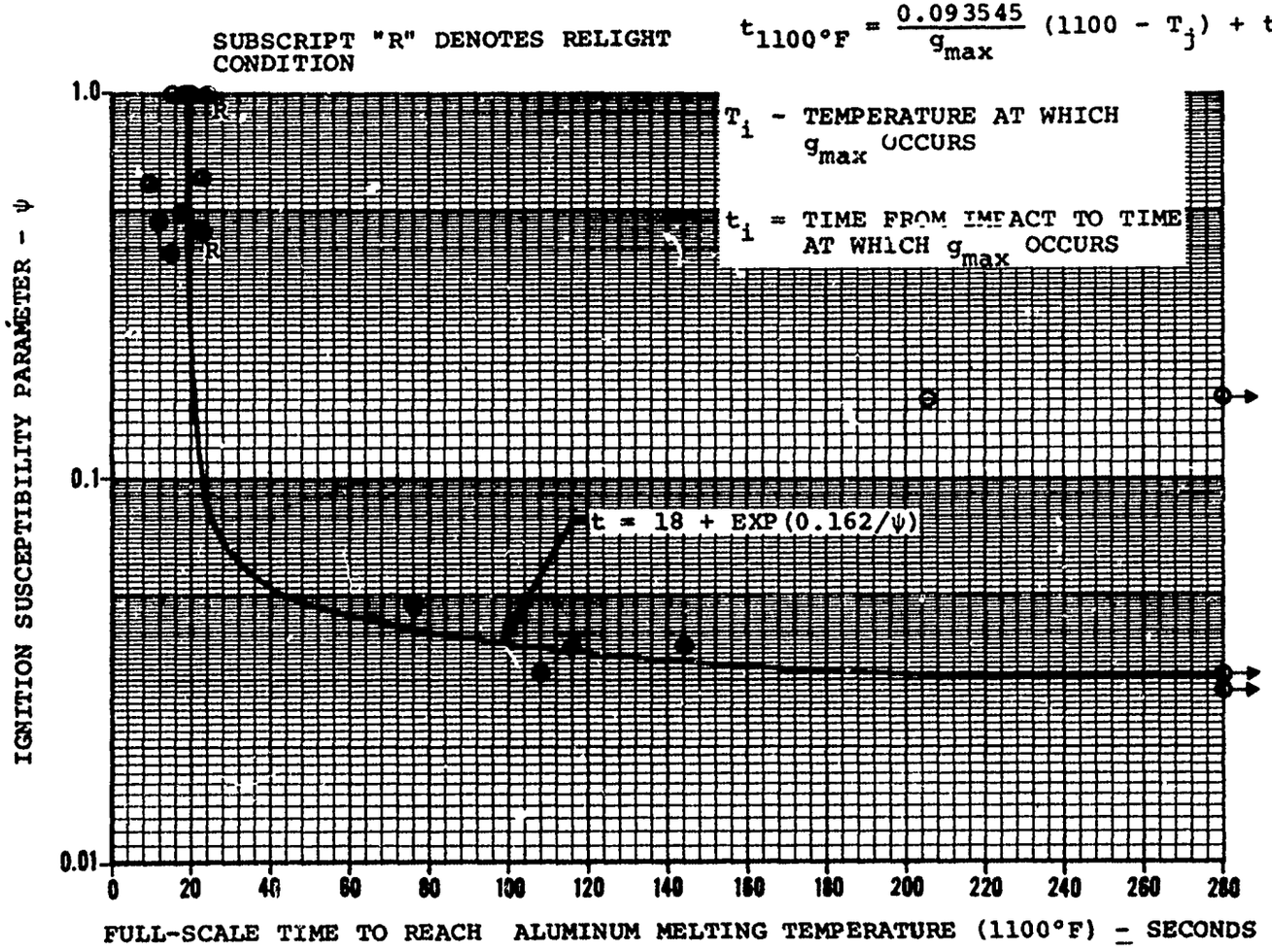


Figure 102. Ignition Susceptibility Parameter Versus Extrapolated Time to Reach Aluminum Melting Temperature for On-Board (Engine Simulator) Igniter Tests.

## CONCLUSIONS

The following conclusions are drawn as a result of this test program:

1. The results of this test program verified that kerosene-base emulsified fuels are an effective method of reducing the postcrash fire hazard.

2. The screening test configurations and procedures that were designed and utilized in this program are valid correlative mechanisms representative of the crash environment on a laboratory scale.

3. As opposed to the high-rate atomization and dispersion characteristics of liquid fuels, emulsified fuels were found to resist atomization and dispersion when subjected to identical crash environmental conditions.

4. Once certain physical properties are known, emulsified fuel fire-hazard susceptibility ratings can be predicted based on the empirical relationships generated during this program.

5. A critical ignition susceptibility parameter value was obtained which allows screening test criteria to be useful in predicting crash impact performance in the full-scale environment.

6. For the emulsified fuels tested, the dependence of yield stress and internal phase, base fuel composition on the safety of fuels was shown.

7. Three emulsified fuels were found which portray a nonhazardous postcrash fire environment within the crash survival envelope: (1) EF8R-104H, (2) EF8R-104, and (3) Jet-A EXP-4.

8. Gelled fuels, although not performing as well as emulsions in a crash environment, strongly indicated a sizeable safety advantage over liquid fuels.

9. The Jet-A gel #1 performed much better in a crash/postcrash fire environment than the Jet-A gel #2.

## RECOMMENDATIONS

Based on the results of this program, it is recommended that:

1. Screening tests be conducted on the EF8R-104 emulsion to further verify its safety performance criteria.

2. Screening tests be conducted on the Jet-A gel #1, the Jet-A gel #2, and one or more higher viscosity gels to obtain safety performance criteria for gelled fuels.

3. Development of a JP-8 or Jet-A internal phase emulsion with a yield stress in the order of 300 to 400 dynes/$cm^2$ be pursued to ease aircraft fuel systems compatibility, if followed by an appropriate safety screening evaluation.

4. Full-scale helicopter crash tests be conducted using an optimal nonhazardous emulsified fuel and an optimal gelled fuel to further verify the safety of modified fuels.

5. Aircraft fuel system compatibility tests be performed to determine system operational criteria when emulsified fuels are used.

## LITERATURE CITED


1. Wilkinson, W. L., NON-NEWTONIAN FLUIDS, FLUID MECHANICS, MECHANICS, MIXING AND HEAT TRANSFER, Pergamon Press, New York, 1960.

2. Harrison, V. G. W., PROCEEDINGS OF THE SECOND INTERNATIONAL CONGRESS ON RHEOLOGY, Oxford 26-31, July 1953, Academic Press, New York, 1964.

3. Eirich, F. R., RHEOLOGY THEORY AND APPLICATION, Academic Press, New York, 1956, Vol. 1, 2, 3, 4.

4. Green, Henry, INDUSTRIAL RHEOLOGY AND THEOLOGICAL STRUCTURES, John Wiley and Sons, New York, 1949.

5. U. S. Army Fuels and Lubricants Research Laboratory Paper II.F., STUDIES RELATING TO FUEL SAFETY, 1 March - 1 April 1969.

6. Kuchta, Joseph M., et.al., FLAMMABILITY CHARACTERISTICS FOR HIGH TEMPERATURE HYDROCARBON FUELS, WADC Technical Report 59-663, Wright Air Development Division, Wright-Patterson Air Force Base, Ohio, February 1960, AD 236661.

7. Zabetakis, Michael G., et.al., RESEARCH ON THE FLAMMABILITY CHARACTERISTICS OF AIRCRAFT FUELS, WADC Technical Report 52-35, Supplement 4, Wright Air Development Center, Wright-Patterson Air Force Base, Ohio, January 1956, AD 91875.

8. Rothe, Victor E., POSTCRASH FIRE RESEARCH, Aviation Safety Engineering and Research, a Division of Flight Safety Foundation, a paper presented at the Flight Safety Foundation International Air Safety Seminar, New York, New York, October 1964.

TABLE IV. WIND SHEAR TEST CONDITIONS AND ASSOCIATED DATA

| Run No. | Fuel | Yield Stress (τ) | $T_{Fuel}$ (°F) | $T_{Amb}$ (°F) | $V_{Air}$ (fps) | F/A | Droplet Diameter d(in) | Photographs Taken* | Comments |
|---|---|---|---|---|---|---|---|---|---|
| WT001 | JP-4 | | 66 | 77 | 80 | | 0.030 | 1 | |
| WT002 | JP-4 | | 66 | 77 | 75 | | 0.035 | 1 | |
| WT003 | JP-4 | | 66 | 82 | 80 | | 0.038 | 1 | |
| WT004 | JP-4 | | 66 | 88 | 75 | | 0.030 | 1 | |
| WT005 | JP-4 | | 66 | 88 | 70 | | 0.0375 | 1 | |
| WT006 | JP-4 | | 66 | 88 | 65 | | 0.060 | 1 | |
| WT007 | JP-4 | | 66 | 88 | 60 | | 0.025 | 1 | |
| WT008 | JP-4 | | 66 | 88 | 55 | | 0.030 | 1 | |
| WT009 | JP-4 | | 66 | 88 | 50 | | 0.030 | 1 | |
| WT010 | JP-4 | | 66 | 88 | 45 | | 0.050 | 1 | |
| WT011 | JP-4 | | 66 | 88 | 40 | | 0.045 | 1 | |
| WT012 | JP-4 | | 66 | 87 | 35 | | 0.045 | 1 | |
| WT013 | JP-4 | | 66 | 86 | 30 | | 0.040 | 1 | |
| WT014 | EF4-104 | 680 | 74 | 82 | 80 | | | | Calibration Run |
| WT015 | EF4-104 | 1800 | 74 | 88 | 80 | | 0.62 | 1 | Calibration Run |
| WT016 | EF4-104 | 1800 | 74 | 88 | 80 | | | 1 | Photo Missed Data |
| WT017 | EF4-104 | 1800 | 74 | 86 | 80 | | | 1 | Photo Missed Data |
| WT018 | EF4-104 | 1800 | 74 | 84 | 50 | | | 1 | Photo Missed Data |
| WT019 | EF4-104 | 3000 | 68 | 84 | 80 | | Large Strands | 1 | Fuel Strand Ran of Photo |
| WT020 | EF4-104 | 1700 | 68 | 84 | 75 | | Large Strands | 1 | Fuel Strand Ran of Photo |
| WT021 | EF4-104 | 1500 | 68 | 84 | 80 | | Large Strands | 1 | Fuel Strand Ran of Photo |
| WT022 | EF4-104 | 1470 | 68 | 84 | 70 | | Large Strands | 1 | Fuel Strand Ran of Photo |

*Photograph Designation: 1 - Microphotographic Camera, 2 - Full View Still Camera, 3 - Full View 65 Frame-Per-Second Movie Camera, 4 - 500 Frame-Per-Second Movie Camera

TABLE IV. Continued

| Run No. | Fuel | Yield Stress (τ) | $T_{Fuel}$ (°F) | $T_{Amb}$ (°F) | $V_{Air}$ (fps) | F/A | Droplet Diameter d(in) | Photographs Taken* | Comments |
|---|---|---|---|---|---|---|---|---|---|
| WT023 | EF4-104 | 1350 | 68 | 84 | 65 | | | 1 | Photo Missed Flow |
| WT024 | EF4-104 | 1300 | 68 | 82 | 80 | | 0.211 | 1 | |
| WT025 | EF4-104 | 1300 | 68 | 81 | 76 | | 0.035 | 1 | Void Run |
| WT026 | EF4-104 | 475 | 65 | 85 | 80 | | 0.60 | 1 | |
| WT027 | EF4-104 | 475 | 65 | 85 | 70 | | 0.356 | 1 | |
| WT028 | EF4-104 | 475 | 65 | 85 | 60 | | 0.875 | 1 | |
| WT029 | EF4-104 | 475 | 65 | 85 | 50 | | | 1 | Photo Missed Flow |
| WT030 | EF4-104 | 475 | 65 | 85 | 40 | | >1.50 | 1 | Continuous Strand |
| WT031 | EF4R-104 | 400 | 68 | 67 | 100 | (-1) 0.01225 | | | |
| | | | | | | (-2) 0.00788 | 0.04 | 1 | |
| WT032 | EF4R-104 | 400 | 68 | 69 | 80 | (-2) 0.00417 | | | |
| | | | | | | (-4) 0.0102 | 0.125 | 1 | |
| WT033 | EF4R-104 | 400 | 68 | 76 | 80 | | 0.025 | 1 | Photo Missed Flow |
| WT034 | EF4R-104 | 400 | 69 | 76 | 80 | 0.000417 | | | |
| WT035 | EF4R-104 | 400 | 69 | 76 | 100 | | | | Void |
| WT036 | EF4R-104 | 400 | 69 | 77 | 60 | 0.00147 | | | |
| WT037 | EF4R-104 | 600 | 70 | 74 | 100 | | | | |
| WT038 | EF4R-104 | 600 | 70 | 74 | 100 | 0.00588 | 0.04 | 1, 2 | |
| WT039 | EF4R-104 | 600 | 70 | 74 | 60 | 0.00258 | 0.70 | 1, 2 | |
| WT040 | EF4R-104 | 600 | 70 | 73 | 80 | 0.0051 | 0.475 | 1 | |
| WT041 | EF4R-104 | 620 | 66 | 78 | 100 | | | | Void |
| WT042 | EF4R-104 | 620 | 66 | 77 | 100 | 0.00185 | | | |
| WT043 | EF4R-104 | 620 | 66 | 75 | 100 | | | 2 | Void |
| WT044 | EF4R-104 | ≈620 | 66 | 73 | 100 | | 0.05 | 1, 2 | |
| WT045 | EF4R-104 | 504 | 66 | 72 | 100 | | | 2 | Void |

TABLE IV. Continued

| Run No. | Fuel | Yield Stress (τ) | $T_{Fuel}$ (°F) | $T_{Amb}$ (°F) | $V_{Air}$ (fps) | F/A | Droplet Diameter d(in) | Photographs Taken* | Comments |
|---|---|---|---|---|---|---|---|---|---|
| WT046 | JP-4 | | 68 | 67 | 100 | 0.01162 | | 1, 2 | Photo Missed Flow |
| WT047 | JP-4 | | 68 | 69 | 80 | 0.0207 | | 1, 2 | Photo Missed Flow |
| WT048 | JP-4 | | 68 | 72 | 100 | 0.0143 | 0.035 | 1 | |
| WT049 | JP-4 | | 68 | 72 | 80 | 0.00715 | 0.025 | 1, 2 | |
| WT050 | JP-4 | | 68 | 74 | 60 | 0.0362 | 0.035 | 1 | |
| WT051 | JP-4 | | 68 | 75 | 40 | 0.0 | 0.035 | 1, 2 | |
| WT052 | JP-4 | | 68 | 75 | 80 | 0.0415 | 0.025 | 1, 2 | |
| WT053 | EF4R-104 | 2000 | 68 | 77 | 100 | | | 2 | Worked, Vacuum Pumps Off |
| WT054 | EF4R-104 | (1775) 2000 | 68 | 77 | 100 | 0.00233 | | 2 | Worked, Vacuum Pumps Off |
| WT055 | EF4R-104 | (1600) 2000 | 68 | | 80 | 0.0007 | | 2 | Worked, Vacuum Pumps Off |
| WT056 | EF4R0104 | (1350) 2000 | 68 | 76 | 60 | | | 2 | Void |
| WT057 | EF4R-104 | (1250) 2000 | 68 | 75 | 120 | | | 2 | Void |
| WT058 | EF4R-104 | (1200) 2000 | 68 | 74 | 120 | 0.00187 | 0.080 | 1, 2 | |
| WT059 | EF4R-104 | (1200) 2000 | 68 | 74 | 100 | 0.00208 | 0.06 | 1, 2 | |
| WT060 | EF4R-104H | 1600 | 68 | ≈70 | 100 | | 0.10 | 1 | |
| WT061 | EF4R0104H | 1870 | 68 | ≈70 | 100 | | 0.26 | 1, 2 | |
| WT062 | EF4R-104H | 1820 | 68 | ≈70 | 80 | | 1.0 | 1, 2 | |
| WT063 | EF4R0104H | 1670 | 68 | ≈70 | 60 | | Continuous Strand | 1, 2 | |
| WT064 | EF4R-104H | 1650 | 67 | ≈70 | 40 | | Continuous Strand | 1, 2 | |
| WT065 | EF4R-104H | 1750 | 68 | ≈70 | 50 | | Continuous Strand | 1, 2 | Photo Missed Flow |

TABLE IV. Continued

| Run No. | Fuel | Yield Stress (τ) | $T_{Fuel}$ (°F) | $T_{Amb}$ (°F) | $V_{Air}$ (fps) | F/A | Droplet Diameter d(in) | Photographs Taken* | Comments |
|---|---|---|---|---|---|---|---|---|---|
| WT066 | EF4R-104H | 1670 | 68 | ≈70 | 70 | | | 1, 2 | Void, Ran Out of Fuel |
| WT067 | EF4R-104H | 1775 | 68 | ≈70 | 70 | | 1.06 | 1, 2 | |
| WT068 | EF4R-104H | 1830 | 68 | ≈70 | 90 | | 0.10 | 1, 2 | |
| WT069 | EF4R-104H | 1800 | 63 | 59 | 120 | | 0.25 | 2 | |
| WT070 | EF4R-104H | 1775 | 64 | 60 | 120 | | 0.20 | 1, 2 | |
| WT071 | EF4R-104H | 1660 | 64 | 60 | 100 | | 0.30 | 1, 2 | |
| WT072 | EF4R-104H | 1700 | 64 | 62 | 80 | | 0.55 | 1, 2 | |
| WT073 | EF4R-104H | 1700 | 64 | 62 | 60 | | 0.40 | 1, 2 | |
| WT074 | EF4R-104H | 2520 | 68 | 72 | 100 | | 0.25 | 1, 2 | |
| WT075 | EF4R-104H | 2470 | 68 | 72 | 80 | | Continuous Strand | 2 | |
| WT076 | EF4R-104H | 2350 | 69 | 73 | 60 | | | 1, 2 | Void |
| WT077 | EF4R-104H | 2400 | 69 | 75 | 120 | | 0.25 | 2 | |
| WT078 | EF4R-104H | 2620 | 69 | 76 | 60 | | Continuous Strand | 2 | |
| WT079 | EF4R-104H | 1790 | 68 | 76 | 100 | | | 3, 4 | |
| WT080 | EF4R-104H | 1790 | 68 | 76 | 80 | | | 3, 4 | |
| WT081 | EF4R-104H | 1790 | 68 | 76 | 60 | | | 3, 4 | |
| WT082 | JP-4 | | 70 | 77 | 60 | 0.000347 | | 3, 4 | |
| WT083 | JP-4 | | 70 | 78 | 100 | 0.000187 | | 3, 4 | |
| WT084 | JP-4 | | 70 | 82 | 40 | 0.000672 | | 3, 4 | |
| WT085 | JP-4 | | 70 | 82 | 30 | 0.000474 | | 3, 4 | |
| WT086 | JP-4 | | 74 | 82 | 60 | 0.000568 | | | |
| WT087 | JP-4 | | 74 | 84 | 80 | 0.000344 | | 3 | |
| WT088 | JP-4 | | 74 | 84 | 80 | 0.000423 | | | |
| WT089 | JP-4 | | 74 | 85 | 100 | 0.000435 | | | |
| WT090 | JP-4 | | 76 | 84 | 120 | 0.000287 | | | |

TABLE IV. Continued

| Run No. | Fuel | Yield Stress (τ) | $T_{Fuel}$ (°F) | $T_{Amb}$ (°F) | $V_{Air}$ (fps) | F/A | Droplet Diameter d(in) | Photographs Taken* | Comments |
|---|---|---|---|---|---|---|---|---|---|
| WT091 | JP-8 | | 66 | 66 | 100 | 0.000149 | | 1 | |
| WT092 | JP-8 | | 66 | 68 | 80 | 0.000257 | | 1 | |
| WT093 | JP-8 | | 66 | 70 | 60 | 0.000441 | | 3, 4 | |
| WT094 | JP-8 | | 66 | 72 | 40 | 0.000606 | | 3, 4 | |
| WT095 | JP-8 | | 66 | 73 | 30 | 0.000366 | | | Impact on Tunnel Floor |
| WT096 | JP-8 | | 66 | 74 | 120 | 0.000286 | | | |
| WT097 | JP-8 | | 66 | 76 | 100 | 0.000389 | | 3, 4 | |
| WT098 | JP-8 | | 66 | 77 | 80 | 0.000341 | | 3, 4 | |
| WT099 | EF8-104H | 1020 | 64 | 62 | 100 | 0.00005 | | | |
| WT100 | EF8-104H | 1130 | 64 | 63 | 80 | 0.000086 | | | |
| WT101 | EF8-104H | 1100 | 68 | 70 | 60 | 0.000166 | | 3, 4 | |
| WT102 | EF8-104H | 1050 | 64 | 70 | 40 | 0.000004 | | 3, 4 | |
| WT103 | EF8-104H | 950 | 64 | 70 | 80 | 0.000118 | | 3, 4 | |
| WT104 | EF8-104H | 1020 | 64 | 68 | 100-80 | 0.000154 | | 3, 4 | Velocity Shifted |
| WT105 | EF8-104H | 1020 | 64 | 70 | 100-80 | 0.000157 | | 3, 4 | May not have had Film for 4 - Velocity Shifted |
| WT106 | EF8-104H | 1020 | 64 | 68 | 100 | 0.000068 | | | |
| WT107 | EF8-104H | 1020 | 64 | 67 | 120 | 0.000044 | | | |
| WT108 | EF8-104H | 750 | 64 | 62 | 40 | 0.0000474 | No Breakup | | |
| WT109 | EF8-104H | 1080 | 64 | 63 | 60 | | | | Ran Out of Fuel |
| WT110 | EF4R-104 | 670 | 68 | 81 | 100 | 0.000147 | | | |
| WT111 | EF4R-104 | 650 | 72 | 82 | 80 | 0.000269 | | | Inconsistent Chromatograph Trace |
| WT112 | EF4R-104 | 690 | 71 | 83 | 60 | 0.000174 | | | Inconsistent Chromatograph Trace |
| WT113 | EF4R-104 | 560 | 70 | 85 | 40 | 0.000185 | | | Inconsistent Chromatograph Trace |

TABLE IV. Continued

| Run No. | Fuel | Yield Stress (τ) | $T_{Fuel}$ (°F) | $T_{Amb}$ (°F) | $V_{Air}$ (fps) | F/A | Droplet Diameter d(in) | Photographs Taken* | Comments |
|---|---|---|---|---|---|---|---|---|---|
| WT114 | EF4R-104 | 640 | 72 | 84 | 100 | 0.000171 | | | Inconsistent Chromatograph Trace |
| WT115 | EF4R-104 | 448 | 72 | 83 | 120 | 0.000145 | | | Inconsistent Chromatograph Trace |
| WT116 | EF4R-104 | 440 | 72 | 86 | 80 | 0.000166 | | | Inconsistent Chromatograph Trace |
| WT117 | EF4R-104 | 440 | 72 | 87 | 60 | 0.000296 | | | Inconsistent Chromatograph Trace |
| WT118 | EF4R-104H | 975 | 66 | 68 | 60 | 0.000324 | | | Void - High SW Wind, 10-40 mph |
| WT119 | EF4R-104H | 1220 | 68 | 67 | 100 | 0.000193 | | | Void - High SW Wind, 10-40 mph |
| WT120 | EF4R-104H | 1325 | 68 | 68 | 80 | 0.000266 | | | Void - High SW Wind, 10-40 mph |
| WT121 | EF4R-104H | 2030 | 68 | 68 | 40 | 0.0000574 | No Breakup | | Void - High SW Wind, 10-40 mph |
| WT122 | EF4R-104H | 1240 | 68 | 69 | 60 | 0.0002196 | | | Void - High SW Wind, 10-40 mph |
| WT123 | EF4R-104H | 1480 | 68 | 70 | 80 | 0.00033 | | | Void - High SW Wind, 10-40 mph |
| WT124 | EF4R-104H | 1250 | 70 | 72 | 100 | 0.000169 | | | Void - High SW Wind, 10-40 mph |
| WT125 | EF4R-104H | 1525 | 68 | 71 | 120 | 0.000243 | | | Void - High SW Wind, 10-40 mph |
| WT126 | EF4R-104H | 1125 | 90 | 86 | 30 | 0.0000238 | | | Fuel Flow Rate Too High |
| WT127 | EF4R-104H | 1290 | 92 | 86 | 40 | 0.000051 | | | Fuel Flow Rate Too High |
| WT128 | EF4R-104H | 1300 | 92 | 87 | 60 | | | | Void |
| WT129 | EF4R-104H | 1130 | 92 | 88 | 80 | 0.0000818 | | | |
| WT130 | EF4R-104H | 1160 | 90 | 87 | 100 | 0.0000387 | | | |
| WT131 | EF4R-104H | 1190 | 90 | 90 | 100 | 0.0000419 | | | |
| WT132 | EF4R-104H | 1210 | 92 | 90 | 120 | 0.0000528 | | | |
| WT133 | EF4R-104H | 1210 | 92 | 90 | 80 | 0.000063 | | | |

TABLE IV. Continued

| Run No. | Fuel | Yield Stress (τ) | $T_{Fuel}$ (°F) | $T_{Amb}$ (°F) | $V_{Air}$ (fps) | F/A | Droplet Diameter d(in) | Photographs Taken* | Comments |
|---|---|---|---|---|---|---|---|---|---|
| WT134 | EF4R-104H | 1220 | 91 | 89 | 60 | 0.0000633 | | | Erratic Fuel Flow |
| WT135 | EF4R-104H | 1125 | 94 | 93 | 40 | 0.0000884 | | | Fuel Flow Too High |
| WT136 | EF4R-104H | 1125 | 94 | 93 | 40 | | | | Void |

TABLE V. IMPACT DISPERSION/ATOMIZATION TEST CONDITIONS AND ASSOCIATED DATA

| Run No. | Fuel | Yield Stress $\tau_y$ (Dynes/cm$^2$) | Piston Velocity (fps) | Fuel Velocity (fps) | Ambient Temperature (°F) | Fuel Temperature (°F) | Surface Temperature (°F) | Fuel/Air Ratio By Volume | Impingement Angle (Degrees) | Comments |
|---|---|---|---|---|---|---|---|---|---|---|
| IT001 | JP-4 | | 30 | 33.3 | | 60 | | | 90 | Ignition Occurred |
| IT002 | JP-4 | | 50 | 50 | | 67 | | | 90 | No Ignition |
| IT003 | JP-4 | | 70 | 62.5 | | 68 | | | 90 | Ignition Occurred |
| IT004 | JP-4 | | 60 | 59.0 | | 68 | | | 90 | Ignition Occurred |
| IT005 | JP-4 | | 40 | 45.5 | | 70 | | | 90 | Ignition Occurred |
| IT006 | JP-4 | | 40 | 40 | | 72 | | | 45 | Ignition Occured |
| IT007 | JP-4 | | 33.3 | 30 | | 70 | | | 45 | Ignition Occurred |
| IT008 | JP-4 | | 50 | 50 | | 70 | | | 45 | No Ignition |
| IT009 | JP-4 | | 60 | 55.5 | | 70 | | | 45 | Ignition Occurred |
| IT010 | JP-4 | | 70 | 71.0 | | 70 | | | 45 | No Ignition |
| IT011 | JP-4 | | 70 | 77.0 | | 70 | | | 15 | Ignition Occurred |
| IT012 | JP-4 | | 30 | 35.6 | | 80 | | | 15 | No Ignition |
| IT013 | JP-4 | | 40 | 41.7 | | 84 | | | 15 | No Ignition |
| IT014 | JP-4 | | 50 | 50 | | 80 | | | 15 | Ignition Occurred |
| IT015 | JP-4 | | 60 | 62.0 | | 80 | | | 15 | Ignition Occurred |
| IT016 | JP-4 | | 40 | 43.5 | | 80 | | | 15 | Ignition Occurred |
| IT017 | JP-4 | | 30 | 33.3 | | 80 | | | 15 | No Ignition |
| IT018 | EF4R-104 | 464 | 30 | 38.5 | | 68 | | | 90 | No Ignition |
| IT019 | EF4R-104 | 464 | 40 | 45.5 | | 68 | | | 90 | No Ignition |
| IT020 | EF4R-104 | 464 | 50 | 50 | | 70 | | | 90 | Slight Ignition |
| IT021 | EF4R-104 | 464 | 60 | 62.0 | | 70 | | | 90 | Slight Ignition |
| IT022 | EF4R-104 | 464 | 70 | | | 70 | | | 90 | Slight Ignition - No Photo |
| IT023 | EF4R-104 | 464 | 70 | 62.0 | | 74 | | | 90 | Slight Ignition |
| IT024 | EF4R-104 | 464 | 50 | 62.0 | | 78 | | | 45 | Ignition Occurred |
| IT025 | EF4R-104 | 472 | 30 | 31.2 | | 62 | | | 45 | No Ignition |

TABLE V. Continued

| Run No. | Fuel | Yield Stress $\tau_y$ (Dynes/cm$^2$) | Piston Velocity (fps) | Fuel Velocity (fps) | Ambient Temperature (°F) | Fuel Temperature (°F) | Surface Temperature (°F) | Fuel/Air Ratio By Volume | Impingement Angle (Degrees) | Comments |
|---|---|---|---|---|---|---|---|---|---|---|
| IT026 | EF4R-104 | 472 | 40 | 40.0 | | 62 | | | 45 | No Ignition |
| IT027 | EF4R-104 | 472 | 60 | 62.5 | | 62 | | | 45 | No Ignition |
| IT028 | EF4R-104 | 472 | 70 | 83 | | 62 | | | 45 | No Ignition |
| IT029 | EF4R-104 | 472 | 50 | 50 | | 68 | | | 45 | No Ignition |
| IT030 | EF4R-104 | 472 | 50 | 50 | | 68 | | | 15 | No Ignition |
| IT031 | EF4R-104 | 472 | 60 | 60 | | 68 | | | 15 | No Ignition |
| IT032 | EF4R-104 | 504 | 70 | 75 | | 64 | | | 15 | No Ignition |
| IT033 | EF4R-104 | 504 | 40 | 38.5 | | 66 | | | 15 | No Ignition |
| IT034 | EF4R-104 | 504 | 30 | 31.0 | | 66 | | | 15 | No Ignition |
| IT035 | EF4R-104H | 1225 | 30 | 33.3 | | 66 | | | 90 | No Ignition |
| IT036 | EF4R-104H | 1225 | 40 | 45.5 | | 66 | | | 90 | No Ignition |
| IT037 | EF4R-104H | 1225 | 50 | 62.5 | | 72 | | | 90 | Slight Ignition |
| IT038 | EF4R-104H | 1225 | 60 | 66.6 | | 72 | | | 90 | Ignition Occurred |
| IT039 | EF4R-104H | 1225 | 70 | 83 | | 72 | | | 90 | No Ignition |
| IT040 | EF4R-104H | 1225 | 50 | 50 | | 72 | | | 45 | No Ignition |
| IT041 | EF4R-104H | 1225 | 60 | 62.5 | | 72 | | | 45 | No Ignition |
| IT042 | EF4R-104H | 1225 | 70 | 71.0 | | 72 | | | 45 | No Ignition |
| IT043 | EF4R-104H | 1225 | 70 | 83.0 | | 72 | | | 90 | No Ignition (Bad Spark) |
| IT044 | JP-8 | | 30 | | | 68 | | | 90 | No Ignition, No Film |
| IT045 | JP-8 | | 40 | | | 68 | | | 90 | No Ignition, No Film |
| IT046 | JP-8 | | 50 | | | 68 | | | 90 | No Ignition, No Film |
| IT047 | JP-4 | | 50 | | | 68 | | | 90 | Ignition Occurred, No Film |
| IT048 | JP-8 | | 60 | | | 68 | | | 90 | No Ignition, No Film |
| IT049 | JP-8 | | 60 | | | 68 | | | 90 | No Ignition, No Film |
| IT050 | JP-4 | | 60 | | | 68 | | | 90 | Ignition Occurred |
| IT051 | JP-4 | | 30 | | | 68 | | | 90 | Ignition Occurred |

TABLE V. Continued

| Run No. | Fuel | Yield Stress $\tau_y$ (Dynes/cm$^2$) | Piston Velocity (fps) | Fuel Velocity (fps) | Ambient Temperature (°F) | Fuel Temperature (°F) | Surface Temperature (°F) | Fuel/Air Ratio By Volume | Impingement Angle (Degrees) | Comments |
|---|---|---|---|---|---|---|---|---|---|---|
| IT052 | JP-8 | | 30 | | | 68 | | | 90 | No Ignition |
| IT053 | JP-4 | | 60 | | | 68 | | | 45 | Ignition Occurred |
| IT054 | JP-8 | | 60 | | | 69 | | | 45 | Slight Ignition |
| IT055 | EF4R-104 | 504 | 60 | | | 68 | | | 90 | Slight Ignition |
| IT056 | EF4R-104 | 504 | 60 | | | 68 | | | 45 | No Ignition |
| IT057 | EF4R-104 | 504 | 30 | | | 68 | | | 90 | No Ignition |
| IT058 | EF8-104H | 660 | 30 | | | 64 | | | 90 | No Ignition |
| IT059 | EF8-104H | 660 | 60 | | | 65 | | | 90 | No Ignition |
| IT060 | EF8-104H | 660 | 60 | | | 66 | | | 45 | No Ignition |
| IT061 | JP-4 | | 30 | | 74 | 70 | 64 | | 90 | No Film, Chromatograph Calibration Run |
| IT062 | JP-4 | | 30 | | | 70 | | | 90 | No Film, Void Run |
| IT063 | JP-4 | | 40 | | 75 | 76 | | | 90 | No Film, Chromatograph Calibration Run |
| IT064 | JP-4 | | 30 | | | 75 | | | 90 | No Film, Chromatograph Calibration Run |
| IT065 | JP-4 | | 40 | | | 76 | | | 90 | No Film, Chromatograph Calibration Run |
| IT066 | JP-4 | | 40 | | | 76 | | | 90 | No Film, Chromatograph Calibration Run |
| IT067 | JP-4 | | 40 | | | 62 | | | 90 | Chromatograph Calibration Run |
| IT068 | JP-4 | | 50 | | 69 | 64 | | | 90 | |
| IT069 | JP-4 | | 47 | | 70 | 66 | | | 90 | Chromatograph Calibration Run |
| IT070 | JP-4 | | 60 | | 78 | 72 | | | 90 | Chromatograph Calibration Run |
| IT071 | JP-4 | | 60 | | 74 | 72 | | | 90 | Chromatograph Calibration Run |

TABLE V. Continued

| Run No. | Fuel | Yield Stress $\tau_y$ (Dynes/cm$^2$) | Piston Velocity (fps) | Fuel Velocity (fps) | Ambient Temperature (°F) | Fuel Temperature (°F) | Surface Temperature (°F) | Fuel/Air Ratio By Volume | Impingement Angle (Degrees) | Comments |
|---|---|---|---|---|---|---|---|---|---|---|
| IT072 | JP-4 | | 70 | | 75 | 73 | | | 90 | Chromatograph Calibration Run |
| IT073 | JP-4 | | 30 | | 74 | 74 | | | 90 | Chromatograph Calibration Run |
| IT074 | JP-4 | | 30 | | | | | | 90 | Chromatograph Calibration Run |
| IT075 | JP-4 | | 30 | | | 74 | | | 45 | Chromatograph Calibration Run |
| IT076 | JP-4 | | 40 | | | | | | 45 | Chromatograph Calibration Run |
| IT077 | JP-4 | | 50 | | 74 | 74 | 80 | | 45 | Chromatograph Calibration Run |
| IT078 | JP-4 | | 60 | | 74 | 74 | 80 | | 45 | Chromatograph Calibration Run |
| IT079 | JP-4 | | 30 | 33.3 | 68 | 66 | 69 | 0.000875 | 45 | |
| IT080 | JP-4 | | 40 | 41.7 | 64 | 66 | 69 | 0.001432 | 45 | |
| IT081 | JP-4 | | 50 | 50 | 65 | 67 | 71 | 0.001635 | 45 | |
| IT082 | JP-4 | | 60 | 62.5 | 66 | 66 | 71 | 0.002040 | 45 | |
| IT083 | JP-4 | | 70 | 69.0 | 66 | 66 | 75 | 0.002744 | 45 | |
| IT084 | JP-4 | | 40 | 38.4 | 75 | 79 | 86 | 0.001439 | 45 | |
| IT085 | JP-4 | | 60 | 59.0 | 78 | 79 | 86 | 0.002628 | 45 | |
| IT086 | JP-4 | | 60 | 59.8 | 78 | 79 | 86 | 0.002074 | 90 | |
| IT087 | JP-4 | | 70 | 70.0 | 79 | 79 | 87 | 0.002301 | 90 | |
| IT088 | JP-4 | | 30 | 27.0 | 79 | 79 | 87 | 0.001967 | 90 | |
| IT089 | JP-4 | | 40 | 32.1 | 79 | 79 | 87 | 0.001915 | 90 | |
| IT090 | JP-4 | | 50 | | 76 | 79 | 82 | 0.002326 | 90 | No Film |
| IT091 | EF4R-104 | 536 | 30 | 22.35 | 68 | 60 | 67 | 0.0002053 | 90 | |
| IT092 | EF4R-104 | 536 | 40 | 29.60 | 68 | 62 | 67 | 0.0006644 | 90 | |

TABLE V. Continued

| Run No. | Fuel | Yield Stress $\tau_y$ (Dynes/cm$^2$) | Piston Velocity (fps) | Fuel Velocity (fps) | Ambient Temperature (°F) | Fuel Temperature (°F) | Surface Temperature (°F) | Fuel/Air Ratio By Volume | Impingement Angle (Degrees) | Comments |
|---|---|---|---|---|---|---|---|---|---|---|
| IT093 | EF4R-104 | 536 | 50 | 38.3 | 69 | 64 | 67 | 0.001082 | 90 | |
| IT094 | EF4R-104 | 536 | 60 | 49.0 | 70 | 69 | 73 | 0.001712 | 90 | |
| IT095 | EF4R-104 | 512 | 70 | 56.0 | 78 | 64 | 80 | 0.000863 | 90 | |
| IT096 | EF4R-104 | 512 | 70 | 57.5 | 77 | 65 | 80 | 0.001710 | 90 | |
| IT097 | EF4R-104 | 512 | 30 | 26.6 | 77 | 68 | 80 | 0.000390 | 45 | |
| IT098 | EF4R-104 | 512 | 40 | 32.0 | 77 | 74 | 80 | 0.0007135 | 45 | |
| IT099 | EF4R-104 | 480 | 50 | 40.0 | 76 | 63 | 77 | 0.0004817 | 45 | |
| IT100 | EF4R-104 | 480 | 50 | 40.0 | 76 | 66 | 77 | 0.000373 | 45 | Designated Run No. IT099 on Film |
| IT101 | EF4R-104 | 480 | 60 | 53.4 | 76 | 67 | 77 | 0.001007 | 45 | |
| IT102 | EF4R-104 | 480 | 70 | 60.0 | 75 | 70 | 77 | 0.001416 | 45 | |
| IT103 | EF4R-104 | 480 | 40 | | 75 | 74 | 77 | 0.000653 | 45 | No Film |
| IT104 | EF4R-104H | 1175 | 30 | 26.9 | 67 | 64 | 68 | 0.0000354 | 45 | |
| IT105 | EF4R-104H | 1175 | 40 | 34.3 | 68 | 64 | 68 | 0.000204 | 45 | |
| IT106 | EF4R-104H | 1175 | 50 | 49.4 | 69 | 66 | 69 | 0.000390 | 45 | |
| IT107 | EF4R-104H | 1175 | 60 | 56.6 | 70 | 66 | 74 | 0.000447 | 45 | |
| IT108 | EF4R-104H | 1175 | 60 | 56.6 | 70 | 66 | 74 | 0.000436 | 45 | |
| IT109 | EF4R-104H | 1100 | 70 | 62.0 | 73 | 64 | 80 | 0.000680 | 45 | |
| IT110 | EF4R-104H | 1100 | 30 | 30.5 | 72 | 64 | 80 | 0.0001456 | 45 | |
| IT111 | EF4R-104H | 1100 | 40 | 35.7 | 74 | 69 | 80 | 0.000466 | 45 | |
| IT112 | EF4R-104H | 1100 | 50 | 43.85 | 74 | 70 | 81 | 0.000409 | 45 | |
| IT113 | EF4R-104H | 1185 | 40 | 33.0 | 74 | 64 | 81 | 0.000203 | 90 | |
| IT114 | EF4R-104H | 1185 | 50 | 34.0 | 72 | 65 | 80 | 0.000245 | 90 | |
| IT115 | EF4R-104H | 1185 | 60 | 44.7 | 74 | 70 | 80 | 0.000475 | 90 | |
| IT116 | EF4R-104H | 1185 | 70 | 52.5 | 74 | 70 | 80 | 0.000592 | 90 | |
| IT117 | JP-8 | | 30 | 32 | 58 | 58 | 60 | 0.0000375 | 90 | |

TABLE V. Continued

| Run No. | Fuel | Yield Stress $\tau_y$ (Dynes/cm$^2$) | Piston Velocity (fps) | Fuel Velocity (fps) | Ambient Temperature (°F) | Fuel Temperature (°F) | Surface Temperature (°F) | Fuel/Air Ratio By Volume | Impingement Angle (Degrees) | Comments |
|---|---|---|---|---|---|---|---|---|---|---|
| IT118 | JP-8 | | 30 | 35 | 58 | 58 | 60 | 0.000125 | 90 | |
| IT119 | JP-8 | | 40 | 35.7 | 60 | 58 | 60 | 0.000101 | 90 | |
| IT120 | JP-8 | | 50 | 41.5 | 66 | 62 | 77 | 0.000221 | 90 | |
| IT121 | JP-8 | | 60 | 50.0 | 66 | 62 | 77 | 0.000340 | 90 | |
| IT122 | JP-8 | | 70 | 52.5 | 66 | 64 | 83 | 0.000408 | 90 | |
| IT123 | JP-8 | | 70 | 55.5 | 66 | 64 | 83 | 0.000422 | 90 | |
| IT124 | JP-8 | | 30 | 32.0 | 54 | 54 | 59 | | 45 | Void Run |
| IT125 | JP-8 | | 30 | 23.8 | 58 | 65 | 66 | 0.000114 | 45 | |
| IT126 | JP-8 | | 40 | 38.5 | 64 | 64 | 75 | 0.000142 | 45 | |
| IT127 | JP-8 | | 50 | 45.5 | 63 | 64 | 75 | 0.000184 | 45 | |
| IT128 | JP-8 | | 60 | 43.5 | 63 | 64 | 75 | 0.000396 | 45 | |
| IT129 | JP-8 | | 70 | 50.0 | 63 | 66 | 63 | 0.000231 | 45 | |
| IT130 | JP-8 | | 78 | 59.0 | 64 | 65 | 64 | 0.000385 | 45 | |
| IT131 | EF8-104H | 740 | 30 | 19.2 | 65 | 60 | 70 | 0.000225 | 45 | Void Run, Possible Fuel Digestion |
| IT132 | EF8-104H | 740 | 40 | 31.2 | 68 | 62 | 70 | 0.000226 | 45 | Void Run, Possible Fuel Digestion |
| IT133 | EF8-104H | 730 | 50 | 37.0 | 72 | 62 | 80 | 0.000162 | 45 | |
| IT134 | EF8-104H | 730 | 60 | 50.0 | 74 | 65 | 84 | 0.000197 | 45 | |
| IT135 | EF8-104H | 730 | 70 | 52.6 | 72 | 71 | 84 | 0.000194 | 45 | |
| IT136 | EF8-104H | 730 | 78 | 56.0 | 74 | 74 | 84 | 0.000203 | 45 | |
| IT137 | EF8-104H | 730 | 40 | 29.5 | 72 | 74 | 84 | 0.000119 | 45 | |
| IT138 | EF8-104H | 780 | 30 | 23.8 | 58 | 54 | 64 | 0.000034 | 90 | |
| IT139 | EF8-104H | 780 | 40 | 29.4 | 56 | 55 | 64 | 0.000088 | 90 | |
| IT140 | EF8-104H | | 50 | 41.0 | 59 | 59 | 74 | 0.0000743 | 90 | |
| IT141 | EF8-104H | 780 | 60 | 50.0 | 58 | 62 | 74 | 0.000132 | 90 | |
| IT142 | EF8-104H | 780 | 70 | 55.5 | 60 | 63 | 78 | 0.000177 | 90 | |
| IT143 | EF8-104H | 780 | 78 | | 62 | 62 | 78 | 0.000176 | 90 | No Film |

TABLE VI. IMPACT IGNITION TEST CONDITIONS AND ASSOCIATED DATA

| Run No. | Fuel | Yield Stress, ($Dynes/cm^2$) | Piston Velocity (fps) | Fuel Velocity (fps) | Ambient Temperature (°F) | Fuel Temperature (°F) | Surface Temperature (°F) | Impact Angle (Degrees) | $\Psi_{JP-4}$ (Calculated) | Ignition Rating | Comments |
|---|---|---|---|---|---|---|---|---|---|---|---|
| IT144 | JP-4 | | 30 | 35.7 | 61 | 62 | 76 | 90 | 1.0 | 4.0 | |
| IT145 | JP-4 | | 40 | 50 | 65 | 63 | 76 | 90 | 1.0 | 4.0 | |
| IT146 | JP-4 | | 50 | 55.5 | 64 | 64 | 76 | 90 | 1.0 | 4.0 | |
| IT147 | JP-4 | | 60 | 58.9 | 66 | 64 | 76 | 90 | 1.0 | 4.0 | |
| IT148 | JP-4 | | 70 | 58.9 | 66 | 66 | 76 | 90 | 1.0 | 4.0 | |
| IT149 | JP-4 | | 30 | 31.25 | 65 | 66 | 78 | 45 | 1.0 | 4.0 | |
| IT150 | JP-4 | | 40 | 38.5 | 66 | 66 | 78 | 45 | 1.0 | 4.0 | |
| IT151 | JP-4 | | 50 | 45.4 | 66 | 66 | 78 | 45 | 1.0 | 4.0 | |
| IT152 | JP-4 | | 60 | 58.8 | 65 | 66 | 82 | 45 | 1.0 | 4.0 | |
| IT153 | JP-4 | | 70 | 55.6 | 66 | 66 | 82 | 45 | 1.0 | 4.0 | |
| IT154 | JP-4 | | 70 | 58.9 | 68 | 68 | 82 | 45 | 1.0 | 4.0 | |
| IT155 | EF4R-104 | 480 | 30 | 25.0 | 70 | 60 | 82 | 90 | 0.2725 | 0 | |
| IT156 | EF4R-104 | 480 | 40 | 31.3 | 72 | 64 | 82 | 90 | 0.442 | 0 | |
| IT157 | EF4R-104 | 480 | 50 | 41.6 | 71 | 68 | 80 | 90 | 0.774 | 0 | |
| IT158 | EF4R-104 | 480 | 60 | 43.5 | 72 | 68 | 80 | 90 | 0.822 | 0 | |
| IT159 | EF4R-104 | 407 | 70 | 50.0 | 78 | 64 | 85 | 90 | 1.0 | 0 | |
| IT160 | EF4R-104 | 407 | 30 | 22.7 | 78 | 67 | 85 | 45 | 0.133 | 1.0 | |
| IT161 | EF4R-104 | 407 | 40 | 32.3 | 78 | 70 | 85 | 45 | 0.273 | 0 | |
| IT162 | EF4R-104 | 487 | 50 | 35.7 | 76 | 66 | 85 | 45 | 0.259 | 0 | |
| IT163 | EF4R-104 | 487 | 60 | 38.5 | 76 | 60 | 85 | 45 | 0.306 | 1.0 | |
| IT164 | EF4R-104 | 487 | 70 | 55.5 | 76 | 66 | 85 | 45 | 0.670 | 1.0 | |
| IT165 | JP-8 | | 30 | 20.5 | 64 | 74 | 86 | 90 | 0.078 | 1.0 | |
| IT166 | JP-8 | | 40 | 40.0 | 75 | 74 | 86 | 90 | 0.14 | 1.0 | |
| IT167 | JP-4 | | 50 | 50.0 | 74 | 74 | 86 | 90 | 1.0 | 4.0 | |

TABLE VI. Continued

| Run No. | Fuel | Yield Stress, $(Dynes/cm^2)$ | Piston Velocity (fps) | Fuel Velocity (fps) | Ambient Temperature (°F) | Fuel Temperature (°F) | Surface Temperature (°F) | Impact Angle (Degrees) | %JP-4 (Calculated) | Ignition Rating | Comments |
|---|---|---|---|---|---|---|---|---|---|---|---|
| IT168 | JP-8 | | 50 | 50.0 | 75 | 75 | 86 | 90 | 0.179 | 2.0 | |
| IT169 | JP-8 | | 60 | 58.8 | 75 | 75 | 82 | 90 | 0.198 | 1.0 | |
| IT170 | JP-8 | | 70 | 62.5 | 75 | 75 | 82 | 90 | 0.202 | 1.0 | |
| IT171 | JP-8 | | 30 | 31.2 | 84 | 83 | 90 | 45 | 0.09 | 2.0 | |
| IT172 | JP-8 | | 40 | 50.0 | 84 | 83 | 90 | 45 | 0.12 | 2.0 | |
| IT173 | JP-8 | | 50 | 58.8 | 86 | 84 | 92 | 45 | 0.148 | 0 | |
| IT174 | JP-8 | | 60 | 55.5 | 85 | 84 | 92 | 45 | 0.130 | 1.0 | |
| IT175 | JP-8 | | 70 | 71.5 | 85 | 84 | 92 | 45 | 0.18 | 1.0 | |
| IT176 | EF4R-104H | 970 | 30 | 20.8 | 86 | 78 | 92 | 90 | 0.086 | 0 | |
| IT177 | EF4R-104H | 970 | 40 | 23.8 | 86 | 78 | 92 | 90 | 0.106 | 0 | |
| IT178 | EF4R-104H | 970 | 50 | 35.7 | 86 | 78 | 94 | 90 | 0.224 | 0 | |
| IT179 | EF4R-104H | 970 | 60 | 45.5 | 89 | 84 | 94 | 90 | 0.369 | 1.0 | |
| IT180 | EF4R-104H | 970 | 70 | 52.6 | 90 | 84 | 97 | 90 | 0.496 | 1.0 | |
| IT181 | EF4R-104H | 1020 | 30 | 31.2 | 89 | 76 | 97 | 45 | 0.092 | 0 | |
| IT182 | EF4R-104H | 1020 | 40 | 40.0 | 90 | 78 | 96 | 45 | 0.138 | 1.0 | |
| IT183 | EF4R-104H | 1020 | 50 | 41.6 | 90 | 80 | 96 | 45 | 0.148 | 0 | |
| IT184 | EF4R-104H | 1020 | 60 | 47.6 | 92 | 82 | 96 | 45 | 0.190 | 3.0 | |
| IT185 | EF4R-104H | 1020 | 70 | 55.5 | 90 | 84 | 96 | 45 | 0.2 | 3.0 | |
| IT186 | EF8-104H | 440 | 30 | 26.3 | 97 | 80 | 102 | 90 | 0.0319 | 0 | |
| IT187 | EF8-104H | 440 | 40 | 43.5 | 98 | 80 | 102 | 90 | 0.135 | 1.0 | |
| IT188 | EF8-104H | 440 | 50 | 41.6 | 100 | 85 | 102 | 90 | 0.122 | 0 | |
| IT189 | EF8-104H | 440 | 60 | 50.0 | 98 | 91 | 102 | 90 | 0.177 | 0 | |
| IT190 | EF8-104H | 440 | 70 | 55.5 | 96 | 95 | 102 | 90 | 0.190 | 0 | |
| IT191 | EF8-104H | 425 | 30 | 22.7 | 98 | 78 | 102 | 45 | 0.0113 | 0 | |
| IT192 | EF8-104H | 425 | 40 | 38.4 | 99 | 78 | 106 | 45 | 0.0375 | 1.0 | |
| IT193 | EF8-104H | 425 | 50 | 50.0 | 99 | 77 | 106 | 45 | 0.0791 | 1.0 | |

TABLE VI. Continued

| Run No. | Fuel | Yield Stress, (Dynes/cm$^2$) | Piston Velocity (fps) | Fuel Velocity (fps) | Ambient Temperature (°F) | Fuel Temperature (°F) | Surface Temperature (°F) | Impact Angle (Degrees) | $\psi_{JP-4}$ (Calculated) | Ignition Rating | Comments |
|---|---|---|---|---|---|---|---|---|---|---|---|
| IT194 | EP8-104H | 425 | 60 | 50.0 | 99 | 76 | 106 | 45 | 0.0791 | 0 | |
| IT195 | EP8-104H | 425 | 70 | 52.7 | 98 | 77 | 106 | 45 | 0.0858 | 0 | |
| IT196 | JP-4 | | 30 | 25.0 | 98 | 78 | 108 | 90 | 1.0 | 4.0 | |
| IT197 | JP-4 | | 40 | 35.7 | 98 | 75 | 108 | 90 | 1.0 | 4.0 | |
| IT198 | JP-4 | | 50 | 50.0 | 95 | 73 | 106 | 90 | 1.0 | 4.0 | |
| IT199 | JP-4 | | 60 | 55.5 | 96 | 74 | 104 | 90 | 1.0 | 4.0 | |
| IT200 | JP-4 | | 70 | 55.6 | 96 | 74 | 104 | 90 | 1.0 | 4.0 | |
| IT201 | JP-4 | | 30 | 26.3 | 88 | 64 | 96 | 45 | 1.0 | 4.0 | |
| IT202 | JP-4 | | 40 | 32.3 | 85 | 64 | 96 | 45 | 1.0 | 3.0 | |
| IT203 | JP-4 | | 50 | 50.0 | 86 | 65 | 96 | 45 | 1.0 | 4.0 | |
| IT204 | JP-4 | | 60 | 52.7 | 85 | 66 | 96 | 45 | 1.0 | 4.0 | |
| IT205 | JP-4 | | 70 | 59.0 | 85 | 66 | 96 | 45 | 1.0 | 4.0 | |
| IT206 | JP-8 | | 30 | 20.0 | 86 | 80 | 94 | 90 | 0.088 | 1.0 | |
| IT207 | JP-8 | | 40 | | 67 | 70 | 94 | 90 | | | Void Run |
| IT208 | JP-8 | | 50 | 50.0 | 87 | 68 | 94 | 90 | 0.178 | 1.0 | |
| IT209 | JP-8 | | 60 | 50.0 | 88 | 68 | 94 | 90 | 0.178 | 2.0 | |
| IT210 | JP-8 | | 70 | 55.6 | 89 | 68 | 98 | 90 | 0.190 | 2.0 | |
| IT211 | JP-8 | | 70 | 55.6 | 86 | 68 | 98 | 45 | 0.136 | 1.0 | |
| IT212 | JP-8 | | 30 | 23.8 | 93 | 70 | 96 | 45 | 0.085 | 1.0 | |
| IT213 | JP-8 | | 40 | 37.0 | 93 | 71 | 96 | 45 | 0.095 | 1.0 | |
| IT214 | JP-8 | | 50 | 52.6 | 93 | 72 | 96 | 45 | 0.125 | 2.0 | |
| IT215 | JP-8 | | 60 | 58.9 | 93 | 72 | 96 | 45 | 0.148 | 2.0 | |
| IT216 | EP4R-104 | 290 | 30 | 22.7 | 93 | 84 | 107 | 90 | 0.472 | 0 | |
| IT217 | EP4R-104 | 290 | 40 | 34.5 | 94 | 82 | 107 | 90 | 0.928 | 0 | |
| IT218 | EP4R-104 | 290 | 50 | 41.7 | 93 | 81 | 107 | 90 | 1.0 | 0 | |
| IT219 | EP4R-104 | 290 | 60 | 50 | 92 | 81 | 107 | 90 | 1.0 | 0 | |

TABLE VI. Continued

| Run No. | Fuel | Yield Stress (Dynes/cm$^2$) | Piston Velocity (fps) | Fuel Velocity (fps) | Ambient Temperature (°F) | Fuel Temperature (°F) | Surface Temperature (°F) | Impact Angle (Degrees) | $\psi_{JP-4}$ (Calculated) | Ignition Rating | Comments |
|---|---|---|---|---|---|---|---|---|---|---|---|
| IT220 | EF4R-104 | 290 | 70 | 55.6 | 93 | 78 | 107 | 90 | 1.0 | 3.0 | |
| IT221 | EF4R-104 | 376 | 30 | 29.4 | 83 | 73 | 94 | 45 | 0.254 | 1.0 | |
| IT222 | EF4R-104 | 376 | 40 | 38.5 | 83 | 72 | 94 | 45 | 0.457 | 0 | |
| IT223 | EF4R-104 | 376 | 50 | 45.5 | 83 | 72 | 94 | 45 | 0.640 | 0 | |
| IT224 | EF4R-104 | 376 | 60 | 50.0 | 84 | 72 | 94 | 45 | 0.763 | 1.0 | |
| IT225 | EF4R-104 | 376 | 70 | 55.5 | 84 | 72 | 94 | 45 | 0.887 | 2.0 | |
| IT226 | EF4R-104H | 1055 | 30 | 31.2 | 86 | 78 | 94 | 45 | 0.088 | 0 | |
| IT227 | EF4R-104H | 1055 | 40 | 40.0 | 87 | 77 | 94 | 45 | 0.131 | 1.0 | |
| IT228 | EF4R-104H | 1055 | 50 | 47.6 | 86 | 77 | 94 | 95 | 0.179 | 3.0 | |
| IT229 | EF4R-104H | 1055 | 60 | 55.6 | 86 | 76 | 94 | 45 | 0.244 | 1.0 | |
| IT230 | EF4R-104H | 1055 | 70 | 62.5 | 86 | 77 | 94 | 45 | 0.310 | 0 | |
| IT231 | EF4R-104H | 1055 | 50 | 47.6 | 89 | 76 | 94 | 45 | 0.179 | 0 | |
| IT232 | EF4R-104H | 1055 | 30 | 31.2 | 88 | 76 | 94 | 45 | 0.156 | 0 | |
| IT233 | EF4R-104H | 970 | 40 | 37.0 | 84 | 78 | 88 | 90 | 0.242 | 0 | |
| IT234 | EF4R-104H | 970 | 50 | 43.5 | 83 | 76 | 88 | 90 | 0.336 | 3.0 | |
| IT235 | EF4R-104H | 970 | 60 | 55.6 | 80 | 74 | 88 | 90 | 0.554 | 1.0 | |
| IT236 | EF4R-104H | 970 | 70 | 52.6 | 81 | 73 | 91 | 90 | 0.497 | 1.0 | |
| IT237 | EF8-104H | 535 | 30 | 29.4 | 85 | 78 | 91 | 90 | 0.0323 | 0 | |
| IT238 | EF8-104H | 535 | 40 | 38.5 | 82 | 77 | 91 | 90 | 0.0755 | 0 | |
| IT239 | EF8-104H | 535 | 50 | 41.7 | 82 | 72 | 98 | 90 | 0.100 | 0 | |
| IT240 | EF8-104H | 535 | 60 | 50 | 82 | 72 | 98 | 90 | 0.160 | 0 | |
| IT241 | EF8-104H | 535 | 70 | 55.6 | 82 | 72 | 98 | 90 | 0.186 | 1.0 | |
| IT242 | EF8-104H | 465 | 30 | 23.8 | 83 | 78 | 102 | 45 | 0.0109 | 0 | |
| IT243 | EF8-104H | 465 | 40 | 40.0 | 84 | 78 | 102 | 45 | 0.0364 | 0 | |
| IT244 | EF8-104H | 465 | 50 | 47.6 | 84 | 78 | 102 | 45 | 0.0603 | 1.0 | |
| IT245 | EF8-104H | 465 | 60 | 50.0 | 85 | 72 | 102 | 45 | 0.0715 | 0 | |
| IT246 | EF8-104H | 465 | 70 | 55.6 | 86 | 72 | 102 | 45 | 0.099 | 0 | |

TABLE VI. Continued

| Run No. | Fuel | Yield Stress ($Dynes/cm^2$) | Piston Velocity (fps) | Fuel Velocity (fps) | Ambient Temperature (°F) | Fuel Temperature (°F) | Surface Temperature (°F) | Impact Angle (Degrees) | $\psi_{JP-4}$ (Calculated) | Ignition Rating | Comments |
|---|---|---|---|---|---|---|---|---|---|---|---|
| IT247 | JP-8 | | 70 | 62.5 | 87 | | 102 | 45 | 0.16 | 1.0 | |
| IT248 | JP-8 | | 30 | 34.5 | 89 | | 102 | 4[illegible] | 0.092 | 1.0 | |
| IT249 | JP-8 | | 30 | 33.3 | 90 | 66 | 102 | 45 | 0.090 | 1.0 | |
| IT250 | JP-8 | | 40 | 47.6 | 89 | 64 | 102 | 45 | 0.113 | 1.0 | |
| IT251 | JP-8 | | 50 | 41.7 | 94 | 65 | 108 | 45 | 0.101 | 1.0 | |
| IT252 | JP-8 | | 60 | 47.6 | 93 | 66 | 108 | 45 | 0.113 | 1.0 | |
| IT253 | JP-8 | | 70 | 58.9 | 92 | 66 | 108 | 45 | 0.149 | 1.0 | |
| IT254 | JP-8 | | 30 | 21.7 | 92 | 66 | 108 | 90 | 0.089 | 1.0 | |
| IT255 | JP-8 | | 40 | 31.2 | 92 | 66 | 102 | 90 | 0.105 | 2.0 | |
| IT256 | JP-8 | | 50 | 45.5 | 93 | 67 | 108 | 90 | 0.163 | 1.0 | |
| IT257 | JP-8 | | 60 | 50.0 | 93 | 68 | 108 | 90 | 0.179 | 1.0 | |
| IT258 | JP-8 | | 70 | 55.6 | 93 | 68 | 108 | 90 | 0.190 | 1.0 | |
| IT259 | JP-8 | | 78 | 55.6 | 93 | 68 | 108 | 90 | 0.190 | 1.0 | |
| IT260 | EF4R-104 | 370 | 30 | 27.8 | 82 | 76 | 94 | 45 | 0.237 | 1.0 | |
| IT261 | EF4R-104 | 370 | 40 | 25.0 | 82 | 74 | 94 | 45 | 0.190 | 0 | |
| IT262 | EF4R-104 | 370 | 50 | 41.7 | 84 | 72 | 94 | 45 | 0.560 | 3.0 | |
| IT263 | EF4R-104 | 370 | 60 | 55.6 | 84 | 72 | 94 | 45 | 0.904 | 1.0 | |
| IT264 | EF4R-104 | 370 | 70 | 58.8 | 86 | 72 | 100 | 45 | 0.951 | 1.0 | |
| IT265 | EF4R-104 | 390 | 40 | 33.3 | 86 | 76 | 100 | 45 | 0.310 | 1.0 | |
| IT266 | EF4R-104 | 390 | 40 | 35.7 | 87 | 78 | 100 | 90 | 0.733 | 9 | |
| IT267 | EF4R-104 | 390 | 50 | 50.0 | 86 | 78 | 100 | 90 | 1.0 | 1.0 | |
| IT268 | EF4R-104 | 390 | 60 | 50.0 | 87 | 78 | 100 | 90 | 1.0 | 3.0 | |
| IT269 | EF4R-104 | 390 | 70 | 58.8 | 87 | 78 | 100 | 90 | 1.0 | 1.0 | |
| IT270 | EF4R-104H | 950 | 30 | 27.8 | 89 | 80 | 110 | 45 | 0.080 | 0 | |
| IT271 | EF4R-104H | 950 | 40 | 35.7 | 91 | 80 | 110 | 45 | 0.119 | 1.0 | |
| IT272 | EF4R-104H | 950 | 50 | 50.0 | 91 | 78 | 110 | 45 | 0.223 | 3.0 | |

TABLE VI. Continued

| Run No. | Fuel | Yield Stress ($Dynes/cm^2$) | Piston Velocity (fps) | Fuel Velocity (fps) | Ambient Temperature (°F) | Fuel Temperature (°F) | Surface Temperature (°F) | Impact Angle (Degrees) | $\Psi_{JP-4}$ (Calculated) | Ignition Rating | Comments |
|---|---|---|---|---|---|---|---|---|---|---|---|
| IT273 | EF4R-104H | 950 | 60 | 57.2 | 92 | 78 | 110 | 45 | 0.295 | 1.0 | |
| IT274 | EF4R-104H | 950 | 70 | 55.6 | 92 | 78 | 110 | 45 | 0.278 | 1.0 | |
| IT275 | EF4R-104H | 1000 | 40 | 41.6 | 94 | 81 | 110 | 90 | 0.295 | 0 | |
| IT276 | EF4R-104H | 1000 | 50 | 50.0 | 94 | 80 | 110 | 90 | 0.432 | 0 | |
| IT277 | EF4R-104H | 975 | 60 | 50.0 | 92 | 83 | 100 | 90 | 0.440 | 1.0 | |
| IT278 | EF4R-104H | 975 | 70 | 58.8 | 92 | 80 | 100 | 90 | 0.608 | 1.0 | |
| IT279 | EF4R-104H | 975 | 30 | 31.2 | 92 | 78 | 100 | 90 | 0.167 | 0 | |
| IT280 | EF8-104H | 455 | 30 | 31.2 | 93 | 91 | 106 | 45 | 0.0195 | 0 | |
| IT281 | EF8-104H | 455 | 40 | 38.5 | 94 | 90 | 106 | 45 | 0.0332 | 0 | |
| IT282 | EF8-104H | 455 | 50 | 55.6 | 94 | 86 | 106 | 45 | 0.099 | 1.0 | |
| IT283 | EF8-104H | 455 | 60 | 55.6 | 94 | 79 | 106 | 45 | 0.099 | 0 | |
| IT284 | EF8-104H | 455 | 70 | 58.8 | 94 | 78 | 109 | 45 | 0.120 | 1.0 | |
| IT285 | EF8-104H | 455 | 40 | 41.6 | 95 | 79 | 109 | 90 | 0.120 | 1.0 | |
| IT286 | EF8-104H | 450 | 50 | 50.0 | 96 | 91 | 109 | 90 | 0.177 | 1.0 | |
| IT287 | EF8-104H | 450 | 60 | 55.6 | 96 | 88 | 109 | 90 | 0.190 | 0 | |
| IT288 | EF8-104H | 450 | 70 | 62.5 | 98 | 85 | 109 | 90 | 0.202 | 1.0 | |

TABLE VII. SIMULATED FULL-SCALE TEST CONDITIONS AND ASSOCIATED DATA

| Run No. | Fuel | Average Yield Stress or Viscosity* | Fuel Temp. (°F) | Ambient Temp. (°F) | Surface Temp. (°F) | Wind Velocity (MPH) and Direction | Impact Velocity (ft/sec) | Barometric Reading (in. Hg) | Relative Humidity (%) | Calculated $\psi_{JP-4}$ | Igniter Type** | Comments |
|---|---|---|---|---|---|---|---|---|---|---|---|---|
| 1 | JP-4 | - | 98 | 94 | 110 | 0-6 W | 63.7 | 29.91 | 15 | 1.0 | 1 | Hazardous |
| 2 | JP-8 | - | 98 | 88 | 111 | 7-10 W-SW | 64.7 | 28.65 | 26 | 0.16 | 1 | Hazardous |
| 3 | EF4R-104 | 283 | 98 | 90.5 | 113 | 0-8 S-SW | 63.5 | 28.57 | 11 | 1.0 | 1 | Hazardous |
| 4 | EF4R-104H | 807 | 100 | 86 | 117 | 0-7 S-SE | 60.2 | 28.66 | 20 | 0.408 | 1 | Hazardous |
| 5 | EF8R-104H | 1570 | 101 | 84 | 103 | 0-9 W-SW | 60.5 | 28.89 | 26 | 0.028 | 1 | Nonhazardous |
| 6 | Jet-A EXP-4 | 1467 | 103 | 87 | 112 | 0-5 S-SE | 62.5 | 30.03 | 27 | 0.032 | 1 | Nonhazardous |
| 7 | JP-4 EXP-4 | 800 | 101 | 88 | 115 | 0-8 W-NW | 65.6 | 29.93 | 21 | 0.49 | 1 | Hazardous |
| 8 | JP-4 | - | 98 | 81 | 100 | 0-6 E-NE | 66.6 | 28.78 | 42 | 1.0 | 2 | Hazardous |
| 9 | JP-4 | - | 100 | 85 | 110 | 0-6 W-SW | 66.6 | 28.71 | 27 | 1.0 | 2 | Hazardous |
| 10 | JP-8 | - | 102.5 | 85 | 113 | 0-6 W-SW | 66.6 | 28.69 | 26 | 0.16 | 2 | Nonhazardous |
| 11 | JP-8 | - | 103 | 68 | 91 | 0-6 E-SE | 65.7 | 28.88 | 14 | 0.16 | 2 | Hazardous |
| 12 | EF4R-104 | 253 | 102 | 74.5 | 109 | 0-7 S-SW | 65.2 | 28.78 | 11 | 1.0 | 2 | Hazardous |
| 13 | EF4R-104 | 349 | 99 | 74 | 93 | 5-10 S-SW | 66.2 | 28.78 | 11 | 1.0 | 2 | Hazardous |
| 14 | EF4R-104H | 825 | 100 | 80 | 100 | 0-5 W-SW | 67.8 | 28.68 | 11 | 0.504 | 2 | Hazardous |
| 15 | EF4R-104H | 761 | 103 | 80 | 105 | 0-5 S | 65.5 | 28.81 | 19 | 0.50 | 2 | Hazardous |
| 16 | EF8R-104H | 1680 | 103 | 85 | 114 | 0-5 W-SW | 66.0 | 28.77 | 13 | 0.032 | 2 | Nonhazardous |
| 17 | EF8R-104H | 1570 | 101.5 | 86 | 110 | 0-5 W | 66.2 | 28.71 | 11 | 0.0358 | 2 | Nonhazardous |
| 18 | Jet-A EXP-4 | 1253 | 99.5 | 86 | 113 | 5-7 S-SW | 65.4 | 28.67 | 15 | 0.051 | 2 | Nonhazardous |
| 19 | Jet-A EXP-4 | 1360 | 98.0 | 89 | 115 | 0-6 W-SW | 64.1 | 28.65 | 12 | 0.0411 | 2 | Nonhazardous |
| 20 | JP-4 EXP-4 | 601 | 99 | 80 | 96 | 0-7 S-SE | 65.2 | 28.77 | 24 | 0.69 | 2 | Hazardous |
| 21 | JP-4 EXP-4 | 723 | 101 | 82.5 | 110 | 5-7 S-SE | 66.0 | 28.76 | 22 | 0.58 | 2 | Hazardous |
| 22 | JP-4 | - | 101 | 74 | 91 | 0-5 W-SW | 65.2 | 28.88 | 37 | 1.0 | 3 | Hazardous |
| 23 | JP-4 | - | 97 | 71 | 93 | 7-10 W-SW | 65.0 | 29.87 | 15 | 1.0 | 3 | Hazardous |

* Yield stress is given in Dynes/cm$^2$; viscosity is given in centipoise.
**Igniter type is designated as: 1 - open-flame igniters, 2 - spark/hot-surface igniter, and 3 - on-board engine simulator.

TABLE VII. Continued

| Run No. | Fuel | Average Yield Stress or Viscosity* | Fuel Temp. (°F) | Ambient Temp. (°F) | Surface Temp. (°F) | Wind Velocity (MPH) and Direction | Impact Velocity (ft/sec) | Barometric Reading (in. Hg) | Relative Humidity (%) | Calculated $\Psi_{JP-4}$ | Igniter Type** | Comments |
|---|---|---|---|---|---|---|---|---|---|---|---|---|
| 24 | JP-8 | - | 101 | 76 | 91 | 0-6 W | 66.2 | 28.92 | 6 | 0.162 | 3 | Nonhazardous |
| 25 | JP-8 | - | 103 | 78 | 99 | 5 SW | 65.5 | 28.88 | 11 | 0.161 | 3 | Nonhazardous |
| 26 | EF4R-104 | 349 | 97 | 78 | 93 | 6 W-SW | 64.1 | 28.82 | 9 | 1.0 | 3 | Hazardous |
| 27 | EF4R-104 | 325 | 101 | 79 | 97 | 5 S | 65.0 | - | - | 1.0 | 3 | Hazardous*** |
| 28 | EF4R-104H | 877 | 103 | 81 | 99 | 7 E-SE | 65.4 | - | - | 0.44 | 3 | Hazardous*** |
| 29 | EF4R-104H | 693 | 102 | 78 | 91 | 8 E | 65.5 | 29.01 | 22 | 0.589 | 3 | Hazardous |
| 30 | EF8R-104H | 1533 | 102 | 80 | 101 | 7 S-SE | 61.1 | 28.89 | 17 | 0.0312 | 3 | Nonhazardous |
| 31 | EF8R-104H | 1520 | 103 | 74 | 90 | 8 SE | 64.5 | 28.93 | 28 | 0.0363 | 3 | Nonhazardous |
| 32 | Jet-A EXP-4 | 1207 | 103 | 75 | 97 | 5 S | 65.8 | 28.90 | 16 | 0.047 | 3 | Nonhazardous |
| 33 | Jet-A EXP-4 | 1517 | 103 | 78 | 99 | 5 NW | 65.5 | 28.82 | 13 | 0.0368 | 3 | Nonhazardous |
| 34 | JP-4 EXP-4 | 735 | 103 | 79 | 95 | 5 S | 65.5 | 28.79 | 11 | 0.498 | 3 | Hazardous*** |
| 35 | JP-4 EXP-4 | 690 | 100 | 76 | 95 | 7 S | 66.2 | 28.78 | 14 | 0.607 | 3 | Hazardous |
| 36 | JP-4 | - | 98 | 75 | 97 | 5 SW | 65.7 | 28.77 | 14 | 1.0 | 3 | Nonhazardous |
| 37 | EF4R-104 | 381 | 100 | 77 | 101 | 6 S-SW | 64.5 | 28.82 | 14 | 1.0 | 3 | Hazardous |
| 38 | EF4R-104H | 798 | 100 | 74 | 90 | 0 | 64.75 | 28.95 | 14 | 0.387 | 3 | Hazardous |
| 39 | JP-8 | - | 97 | 73 | 93 | 6 SW | 64.5 | 28.92 | 13 | 0.16 | 3 | Nonhazardous |
| 40 | EF8R-104H | 1810 | 98 | 72 | 98 | 7 S-SW | 65.0 | 28.92 | 17 | 0.0283 | 3 | Nonhazardous |
| 41 | Jet-A EXP-4 | 1755 | 98 | 73 | 107 | 7 W-NW | 65.0 | 28.90 | 14 | 0.0308 | 3 | Nonhazardous |
| 42 | JP-4 EXP-4 | 800 | 100 | 70 | 93 | 7 SW | 63.5 | 28.61 | 16 | 0.47 | 3 | Hazardous |
| 43 | EF8R-104 | 665 | 103 | 66 | 86 | 8 | 66.6 | 28.31 | 19 | 0.105 | 1 | Nonhazardous |
| 44 | EF8R-104 | 568 | 103 | 60 | 71 | 0-6 S-SE | 64.5 | 28.84 | 25 | 0.1185 | 2 | Nonhazardous |
| 45 | EF8R-104 | 643 | 102 | 63 | 83 | 8-13 SW | 63.5 | 28.77 | 16 | 0.100 | 2 | Nonhazardous |

* Yield stress is given in Dynes/cm$^2$; viscosity is given in centipoise.
** Igniter type is designated as: 1 - open-flame igniters, 2 - spark/hot-surface igniter, and 3 - on-board engine simulator.
***Burner malfunction, relight second actuation of burner cycle.

TABLE VII. Continued

| Run No. | Fuel | Average Yield Stress or Viscosity* | Fuel Temp. (°F) | Ambient Temp. (°F) | Surface Temp. (F°) | Wind Velocity (MPH) and Direction | Impact Velocity (ft/sec) | Barometric Reading (in. Hg) | Relative Humidity (%) | Calculated $\psi_{JP-4}$ | Igniter Type** | Comments |
|---|---|---|---|---|---|---|---|---|---|---|---|---|
| 46 | EF8R-104 | 693 | 99 | 60 | 78 | 8-10 S-SE | 64.5 | 28.93 | 35 | 0.0914 | 3 | Nonhazardous |
| 47 | EF8R-104 | 673.3 | 100 | 62 | 80 | 3 S | 61.6 | 29.45 | 34 | 0.0844 | 3 | Hazardous (Marginal) |
| 48 | EF8R-104 | 618 | 103 | 71 | 85 | 6 SW | 65.6 | 29.75 | 15 | 0.109 | 3 | Nonhazardous |
| 49 | Jet-A Gel #1 | 68.0 cP | 103 | 72 | 92 | 0-3 SW | 65.6 | 28.87 | 22 | - | 1 | Nonhazardous |
| 50 | Jet-A Gel #1 | 67.1 cP | 103 | 77 | 97 | 0-5 SW | 65.1 | 28.79 | 19 | - | 2 | Nonhazardous |
| 51 | Jet-A Gel #1 | 129 cP | 101 | 87 | 101 | 5-7 S-SE | 62.5 | 28.77 | 17 | - | 2 | Nonhazardous |
| 52 | Jet-A Gel #1 | 129 cP | 103 | 82 | 101 | 0-4 S-SE | 61.6 | 28.75 | 19 | - | 3 | Hazardous |
| 53 | Jet-A Gel #2 | 40.7 cP | 98 | 67 | 84 | 0-7 S | 64.5 | 28.82 | 39 | - | 1 | Hazardous (Marginal) |
| 54 | Jet-A Gel #2 | 21.9 cP | 100 | 70 | 80 | 8-12 S-SE | 64.5 | 28.71 | 17 | - | 2 | Hazardous |
| 55 | Jet-A Gel #2 | 24.7 cP | 102 | 73 | 91 | 10 S-SW | 66.5 | 28.63 | 13 | - | 2 | Hazardous |
| 56 | Jet-A Gel #1 | 61.0 cP | 97 | 67 | 88 | 0-7 SW | 64.5 | 28.85 | 10 | - | 3 | Hazardous |
| 57 | Jet-A Gel #1 | 42.0 cP | 100 | 74 | 87 | 6-11 S-SW | 60.4 | 28.64 | 15 | - | 3 | Hazardous |
| 58 | Jet-A Gel #2 | 27.9 cP | 99 | 56 | 76 | 6-9 S | 65.5 | 30.04 | 64 | - | 3 | Hazardous |
| 59 | Jet-A Gel #2 | 34.0 cP | 102 | 61 | 78 | 8-12 S | 64.5 | 29.85 | 39 | - | 3 | Hazardous |
| 60 | Jet-A Gel #2 | 31.6 cP | 102 | 63 | 81 | 6-10 S-SW | 65.5 | 29.78 | 31 | - | 3 | Hazardous |

* Yield stress is given in Dynes/cm$^2$; viscosity is given in centipoise.
**Igniter type is designated as: 1 - open-flame igniters, 2 - spark/hot-surface igniter, and 3 - on-board engine simulator.